UNIVERSITY OF SOUTHAMPTON

FACULTY OF PHYSICAL SCIENCES AND ENGINEERING

School of Electronics and Computer Science

Dielectric Properties of Hexagonal Boron Nitride Polymer Nanocomposites

by

Raed Ayoob

Thesis for the degree of Doctor of Philosophy

June 2017

UNIVERSITY OF SOUTHAMPTON

ABSTRACT

FACULTY OF PHYSICAL SCIENCES AND ENGINEERING

Electrical Engineering

Thesis for the degree of Doctor of Philosophy

DIELECTRIC PROPERTIES OF HEXAGONAL BORON NITRIDE POLYMER NANOCOMPOSITES

Raed Ayoob

There is a growing research interest in polymer nanocomposite materials due to their potential in enhancing dielectric properties. However, a considerable amount of variability exists in the literature regarding the electrical performance of polymer nanocomposites, and therefore the underlying mechanisms underpinning their electrical properties are still far from fully understood. Possible reasons for the existing inconsistencies could be due to different material preparation techniques, different nanoparticle dispersion states, unknown filler content, inconsistent sample storage conditions, and unknown water level content in the samples. Determining the principal factors that dominate the electrical behaviour of polymer nanocomposites could allow engineers to tailor the electrical properties of dielectrics for their specific application. As a result, the work reported in this thesis was mainly set out to explore the factors governing the electrical properties of polymer nanocomposites such that the inconsistencies in the literature can be better understood, and consequently eliminated. This thesis investigated the performance of hexagonal boron nitride (hBN) nanocomposites based on two thermoplastic polymers: polystyrene and polyethylene.

Prior to producing any nanocomposites, the hBN particles were characterised using different techniques. The characterisation primarily revealed that the boron nitride particles are in the hexagonal form and the surface of hBN contains a scarce amount of hydroxyl groups. Polystyrene nanocomposites were prepared containing identical amounts of hBN dispersed in different solvents in an attempt to obtain different dispersion states, as a result of different hBN/solvent interactions. The effect of solvent processing was negligible on the dispersion state of the hBN in the polystyrene; no observable difference in the dispersion and electrical

properties was reported although the presence of hBN resulted in a slight increase in the breakdown strength relative to the unfilled polystyrene.

A range of polyethylene nanocomposites were produced containing different amounts of hBN to understand the effect of the dispersion or aggregation state of the hBN on the breakdown strength. The results revealed that the nanocomposites, regardless of the morphology, exhibited a monotonic increase in breakdown strength with increasing hBN content from 2 wt % to 30 wt %, while maintaining the low dielectric losses of the unfilled polyethylene. While the hBN was found to have a strong nucleating effect on the polyethylene, it was determined that the local change in morphology was not the cause of the enhanced breakdown strength as both the polyethylene nanocomposites obtained by rapid crystallisation, where the development of spherulites was suppressed, and the amorphous polystyrene nanocomposites, also exhibited an improved breakdown strength. Further experiments indicated that the polyethylene nanocomposites did not absorb any moisture from the environment in ambient conditions, and absorbed a very small amount of water even in the 30 wt % polyethylene/hBN nanocomposite when completely immersed in water. Dielectric spectroscopy measurements revealed that the surface hydroxyl groups on the hBN are most likely located only on the edge surfaces of the hBN rather than basal surfaces. The water was most likely loosely bound to the hBN particles, where local water clusters formed. It was remarkable that a percolating water network was not formed in a nanocomposite consisting of an already percolating hBN network, which was largely attributed to the surface chemistry of hBN. Despite the presence of water in the system, the hBN nanocomposites continued to exhibit an enhanced breakdown strength in comparison to the unfilled polyethylene. Therefore, this thesis demonstrated that the electrical behaviour of polymer nanocomposites is most likely dominated by the surface state of the nanoparticles and how the particles interact with the charge carriers; any other effects due to local morphological changes or nanoparticle dispersion are considered to be secondary reasons for changes in the electrical properties.

Table of Contents

List of Tables

List of Figures

DECLARATION OF AUTHORSHIP

I, Raed Ayoob, declare that this thesis and the work presented in it are my own and has been generated by me as the result of my own original research.

Dielectric Properties of Hexagonal Boron Nitride Polymer Nanocomposites

I confirm that:

1. This work was done wholly or mainly while in candidature for a research degree at this University;
2. Where any part of this thesis has previously been submitted for a degree or any other qualification at this University or any other institution, this has been clearly stated;
3. Where I have consulted the published work of others, this is always clearly attributed;
4. Where I have quoted from the work of others, the source is always given. With the exception of such quotations, this thesis is entirely my own work;
5. I have acknowledged all main sources of help;
6. Where the thesis is based on work done by myself jointly with others, I have made clear exactly what was done by others and what I have contributed myself;
7. Parts of this work have been, and will be, published as:

    i. R. Ayoob, T. Andritsch, and A. S. Vaughan, "Electrical Breakdown Strength of Boron Nitride Polyethylene Nanocomposites," in *The Seventh UHVnet Colloquium,* United Kingdom, 2014.

    ii. R. Ayoob, T. Andritsch, and A. S. Vaughan, "The Effect of Exfoliation on the Breakdown Strength of Polystyrene Boron Nitriide Composites," in *IEEE Conference on Electrical Insulation and Dielectric Phenomena*, United States, 2014, pp. 675-678.

    iii. R. Ayoob, T. Andritsch, and A. S. Vaughan, "The Effect of Material Processing on the Dielectric Properties of Polystyrene Boron Nitride Nanocomposites," in *IEEE Electrical Insulation Conference*, United States, 2015, pp. 333-336.

    iv. R. Ayoob, T. Andritsch, and A. S. Vaughan, "Material Processing of Polystyrene Boron Nitride Nanocomposites," in *Early Career Researchers Colloquium*, United Kingdom, 2015.

v. R. Ayoob, T. Andritsch, and A. S. Vaughan, "Water Absorption Behaviour in Polyethylene Boron Nitride Nanocomposites," in *IEEE Conference on Dielectrics*, France, 2016, pp. 784-787.

vi. R. Ayoob, T. Andritsch, and A. S. Vaughan, "Enhanced Dielectric Properties in Polyethylene/Hexagonal Boron Nitride Nanocomposites," *ACS Applied Materials & Interfaces*, Manuscript Submitted, 2017.

vii. R. Ayoob, T. Andritsch, and A. S. Vaughan, "The Effect of Water Absorption on the Dielectric Properties of Polyethylene/Hexagonal Boron Nitride Nanocomposites," *Journal of Materials Chemistry*, Manuscript Written, 2017.

viii. R. Ayoob, T. Andritsch, and A. S. Vaughan, "Electrical Properties of Hydrophobic Polyethylene Nanocomposites Based on a Hexagonal Boron Nitride Filler," *IEEE Transactions on Nanotechnology*, Manuscript Written, 2017.

ix. R. Ayoob, T. Andritsch, and A. S. Vaughan, "The Effect of Solvent Processing on the Dispersion State of Polystyrene/Hexagonal Boron Nitride Nanocomposites," *Journal of Applied Physics D*, Manuscript Written, 2017.

x. R. Ayoob, T. Andritsch, and A. S. Vaughan, "Structure-Property Relationship in Polyethylene/Hexagonal Boron Nitride Nanocomposites," *IEEE Transactions on Dielectrics and Electrical Insulation*, Manuscript Under Preparation, 2017.

Signed: .....

Date: .....

Acknowledgements

I would like to thank both my supervisors, Dr Thomas Andritsch and Professor Alun Vaughan, for their continuous support and guidance. I am grateful for all their invaluable discussions and expertise, without which this thesis would not have been possible. I would also like thank Professor Steve Beeby, the internal examiner for my first year viva and MPhil to PhD upgrade viva, whose useful suggestions have helped me complete my final thesis.

My thanks extends to Dr Alex Holt, whose considerable help and support has helped me get started with my PhD project in the lab. I am grateful to many of the members of the Tony Davies High Voltage Laboratory for their useful discussions over the years. In particular, I express my gratitude to Dr Ian Hosier, Dr Matt Praeger, Mr Fuad Alhabill, Mr Yan Wang, Ms Istebreq Saeedi, and Dr Stelios Christou. Many thanks to all the friends I have made in Southampton over the past 7 years for all their support. Special thanks goes to Zubair and Ali for their constant help and support over the past 15 years.

I am very grateful to my colleagues at Edif ERA, particularly Mr Duncan Humphrey and Mr Bob Dean, for their complete support over the past few months. Furthermore, their expertise in high voltage electrical engineering has helped me gain valuable industrial experience whilst writing the thesis during the final year of my PhD.

Most of all, I thank my parents, sisters, and brothers for their unconditional love, endless support, and constant encouragement. No words can describe my gratitude and appreciation for all that you have given me in my life. Finally, I sincerely thank Hawra for her constant support and motivation when I have needed it the most.

Abbreviations

AC	Alternating current
Al_2O_3	Aluminium oxide
aPS	Atactic polystyrene
ASTM	American Society for Testing and Materials
CB	Chlorobenzene
DC	Direct current
DCM	Dichloromethane
DSC	Differential scanning calorimetry
FTIR	Fourier transform infrared
hBN	Hexagonal boron nitride
HDPE	High density polyethylene
IPA	Isopropyl alcohol
LDPE	Low density polyethylene
MgO	Magnesium oxide
MMT	Montmorillonite
PE	Polyethylene
PS	Polystyrene
PVC	Polyvinyl chloride
RH	Relative humidity
SEM	Scanning electron microscopy
Tanδ	Dielectric loss tangent

TGA	Thermogravimetric analysis
TiO_2	Titanium dioxide
TOL	Toluene
XRD	X-Ray diffraction
ZnO	Zinc oxide

Symbols

α	Weibull scale parameter
β	Weibull shape parameter
δ	Phase lag
δ_s	Solubility parameter
ε_0	Permittivity of free space
ε^*	Complex relative permittivity
ε'	Real relative permittivity
ε''	Imaginary relative permittivity
ε'_c	Real relative permittivity of the composite
ε'_m	Real relative permittivity of the matrix
ε'_p	Real relative permittivity of the particle
λ	X-Ray wavelength
σ	Electrical conductivity
χ	Crystallinity
ω	Angular frequency
ω_f	Weight fraction of polymer
ΔH	Enthalpy of melting
ΔH_0	Enthalpy of a 100% crystalline material
d	Interlayer spacing
D	Electric displacement
E	Electric field

E_b	Breakdown field
I	Current
T_c	Crystallisation temperature
T_{c1}	Lower peak crystallisation temperature
T_{c2}	Upper peak crystallisation temperature
T_g	Glass transition temperature
T_{m1}	Lower peak melting temperature
T_{m2}	Upper peak melting temperature
T_{10}	Thermal degradation temperature at 10% of mass degradation
T_{50}	Thermal degradation temperature at 50% of mass degradation
V	Voltage
V_b	Breakdown voltage
2θ	Diffraction angle

اهداء الى سر سعادتي و ابتسامتي و نجاحي.....

عائلتي الحبيبة

Chapter 1: Introduction

The availability of reliable and affordable supplies of energy that do not lead to significant climate change is one of the most pressing challenges of present times and is one that affects both developed and developing economies [1]. This is forcing a paradigm shift in the way we generate electricity, from large centralised power stations, that frequently rely upon fossil fuels, to a much more diversified – both in terms of their nature and location – sources. For example, the adoption of renewable generation involving off-shore wind necessarily requires the transmission of large amounts of energy from the point of production to centres of demand [2]. All electrical systems rely upon insulation and, as the demands placed on power systems increase, for example through a desire to reduce the size of insulation systems in order to aid heat dissipation or to exploit high voltage transmission, so do the demands placed on the insulation. The critical enabling role played by dielectric materials in facilitating the evolution of next-generation generation and transmission infrastructures has led to significant related research efforts, and a topic that has received particular attention is that of nanocomposite dielectrics – nanodielectrics [3]. The potential of nanodielectrics was first highlighted by Lewis in 1994 [4] albeit that such systems had received much attention for many years in connection with other applications. Lewis proposed that the addition of nanometric sized particles in a polymer would form interfaces that highly influence the dielectric properties of the resulting nanodielectrics material. This idea has captured the interest of many researchers worldwide, as the present dielectric materials could benefit from improvements in properties such as dielectric strength, dielectric loss, and thermal conductivity.

1.1 The Emergence of Polymer Nanocomposites

Composite materials are not a new topic of research as polymer composites based on a clay filler have been explored in the past. In the 1980's and early 1990's, research by Toyota on the exfoliation of clay in nylon-6 demonstrated major improvements in mechanical properties, such as improved tensile strength and elongation at break, and thermal properties, such as improved thermal resistance and fire retardant properties. In 1985, polymer clay nanocomposites were invented at Toyota central Research Laboratories in Japan when they introduced the Nylon-6/montmorillonite nanocomposites. These new materials found

applications in the automotive, electric, and food industry [5]. It was only in 1991 when the first commercial engineering application of these nanocomposites was realised by Toyota, in collaboration with Ube, when nylon-6/clay nanocomposites were used as timing belt covers in their cars. This successful pioneering work by Toyota initiated the development and use of polymer nanocomposites in the automotive industry. Nylon-6/clay nanocomposites were introduced by Unitika, a materials manufacturing company in Japan, for engine covers used in Mitsubishi's gasoline direct injection engines [6]. As automotive companies began to notice the advantages of using these new materials, different types of polymer nanocomposites were produced. Polyolefin/clay nanocomposites found useful applications as step assistant components for GMC safari and Chevrolet astro vans in 2001 when they were introduced by General Motors and Basell. The same nanocomposites were also used in Chevrolet Impala doors. Polypropylene/clay nanocomposites were used by Honda for structural seat backs recently. Additionally, nylon-12/clay nanocomposites were used by Ube in fuel system components [7]. As the potential for these materials has been realised in the automotive industry, the possibilities for polymer nanocomposites as electrical insulators in the power industry were still not explored yet.

Early experimental work in 1999 by Henk et al. [8] has shown that by incorporating silica nanoparticles in polymers, the voltage endurance could be improved with a reduction in filler size. However, these materials were still not considered in electrical insulation applications. A global interest in nanodielectrics originated in 2002 after Nelson et al. [9] experimentally revealed some of the potentials of nanodielectrics, such as the rapid decay of space charge in nanofilled systems compared to microfilled systems. The trend in nanodielectrics research is shown in Figure 1.1, where the number of publications related to research in nanodielectrics, exploring several dielectric properties, has dramatically increased after Nelson's paper. The rapid growth of nanodielectrics research started a new global interest to develop new materials with potentially enhanced dielectric properties.

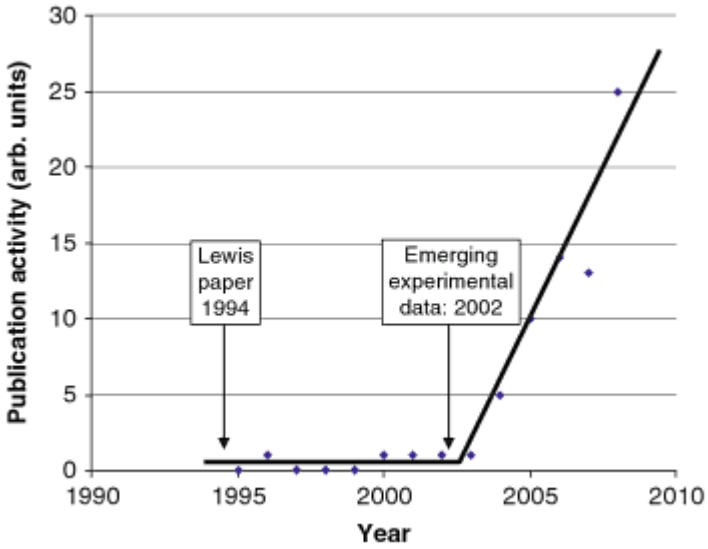

Figure 1.1: Trend in nanodielectrics publication

1.2 Electrical Properties of Polymer Nanocomposites

There are large possibilities for polymer nanocomposites to improve insulating properties such as dielectric breakdown strength, partial discharge resistance, electrical tree growth, and dielectric losses. The enhancement of breakdown strength is one of the most attractive properties of polymer nanocomposites. For example, Wang et al. [10] reported an increase in breakdown strength in LDPE/MgO nanocomposites where the breakdown strength increased upon the addition of 1 wt % of MgO, and then started to progressively decrease when 3 wt % and 5 wt % of MgO were added, although the breakdown strength in these nanocomposites was still higher than the breakdown strength of the unfilled LDPE. Similarly, Chen et al. [11] reported a similar pattern in in epoxy/TiO_2 nanocomposites where the breakdown strength increased as 0.5 wt % of TiO_2 was added, and started to decrease with higher TiO_2 loading. A similar pattern in breakdown strength was also observed in PVC/ZnO nanocomposites [12]. Li et al. [13] investigated the breakdown behaviour of micro and nano Al_2O_3 epoxy composites and reported a 56 % decrease and a 5% increase in breakdown strength for the 60 wt % micro composite and the 5 wt % nanocomposite respectively. They claimed that an electrical tree forms, when the electric field is applied, which rapidly grows when it encounters the microfiller polymer interface, which they referred to as defects, thus decreasing the breakdown strength relative to the unfilled epoxy. They also state that these "defects" do not exist in a nanocomposite, which is why the increase the breakdown strength was observed. In a similar study, the 5 vol % addition of nano barium-titanate into epoxy has been observed to enhance the breakdown strength by 21% relative to the unfilled epoxy [14]. However, in another study [15], the breakdown

strength of polyethylene/aluminium nanocomposites was shown to be lower than the base polymer for all loading levels, even with surface modification of the nanoparticles. Additionally, Lau et al. [16] showed that that adding silica nanoparticles to a polyethylene matrix reduced the breakdown strength when the surface of nanoparticles was not modified. However, after surface modification, the breakdown strength of the nanocomposite system increased relative to the systems with the unmodified nanoparticles, yet the breakdown strength was still lower than the unfilled polymer. So it is not reasonable to say that nanodielectrics necessarily exhibit improved breakdown strength, as there are appears to be many factors determining their behaviour, and it has been shown that some nanofillers have an undesirable effect on the breakdown behaviour.

The dielectric response of dielectrics is a topic of great interest as the dielectric losses provide an idea of how efficient the material is at storing or dissipating energy. The addition of nanoparticles into a polymer causes changes in the dielectric response of the system due to the presence of the interfacial zones. Nelson et al. [17] prepared epoxy/TiO_2 microcomposites and nanocomposites where, at low frequencies between 0.01 Hz to 100 Hz, the microcomposite had a higher real relative permittivity than both the base epoxy and the nanocomposite, due to the high relative permittivity of the filler compared to the epoxy. At frequencies above 1 kHz, the epoxy, microcomposite, and the nanocomposite had roughly the same real relative permittivity. However, at frequencies below 1 kHz, the real relative permittivity of the nanocomposite was below that of the microcomposite and the base epoxy. This result is not consistent with conventional mixing rules as the permittivity is presumed to have a value that lies between the permittivity of the polymer and the nanofiller. The authors suggested that the nanoparticles act as barriers for the epoxy chain movement, as a change in morphology was observed, and the small size of the nanoparticles restricts dipolar reorientation, resulting in the lower real permittivity. Singha et al. [18] studied the dielectric response of epoxy/TiO_2 and epoxy/ZnO nanocomposites as well as epoxy/TiO_2 microcomposites. At low frequencies, the epoxy had a high permittivity value as the dipole moments in the epoxy chains have enough time to orient themselves with the applied field. At high frequencies, the dipole moments do not have enough time to orient themselves with the alternating field, resulting in a decreasing permittivity value with increasing frequency. The same behaviour was observed in the microcomposite and nanocomposite systems with various nanofiller loading levels. Due to the presence of Ti^{4+} and O^{2-} ions, the TiO_2 microcomposite and nanocomposite systems exhibited strong ionic polarisation resulting in a high static permittivity value. For the nanocomposites containing 0.1 wt % and 0.5 wt %

filler content, the permittivity values were slightly lower than those of the unfilled epoxy and at loading levels of 1 wt %, 5 wt %, and 10 wt %, the permittivity was higher than the unfilled epoxy. Similarly, for loading levels of 0.1 wt %, 0.5 wt %, and 1 wt %, the ZnO nanocomposites also exhibited a reduced permittivity relative to the unfilled epoxy. The authors suggested that the mobility of dipolar groups is restricted upon the addition of nanofillers, resulting in a reduced permittivity. At frequencies just below 1 kHz for loading levels of 5 wt % and 10 wt % for both the TiO_2 microcomposites and nanocomposites, the permittivity increased rapidly with decreasing frequency, due to the influence of ionic polarisation. At frequencies above 1 kHz, interfacial polarisation occured in the microcomposite system due to the presence of impurities and excess free charges, which are not bound to the surface of the particles. In epoxy/MgO nanocomposites [19], the permittivity was shown to be lower than the unfilled epoxy for varying MgO loading levels ranging from 0.5 wt % to 10 wt %. In epoxy/Al_2O_3 nanocomposites [19], the permittivity of the nanocomposites containing alumina (Al_2O_3) loading levels from 0.5 wt % to 5 w t% was lower than the unfilled epoxy but higher nanocomposite containing 10 wt % of alumina. The reasons for the lower permittivity was attributed to the immobilisation of the polymer chains as a result of nanoparticle surface modification. On the other hand, a polyethylene/silica nanocomposite [20], with a silica loading level of 2 wt % to 10 wt %, was found to have a larger real relative permittivity and larger losses, which increased with decreasing frequency. Similarly, the dielectric response of polyethylene/silicon nitride nanocomposites [21] have shown that both the real permittivity and dielectric losses are much larger than that of the unfilled polyethylene, and both increase significantly with decreasing frequency. Thus, many varied results of the dielectric response are reported in the literature and, again, they all depend on the combination of materials; no universal models exist to explain the electrical properties of nanodielectrics. Table 1.1 lists some properties of nanocomposites relative to the relevant unfilled polymer, which demonstrates the variability in the literature.

Table 1.1: Electrical properties of nanodielectrics

Polymer nanocomposite	**Filler content**	**Properties investigated**
LDPE/magnesium oxide [22]	1 wt %	Breakdown (increased)
Polyurethane/mica [23]	1, 2, 3, 4, 5, 10 wt %	Breakdown (increased)
Epoxy/alumina [24]	0.1, 1, 5 wt %	Breakdown (decreased from 0.1 and 1 wt % and increased for 5 wt %)
LDPE/alumina [25]	0.1, 1, 2, 5, 10 wt %	Breakdown (increased),
LDPE/titanium dioxide [25]	0.1, 1, 2, 5, 10 wt %	Breakdown (increased from 0.1 to 2 wt % then decreased)
Epoxy/alumina [26] and Epoxy/aluminium nitride [26]	0.5, 2, 5, 10 wt %	Breakdown (unchanged)
Epoxy/magnesium oxide [26]	0.5, 2, 5, 10 wt %	Breakdown (increased for 0.5 wt % then decreased)
Epoxy/silica [26]	0.5, 2, 5, 10 wt %	Breakdown (increased for 0.5 wt % then decreased)
Polyethylene/silica [27]	0.1, 0.5, 1, 2, 5 wt %	Breakdown (increased from 0.1 to 0.5 wt %then decreased)
Epoxy/alumina [28]	0.1, 1, 5 wt %	Breakdown (decreased from 0.1 to 1 wt % and increased in 5 wt %)
Polyethylene/silica [29]	2, 5, 10 wt %	Breakdown (decreased)
Epoxy/titanium dioxide [30]	0.5 wt %	Permittivity (decreased)
Epoxy/alumina [31]	2 wt %	Permittivity (decreased)

The main underlying cause for the property changes in polymer nanocomposites is considered, by the majority of researchers, to be the presence of the interface when nanoparticles are introduced [13], [40]–[43]. One of the main difference between nanoparticle and microparticle inclusions is the large specific surface area associated with nanoparticles. Figure 1.2 illustrates the relationship between the surface area per unit volume and the radius of the particle. It can be seen that as the radius of the particle becomes less than 100 nm, the surface area considerably increases, which has led to the notion that the surface area of the polymer/nanoparticle interface becomes the most dominant feature.

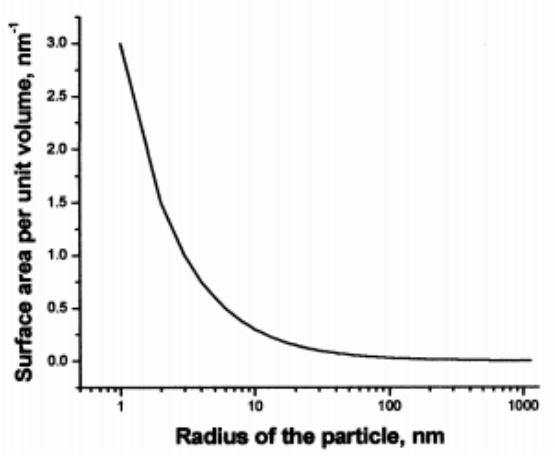

Figure 1.2: Surface area of nanocomposites as a function of particle size [3]

The interaction zone is considered to be a new material that is different from the constituent elements of the nanocomposite: the polymer matrix and the nanofiller. Figure 1.3 shows how the interaction zone might look like for microparticles and nanoparticles

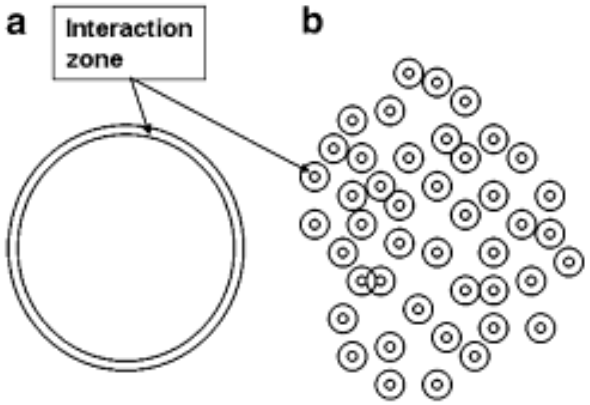

Figure 1.3: Interaction zone for (a) microparticles and (b) nanoparticles [3]

It can be seen the interface volume is significantly increased as the particle size is reduced, implying that the interphase constitutes most of the bulk material of the nanocomposite [3]. This is why a considerable effort has been devoted to modifying the internal surfaces of nanoparticles, as to vary the polymer/nanofiller interactions, thereby changing local properties; therefore, the desired material properties can be achieved by properly engineering the interface. Many theoretical models have been proposed [32], [35], [37], [38] to explain the behaviour of the interface; however, such models are not universal and have been developed to explain a certain set of experimental results. As this interaction zone is not sufficient in explaining the unusual experimental results in polymer nanocomposites, it appears that other factors might be dominating the electrical performance of polymer nanocomposites, which should be explored in order to understand the mechanisms governing the electrical properties of nanodielectrics.

1.3 Research Motivation

Increased power requirements stresses the importance for the design of high-performance and novel insulating materials. The addition of nanoparticles to existing polymers has been studied, attempted and tested in the last decade, to produce new materials with improved dielectric properties. Although research on nanodielectrics has been carried out for the last decade, this does not mean that that the subject is entirely understood. Indeed, very many of the underlying principles remain uncertain, such as the polymer/nanofiller interface, and consequently, researchers are still exploring solutions to common challenges faced by nanodielectrics, such as nanoparticle agglomeration. There are large prospects for the use of nanofillers in polymers to enhance the polymer's dielectric properties. However, the addition of nanofillers does not always lead to improved insulation; it is common to observe a degraded performance in polymer nanocomposite. Understanding the reasons behind this unusual behaviour and variability remains to be a challenge in the present day, which needs to be addressed.

1.4 Research Objectives

The goal of this research is to give insights into some of the reasons behind the inconsistencies reported in the literature regarding the electrical properties of polymer nanocomposites. The thesis mainly sets out to give an insight into the dominant factors affecting the electrical properties of polymer nanocomposites. Therefore, the work reported here is set out to understand the effect of hexagonal boron nitride (hBN) filler on the

dielectric properties of polystyrene and polyethylene nanocomposites. In particular, the goals of this thesis were to:

i) Investigate the chemical interactions between the hexagonal boron nitride filler and different solvents.

   Hypothesis: Chemical interactions between the hexagonal boron nitride particles and different solvents lead to different nanoparticle dispersion states, and therefore different electrical properties.

ii) Investigate the effect of nanoparticle agglomeration on the electrical properties of polymer nanocomposites.

   Hypothesis: The effect of particle agglomeration is not the dominant factor in determining the electrical properties of polymer nanocomposites and does not always lead to deteriorated electrical properties as always reported in the literature.

iii) Investigate the role of surface chemistry of the nanoparticles, or the interface, in determining the electrical properties of polymer nanocomposites.

   Hypothesis: The effect of water absorption on the electrical properties of nanodielectrics is more dominant than the effect of nanoparticle dispersion or agglomeration.

1.5 Thesis Contributions

- The first contribution of this thesis is presented through the results in Chapter 6, which tested the second hypothesis listed in Section 1.4. The results in Chapter 6 showed a monotonic increase in breakdown strength with increasing hBN content, up to 30 wt % of hBN, despite the presence of large hBN agglomerates and a percolating hBN network. As opposed to the results reported in the literature, which always show a drastic reduction in the breakdown strength of nanodielectrics at the percolation threshold, the unexpected results presented in this thesis show that this is not always true since the percolation of hBN in this work did not lead to deteriorated electrical properties. Therefore, these results suggest that the breakdown strength and charge transport have less to do with the distribution of the nanofiller and much more with how the nanofiller interacts with the charge carriers; the dispersion of the hBN particles is not the main factor to consider when trying to improve the electrical

properties in hBN based nanocomposites. This is an important contribution to the field of nanodielectrics as most researchers attempt to improve nanoparticle dispersion in order to improve the electrical properties, and this thesis shows that this is unnecessary when the appropriate nanofiller is chosen for the required application.

- The second contribution of this thesis is presented through the results in Chapter 7, which tested the third hypothesis listed in Section 1.4. The results presented in Chapter 7 showed that polyethylene/hBN nanocomposites absorb no water under ambient conditions and insignificant amount of water when completely immersed in water, where they continue to exhibit an improved breakdown strength even in the most humid conditions; this has not been reported elsewhere in the literature. While the available literature on water absorption in polymer nanocomposites is limited, most of the published literature are studies on the water absorption of silica based nanocomposites, which are always shown to absorb a significant amount of water in both ambient and wet conditions. The main difference seen in this study and the published results in the literature is attributed to the different surface states of the fillers; the hydrophilic and spherical surface of silica is surrounded by hydroxyl groups and therefore readily absorbs water to form conducting water shells whereas the hydrophobic surface of hBN does not favour water absorption due to the presence of a small amount of hydroxyl groups on the edge surfaces which cannot form water shells around the entire hBN particles. These results suggest that the surface chemistry of the nanoparticles, rather than the dispersion of nanoparticles within the polymer, affects how they interact with the charge carriers and may be the dominating factor in determining the electrical performance of nanodielectrics; the breakdown strength of nanocomposites is believed to be largely dominated by the presence of water rather than structural or nanoparticle agglomeration effects.

The work presented in this thesis has not been reported previously in the literature due to the very limited research on hBN nanocomposites for high voltage applications, and therefore the contributions listed above are important for two main reasons. First, the improvement in breakdown strength, especially at the percolation threshold, is a significant contribution as this allows the synthesis of a composite system with enhanced breakdown strength and thermal conductivity, which was also demonstrated in Chapter 6. The thermal conductivity of composite systems below the percolation threshold is either very minimal or reduced, due to the presence of interfaces which result in phonon scattering; percolation is required to achieve efficient phonon transport. Since most of the available studies in the literature report

a decrease in breakdown strength at the percolation threshold, one of the biggest challenges in the field of nanodielectrics is producing a material which exhibits significant enhancements in both the dielectric breakdown strength and thermal conductivity. Therefore, this thesis showed that one property does not need to be improved at the expense of the other as they can both be simultaneously improved. These two properties, along with the improved breakdown strength in humid conditions, are the two of the most important properties for insulation materials in high voltage cables. Second, the results of the thesis provide an understanding of the mechanisms that dominate the electrical properties of polymer nanocomposites, which could enable future researchers in designing improved insulation materials for high voltage cable systems.

1.6 Thesis Outline

Chapter 1 presents an introduction to polymer nanocomposites, some of the variability in the literature regarding the electrical properties of nanocomposites, and the objectives of the research.

Chapter 2 presents a brief literature review of hBN composites used for high voltage applications to highlight the novelty in this thesis.

Chapter 3 contains the experimental techniques used in this research. The theoretical background of the experimental procedures is also provided.

Chapter 4 contains the experimental work on the characterisation of the hBN particles.

Chapter 5 explores the effect of solvent processing on the dielectric properties of polystyrene/hBN nanocomposites.

Chapter 6 explores the effect of hBN content on the dielectric properties of polyethylene/hBN nanocomposites.

Chapter 7 explores the effect of water absorption on the electrical properties of polyethylene/hBN nanocomposites.

Chapter 8 includes a summary of the findings, major conclusions, and suggestions for possible future work.

Chapter 2: A Review of Hexagonal Boron Nitride Composites for High Voltage Applications

2.1 Introduction

The 20th century witnessed remarkable advances in the field of high voltage electrical insulation. Naturally occuring materials such as asphalt and mica were used in the early 1900's until 1925, when the first synthetic materials such as phenolic and alkyd resins were produced [39]. A polymeric insulator, polyvinylchloride, was introduced in 1936 as a substitute for some of the natural materials, but it was limited to low voltage applications due to its high electrical losses. The knowledge and processing of insulation materials has increased in the 1940's and 1950's, which led to the synthesis of a considerable number of polymeric insulators such as polyethylene, polystyrene and polypropylene [40]. These materials were suitable for applications involving high electrical stresses as they have a high dielectric breakdown strength. High voltage cables with polyethylene insulation were used in the 1950's at 15 kV [41]. The study of the underlying physics and chemistry of insulators led to major breakthroughs in the 1960's [42]. This in turn led to the development and use of extruded polyethylene, cross-linked polyethylene (XLPE), and thin polypropylene films in high voltage systems [40].

The 1970's revolved around the investigation of electrical treeing failure mechanisms, which were a result of impurities or voids [43]. The main example is XLPE , which was never expected to fail but did due to electrical and water treeing. Therefore, a considerable effort was put into the study of these failure mechanisms in polyethylene as it was widely used in electrical insulation [44]. Morphological characterisation of XLPE using scanning electron microscopy (SEM) and transmission electron microscopy (TEM) helped researchers understand the changes in the structure of polyethylene under high voltage stresses, therefore enabling further developments in controlling the morphology of polyethylene [45]. The concept of high-voltage, direct current (HVDC) transmission emerged in the 1990's, which introduced the possibility of the use of polyethylene as an insulating materials for HVDC links, although the problem of space charge build up arose for the case of DC cables [46]. As an alternative, there were prospects for the use of fillers in low density polyethylene and blends of polyethylene to tailor its electrical properties and reduce the formation of space

charge [47]. The current stage into polymeric insulation research involves nanotechnology for high voltage applications, which was initiated at the start of the 21st century and remains a subject of research today [3].

2.2 Thermal Conductivity

The current rating of high voltage cables is largely determined by the rate of heat transfer through the insulation. The copper or aluminum conductors, which carry the current, have a much larger thermal conductivity than the insulation material, which is mainly made of cross-linked polyethylene (XLPE). Therefore, improvements in the thermal conductivity of the insulation could lead to an improved current rating of the cable, and consequently the cross section of the copper conductors can be effectively reduced. The reduction in the amount of used copper could lead to large reductions in the production costs of the cable, as copper is the most expensive component in high voltage cable systems. Thermal dissipation is a topic that is of great technological importance and, consequently, the potential of composite systems as a route to improved material characteristics has been studied by many workers. Increasing the thermal conductivity in composite systems requires the formation of a percolating network of particles with high thermal conductivity as this would achieve a thermal pathway for efficient phonon transport, whereas a well dispersed nanocomposite system results in a large interphase, as illustrated in Figure 2.1, which would significantly enable phonon scattering at the interfacial boundaries, and consequently either lead to a reduction or a minimal increase in the thermal conductivity.

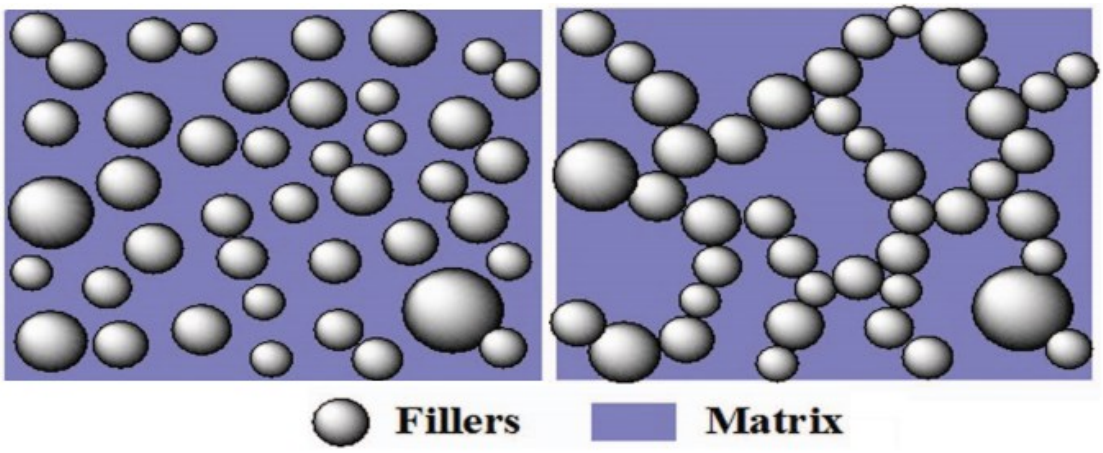

Figure 2.1: A representation of a polymer composite with a reasonable particle dispersion (left) and a poor particle dispersion (right) [48]

While the electrical properties of nanocomposites are generally poorly understood and ambiguous, the thermal conductivity is a much better understood property and the reported literature on the thermal conductivity of composite systems is much more consistent than the reported literature on the electrical properties. For example, Zhou et al. [49] reported a monotonic increase in the thermal conductivity with increasing hBN content in polyethylene/hBN composites incorporating hBN particles with an average particle size of 0.5 μm. The thermal conductivity of the unfilled HDPE, which was reported as 0.26 W/m.K, was increased to 0.45 W/m.K in the 15 vol % composite, 0.76 W/m.K in the 25 vol % composite, and 1.02 W/m.K in the 35 vol % composite. Similar results were presented by Vanga-Bouanga et al. [50] who reported an increase in the thermal conductivity of a 50 wt % ultra-high-molecular-weight polyethylene (UHMWP)/hBN microcomposite and a nanocomposite. The thermal conductivity of the unfilled UHMWP was 0.33 W/m.K whereas it increased to 0.69 W/m.K and 0.52 W/m.K in the microcomposite and nanocomposite respectively. Zhou et al. [51] reported a monotonic increase in thermal conductivity with increasing hBN content in epoxy/hBN composites, where the thermal conductivity in the unfilled epoxy increased from 0.22 W/m.K to 1.34 W/m.K as 50 wt % of hBN particles were added into the epoxy. Similarly, Du et al. [52] reported a monotonic increase in the thermal conductivity with increasing hBN content in polyimide/hBN composites, where the thermal conductivity in the unfilled polyimide increased from 0.38 W/m.K to 2.58 W/m.K in the 80 wt % composite.

The use of thermally conductive particles such as hBN in polymers does not always lead to an increase in thermal conductivity. For example, Heid et al. [53] reported a very small change in thermal conductivity in epoxy/hBN nanocomposites with a low filler concentration, where the thermal conductivity of the epoxy changed from 0.171 W/m.K in the unfilled epoxy to 0.177 W/m.K, 0.179 W/m.K, and 0.201 W/m.K in the 1 wt %, 2 wt %, and 5 wt % epoxy/hBN composites respectively. Similarly, Reading et al. [54] reported a change from ~0.22 W/m.K in the unfilled epoxy to 0.25 – 0.33 W/m.K in a range of 10 wt % hBN composites with a range of hBN particle sizes. However, a reduction in thermal conductivity is sometimes reported in composite systems containing thermally conductive particles. For example, Saysouk et al. [55] compared the thermal conductivity of polyimide composites based on a 120 nm hBN filler and a 40 nm cBN filler, where the cBN refers to the cubic form of boron nitride, and found that the thermal conductivity of the polyimide/cBN composites at low concentrations was lower than the thermal conductivity of the unfilled polyimide whereas an increase in thermal conductivity was reported in the

polyimide/hBN composites at all hBN concentrations, despite hBN having a lower thermal conductivity than cBN [56], [57]. The thermal conductivity in the hBN composites increased with increasing hBN content, which increased from 0.21 W/m.K in the unfilled polyimide to 0.56 W/m.K in the 29 vol % hBN composite. In contrast, the thermal conductivity in the cBN composite initially decreased with increasing cBN content, up to 20 vol %, from 0.21 W/m.K to 0.12 W/m.K, and then it was found to increase to 0.25 W/m.K in the composite containing 57 vol % of cBN. It could be that a higher amount of cBN was required to reach percolation, in comparison to the hBN composites, due to the much smaller size of the cBN particles which would then effectively lead to an increase in the thermal conductivity.

2.3 Dielectric Breakdown Strength

While percolation is required in order to effectively improve the thermal conductivity, a significant reduction in the breakdown strength of nanocomposites at the percolation threshold was always reported. For example, the addition of 45 vol % of silica in a polymethyl methacrylate (PMMA) polymer caused the breakdown strength to reduce from ~800 V/μm, in the unfilled PMMA, to ~340 V/μm [58]. Similarly, the breakdown strength of a 20 vol % poly(vinylidene fluoride-co-hexafluoro propylene)/barium titanate ($BaTiO_3$) nanocomposite decreased from ~380 V/μm, in the unfilled polymer, to ~230 V/μm [59]. Therefore, one of the biggest challenges in the field of nanodielectrics is to simultaneously improve the breakdown strength and thermal conductivity, as most commonly one property is always significantly improved at the expense of the other property.

The breakdown strength of hBN based nanocomposites at or above the percolation threshold has not yet been explored in the literature, which highlights the importance of the results presented in this thesis. However, some researchers have studied the breakdown strength behaviour of hBN based nanocomposites in the past, although there exists some variability in the reported data. Andritsch et al. [60] investigated the short-term DC breakdown strength of 10 wt % epoxy/hBN nanocomposites and microcomposites using 4 different hBN particle sizes, and they noticed an increase in breakdown strength with decreasing hBN particle size although all composites exhibited a breakdown strength higher than the unfilled epoxy. They reported an increased breakdown strength from 162.6 kV/mm in the unfilled epoxy to 172.3 kV/mm, 180.3 kV/mm, 196.3 kV/mm, and 230.6 kV/mm in the nanocomposites containing 10 wt % of hBN with a particle size of 5 μm, 1.5 μm, 0.5 μm, and 70 nm respectively. The authors stated the increase in breakdown strength with decreasing particle

size is typically attributed to the increase of the size of the interfaces, although they found this result surprising as the surface of the hBN particles was not functionalised. This suggests that the presence of interfaces may not be as significant in determining the electrical properties as initially proposed by Lewis [4], where he argued that interfaces are the dominant factor in tailoring the electrical properties of polymer nanocomposites – an idea that was, and still is to this day, adopted by many researchers in the nanodielectrics community.

The same 70 nm hBN particles used previously by Andritsch et al. [60] were used by Tsekmes et al. [61], [62], where they modified the surface of the hBN particles to investigate the trend in both the AC and DC breakdown strength behaviour in epoxy/hBN nanocomposites with varying hBN content. In the case of the AC breakdown behaviour, the breakdown strength changed from ~42 kV/mm in the unfilled epoxy to ~44 kV/mm, ~51 kV/mm, ~48 kV/mm, and ~36 kV/mm in the nanocomposites containing 0.2 vol %, 0.6 vol %, 1 vol %, and 5 vol % of hBN respectively. In the case of the DC breakdown behaviour, the authors reported a similar trend where the breakdown strength changed from ~251 kV/mm in the unfilled epoxy to ~260 kV/mm, ~281 kV/mm, ~242 kV/mm, and ~176 kV/mm in the nanocomposites containing 0.2 vol %, 0.6 vol %, 1 vol %, and 5 vol % of hBN respectively. The authors attributed the increase in breakdown strength in the nanocomposites with low hBN loading levels to the lower dielectric losses and higher thermal conductivity in comparison to the unfilled epoxy, which can ultimately aid heat dissipation and prevent thermal runaway. Regarding the nanocomposites with a high hBN loading level, the authors attributed their decreased breakdown strength to their higher dielectric losses and the higher possibility of the presence of structural imperfections as the filler content increases, resulting in a composite material with an increased mass density than the unfilled epoxy, which highly increases the likelihood of void formation. Indeed, the study of Wang et al. [63], [64] highlighted the importance of void formation on the breakdown strength of epoxy/hBN nanocomposites, where they produced composites containing up to 80 wt % of hBN, which in some cases resulted in a 56.3 % reduction in breakdown strength in comparison to the unfilled epoxy due to the large void content.

Zhou et al. [51] studied the effect of hBN loading level on the breakdown strength of epoxy/hBN composites using a 0.5 μm hBN particle size. In a 10 wt % composite, the breakdown strength was very similar to the unfilled epoxy, which exhibited a breakdown strength of 32 kV/mm, however the breakdown strength started to decrease as the hBN content further increased; there was a 50 % reduction in breakdown strength in the 50 wt %

composite which exhibited a breakdown strength of 16 kV/mm. This decrease in breakdown strength at high filler loading levels was attributed to the presence of defects such as voids, as a result of difficulties in material processing at high filler content due to the rapid increase in the viscosity of the epoxy/hBN mixture. Indeed, this observation was demonstrated by Chung et al. [65] who reported an increase in both the density and porosity in epoxy/hBN composites with increasing hBN content. The authors prepared a range of epoxy/hBN composites containing up to 80 vol % of two different types of hBN particles with a 3.6 μm and a 10.6 μm particle size in an attempt to improve the thermal conductivity of the system. They found that the composites containing the two different hBN particles followed the same trend, where both the value of the density and porosity increased with increasing hBN content, and there was a rapid increase in the value of porosity at a 50 vol % hBN content which resulted in a 20 % porosity. This behaviour was ascribed to the increased viscosity of the epoxy/hBN mixture at higher filler contents, where the voids are less easily filled due to the poor flow of the epoxy/hBN mixture and the poor contact between the epoxy and the hBN particles, which resulted in an increased volume of voids.

While some studies report an initial increase in breakdown strength at low hBN content and then a decrease in breakdown strength at high hBN content, some authors have reported that the incorporation of hBN particles result in a decrease in breakdown strength regardless of the hBN content. For example, Heid et al. [53] prepared epoxy/hBN composites with a range of hBN formulations by adding two different hBN particles, with a mean particle size of 0.5 μm and 9 μm, and reported a similar breakdown strength trend for both composites. The breakdown strength of the unfilled epoxy was 160 kV/mm, which decreased after including any amount of hBN. The breakdown strength of the 1 wt %, 2 wt %, and 5 wt % composites including the 0.5 μm hBN particles was 142 kV/mm, 140 kV/mm, and 134 kV/mm respectively. Similarly, the breakdown strength of the 1 wt %, 2 wt %, and 5 wt % composites including the 9 μm hBN particles was 144 kV/mm, 133 kV/mm, and 132 kV/mm respectively. These breakdown strength results are not consistent with the results presented by Andritsch et al. [60] and Tsekmes et al. [61], [62] where they noticed an improvement in breakdown strength even when a higher hBN content and larger hBN particles were used. In another study, Reading et al. [54] prepared a total of seven different 10 wt % epoxy/hBN composites with a mean hBN particle size of 0.4 μm, 0.5 μm, 3-5 μm, 5 μm, 7-15 μm, 9 μm, and 45 μm which exhibited a breakdown strength of 37.9 kV/mm, 40.1 kV/mm, 39.7 kV/mm, 37.9 kV/mm, 41.0 kV/mm, 36.3 kV/mm, and 39.5 kV/mm respectively in comparison to the breakdown strength of 37.0 kV/mm in the unfilled epoxy. While the

authors state that some of these composites exhibited a significant increase in breakdown strength relative to the unfilled epoxy, the results are considered to be statistically similar to each other where the observed changes could be due to experimental uncertainties. Moreover, the authors did not include any information about the confidence bounds in the Weibull plots or any uncertainties, which could reveal more information about the significance of the changes in the measured breakdown strength values.

These results which show a decrease or no change in breakdown strength are inconsistent with the results presented by Andritsch et al. [60] and Tsekmes et al. [61], [62], which suggests that there is a different factor which is causing this different behaviour. The complexity of relating physical properties to the breakdown strength in epoxy composite systems has been highlighted in the work of Nguyen et al. [66], where the authors reported that the inclusion of silica particles significantly affected the stoichiometry of the epoxy, which resulted in a stoichiometry with an excess hardener which was then related to the decrease in breakdown strength. To confirm this result, the authors deliberately prepared similar nanocomposites by changing the stoichiometry of the epoxy and found that by preparing nanocomposites with a stoichiometry incorporating an excess hardener, a similar decrease in breakdown strength was observed, and therefore concluded that the presence of nanoparticles could perturb the epoxy curing process and consequently change the stoichiometry, which ultimately can cause a decrease in breakdown strength. While this effect is not expected to be a consequence in all epoxy based nanocomposite systems, the decreased or unchanged breakdown strength results presented by Heid et al. [53] and Reading et al. [54] could be an effect of a change of stoichiometry rather than an effect of the hBN particle inclusions, which further highlights the difficulties in the material preparation of epoxy composites.

Composite systems based on an hBN filler have also been used in polymer others than epoxy in an attempt to improve the breakdown strength. For example, Xing et al. [67] prepared hBN nanocomposites by adding amide-functionalised boron nitride nanosheets (BNNSs) into a supramolecular polymer network, formed by a condensation reaction between fatty di-acids, fatty tri-acids, and diethylene triamine. The authors reported a monotonic increase in both the dielectric breakdown strength and electrical resistivity with increasing hBN content up to 8 vol % relative to the unfilled polymer. In a well dispersed polymer nanocomposite containing 8 vol % of hBN, the dielectric breakdown strength increased from 67.6 MV/m to 232.6 MV/m and the electrical resistivity increased from 3.08×10^{9} Ω.m to 2.78×10^{11} Ω.m. The authors attributed the improvement in the dielectric properties to the

enhanced Young's Modulus of the polymer nanocomposites, which increased from 1.5 MPa to 45 MPa in the 8 vol % nanocomposite, which may delay the onset of electromechanical breakdown. While many polymer breakdown theories exist, a filamentary electromechanical breakdown mechanism was in fact proposed by John Fothergill in 1991 [68], where he argued that breakdown in polymers may occur by the propagation of a filamentary-shaped mechanical crack, which leads to the release of electrostatic energy and electromechanical strain energy stored in the polymer due to the applied electric field. Although it is difficult to confidently determine the exact cause of breakdown in polymers, their study nevertheless highlighted some of the potential enhancements in electrical properties due to the incorporation of hBN particles into a polymer, regardless of the involved breakdown mechanism.

While most of the existing literature on the breakdown strength of hBN composites for high voltage applications were studies based on thermosetting epoxy composites, a very limited studies of hBN composites based on thermoplastics have been reported. For example, Du et al. [69] studied the breakdown strength behaviour in polypropylene/hBN nanocomposites and microcomposites, where the former exhibited an increase in breakdown strength with increasing hBN content whereas the latter exhibited a decrease in breakdown strength with increasing hBN content. The breakdown strength increased from 289 kV/mm to 300 kV/mm, 320 kV/mm, and 336 kV/mm in the nanocomposites containing 3 wt %, 6 wt %, and 9 wt % of hBN particles respectively whereas the breakdown strength decreased from 289 kV/mm to 279 kV/mm, 273 kV/mm, and 243 kV/mm in the microcomposites containing 3 wt %, 6 wt %, and 9 wt % of hBN particles respectively, although some of the confidence bounds in their presented Weibull plots seemed to overlap, especially at higher probabilities of failure. They described the decrease in breakdown strength in the microcomposites, which contained 10 μm hBN particles in comparison to the 50 nm hBN particles in the nanocomposites, to the formation of voids and defects. As the study of Andritsch et al. [60] described earlier showed a slight increase in breakdown strength in hBN composites containing hBN particles 5 μm in size, there appears to be a critical hBN particle size which will negatively influence the breakdown strength if it is exceeded, as highlighted in these two studies.

Another hBN composite system based on a thermoplastic polymer matrix was investigated by Vanga-Bouanga et al. [50] who prepared 50 wt % hBN composites by adding two hBN particles with a mean particle size of 11 μm and 70 nm in a UHMWP polymer. The breakdown strength of the unfilled UHMWP sample was 78 kV/mm while the breakdown

strength of the composites was reduced – the microcomposite exhibited a breakdown strength of 66 kV/mm and the nanocomposite exhibited a breakdown strength of 74 kV/mm. The authors attributed the decrease in breakdown strength to the presence of defects and voids, which is more significant in the microcomposite. While this may have some impact in a composite with such a high filler loading, the reliability of the presented data is questionable as the confidence bounds in the Weibull plot of the three materials overlap. If this reduction in breakdown strength is in fact significant, one must consider all the factors that could cause this reduction. In particular, the authors stated that the materials were synthesized using a ball milling process in a zirconium oxide crucible, which could introduce some impurities in the system. Indeed, Zhu et al. [70] used a ball milling processes using zirconia balls to grow boron nitride nanotubes (BNNTs) on the surface of silicon carbide fibres, and noticed two additional peaks in the X-Ray photoelectron spectroscopy (XPS) spectrum of the as-milled boron powder, which were attributed to the residual contamination of the zirconium dioxide (ZrO_2) from the ball milling process. Similarly, Bansal et al. [71] prepared a boron nitride composite by adding 4 wt % of BNNT into barium calcium aluminosilicate (BCAS) using a zirconia ball milling process, and noticed the presence of unusual inclusions in the SEM, which were later confirmed by energy dispersive X-Ray (EDX) analysis to be zirconia impurities. Electrical properties are extremely sensitive to residual chemical impurities and therefore the decrease in breakdown strength in the 50 wt % composites discussed above could be attributed to the presence of zirconia impurities, and therefore the employed material processing technique should be critically evaluated and chosen for the desired purpose and application of the produced material. A summary of the breakdown strength behaviour of the various hBN based composite systems reported in the literature is presented in Table 2.1.

Table 2.1: Breakdown strength of various hBN based composite systems

Polymer	**hBN content**	**hBN particle size**	**Breakdown Strength**
Epoxy	10 wt %	70 nm – 5000 nm	Increased in all systems
Epoxy	0.1 vol % - 5 vol%	70 nm	Increased in 0.1 vol % to 1 vol % and decreased in 5 vol %.
Epoxy	10 wt % - 50 wt %	500 nm	Unchanged in 10 wt % and decreased in 20 wt % to 50 wt %
Epoxy	1 wt % - 5 wt %	500 nm – 9000 nm	Decreased in all systems.
Epoxy	1 wt % - 5 wt %	9 μm	Decreased in all systems.
Epoxy	10 wt %	0.4 μm – 45 μm	Unchanged in all systems.
Supramolecular polymer network	5 vol % - 8 vol %	200 nm	Increased with increasing hBN vol %
Polypropylene	3 wt % - 9 wt %	50 nm	Increased with increasing hBN wt %
Polypropylene	3 wt % - 9 wt %	10 μm	Decreased with increasing hBN wt %
UHMWP	50 wt %	70 nm, 11 μm	Decreased in both systems

2.4 The Effect of Water Absorption

One of the first studies investigating the effect of water absorption on the electrical properties of polymer nanocomposites was reported by Zou et al. [72]–[74], based on epoxy/silica nanocomposites, who later proposed a water shell model based on their findings. They found that the unfilled epoxy can absorb up to 2.7 wt % of water in a 100 % relative humidity (RH) environment, and can also absorb water ~0.6 wt % of water in a 30 % RH environment. However, they found that the nanocomposites absorbed a significantly higher amount of water than the unfilled epoxy, where the 3 wt % nanocomposite absorbed ~3.5 wt % of water while the 9 wt % nanocomposite absorbed ~4.3 wt % of water. They concluded that water shells formed around the silica nanoparticles and these water shells overlapped in the nanocomposites containing a high silica content, which was manifested in dielectric spectroscopy measurements as two parallel slopes, of a value ~ -1, in the real and imaginary capacitance data. In physical terms, charge carrier movement is more likely to occur through the conductive paths of the overlapping water shells, as illustrated in Figure 2.2, which would consequently lead to deteriorated electrical properties.

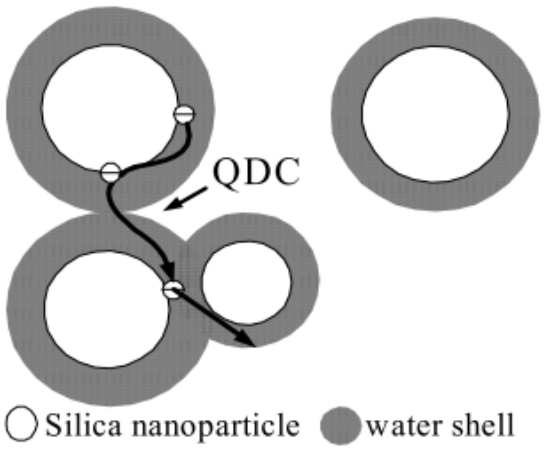

Figure 2.2: Overlapping water shells (grey) around silica nanoparticles (white) [74]

Similar results were reported by Hui et al. [75], where they reported that silica/XLPE nanocomposites absorbed a significantly larger amount of water than the unfilled XLPE; the XLPE, 5 wt % nanocomposite, and 12.5 wt % nanocomposite absorbed 0.02 wt %, 0.40 wt %, and 1.40 wt % of water respectively. The 12.5 wt % nanocomposite exhibited a significant increase in both the real and imaginary permittivity with decreasing frequency,

which suggested that a percolation of water shells was likely to have occurred. The likelihood of the formation of a percolating water network in silica based nanocomposites is ascribed to the highly hydrophilic surface of nanosilica, which contains a large amount of hydroxyl groups, as illustrated in Figure 2.3, which can readily absorb moisture from the environment either in ambient or wet conditions.

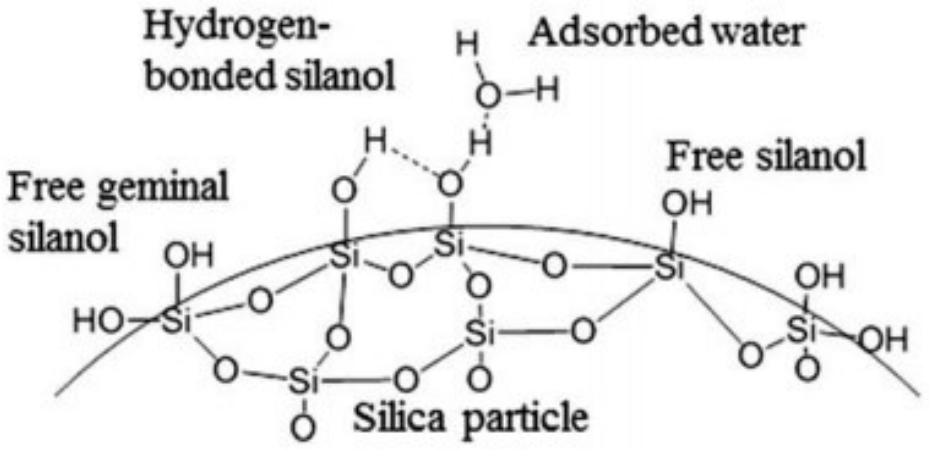

Figure 2.3: Hydroxyl groups on the surface of a silica particle [76]

In order to change the surface of silica and render it hydrophobic, Lau et al. [77] studied the effect of surface functionalisation on the dielectric response of polyethylene/silica nanocomposites. They found that by functionalising the surface of silica with trimethoxy(propyl)silane, the majority of the hydroxyl groups on the surface were replaced with propyl groups. As a result, the water absorption and the dielectric losses in the functionalised nanocomposites were significantly reduced, which highlighted the importance of the surface state of the nanoparticles. In terms of the effects of dispersion, Hosier et al. [21] compared the water absorption behaviour in polyethylene nanocomposites based on two fillers, namely silica and silicon nitride, where the silicon nitride nanocomposites exhibited a much better dispersion in comparison to the silica nanocomposites. Despite the better dispersion of the silicon nitride nanocomposites, the 10 wt % silicon nitride nanocomposite exhibited much larger losses, where the slope of the real and imaginary permittivity was close to -1, in comparison to the silica nanocomposites under wet conditions. After repeatedly running MATLAB simulations, the authors demonstrated that percolation of water shells always occurred in the 10 wt % silicon nitride nanocomposite where a complete path between the two ends of the model volume was

always formed through the interconnecting water shells. An image of the numerical model was reprinted from their publication [21] and is shown in Figure 2.4, which shows the percolation of water shells in a well dispersed 10 wt % polyethylene/silicon nitride nanocomposite system. Their study demonstrated that a well-dispersed nanocomposite can sometimes lead to deteriorated electrical properties under certain environmental conditions, and therefore proper dispersion of nanoparticles may not always be desirable.

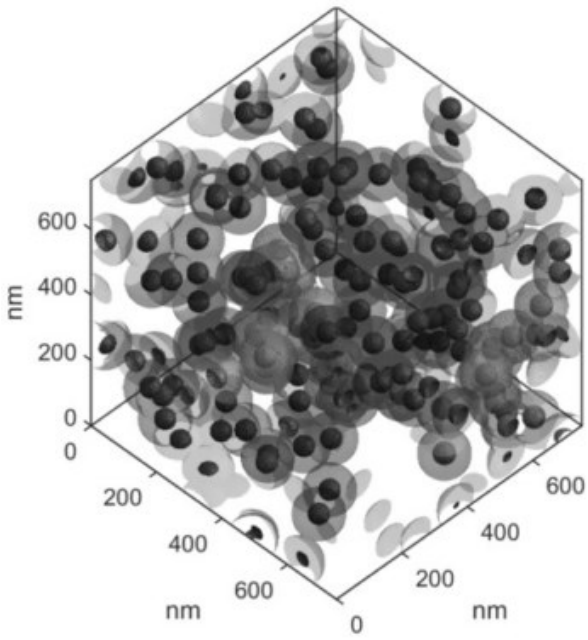

Figure 2.4: Percolation of water shells in a well dispersed 10 wt % nanocomposite [21]

While the above literature mainly covers the water absorption of behaviour of silica based nanocomposites, the available literature on the water absorption behaviour of hBN based nanocomposites is extremely limited. Tsekmes et al. [61], [62] found that the breakdown strength of thermally treated epoxy/hBN nanocomposites, where the samples were placed in a vacuum oven at 140 °C for 120 hours, were always higher than the nanocomposites which were not thermally treated. The authors explain that the thermally treated samples contain less water than the untreated samples, and therefore they exhibit a larger breakdown strength; however, the Weibull confidence bounds of all samples overlap and therefore the differences in the measured values of the breakdown strength is not very significant. Marx et al. [78] found that epoxy/hBN nanocomposites stored in a 50 % RH environment at 50 °C absorbed 0.9 % of water while the unfilled epoxy absorbed 1.2 % of water, and therefore the 0.9 % increase in mass was attributed to the water absorption of the hydrophilic epoxy matrix rather than the boron nitride particles. In contrast to silica particles, the surface of hBN particles

does not contain many hydroxyl groups and any hydroxyl groups were found to be located on the edge surfaces of the hBN platelets rather than the basal surfaces, as shown in the representation of the structure of hBN in Figure 2.5.

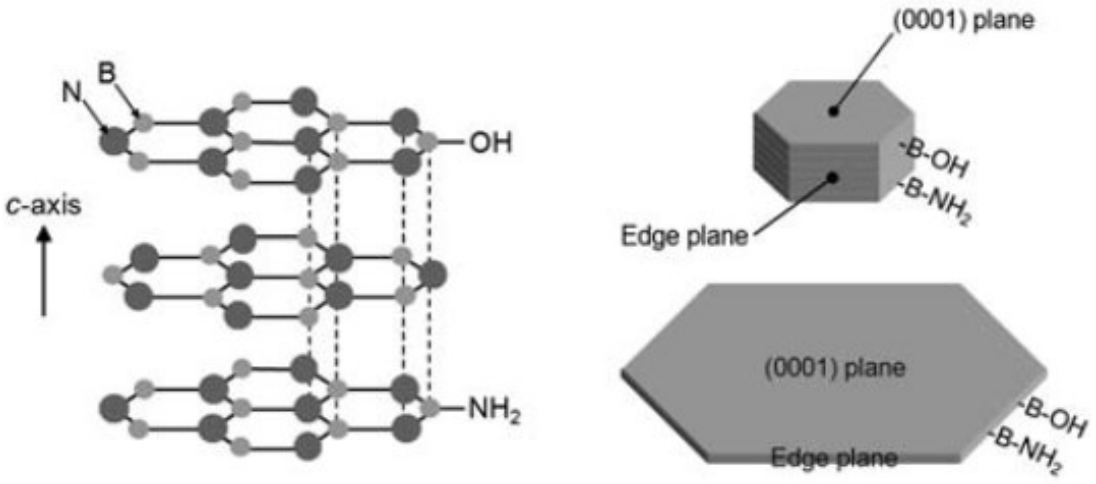

Figure 2.5: Hydroxyl groups on the edge surface of hBN platelets [79]

2.5 Justification for the Choice of Hexagonal Boron Nitride

The review of the literature on hBN composite systems has shown a promising use of hBN in polymers to improve their properties for high voltage cable systems, as a number of reports have shown that hBN was used to facilitate composites with desirable thermal and electrical characteristics. The choice of hBN in this study is based upon three factors: hBN is characterised by high thermal conductivity, high dielectric breakdown strength, and is hydrophobic in nature, which are all highly desirable properties for electrical insulation systems. In contrast to many spherical particles, the surface of hBN is not surrounded with hydroxyl groups and therefore at the percolation limit, the composite can still exhibit enhanced electrical performance, as conductive pathways may not formed, provided that the material synthesis route minimises the formation of voids in the resultant nanocomposite. Most of the reported literature is based on epoxy/hBN composites, and therefore work on polyethylene/hBN composites for high voltage cable systems is yet to be reported as the current cable insulation materials are polyethylene based materials. Additionally, the use of cables in wet conditions, such as underground or in the sea, requires the understanding of how the insulation material interacts with water since electrical properties are very sensitive

to water. The available literature on hBN composite systems has not yet addressed two main key points: the use of hBN composite systems at the percolation threshold for high voltage applications, to improve both electrical and thermal properties, and a detailed assessment of the water absorption behaviour in these systems. These two studies could improve the design of the current insulation systems and help in the understanding of the key mechanisms dominating the electrical properties of polymer nanocomposites, and therefore the contributions of this thesis, previously listed in Section 1.5, are based on these studies.

Chapter 3: Experimental Methods and Theory

3.1 Introduction

A polymer is a material made from multiple repeating groups of atoms, termed monomers, linked to each other by covalent bonds. Polymerisation is a process involving the chemical reaction of monomers to convert them into polymers [80]. Polystyrene in its atactic form (aPS) was used which enables the nanofiller dispersion to be readily imaged without the influence of any morphological effects. Polyethylene (PE) is the polymer of primary interest in this study as the insulation materials used in high voltage cables are primarily polyethylene-based materials [41]. Hexagonal boron nitride was used in this study due to its high thermal conductivity, high breakdown strength, and hydrophobicity [81]. The structures of hBN, polystyrene, and polyethylene are discussed in more detail in Chapter 4, Chapter 5, and Chapter 6 respectively. This chapter is set out to describe all the experimental techniques used in this study, along with the background theory and purpose of each procedure.

3.2 Polymer Nanocomposite Preparation Method

There are many methods for the preparation of polymer nanocomposites. Solvent blending has been chosen as the preparation route in this work, as it produces low-scale high-quality materials allowing researchers to examine different material formulations before attempting large-scale industrial manufacturing. This procedure involves the use of a solvent to dissolve the polymer, followed by the use of a non-solvent to induce precipitation of the polymer.

A polar, volatile non-solvent must be selected for precipitation, as their low boiling points makes them easy to remove from the solution to produce a dry material [82]. Solubility of a polymer is an important parameter that needs to be considered before using the solvent blending method. The Solubility parameter δ_s describes the solvency characteristics of a solvent, which is represented by a numerical value. Therefore two materials are said to be miscible when they have similar values of the Solubility parameter δ_s [83]. Some examples of suitable solvents and non-solvents for some polymers are provided in Table 3.1. Therefore, dichlorobenzene, toluene, and dichloromethane were selected as suitable solvents and methanol/isopropyl alcohol (IPA) were selected as suitable non-solvents for the preparation of polystyrene-based nanocomposites. Xylene and methanol/isopropyl alcohol

were selected as suitable solvents and non-solvents respectively to prepare the polyethylene nanocomposites through the solvent blending method.

Table 3.1: Suitable solvents for different polymers

Polymer	**Solvent**	**Non-Solvent**
Polyethylene	Xylene, decaline, and trichlorobenzene	Acetone, methanol, isopropyl alcohol
Polystyrene	Toluene, chlorobenzene, and dichloromethane	Methanol and isopropyl alcohol
Polyvinyl chloride	Tetrahydrofuran, dimethylformamide, and Methyl ethyl ketone	Methanol, heptane, and acetone

3.3 Scanning Electron Microscopy

Scanning electron microscopy (SEM) is used to study the distribution of nanofillers and in the polymer nanocomposites and the changes in morphology in the polymer upon the addition of the nanofillers. In a scanning electron microscope, an electron gun directs a beam of electrons at the sample, which are accelerated to produce an energy typically between 1 keV and 30 keV. The electron beam is then demagnified by a condenser lens and an objective lens until the beam has a diameter of 2-10 nm when it is incident upon the sample. The electron beam is scanned across the sample by scan coils, and the number of low energy secondary electrons and other forms of radiations emitted from points on the surface are counted by a detector. The beam position on the sample is digitally controlled to produce an image on a computer screen. A field emission gun scanning electron microscope offers high performance and high resolution, as compared with the normal scanning electron microscope, due to larger probe currents and smaller electron beam diameters where the electrons are emitted from a tungsten wire with a very sharp tip [84].

A good knowledge of the distribution of crystalline and amorphous regions in polymers is necessary to fully characterise the material. Chemical etching has been shown to be successful to resolve the crystalline structure from the amorphous region in the material, thus both phases can be examined. The chemical etchant selectively attacks the amorphous regions leaving crystalline regions in the surface which can be examined using the SEM. In this study, permanganic etching [85] has been used to provide morphological information concerning both the structure of polymer matrices and the distribution of filler particles. For all samples examined using the SEM, samples of ~220 μm in thickness were produced by heating at 180 °C, followed by pressing at the same temperature with a load of 5 tons, where the resulting material was then cut into 1 cm x 1 cm samples. Potassium permanganate was gradually added to an etchant mixture composed of 5:2:2 parts sulphuric acid: phosphoric acid: water for the polystyrene materials and an etchant mixture composed of 5:2:1 parts sulphuric acid: phosphoric acid: water for the polyethylene materials. The resulting etching reagent was stirred for 15 min without heat to give a 1% solution. The samples were transferred to empty vials in which ~10 mL of the etchant mixture was added and shaken for 4 h. The samples were then quenched in a solution of 25% hydrogen peroxide and 75% quench mixture, composed of 2:7 parts sulphuric acid: water. Finally, the samples were rinsed in distilled water and then methanol (for the polystyrene materials) or acetone (for the polyethylene materials), then left to dry before being gold coated, to prevent charge accumulation on the surface of the sample during examination in the SEM. A JEOL Model JSM-6500F scanning electron microscope was used An Emitech K550X sputter coater was used to coat the samples with gold; a 25 mA current was used for 3 min.

3.4 X-Ray Diffraction

X-Ray diffraction (XRD) was used to study the crystal structure of the hexagonal boron nitride particles as well as the intercalation or exfoliation state of hBN in the polymers. A filament is heated to produce a beam of electrons, which is accelerated in vacuum by a high voltage and bombards a target material, such as copper (Cu) or Molybdenum (Mo). The high energy electron beam causes the emission of electrons from the first inner shell (K-shell, n = 1) of the target material whereupon electrons from the outer, higher energy shells (L-shell, n = 2 or M-Shell, n = 3) fill up the vacant lower energy states. The transition of electrons from higher energy levels to lower energy levels results in the generation of X-Rays. In XRD measurements, X-Rays with wavelengths termed K_α and K_β are usually specified and are generated when electrons drop from n = 2 to n = 1 and from n = 3 to n = 1

respectively. Filtering is required to produce monochromatic X-Rays, which are then collimated and directed towards the sample. The X-Ray beam interacts with the electrons in the atoms in the test sample, which then causes the X-Ray waves to diffract and interfere with each other [86]. X-Rays which constructively interfere are of primary interest in XRD experiments and this is described by Bragg's law:

$$2dsin\theta = n\lambda \tag{3.1}$$

where d is the distance between the atoms in the crystal, θ is the angle between the incident X-Rays and the diffracting plane, n is an integer representing the order of diffraction, and λ is the wavelength of the X-Ray radiation.

Results from XRD measurements are usually plots of intensity as a function of 2θ, which is the angle between the transmitted and the diffracted waves. As the detector/sample rotates, the intensity of the X-Rays is detected and recorded. When Bragg's law is satisfied, constructive interference occurs, which causes a maximum in the intensity to be recorded at that specific geometry which corresponds to a certain 2θ value. The structure of the material can then be deduced from the position of the peaks in the consequent intensity plots.

Samples 1 mm in thickness were produced for XRD measurements. XRD data were gathered using a Bruker D2 phaser second generation equipment. A copper detector is used with the Cu K_α corresponding to a wavelength of 0.15418 nm; the generated X-Rays were filtered using a nickel K_β filter to obtain monochromatic X-rays with only K_α wavelength. The beam of electrons was accelerated in the vacuum tube at a potential of 30 kV with a 10 mA value of current. The 2θ values were scanned from 5° to 80° with a 0.02° increment and 2 s step time. After the scan is complete, the computer then outputs an intensity plot as a function of 2θ, which is then analysed.

3.5 Fourier Transform Infrared Spectroscopy

Fourier transform infrared (FTIR) spectroscopy is a technique used to identify the molecular composition of a material. The operation of the FTIR equipment is based on a Michelson interferometer, which consists of a beamsplitter, a fixed mirror, and a moving mirror. The infrared radiation from the source strikes the beamsplitter where 50% of the incident radiation is reflected to the fixed mirror and 50% is transmitted to the moving mirror. Both mirrors reflect the radiation back to the beam splitter, where each beam is split into two

separate beams with one going back to the source and the other to the sample and then the detector. Due to the moving mirror, a difference in the optical path length exists between the two beams that recombine at the beamsplitter. The optical path difference produces an interference pattern, or interferogram, at the detector from the constructive or destructive interference of the two beams. As the source emits a range of frequencies simultaneously, the resultant interferogram at the detector is the sum of all the interferograms corresponding to the different frequencies. The spectrum is then obtained by computing the Fourier transform of the interferogram, which is performed numerically [87]. Before the infrared signal reaches the detector, it has to first pass through the sample. In order for a molecule to absorb infrared radiation, the oscillating electric field component of the infrared radiation must interact with the bonds in the molecule to induce a change in the dipole moment. The molecules will only absorb the infrared radiation with the frequency corresponding to their natural frequency of vibration. This will appear as minima peaks in the transmission spectrum as the intensity of the detected signal decreases due to the infrared absorption. Different molecules will produce different kinds of spectra and thus FTIR can be used to identify and differentiate the molecular structure of different materials.

FTIR spectroscopy measurements of the hBN powder were performed using a Perkin Elmer Spectrum GX spectrometer. The beamsplitter is made up from potassium bromide with a germanium coating. The source is a HeNe laser with a 633 nm wavelength. The spectral data for the powder were collected for wavenumbers in the range of 400 cm^{-1} to 4000 cm^{-1} over 32 scans at 4 cm^{-1} resolution. Before each measurement, a background scan was performed without any sample in the spectrometer. The spectrometer was operated in transmittance mode where the data obtained are plots of transmission % as a function of wavenumber.

3.6 Thermogravimetric Analysis

Thermogravimetric analysis (TGA) is a technique used to measure mass changes of a sample as a function of temperature over a specific temperature range, or isothermally as a function of time, at a constant controlled temperature. The sample is first set on a high precision balance, where the mass of the sample is constantly being monitored throughout the experiment, and is then placed in a furnace, which is used to control the temperature [88]. This technique can be used to quantify the amount of filler in the nanocomposite, water in the system, amount of solvent in the system and the thermal decomposition of the polymers or fillers. A curve with weight percentage as a function of temperature is usually plotted to determine the amount of filler in the nanocomposite and the decomposition behaviour.

Thermogravimetric analysis was mainly used to confirm the filler content of the hBN in the polymer nanocomposite. The thermal degradation temperature of the nanocomposites was also assessed by TGA. A Perkin Elmer 1 TGA with Perkin Elmer Pyris software was used to perform all the measurements. Samples of 5 mg in mass were placed in an aluminium pan and heated from 40 °C to 600 °C at a rate of 10 °C/min in air, and the filler content was approximated by the mass of the remaining residue. The degradation temperatures are determined as the temperatures where the mass of the materials reached 90% and 50% of its initial value.

3.7 Differential Scanning Calorimetry

Differential scanning calorimetry (DSC) is a technique used to study thermal phase transitions in materials. The difference between the rate of heat flow into the desired sample and an inert reference is measured with respect to temperature, to study the thermal properties of the sample. The temperature of the sample pan and the reference pan is increased at the same rate and the heat flow is monitored. During a phase transition, the rate of temperature will no longer be equal between the two pans and the computer controlling the DSC will compensate for this by a power change to maintain the same temperature between the pans. The heat flow as a function of temperature can then be plotted to detect the phase transitions [89].

The phase transitions of interest in the thermal characterisation of polymers include: melting temperature T_m, crystallisation temperature T_c, and the glass transition temperature T_g. The crystalline regions in polymer exhibit melting and crystallisation temperatures while the non-crystalline, or amorphous, regions exhibit a glass transition temperature. DSC was used to study the glass transition behaviour of the amorphous polystyrene nanocomposites and the melting/crystallisation behaviour of the semi-crystalline polyethylene nanocomposites. A Perkin Elmer DSC-7 with Perkin Elmer Pyris software was used to perform all the measurements. The equipment was calibrated using high purity indium with a known melting temperature of 156.6 °C and enthalpy of 28.45 J/g. Samples, 5 mg in mass, were placed in a sealed aluminium pan and heated from 40 °C to 160 °C at a rate of 10 °C/min to study the glass transition and melting/crystallisation behaviour of the polystyrene and polyethylene nanocomposites respectively. The polyethylene nanocomposites samples were cooled from 160 °C to 40 °C at a rate of 5 °C/min to study their crystallisation behaviour. All measurements were performed in a nitrogen atmosphere.

3.8 Dielectric Spectroscopy

Since polymers are widely used as dielectric materials in many applications, it is worth investigating the interaction between the electric field and the dipole moments in the materials. When an electric field is applied between two metallic plates separated by some distance, charges from the electric field source are stored on the plates and the plates become oppositely charged. If a dielectric material is placed between the two plates, the internal charges of the dielectric will distribute themselves to align with the applied electric field [90].

The dielectric material is polarised when subjected to an alternating electric field. Electronic polarisation typically occurs at high frequencies where the applied electric field slightly displaces the electrons in the atoms relative to the nucleus. The applied electric field is usually much weaker than the intra-atomic field at an electron and therefore the electrons only shift very slightly. Atomic polarisation occurs when the electric field disturbs the arrangement of the atomic nuclei in a molecule or lattice. Since the mass of the atom is much larger than the mass of an electron, atomic polarisation occurs at lower frequencies than electronic polarisation. The magnitude of atomic polarisation is usually only one-tenth of that of the magnitude of electronic polarisation. Dipolar polarisation occurs in materials containing molecules that already possess permanent dipole moments, such that they tend to align with the electric field to give a net polarisation in the direction of the electric field. The process of dipole orientation is relatively slow compared to electronic transitions or molecular vibrations. If sufficient time is provided after applying an electric field, the orientation of dipoles will reach equilibrium and maximum polarisation will be achieved, resulting in the highest possible relative permittivity, called the static relative permittivity ε_s. Conversely, if the polarisation of dipoles is measured directly after applying the electric field, no time is allowed for the orientation of dipoles resulting in a low instantaneous relative permittivity, ε_∞ [90].

Consider an alternating electric field, E, with amplitude E_0 and frequency ω, which is applied across a dielectric material:

$$E = E_0 \cos(\omega t) \tag{3.2}$$

This field will produce an alternating polarisation, and dipole orientations will lag behind the field at high enough frequencies, producing a phase lag δ. This can be expressed in the electric displacement, D, which accounts for polarisation, bound charges, and free charges:

$$D = D_0 \cos(\omega t - \delta) \tag{3.3}$$

This equation can be simplified to:

$$D = D_1 \cos(\omega t) + D_2 \sin(\omega t) \tag{3.4}$$

where

$$D_1 = D_0 \cos(\delta) \tag{3.5}$$

and

$$D_2 = D_0 \sin(\delta) \tag{3.6}$$

Since D relates to the bound and free charges, it can also be written as:

$$D = \varepsilon_0 E + P = \varepsilon_0 \varepsilon_r E \tag{3.7}$$

where ε_0 is the permittivity of free space (8.85 x 10^{12} F/m), ε_r is the relative permittivity of the dielectric, and P is the polarisation term.

Rearranging the equation in terms of the relative permittivity:

$$\varepsilon_r = \frac{D}{\varepsilon_0 E} \tag{3.8}$$

Thus the two relative permittivities can be defined:

$$\varepsilon_r' = \varepsilon' = \frac{D_1}{\varepsilon_0 E_0} \tag{3.9}$$

and

$$\varepsilon_r'' = \varepsilon'' = \frac{D_2}{\varepsilon_0 E_0} \tag{3.10}$$

Combining these two permittivities into one quantity:

$$\varepsilon^* = \varepsilon' - j\varepsilon'' \tag{3.11}$$

where ε^* is the complex relative permittivity, ε' is the real part of the permittivity and represents the energy storage in the dielectric, and ε'' is the complex part of the permittivity and represents the energy losses in the dielectric.

An important engineering quantity that relates the real and imaginary permittivities is the dissipation factor, which is expressed as:

$$\tan\delta = \frac{\varepsilon''}{\varepsilon'} \tag{3.12}$$

where *tanδ* is the dissipation factor, or dielectric loss tangent, and is directly proportional to the ratio of the rate of energy loss to the rate of energy storage within the dielectric.

Dielectric spectroscopy was carried out using a Solartron 1296 dielectric interface in combination with a Schlumberger SI 1260 Impedance/phase gain analyser. The Solartron 1296 2A sample holder, designed for testing solid dielectrics at room temperature, was used which consists of two 30 mm diameter parallel electrodes, one fixed in position while the other can be moved to have contact with the sample. The sample holder incorporates a guard ring to reduce fringing effects at the edges of the sample. An AC voltage of 1 V was applied to the sample with a frequency sweep from 10^{-1} Hz to 10^6 Hz at 8 points per decade and 10 cycle integrations per point. Samples 250 μm in thickness were prepared and gold coated before, finally, being tested between the 30 mm diameter electrodes.

3.9 Dielectric Breakdown Strength

Electrical breakdown must occur at some point when a progressively increasing voltage is applied across a dielectric material. A large amount of electrical energy is released at high voltages between the two electrodes and causes breakdown. There exists a maximum voltage that the material can withstand without failing, which leads to the concept of dielectric strength. Dielectric strength is the maximum sustained electric field that can be applied to a dielectric material without failure [91] and is defined by the following equation:

$$E_b = \frac{V_b}{t} \tag{3.13}$$

where E_b is the breakdown field, V_b is the breakdown voltage, and t is the thickness of the dielectric sample.

Since the electrical breakdown strength varies in each test, there is no single defined value of breakdown strength for each material thus a statistical distribution must be used to analyse the breakdown data. The Weibull distribution is often used in systems that fail by the weakest link and in electrical breakdown, there exists a large number of failure mechanisms so the Weibull distribution is suitable for this application; it is common practice to assess the dielectric strength of an electrically insulating material using the two-parameter Weibull distribution with either 90 % or 95 % confidence bounds [92]. For a dielectric material, the probability of failure can be represented by the following two parameter Weibull failure probability function:

$$P_f(E) = 1 - exp\left[-\left(\frac{E}{\alpha}\right)^{\beta}\right] \tag{3.14}$$

where $P_f(E)$ is the cumulative probability of failure at the breakdown value of E, where E is the applied electric field that gradually increases to cause breakdown. The parameter α, the scale parameter which is analogous to the mean of the normal distribution, describes the scale of the distribution and represents the electric field which causes 63.2% of the samples to fail. The parameter β, the shape parameter which is analogous to the standard deviation of the normal distribution, describes the shape of the distribution and provides a measure of spread of the breakdown strength data [90].

The cumulative probability of failure for each data point is approximated by the following equation:

$$P_f(i,n) = P_f(E) = \frac{i - 0.3}{n + 0.4} \tag{3.15}$$

where i is the ranked data point increasing by increments of 1 from the smallest to largest breakdown strength value and n is the total number of breakdown measurements [93].

A standard electrical breakdown test was performed based upon the general considerations laid down in ASTM standard D149-87 [91]. Samples 70 μm in thickness were used for breakdown testing, which are ideal for breakdown testing as samples with larger thicknesses can introduce impurities or voids which would affect the electrical breakdown results. Electrical breakdown measurements are easily affected by sample thickness so samples with known and reproducible geometries are required to obtain reproducible results. The sample for testing was placed between two opposing 6.3 mm steel ball bearing electrodes in a test cell. The test cell was immersed in Dow Corning 200/20cs silicone fluid to prevent surface flashover. The upper electrode, which has a 50 g load applied to it to eliminate the film of oil between the electrode and the sample, is connected to the high voltage supply while the lower electrode is connected to earth. A warm up time of 1 hour is required for the function generator to ensure a stable output prior to the use of the breakdown kit. Before each use, the equipment has to be calibrated to generate a 50 Hz signal with an RMS voltage ramp rate of 50 V/s. The signal from the function generator is fed to the power amplifier, and the amplifier output is then fed to the isolation transformer and the high voltage transformer, which can generate up to 30 kV. An increasing AC voltage at a ramp rate of 50 V/s was applied to the upper electrode until the sample failed. When a sample fails, a voltage is generated across the current sensing resistor which is detected by the tripping relay through the optical isolator. The signal to the power amplifier is then cut off and the voltage is reduced to 0 kV. The relay remains tripped until it is manually reset after the next sample is inserted.

3.10 Electrical Conductivity

When an electric field is applied to a dielectric material placed between two electrodes, the field interacts with the charges inside thus generating an electric current. The electric current usually is a function of time made up of two components where it generally drops with time initially and then reaches a steady state. The first component, the polarisation current, is due to the dipole interactions with the field while the second component, the steady state current, is due to the charge carrier motion [91].

Electrical conductivity testing was performed using a Keithley 6487 pico-ammeter in series with a voltage source, where the samples were placed between two 20 mm gold electrodes. Gold coated samples ~250 μm in thickness and 20 mm in diameter were used in the conductivity tests. A constant voltage test was performed over a period of 3 h to study the time dependence of the conductivity, where current measurements using a pico-ammeter were taken in 15 s increments. The tests were performed at an applied field of 40 kV/mm, due to the voltage limitation of the equipment and to prevent breakdown of the samples. The conductivity calculations were performed numerically using the following equation:

$$\sigma = \frac{VA}{It} \tag{3.16}$$

where σ is the conductivity, V is the applied voltage, A is the cross sectional area of the sample, I is the measured current, and t is the thickness of the sample.

Chapter 4: Characterisation of the Hexagonal Boron Nitride Particles

4.1 Introduction

Graphene is a pure carbon material made of a single layer of carbon atoms arranged in a two-dimensional honeycomb lattice. It is the fundamental building block of three-dimensional graphite, since layers of graphene sheets make up graphite [94]. Hexagonal boron nitride, the most common and stable crystalline form of boron nitride, has a similar lattice structure to the carbon atoms found in graphite, such that it contains an equal number of alternating boron and nitrogen atoms firmly bound together in a honeycomb lattice, consisting of two-dimensional layers stacked on top of each other. Boron nitride has been chosen as the nanofiller in this work because of its attractive electrical and thermal properties such as high breakdown strength and thermal conductivity coupled with its hydrophobic character, as discussed in Chapter 2. Boron nitride (BN) is an inorganic material which exists in three different crystalline forms: hexagonal BN (hBN), cubic BN (cBN), and wurtzite BN (wBN). These crystalline forms of BN have similar structures to carbon lattices where the hBN, cBN, and wBN are analogous to the graphite, diamond, and Lonsdaleite allotropes of carbon [95]. The hBN form, which is the particle used in this study, typically consists of a highly anisotropic layered structure where each layer comprises of strong covalent bonds linking the boron and nitrogen atoms, and the layers are linked to each other via weak van der Waals forces. Within the basal plane, every boron atom is bonded to three nitrogen atoms and vice versa. The B-N bond is polar, due to the electronegative nitrogen atoms, which causes charges to localise closer to the nitrogen atoms rather than the boron atoms [96]. It is electrically insulating in nature due to its wide bandgap, it has a high thermal conductivity, thermal stability, mechanical strength, and chemical stability which makes it very useful in many applications [62]. This chapter is set out to characterise the hBN particles through SEM to determine the aggregation state of the particles, XRD to confirm the hexagonal structure, FTIR to determine the molecular composition, and TGA to determine the thermal stability of the hBN particles.

4.2 Scanning Electron Microscopy

The hBN powder was examined in its as-received state using SEM, before incorporating it into the polymers. The low magnification SEM micrograph in Figure 4.1 shows that the as-received hBN powder is composed of clusters of hBN particles with a considerable amount of agglomeration. The hBN particles appear to form a network of large aggregates with sizes in the micrometer range, as seen from Figure 4.2. Furthermore, it can be seen that many aggregates with different orientations, as seen in Figure 4.3, join together to form larger aggregates. High magnification SEM micrographs show that the crystal structure of hBN has a smooth basal plane with no irregularities on the surface.

The extent of hBN particle agglomeration is highlighted in all the SEM micrographs, where the size of the aggregates is in the order of ~10 μm, which is quite significant for a considered "nanoparticle". Figure 4.4 shows that the bulk hBN powder contains particles of hBN layers consisting of irregularly shaped platelets with a distribution of lateral sizes with a thickness of less than 50 nm. The distribution of lateral sizes is consistent with the lateral average size stated in the datasheet, which is ~900 nm, as the manufacturer will give information about the size of individual particles instead of the size of agglomerates. Although the thickness of each platelet is less than 50 nm, it is clear from the high magnification SEM micrographs that these platelets do not exist individually in an exfoliated state but they are rather stacked on top of each other and are in agglomerated state. It is typical for nanoparticles in powders to exist in an agglomerated state due to the attractive Van der Waals forces between them. Neshastehriz et al. [98] studied hBN powder using the SEM and found that the powder contains a range of agglomerated particles with sizes larger than 30 μm.

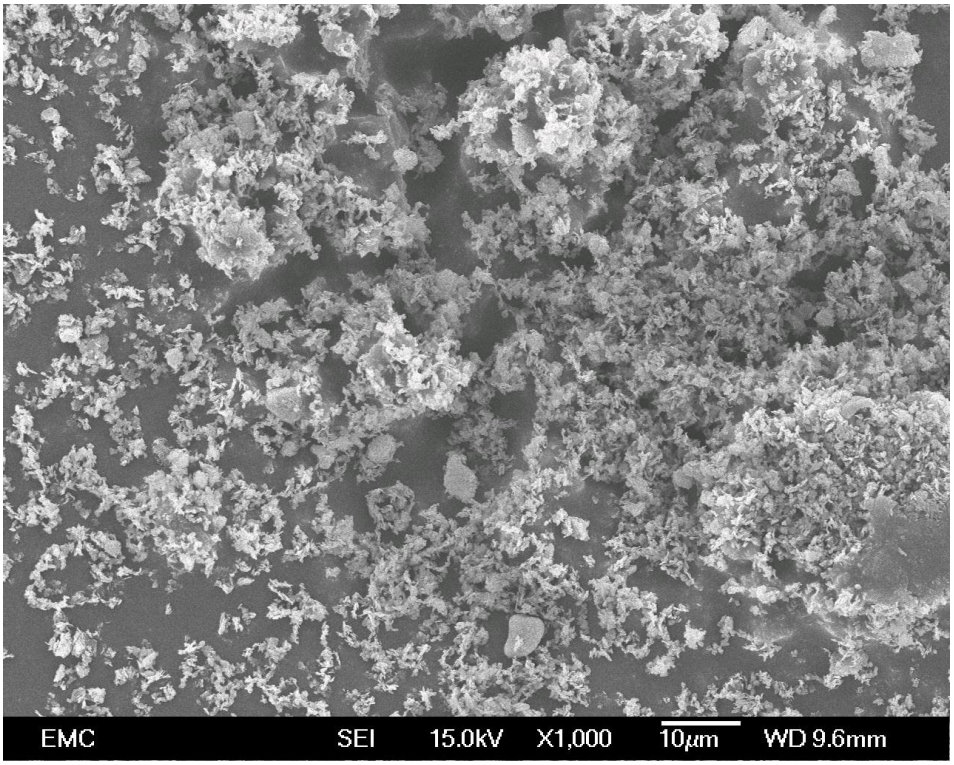

Figure 4.1: Low magnification SEM micrograph of the hBN powder

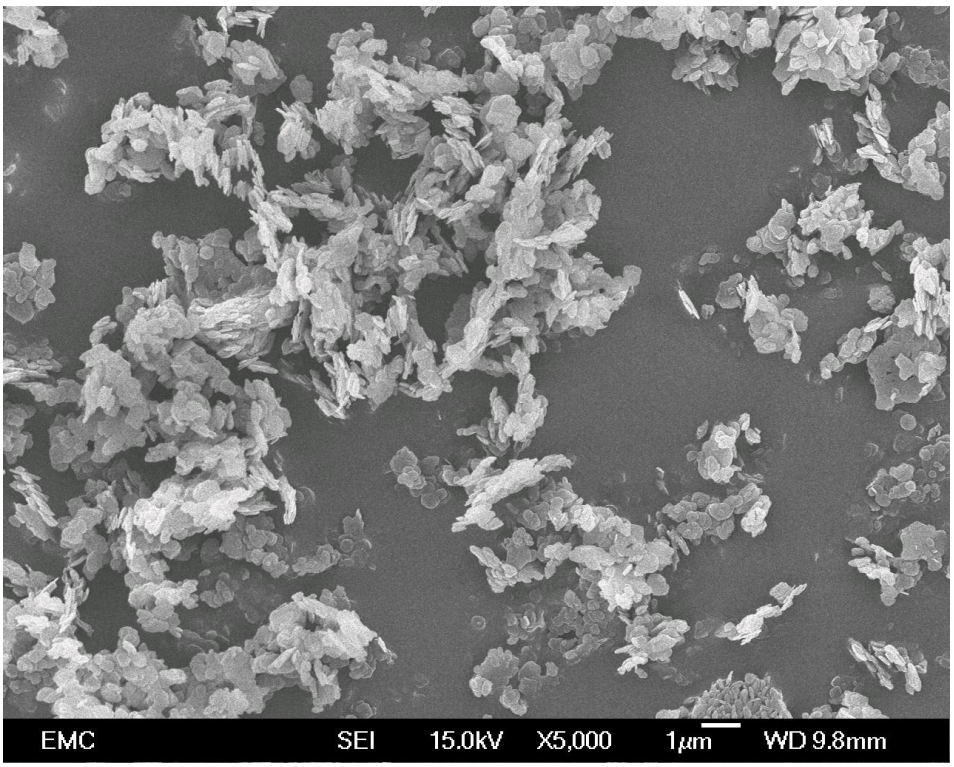

Figure 4.2: A network of large agglomerates in the hBN powder

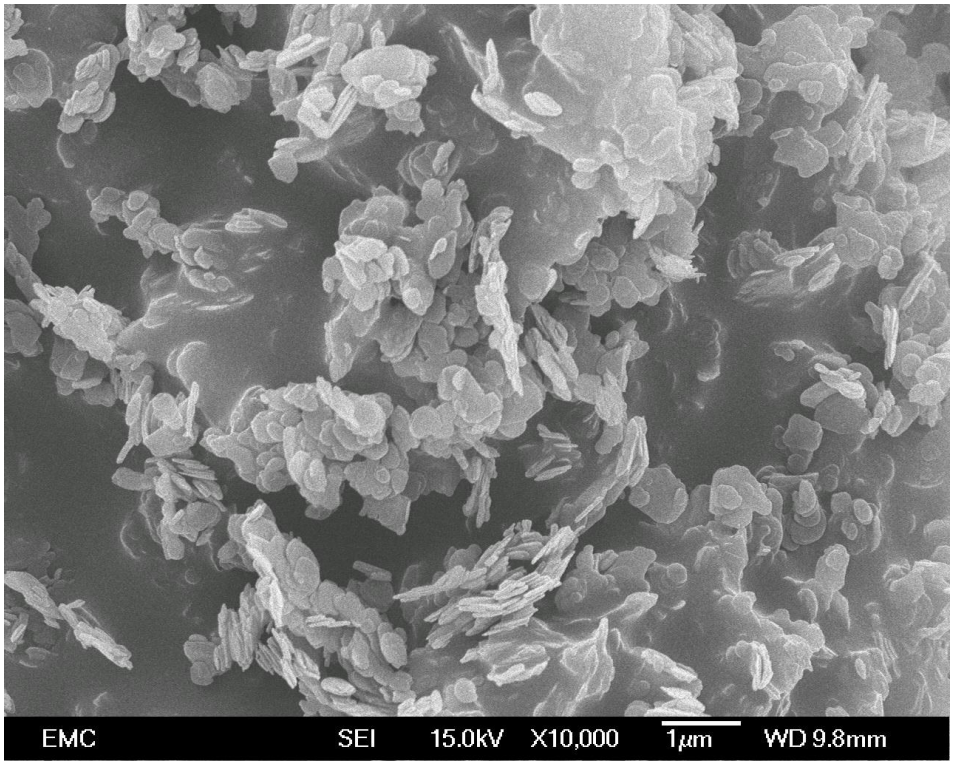

Figure 4.3: SEM micrograph showing the different orientations of the hBN platelets

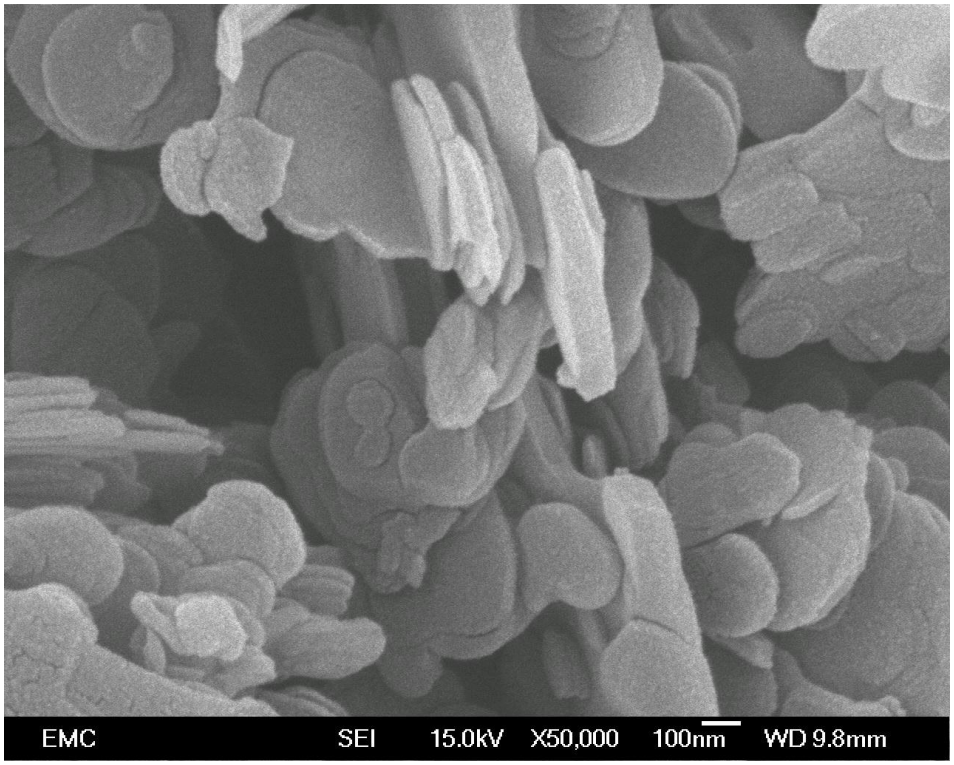

Figure 4.4: High magnification SEM micrograph showing the size of the hBN platelets

4.3 X-Ray Diffraction

Crystal planes are usually denoted by Miller indices, which represent the directional and planar orientations in a crystal lattice unit cell. The Miller indices are represented by three integers: “h”, “k”, and “l” such that (hkl) defines the plane of interest. A few examples of crystal planes represented by the Miller indices are shown in Figure 4.5, where the (xyz) axes correspond to the (hkl) axes.

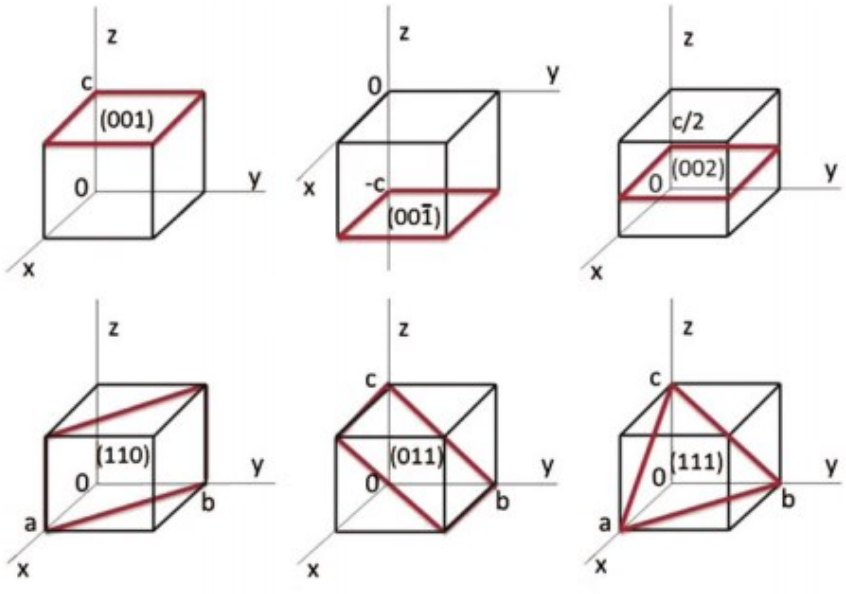

Figure 4.5: The hkl plane representations by Miller indices [99]

For a hexagonal structure unit cell, such as shown in Figure 4.6, “*a*” represents the distance between two points in the “h” and “k” planes, or in-plane orientation, whereas “*c*” represents the distance between two points in the “l” plane, or out-of-plane orientation.

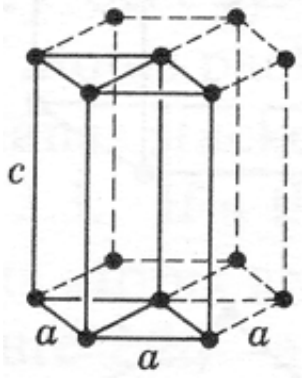

Figure 4.6: Unit cell of a hexagonal structure [100]

With reference to the hexagonal structure of boron nitride, "*c*" is shown in Figure 4.7 (a) and "*a*" is shown in Figure 4.7 (b). It is important to note that "*a*" is not the bond length or the distance between the boron and nitrogen atoms and "*c*" is not the interlayer distance. Unlike graphite which consists only of carbon atoms, the periodicity in hBN is different as it consists of a combination of boron and nitrogen atoms where the distance from one boron atom to the other boron atom between layers corresponds to a distance between two layers. This is due to the alternate stacking of boron and nitrogen atoms on top of each other in the layers such that a boron atom in one layer is located directly on top, or below, the nitrogen atom in the next layer. And since the periodicity of the crystals is of interest, "*a*" and "*c*" are constants representing the periodicity of the lattice in a hexagonal structure. The constants "*a*" and "*c*" are denoted by "a" and "c" in Figure 4.7 where "a" represents the distance between two boron atoms or two nitrogen atoms in the in-plane direction and "c" represents the distance between two boron atoms or two nitrogen atoms in the out-of-plane direction.

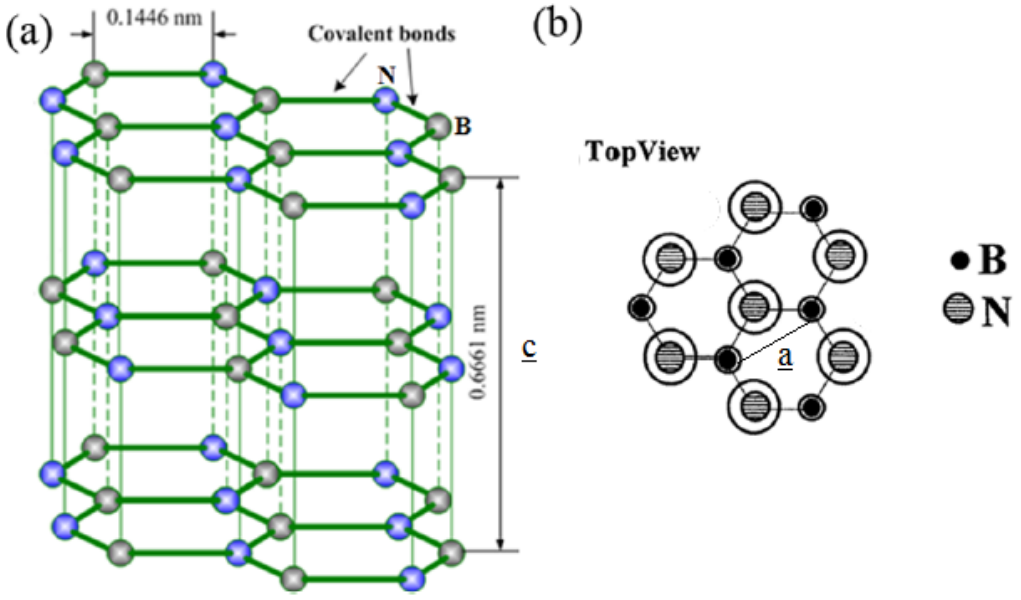

Figure 4.7: (a) The structure of the hBN layers, (b) top view of one hBN layer [94]

The X-Ray diffraction pattern of the hBN powder is shown in Figure 4.8. Several peaks are revealed in the XRD pattern of the hBN powder centred at 2θ values of 26.8°, 40.0°, 42.1°, 48.2°, 54.3°, and 74.6° corresponding to the (002), (100), (101), (102), (004), and (110) planes respectively. A well-defined, sharp narrow peak relative to all other peaks is observed in the (002) plane in the XRD spectrum which confirms the crystalline structure of the hBN

powder consisting of a periodic structure composed of well-ordered stacked crystal planes, which correspond to the stacked hBN layers. A similar diffraction pattern has been reported by the Joint Committee on Powder Diffraction Standards (JCPDS card number 34-0421) obtained from the XRD database, with ± 0.5° variations in 2θ values, thereby confirming the hexagonal crystal structure of the hexagonal boron nitride powder used in this study. Furthermore, the XRD diffraction pattern observed in this study has been reported in many XRD studies of hexagonal boron nitride [101]–[105] having sharp narrow peaks in the (002) plane relative to all other peaks, with small variation in all 2θ values, thus confirming the measurements in this study and the hexagonal structure of the boron nitride.

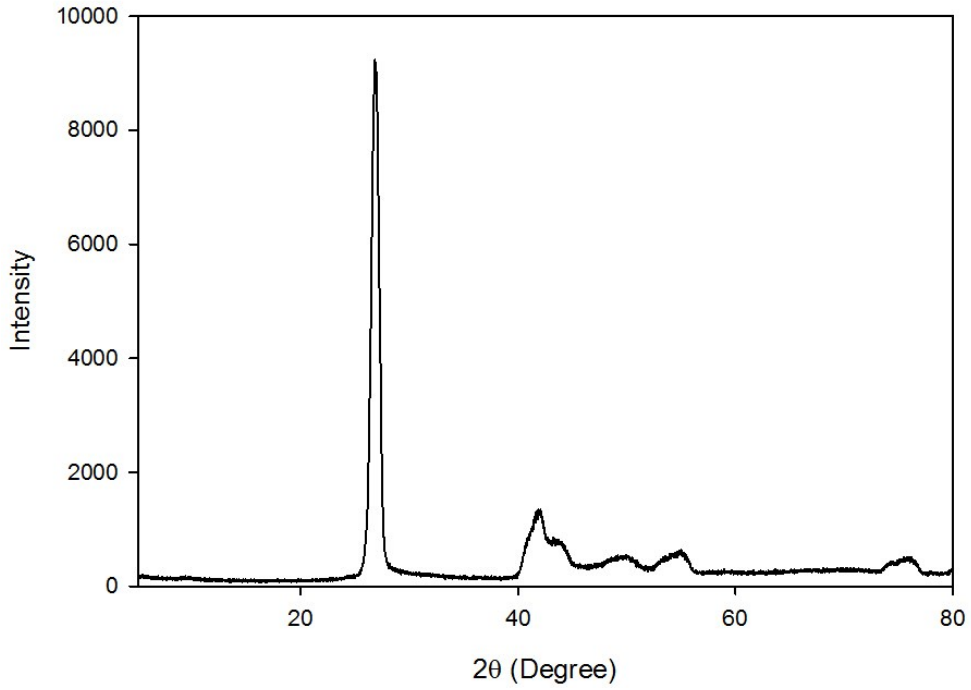

Figure 4.8: X-Ray diffraction pattern of the hBN powder

The peak in (002) plane corresponds to a d-spacing of 3.33 Å, 0.333 nm, when calculated by rearranging Bragg's Law:

$$d = \frac{n\lambda}{2sin\theta} \tag{4.1}$$

The following formula is used to measure the lattice constants in a hexagonal structure:

$$\frac{1}{d_{hkl}^2} = \frac{4}{3}\left(\frac{h^2 + hk + k^2}{a^2}\right) + \frac{l^2}{c^2} \tag{4.2}$$

where d_{hkl} refers to the "*d*" spacing in Bragg's Law. Using simple geometry for hexagonal structures, the interlayer spacing, d_{int}, and the boron-nitrogen bond length, l_{bond}, can be expressed as:

$$d_{int} = \frac{c}{2} \tag{4.3}$$

and

$$l_{bond} = \frac{a}{\sqrt{3}} \tag{4.4}$$

This yields values of:

a = 0.254 nm
l_{bond} = 0.1466 nm
c = 0.666 nm
d_{int} = 0.333 nm

These values are all consistent with the reported values in the literature [94], [106], [107].

4.4 Fourier Transform Infrared Spectroscopy

The FTIR spectrum of the hBN particles is shown in Figure 4.9. The FTIR spectrum shows characteristic peaks of boron nitride in the hexagonal phase, in which the absorption band centred at 1360 cm^{-1} corresponds to the in-plane stretching of the B-N bonds while the absorption band centred at 814 cm^{-1} corresponds to the out-of-plane B-N-B bond bending. Similar observations have been made by other researchers which indicate these absorption bands are characteristic of the hexagonal phase of boron nitride [108]–[110]. The in-plane stretching absorption band is centred at a higher wavenumber than the out-of-plane bending due to the stronger covalent bonds between the boron and nitrogen atoms relative to the

weaker Van der Waals forces involved in the out-of-plane direction. Figure 4.10 shows the direction of the in-plane stretching and out-of-plane bending in hBN.

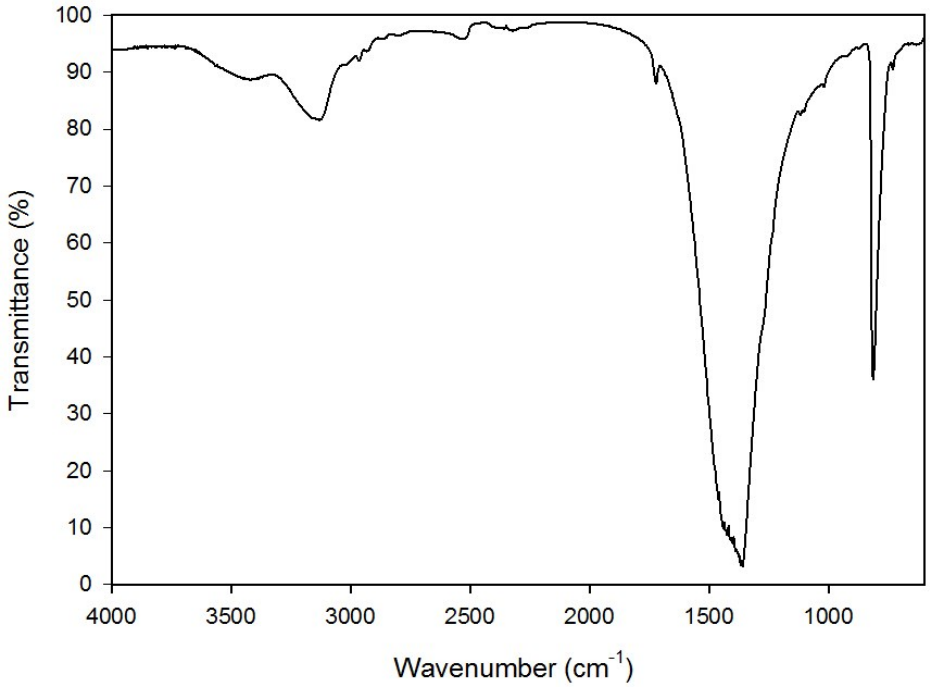

Figure 4.9: FTIR spectrum of the hBN powder

Two smaller absorption bands centred at 3131 cm^{-1} and 3420 cm^{-1} correspond to the stretching of O-H and N-H bonds. Similar characteristic absorption bands of hydroxyl stretching, with a small amount of infrared absorption, in the FTIR spectrum of hBN has been reported elsewhere [108], [110].

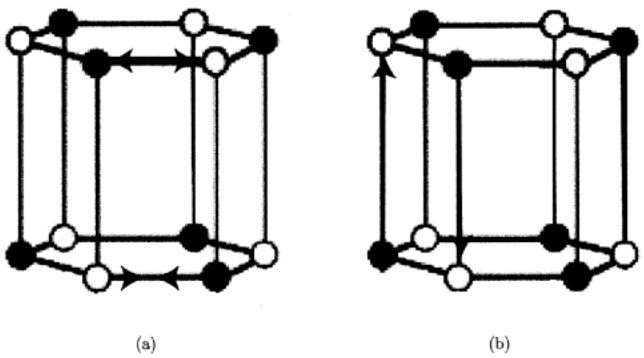

Figure 4.10: (a) In-plane B-N stretching, (b) out-of-plane B-N-B bending [111]

4.5 Thermogravimetric Analysis

Figure 4.11 shows the TGA curve for the hBN powder displaying the weight percent of the powder as a function of temperature. The powder was heated up to 900 °C, where the mass constantly decreased with increasing temperature and experienced a total weight loss of 0.65 % of its initial mass. This mass loss can be attributed to the small amounts of hydroxyl groups which are removed from the surface of the hBN upon heating.

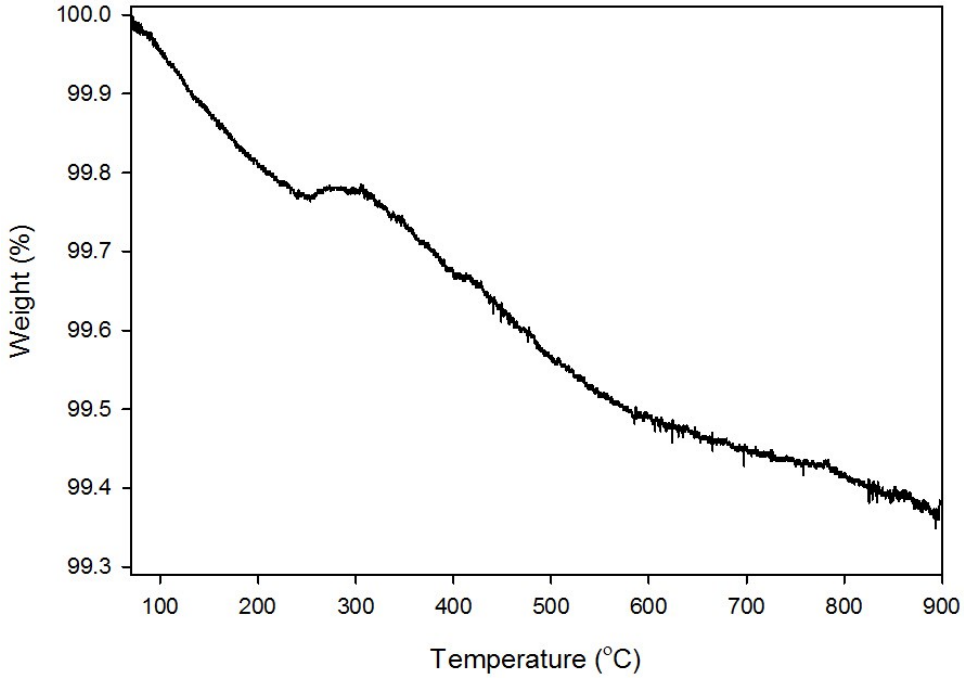

Figure 4.11: TGA curve for the hBN powder

The thermal stability of boron nitride has been widely reported in the past. Huo et al. [108] studied the thermal stability of hBN particles and found that the as-received hBN particles showed no mass change up to 800 °C while modified hBN particles lost up to 2 % of mass due to the degradation of silane molecules. Similarly, Yu et al. [105] reported similar results, where they found that hBN particles remained thermally stable up to 800 °C with no mass change. In their results, they plotted TGA curves with a large weight percent scale and therefore any small mass changes were not observable. Here, a reproducible small mass change was observed which could be considered as insignificant by other researchers when reporting their results. The thermal stability of boron nitride above 900 °C has been investigated by a few researchers. Kostoglou et al. [112] reported that hBN particles

remained thermally stable up to 1000 °C. The mass of the hBN particles suddenly increased by 30 % in the temperature range of 1000 °C – 1200 °C where it was then stable again. The mass increase was attributed to the oxidation of the boron nitride and the formation of boron trioxide (B_2O_3) on the surface of BN. The resistance to oxidation, which occurs at very high temperatures, is due to the combination of high crystallinity and small specific surface area which do not provide readily available sites for oxidation. Wang et al. [113] reported similar results where they used hBN particles with different surface areas and found that the onset oxidation temperature decreased and the mass gain percentage increased with increasing surface area of the BN particles. For all particles, the mass of the particles remained constant up to a temperature of 800 °C – 1000 °C, depending on the surface area of the particles, where a mass gain of up to 35 % was noticed due to the reaction of boron nitride and oxygen to form boron trioxide.

While the boron nitride remained thermally stable up to 900 °C with an insignificant mass change, other types of particles have been reported to exhibit a completely different behaviour. Li et al. [114] performed TGA measurements on functionalised silica and reported that silica nanoparticles can lose between 13 % and 30 % of weight. Similarly, Bracho et al. [115] showed that unmodified silica can lose up to 5 % of its initial mass due to the substantial amount of hydroxyl groups on its surface. Jin et al. [116] showed that pure silica can lose up to 18 % of its initial mass due to water content while functionalised silica can lose only up to 8 % of its initial mass. Guo et al. [117] reported that alumina nanoparticles can lose up to 4 % of their initial mass due to the adsorption of moisture and chemical bonding of hydroxyl groups. While oxide based particles show some mass loss upon heating, similar results have been reported for nitride based particles. Tai et al. [118] reported that unmodified silicon nitride nanoparticles lose up to 4 % of their initial mass due to absorbed water in the particles while modified silicon nitride particles can lose up to 6 % of mass due to the additional degradation of the coupling agent. Peng et al. [119] showed that unmodified aluminium nitride nanoparticles can lose up to 6 % of mass while modified nanoparticles lose up to 8 % of mass due to the decomposition of grafted silane molecules. The amount of mass loss in these type of particles, particularly silica, is very significant in comparison to boron nitride particles, which suggests that boron nitride is highly thermally stable and highly resistant to moisture absorption.

4.6 Conclusion

The hBN particles have been characterised through a range of different methods. SEM analysis of the hBN in the as-received state revealed that the hBN exists largely as agglomerates. The XRD results confirmed that crystalline and periodic structure of the hexagonal form of boron nitride while FTIR results confirmed the molecular composition of hBN. The FTIR and TGA results suggest there is a small amount of hydroxyl groups on the hBN surface. The TGA results also revealed the high thermal stability of the hBN particles. The insignificant TGA mass loss of the hBN particles provided evidence that a small number of hydroxyl groups are available on the surface of hBN particles, thereby rendering the surface hydrophobic relative to other types of particles; this was one of the reasons that hBN particles were used in this study.

Chapter 5: Polystyrene Hexagonal Boron Nitride Nanocomposites

5.1 Introduction

Polystyrene (PS) is a synthetic polymer produced from the monomer styrene resulting in a chemical structure containing CH_2 - $CH(C_6H_5)$ repeating units. The form of polystyrene chosen in this study is atactic polystyrene (aPS), which is amorphous unlike polyethylene which is a semi-crystalline polymer. While polyethylene crystallises from the melt, aPS does not crystallise due to the lack of order in the phenyl group arrangement in the polymer backbone, which produces an amorphous morphology; however, above its glass transition temperature, the molecular mobility of the polymer chains is not restricted and the material changes from a rigid to a rubbery state [120]. Polystyrene is a model system which enables the nanofiller dispersion to be readily imaged, therefore it is ideal for this study. In cases where it could be difficult to distinguish between the boron nitride particles and the crystalline structure of a semi-crystalline polymer, the distinction is very clear in polystyrene as the background matrix is amorphous and does not have any structural changes or interactions with the boron nitride particles

As the material preparation route involves the use of a solvent, the hypothesis of this chapter is that the chemical interactions between the hBN and different solvents lead to different hBN dispersion states, and thus different electrical properties. Therefore the effect of solvent processing on the dielectric properties of polystyrene/hBN nanocomposites are explored in this chapter. A total of six different nanocomposites were prepared with three different solvents: dichloromethane (DCM), toluene (TOL), and chlorobenzene (CB) as they are compatible with PS and have similar surface energy values to hBN, as demonstrated in Appendix A. All the nanocomposites were tested for changes in structural, thermal, and electrical properties relative to an unfilled polystyrene material prepared with the respective solvent. Structural properties were investigated using SEM, to study the dispersion state, and XRD, to study the intercalation or exfoliation state of the hBN in the polystyrene. Thermal properties were investigated using TGA, to confirm the filler content after the decomposition of the polystyrene, and DSC, to investigate changes in the glass transition temperature to reveal information about the interactions between the hBN particles and the polystyrene. To

understand the influence of particle dispersion on the electrical performance of the polystyrene/hBN nanocomposites, electrical properties were investigated using dielectric spectroscopy and dielectric breakdown strength testing to reveal information about the effect of the hBN particles on the dielectric losses and changes in the breakdown behaviour.

5.2 Preparation of the Polystyrene/hBN Nanocomposites

5.2.1 Materials

The polystyrene was obtained from Sigma-Aldrich with a quoted average molecular mass of 192,000 g mol^{-1}. The hBN nanoparticles were obtained from Momentive (grade NX-1) with a quoted particle size of 900 nm.

5.2.2 Solvent Blending Procedure

In all polystyrene/hBN nanocomposites, 10 g of material was produced, including the mass of PS and hBN. For the unfilled aPS, 10 g of the polymer was used. For a 5 wt % aPS/hBN nanocomposite, 9.5 g of aPS and 0.5 g of hBN were used. Two solvent blending methods were used: one involved preparing the materials at room temperature using DCM and the other involved heating the polymer at high temperatures using TOL or CB.

To prepare the polymer nanocomposites at room temperature using DCM as a solvent, 9.5 g of aPS was added to 100 mL of DCM. The required mass of hBN was added to 15 mL of DCM, sonicated using a probe sonicator for 30 min using a half cycle pulse at 60% of the maximum amplitude. The aPS/DCM mixture was stirred using a magnetic stirrer bar for approximately 1 h, until all the polymer had dissolved. After sonication, the hBN was added to the aPS/DCM mixture, and the aPS/hBN/DCM mixture was then poured into a beaker containing 150 mL of the non-solvent (IPA), with quick stirring using a stirring rod to induce precipitation of the polymer nanocomposite. Where the hBN was dispersed in IPA, the desired amount of hBN was sonicated in 15 mL of IPA prior to being added to 150 mL of IPA, with quick stirring. Afterwards, the aPS/DCM mixture, after the aPS had dissolved, was added to the IPA/hBN solution and stirred to precipitate the polymer nanocomposite. The resulting nanocomposite gel was kept at ambient conditions in a ventilated fume cupboard for 7 days; the mass of the gel was monitored daily to confirm that most of the solvent had evaporated. The material was then further dried in a vacuum oven at 60 °C for 3 days before being melt pressed at 180 °C for 3 minutes, to remove any gas bubbles or residual solvent.

To prepare the polymer nanocomposites at high temperatures using either TOL or CB, 9.5 g of aPS was added to 100 mL of the appropriate solvent. The mixture was heated to the boiling point of the solvent, i.e. 111 °C and 131 °C for TOL and CB respectively, while simultaneously being stirred with a magnetic stirrer bar. After the solvent started boiling, the heat was lowered to allow the solution to boil gently. The mixture was left at low heat until all the polymer had dissolved. The sonicated hBN was added to the aPS/solvent mixture and the hot aPS/hBN/solvent mixture was poured quickly into a beaker containing 150 mL of IPA with simultaneous, vigorous, stirring, such that rapid precipitation of the polymer nanocomposite occurred. The procedure was repeated again to produce different materials where the hBN was dispersed in IPA, as described previously where the materials using DCM were prepared. The same drying procedure was followed as described above.

The unfilled polystyrene samples, without any hBN particles, were prepared through the same way with the three different solvents. Samples of the as-received polystyrene (PS/REF), which was in the form of pellets, were also prepared. The PS/REF samples, which were the reference samples, were prepared by melt pressing in order to understand the effect of solvent processing on the properties of the unfilled polystyrene polymer.

5.2.3 Material Formulations

The materials listed in Table 5.1 are denoted by “PSBN/SOLVENT/NON-SOLVENT/X” where the “PSBN” refers to a polystyrene/hBN nanocomposite, the “SOLVENT” is the name of the solvent (DCM, TOL, or CB), the “NON-SOLVENT” is IPA in all cases, and the “X” refers to the wt % of hBN. The asterisk placed on the solvent or non-solvent refers to the solvent in which the hBN was dispersed during material processing.

Table 5.1: Polystyrene/hBN nanocomposite formulations

Material	Polystyrene solvent	hBN Solvent	Polystyrene content (wt %)	hBN content (wt %)
PS/REF	-	-	100	0
PSBN/DCM/IPA/0	DCM	-	100	0
PSBN/TOL/IPA/0	TOL	-	100	0
PSBN/CB/IPA/0	CB	-	100	0
PSBN/DCM*/IPA/5	DCM	DCM	95	5
PSBN/DCM/IPA*/5	DCM	IPA	95	5
PSBN/TOL*/IPA/5	TOL	TOL	95	5
PSBN/TOL/IPA*/5	TOL	IPA	95	5
PSBN/CB*/IPA/5	CB	CB	95	5
PSBN/CB/IPA*/5	CB	IPA	95	5

5.3 Thermogravimetric Analysis

TGA was used to confirm the filler content of the hBN in the nanocomposites. Repeated experiments have shown that there is a variation of ~4 °C in the temperature measurements and 0.3 % in the weight percent measurements. Figure 5.1 shows the TGA curves of the six different nanocomposites and the as-received polystyrene. The as-received polystyrene (PS/REF) was the only polystyrene included in Figure 5.1 for clarity, since the other unfilled polystyrene samples all exhibit identical behaviours. The thermal degradation of polystyrene occurs in the temperature range of 350 °C to 450 °C, which is consistent with published results [121]–[123], to yield a char residue of 0.2 %, which suggests that the polystyrene is fully decomposed. No mass loss is observed between 100 °C to 200 °C, the temperature range where the solvents boil, suggesting that no residual solvent or moisture is in the system. The TGA results are summarised in Table 5.2, which confirms that all nanocomposites contain the expected amount of hBN, within slight variations, in the polystyrene matrix. While TGA was just used to confirm the filler content, it was noticed

that all nanocomposites degrade at a higher temperature relative to the unfilled polystyrene, suggesting that the presence of the hBN particles improves the thermal stability of the system and therefore the terms, T_{10} and T_{50}, in Table 5.2 are the temperatures at which 10 % and 50 % of the sample mass has degraded.

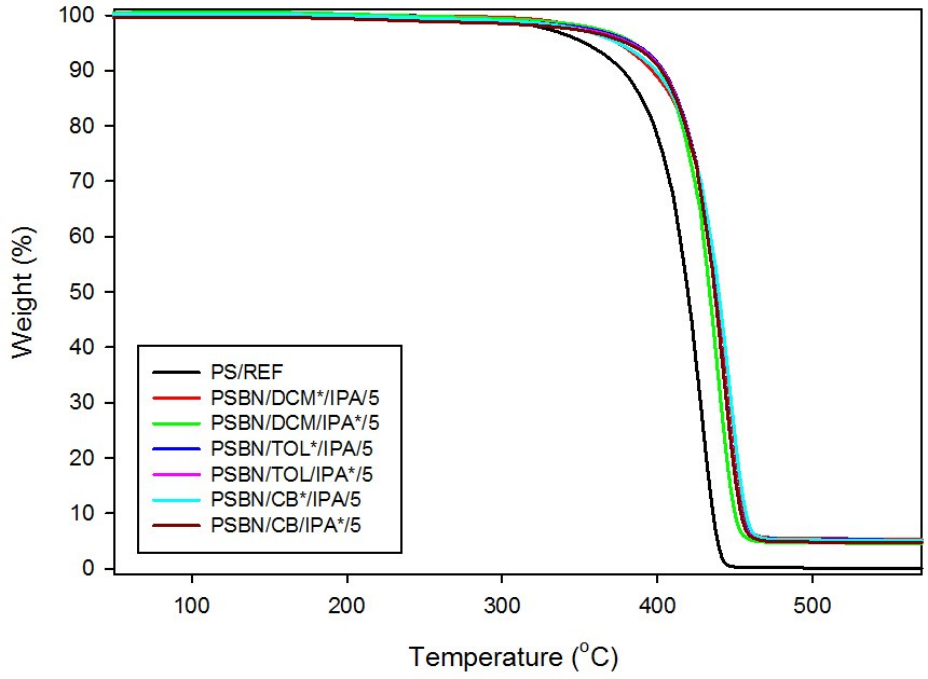

Figure 5.1: TGA curves for the different polystyrene/hBN nanocomposites

Table 5.2: Decomposition temperatures and residue for the polystyrene/hBN nanocomposites

Material	Residue (wt %)	$T_{10\%}$ (°C)	$T_{50\%}$ (°C)
PS/REF	0.02	379	419
PSBN/DCM/IPA/0	0.07	383	421
PSBN/TOL/IPA/0	0.05	385	416
PSBN/CB/IPA/0	0.03	382	418
PSBN/DCM*/IPA/5	5.28	399	438
PSBN/DCM/IPA*/5	4.53	402	434
PSBN/TOL*/IPA/5	5.13	404	437
PSBN/TOL/IPA*/5	4.89	403	437
PSBN/CB*/IPA/5	5.04	397	439
PSBN/CB/IPA*/5	4.65	403	440

5.4 Scanning Electron Microscopy

Figure 5.2, Figure 5.3, and Figure 5.4 show the SEM micrographs of all the six nanocomposites. The use of polystyrene becomes clear after looking at the SEM images as no morphological effects are observed, as seen from the clear amorphous backgroud, which allows the dispersion state of the hBN to be studied. The SEM micrographs reveal that the hBN exists in various different forms, which can be distinguished by variations in the secondary electron (SE) emission that they generate. The agglomerates typically give rise to relatively high SE emission, which indicates that they correspond to regions of high rugosity; this, in turn, implies that they contain many layers of hBN. Additionaly, many more hBN objects are present which contain relatively low internal contrast. This indicates that the surface is relatively flat, and therfore suggests that they contain relatively fewer hBN layers. These structues cannot be referred to as exfoliated hBN, but it is believed that they are likely to correspond to simple tactoids.

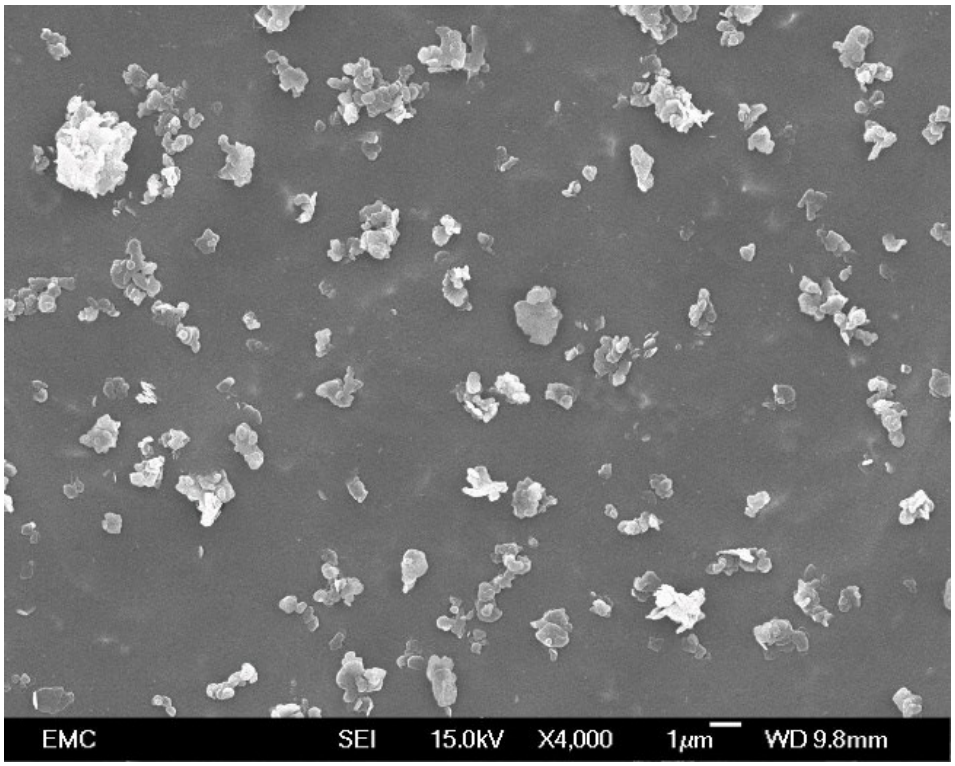

(a)

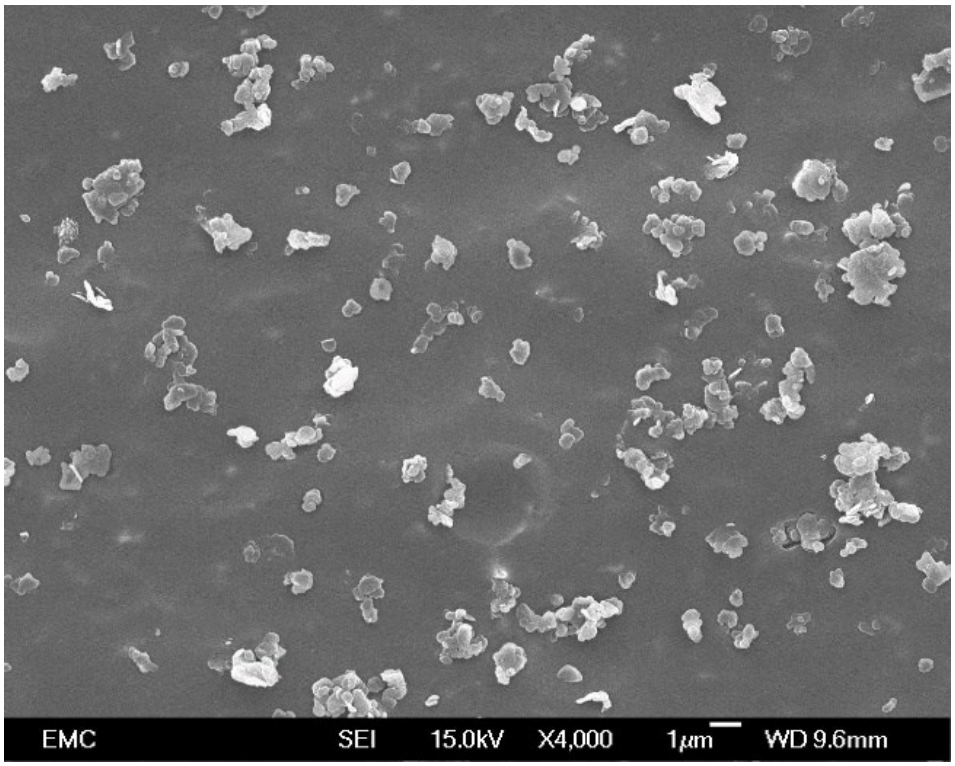

(b)

Figure 5.2: SEM micrographs of (a) PSBN/DCM*/IPA/5, (b) PSBN/DCM/IPA*/5

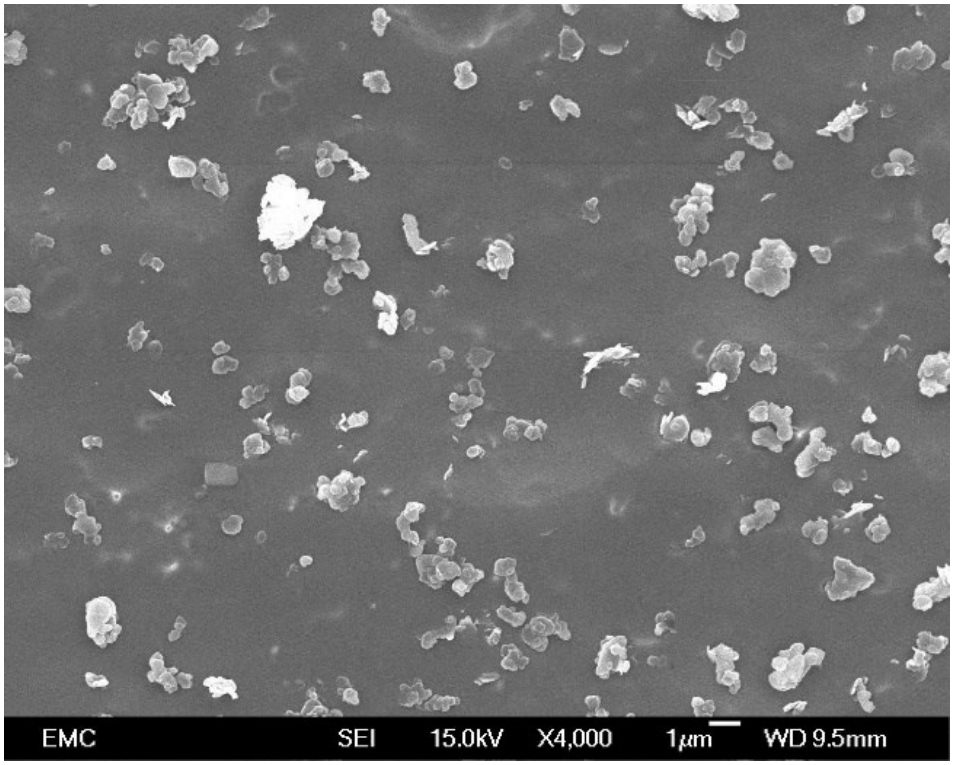

(a)

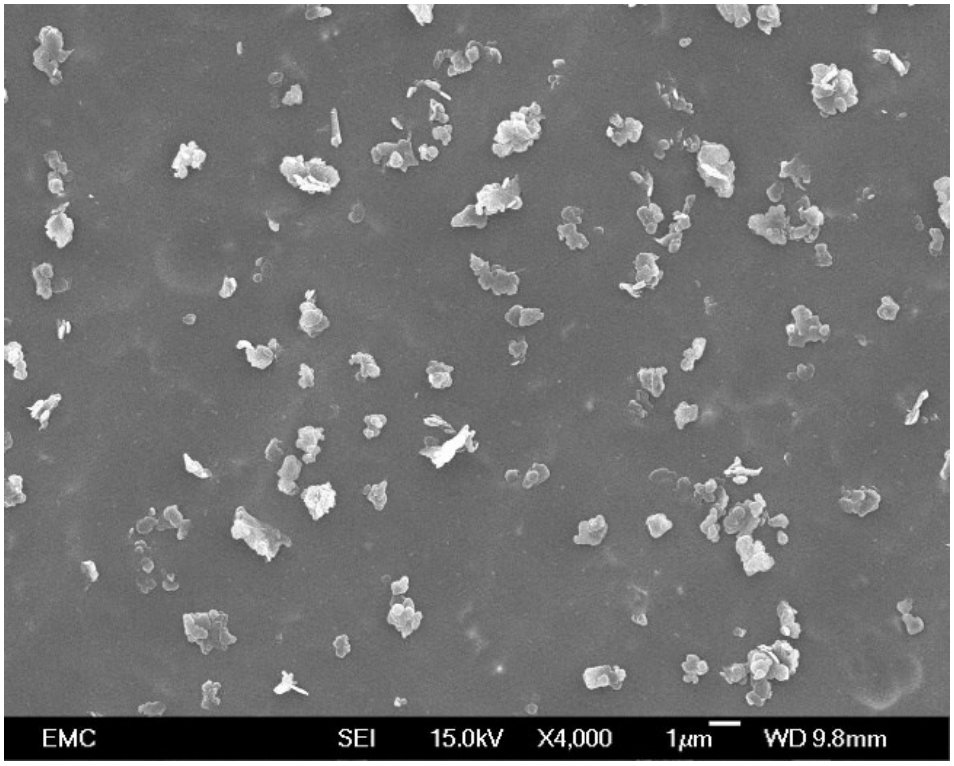

(b)

Figure 5.3: SEM micrographs of (a) PSBN/TOL*/IPA/5, (b) PSBN/TOL/IPA*/5

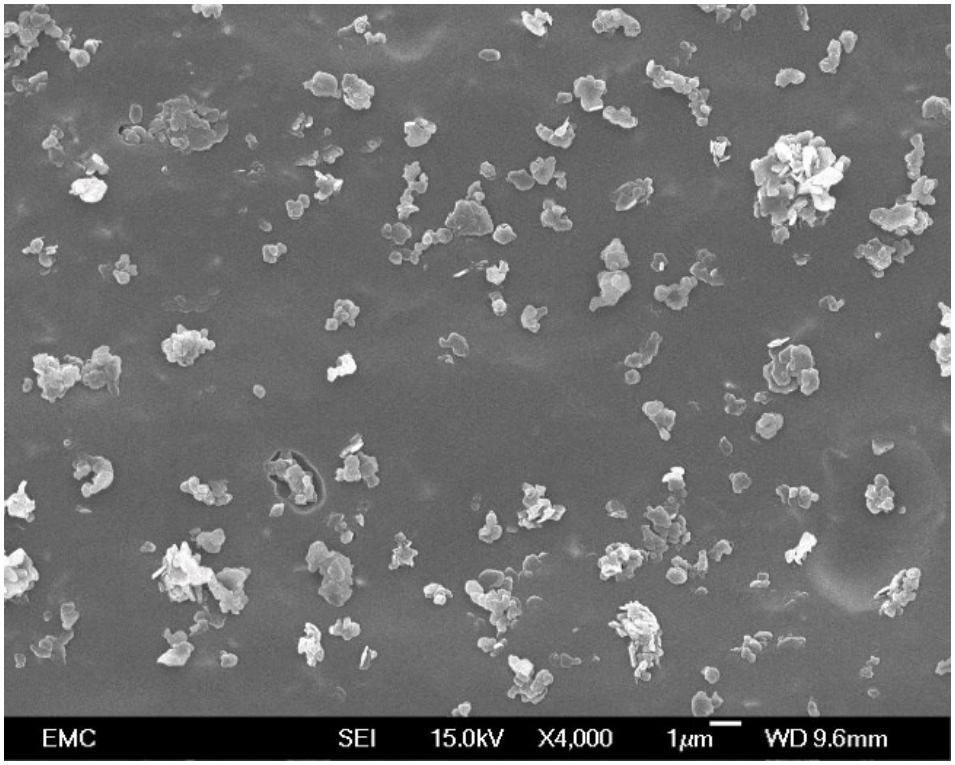

(a)

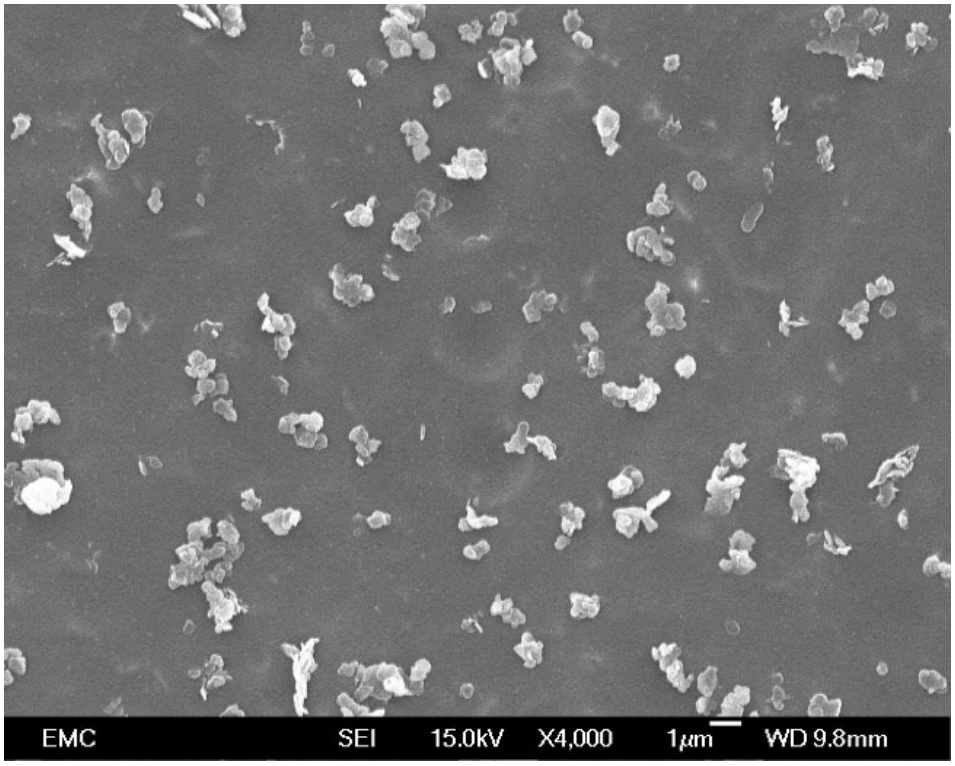

(b)

Figure 5.4: SEM micrographs of (a) PSBN/CB*/IPA/5, (b) PSBN/CB/IPA*/5

When looking at the SEM micrographs of all the nanocomposites, there does not seem to be an observable difference in the dispersion state of the hBN in the polystyrene, as all systems contain clustered hBN particles and thin hBN tactoids. This suggests that there are similar hBN/solvent and polymer/solvent interactions in all solvents. In all the nanocomposites, the hBN appears to be uniformly distributed in the polymer matrix, but a number of agglomerates of various sizes in all the materials exists, as seen from the SEM micrographs. These agglomerates are introduced from the as-received hBN powder, which itself contained many agglomerated structures which could not be completely separated into smaller constituents by sonication. All agglomerates in the nanocomposites are less than 5 μm in size and the structures containing relatively few layers of hBN, identified by the objects with low internal contrast in the SEM micrographs, appear to be more abundant in the nanocomposites than the highly agglomerated structures.

There doesn't seem to be an observable change in the final dispersion state of the hBN platelets when they were processed in either the IPA, prior to being added to the polymer, or when they were processed in the solvent used to dissolve the polystyrene. Since the dispersion state of the hBN in all nanocomposites is very similar with no significant changes, this suggests that liquid exfoliation, or dispersion methods in solution might not be effective in dispersing the hBN platelets. It was initially presumed that sonicating the hBN in different solvents would result in different dispersion states,; however, this is clearly not the case which suggests that these solvents are equally effective at dispersing the hBN platelets. Since there is a small amount of large agglomerates relative to the thin tactoids in the nanocomposites, the dispersion of the hBN in the polymer is considered to be adequate even though the degree of exfoliation cannot be deduced solely from the SEM images.

5.5 X-Ray Diffraction

XRD was used to further evaluate the dispersion state of the hBN particles in the polystyrene. Figure 5.5 shows the XRD patterns of the PSBN nanocomposites relative to the hBN powder. The polystyrene diffraction pattern is clear, with two very broad peaks centred at 2θ values of ~9° and ~19° belonging to the amorphous phase of the atactic polystyrene. These wide peaks with low intensities appear due to the disordered non-crystalline structure of atactic polystyrene which lacks any structural periodicity. This is a standard XRD pattern of polystyrene which has been seen elsewhere [124]–[126]. The presence of the hBN peak in all nanocomposites is very clear, and it is positioned very close to the peak of the starting hBN powder which suggests that there is little to no intercalation. This indicates that the thin

tactoids presents in the SEM images are not exfoliated sheets but rather stacked hBN platelets composed of a few layers.

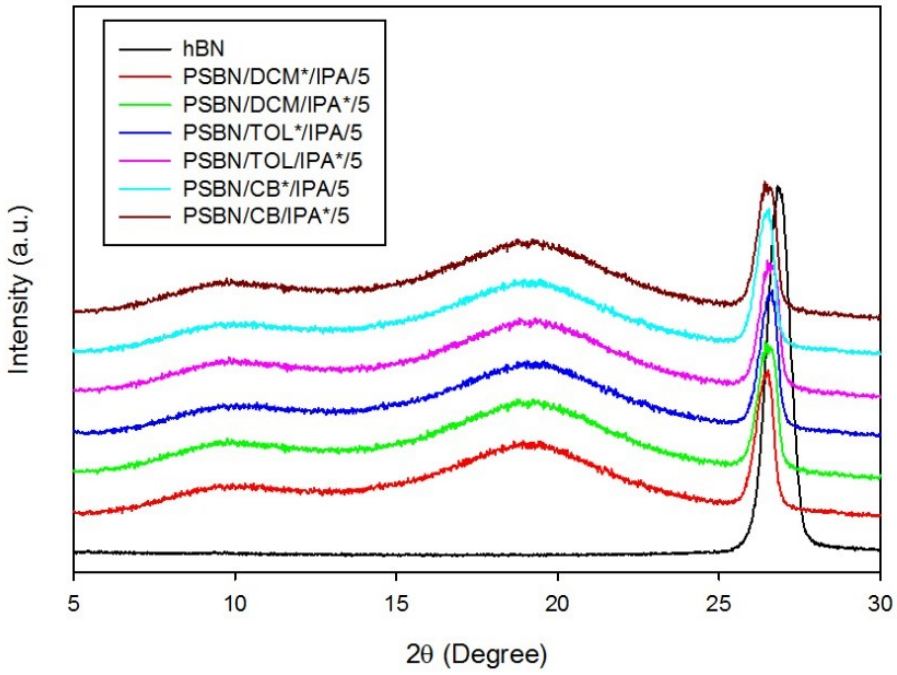

Figure 5.5: XRD patterns for the different polystyrene/hBN nanocomposites

Figure 5.6 closely shows the position of the hBN peak in the nanocomposites relative to the hBN powder. The figure shows that the hBN peak in the nanocomposites slightly shifts to lower 2θ values and, according to Bragg's law, a decrease in 2θ results in an increase in the interlaying distance which suggests some intercalation. However, a closer look at the figure reveals that this decrease in 2θ values is less than 1° which is within experimental uncertainty. Cao et al. [127] reported no change in 2θ value in the XRD results of pristine hBN and exfoliated hBN; however, a broader peak was observed in the exfoliated hBN which suggests a smaller thickness. The 2θ values with their corresponding interlayer distances are shown in Table 5.3 for all the nanocomposites. The similarity in the interlayer distance of all the nanocomposites is consistent with the SEM results where all nanocomposites exhibited a similar hBN dispersion state. The interlayer distance values of all the nanocomposites are all very similar and very slightly higher than the interlayer distance of the hBN powder, even though the difference is very negligible, which suggests little to no intercalation. The difficulties in the intercalation/exfoliation of hBN platelets has been widely reported by many researchers in the literature [128]–[131]. Unlike its carbon

counterpart, graphite, the B-N bonds in hBN are polar due to the differences in electronegativity between the boron and nitrogen atoms. The nature of the stacked hBN layers such that a nitrogen atom lies directly on top of a boron atom will give rise to additional interlayer forces, due to the charged boron and nitrogen atoms, with stronger electrostatic interactions than in graphite, which contains non-polar carbon bonds, despite having the same interlayer distance [106]. For this reason, hBN is harder to exfoliate which explains why the solvents alone in this study were insufficient at exfoliating or even intercalating the hBN layers.

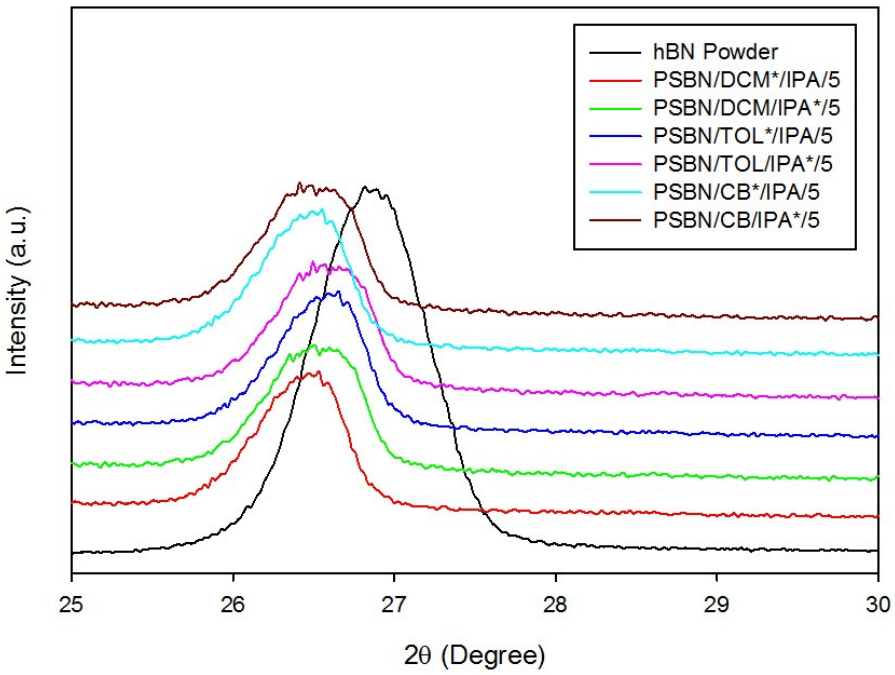

Figure 5.6: Changes in the XRD pattern in the polystyrene/hBN nanocomposites

Table 5.3: Interlayer spacing of the polystyrene/hBN nanocomposites

Material	2θ	Interlayer spacing (nm)
hBN	26.8191 °	0.33241
PSBN/DCM*/IPA/5	26.5355 °	0.33590
PSBN/DCM/IPA*/5	26.4950 °	0.33641
PSBN/TOL*/IPA/5	26.5963 °	0.33515
PSBN/TOL/IPA*/5	26.5557 °	0.33565
PSBN/CB*/IPA/5	26.4747 °	0.33666
PSBN/CB/IPA*/5	26.4139 °	0.33742

5.6 Differential Scanning Calorimetry

DSC was used to measure the glass transition temperature of the materials, which provides information about the interaction between the polystyrene and the hBN. The glass transition temperature of all materials is shown in in Table 5.4. Repeated experiments have shown that there is a variation of ~4 °C in the temperature measurements. An unexpected observation is that the glass transition temperatures, T_g, for all the polystyrene samples are not similar. The T_g of polystyrene has been studied in the past by many researchers and is reported to be ~100 °C [132]–[134]. The T_g of the PS/REF and the PS/DCM are similar and close to the literature value yet they are larger by ~8 °C than the T_g of the PS/TOL and PS/CB systems, which are also similar. Taking into account their chemical structures and their high boiling points, it is speculated that toluene and chlorobenzene act as plasticisers for polystyrene which effectively lower the T_g of polystyrene from 99.8 °C to 91.3 °C and 90.8 °C in the presence of toluene and chlorobenzene respectively. When the polystyrene gel was dried off, some of the solvent molecules surrounding the polymer chains may have evaporated, however, some of the solvent molecules that are intercalated between the polymer chains may get entrapped and the thermal energy provided from the drying procedure might not be sufficient to evaporate the solvent molecules, thus leaving a very small amount of residual solvent. Yoshioka et al. [135] has shown that the presence of varying amounts of chloroform, benzene, and toluene in polystyrene results in drastic decrease in T_g, thus highlighting the

plasticising effects of these solvents on polystyrene. It is important to note that that if there is any residual solvent, the amount is too small to even be detected in the TGA measurements. The plasticising effect is not observed when DCM was used to dissolve polystyrene due to its dissimilarity in chemical structure, low boiling point, and high volatility which allows it to evaporate rapidly.

Table 5.4: Glass transition temperatures of the polystyrene/hBN nanocomposites

Material	**T_g (°C)**
PS/REF	99.8
PSBN/DCM/IPA/0	99.3
PSBN/TOL/IPA/0	91.3
PSBN/CB/IPA/0	90.8
PSBN/DCM*/IPA/5	98.7
PSBN/DCM/IPA*/5	99.5
PSBN/TOL*/IPA/5	92.1
PSBN/TOL/IPA*/5	91.5
PSBN/CB*/IPA/5	91.2
PSBN/CB/IPA*/5	90.6

The T_g of the polystyrene/hBN nanocomposites are always compared to the T_g of the polystyrene sample which was prepared using the same solvent. The T_g of the nanocomposites in comparison to the unfilled polystyrene dissolved using the same solvent are very similar and within experimental uncertainties. For example, the T_g of PSBN/TOL/IPA/0, PSBN/TOL*/IPA/5, and PSBN/TOL/IPA*/5 are 91.3 °C, 92.1 °C, and 91.5 °C respectively, which are within experimental uncertainties. This is contrary to some of the published results where an increase in T_g has been reported in hBN nanocomposites [136], [137], however, this increase in T_g was directly related to the dispersion of the hBN in the polymer. Indeed, Cao et al. [138] prepared 5 wt % polyurethane/clay nanocomposites using two processing methods, which resulted in different clay dispersions, and found an increase in T_g in the nanocomposite with better dispersion containing exfoliated structures.

However, Torre et al. [139] noticed a different effect in polystyrene/MMT nanocomposites where the T_g of the nanocomposites prepared by solution intercalation using toluene decreased from 90 °C to 65 °C, whereas the T_g of the nanocomposites prepared by melt intercalation remained unchanged relative to the unfilled polymer. This could be ascribed to entrapment of the toluene solvent, which is also observed in this study.

The dispersion of the hBN in either the solvent or the non-solvent does not affect the T_g, due to the similar dispersion state of the hBN in the polystyrene in the two cases which did not result in exfoliated structures; the lack of change of T_g in the nanocomposites relative to the unfilled polystyrene suggests that there are weak interactions between the hBN and the polystyrene. A good dispersion of the hBN, which results in the exfoliation or intercalation of the hBN layers, can restrict the motion of polymer chains which in turn increases the glass transition temperature. Since no exfoliation or intercalation is evident, the chain mobility is not significantly affected, which results in very small changes in the T_g. This is consistent with the XRD results where a lack of intercalation was observed, most possibly due to the presence of large hBN particles as evinced in the SEM micrographs.

5.7 Dielectric Spectroscopy

Dielectric spectroscopy was used to investigate the dielectric response of the materials and the dielectric losses in the system due to the presence of the hBN particles. Figure 5.7 shows the real permittivity of all the unfilled polystyrene materials. The real relative permittivity behaviour of the PS/REF and all solution processed polystyrene samples is identical. This behaviour is characterised by a frequency independent real permittivity with a value of ~2.60 across the entire measured frequency range, as also reported elsewhere [140], [141], due to the non-polar nature of polystyrene which contains no permanent dipoles. The imaginary permittivity of all four polystyrene materials is shown in Figure 5.8 and is also similar, characterised by a frequency independent behaviour with very low losses (~10^{-3}). This corresponds to very low calculated tanδ values of all the polystyrene materials, in the range of ~10^{-3}, and is reported in the literature to be less than 10^{-4} [142], which is beyond the measurement capabilities of the equipment used here as the values of the imaginary permittivity are also within the noise limit of the equipment.

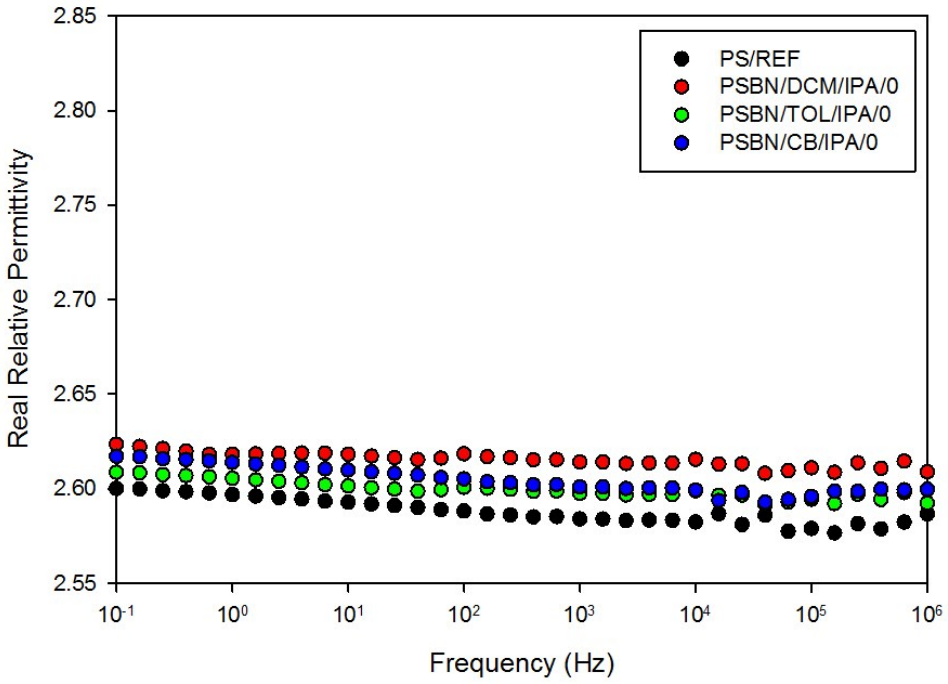

Figure 5.7: Real relative permittivity of all the different polystyrene materials

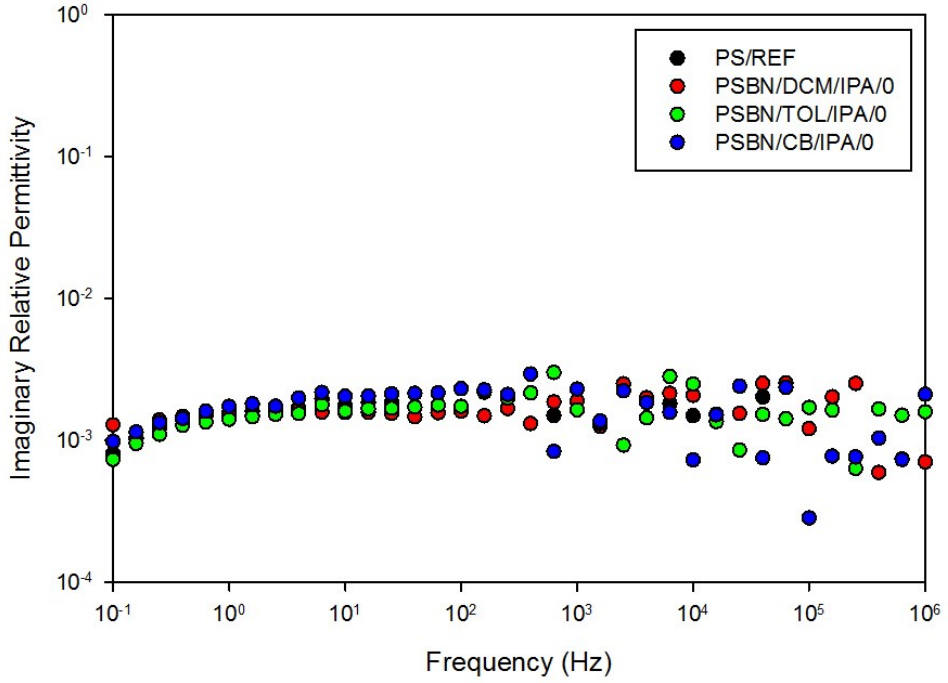

Figure 5.8: Imaginary relative permittivity of all the different polystyrene materials

Figure 5.9 shows the real relative permittivity of all the six nanocomposites relative to the unfilled polystyrene (PS/REF) only, as the solution processed polystyrene materials exhibit a similar dielectric response. The dielectric response of all the nanocomposites is very similar with no apparent differences in either the real or imaginary permittivity. The real relative permittivity of all the nanocomposites is also frequency independent with a slightly higher permittivity relative to the unfilled polystyrene, with a value of ~2.72. The variation in the values of the real relative permittivity is a result of measurement uncertainties (± 0.05), which has been determined from repeated experiments. The higher value of the real permittivity of the nanocomposites is attributed to the presence of the hBN filler in the polystyrene, and this is consistent with published work on hBN nanocomposites [136], [143], [144]; the permittivity increase in the nanocomposites is very small due to the small quantity of hBN in the system. The frequency independent behaviour suggests that the nanocomposites are dry as no low frequency permittivity increases are observed. In another hBN system, Tsekmes et al. [145], [146] evaluated the role of boron nitride distribution in epoxy on the dielectric response of the nanocomposites by preparing the materials through different processing techniques, which resulted in slightly different particle dispersions in the epoxy matrix. They noticed that while all processing techniques result in different particle distributions, they all lead to well dispersed systems. They suggest that the filler content and water uptake play a major role in determining the dielectric response rather than the distribution of the particles. As the drying procedure removed all water from the systems in this study, no change in the dielectric response was observed. Even if there were some differences in the dispersion of the hBN in the materials processed with different solvents, the change in the dielectric response would not very significant without changing the filler content.

Many researchers have reported opposite effects at low filler loading levels with a lower real permittivity than the unfilled polymer. Wang et al. [147] found that the real permittivity and dielectric losses of polystyrene/clay nanocomposites, at 1.5 wt % and 2.5 wt % of clay with different intercalating agents, are significantly lower than that of the pure polystyrene. They attribute this decrease in permittivity to the confinement of the polystyrene molecular chains in the presence of exfoliated clay structures, which restrict the chain mobility which in turn reduces the dielectric losses. Similar results have been reported with various different types of fillers with different sizes at low filler content in epoxy systems, which were also attributed to the restriction of chain mobility especially when they epoxy groups bond with the surface of the particle [148]–[152].

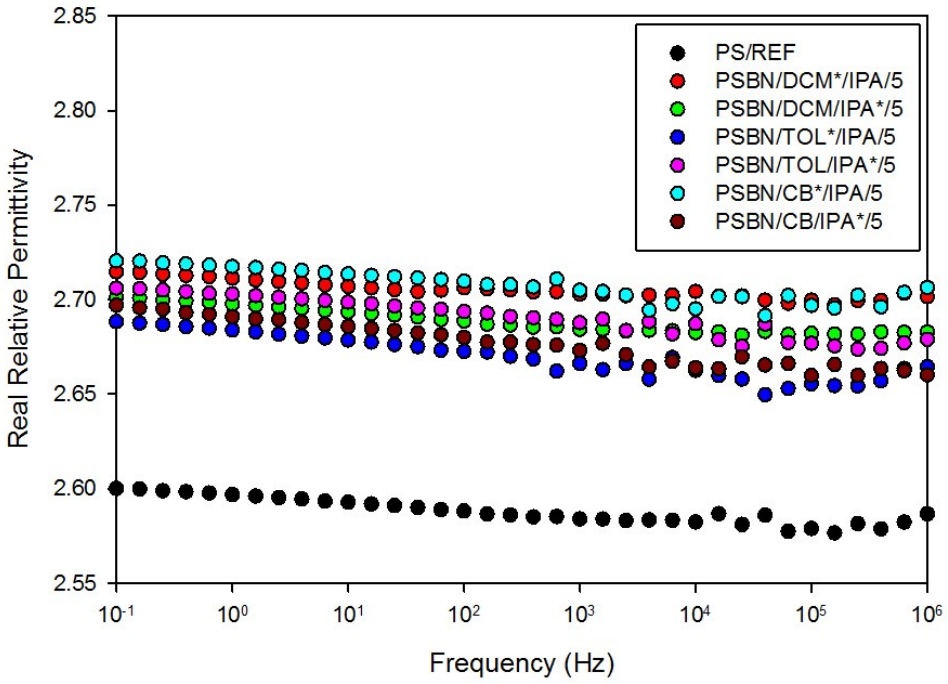

Figure 5.9: Real relative permittivity of the polystyrene/hBN nanocomposites

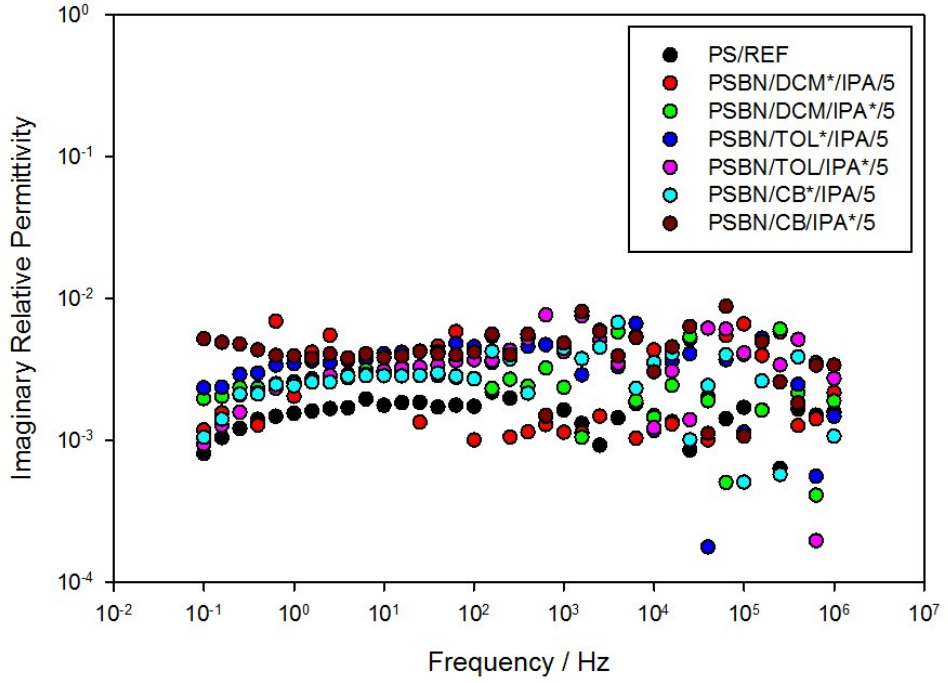

Figure 5.10: Imaginary relative permittivity of the polystyrene/hBN nanocomposites

While the previously mentioned studies highlighted the effect of the size of the filler on the permittivity of the material, this type of behaviour does not conform to the established dielectric mixing laws for composites which assumes the permittivity of the composite is generally a combination of both the filler and the polymer. This is due to the effect of the interphase brought about by nanostructuration, which is not observed in this study as the effect of the relatively high filler content with a larger permittivity dominates the effect of chain mobility restriction.

Figure 5.10 shows the imaginary permittivity of all the nanocomposites. The imaginary permittivity behaviour of the nanocomposites is similar to that of the unfilled polystyrene, where a slight increase is noticed, and is characterised by very low losses ($\sim 10^{-3}$) which cannot be measured accurately by the equipment, resulting in scattered points across the measured frequency range. Although the imaginary permittivity values of the nanocomposites might be slightly higher than the unfilled polystyrene, possibly due to interfacial polarisation at the nanoparticle interface, they are within the noise limit of the equipment, and therefore the nanocomposites can be said to be low loss materials. Generally, the addition of particles introduces some interfacial polarisation due to the permittivity differences between the organic polymer and the inorganic particles, which introduces discontinuities. These inorganic particles usually contain surface functional groups such as hydroxyl groups which can be a source of charge carriers that can result in an increase in the tanδ term. Praeger et al. [140] found that the real and imaginary permittivity of 2.5 wt % polystyrene/silica nanocomposites increased in the low frequency region, which was attributed to a low frequency relaxation process, whereas the unfilled polystyrene showed no frequency dependent behaviour. Similar observations were made by Huang et al. [153], [154] in polyethylene/alumina nanocomposites at alumina filler loadings above 12 wt %, which was attributed to the interfacial polarisation between the polyethylene and the alumina particles. The small changes in the imaginary permittivity of the nanocomposites relative to the unfilled polystyrene, which can be as a result of uncertainties, suggests there is minimal interfacial polarisation between the aPS and hBN, and thus very small difference in the dielectric losses were observed, which may be due to the low filler content. For high voltage power applications, the dielectric response at power frequencies of 50 – 60 Hz is of primary concern. The tanδ term is an important electrical engineering parameter as it provides information about the dielectric losses of the material. No apparent change in the dielectric losses are seen since the changes in the real and imaginary relative permittivity of the nanocomposites are very small in the nanocomposites. Although polystyrene cannot be used

as an insulator in high voltage cables, this low loss quality which is unaffected by the presence of the hBN filler is an attractive dielectric property as the presence of nanofillers usually introduces significant losses to the base material.

5.8 Dielectric Breakdown Strength

To investigate the effect of the hBN dispersion state in the nanocomposites on the electrical performance, the dielectric breakdown strength of all the prepared nanocomposites was measured. Figure 5.11 shows a Weibull plot of the four different polystyrene materials, which clearly shows that the four systems exhibit very similar breakdown behaviour with an electrical breakdown field of 190 kV/mm ± 2 kV/mm, and all the confidence bounds overlap. Therefore, the effect of solution processing on the breakdown behaviour of polystyrene can be considered to be negligible. Although the DSC results suggested some residual solvent in the polystyrene materials prepared using toluene and chlorobenzene, and if this is indeed present in the system, it does not influence the breakdown behaviour of the materials. However, the work of Sabuni et al. [155] by adding 2.7 wt % of an ester type plasticiser in polystyrene, the dielectric breakdown strength reduced from a maximum of 7.42 MV/cm to 6.56 MV/cm . However, as a relatively small decrease in breakdown strength was observed at a 2.7 wt % plasticiser content, the lack of change in breakdown strength in this case is reasonable as the content of plasticiser, if present, is undetectable due to its very low amount.

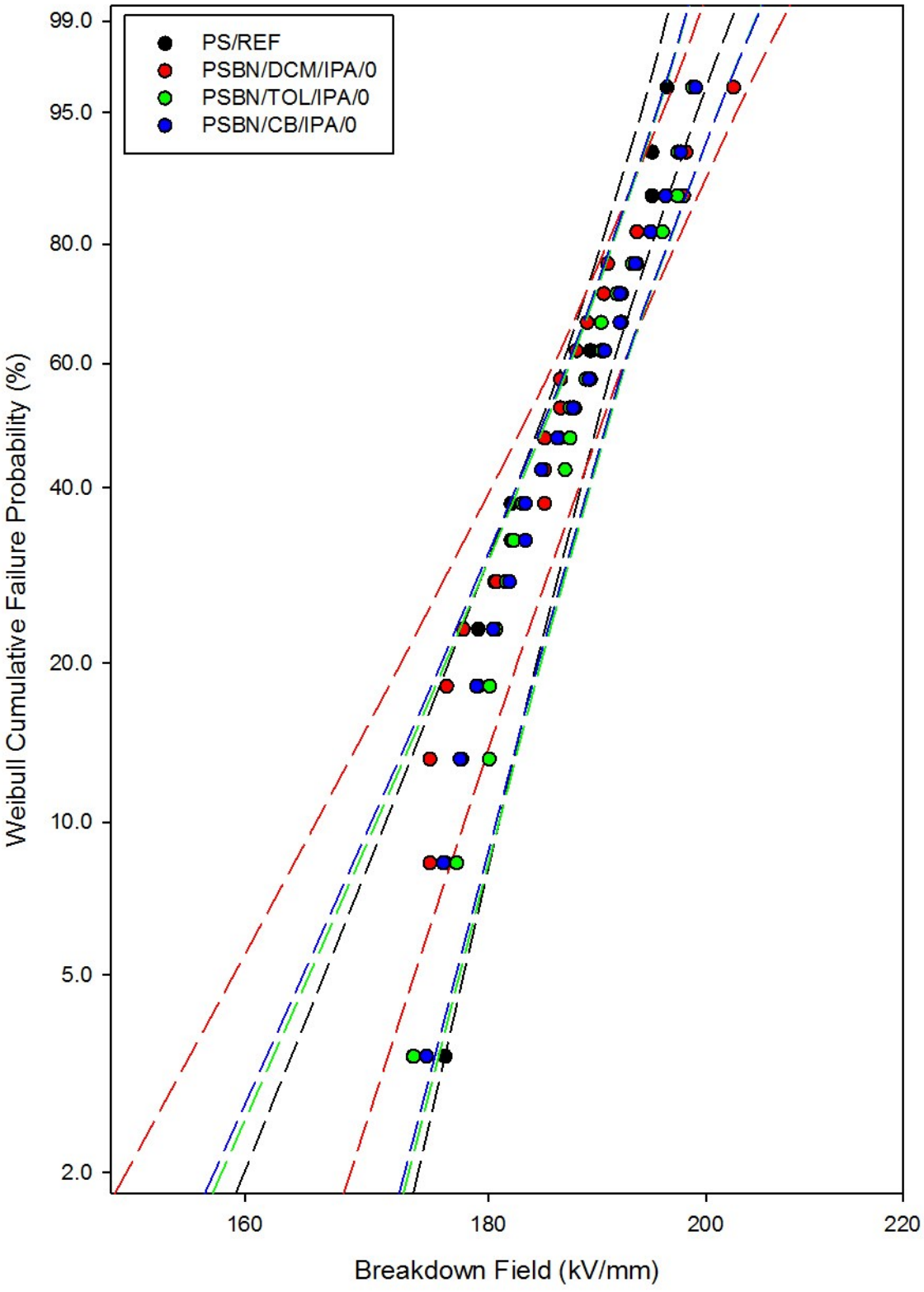

Figure 5.11: Weibull plots of all the polystyrene materials

Figure 5.12 shows the Weibull plot of the reference polystyrene with the six nanocomposites, where that all nanocomposites exhibit a comparable breakdown strength that is slightly larger than the unfilled polystyrene. However, the breakdown strength values of the nanocomposites and the unfilled polystyrene appear to be similar when the uncertainty limits are considered. The Weibull parameters for all the materials are listed in Table 5.5.

Table 5.5: Weibull parameters of all the polystyrene/hBN nanocomposites

Material	**Scale parameter α (kV/mm)**	**Shape parameter β**
PS/Ref	189 ± 2	33 ± 9
PSBN/DCM/IPA/0	190 ± 3	24 ± 6
PSBNTOL/IPA/0	191 ± 2	30 ± 9
PSBN/CB/IPA/0	191 ± 2	29 ± 8
PSBN/DCM/IPA/5	195 ± 3	24 ± 7
PSBN/IPA/DCM/5	195 ± 4	23 ± 6
PSBN/TOL/IPA/5	195 ± 3	29 ± 8
PSBN/IPA/TOL/5	196 ± 3	27 ± 7
PSBN/CB/IPA/5	197 ± 3	30 ± 8
PSBN/IPA/CB/5	196 ± 3	29 ± 8

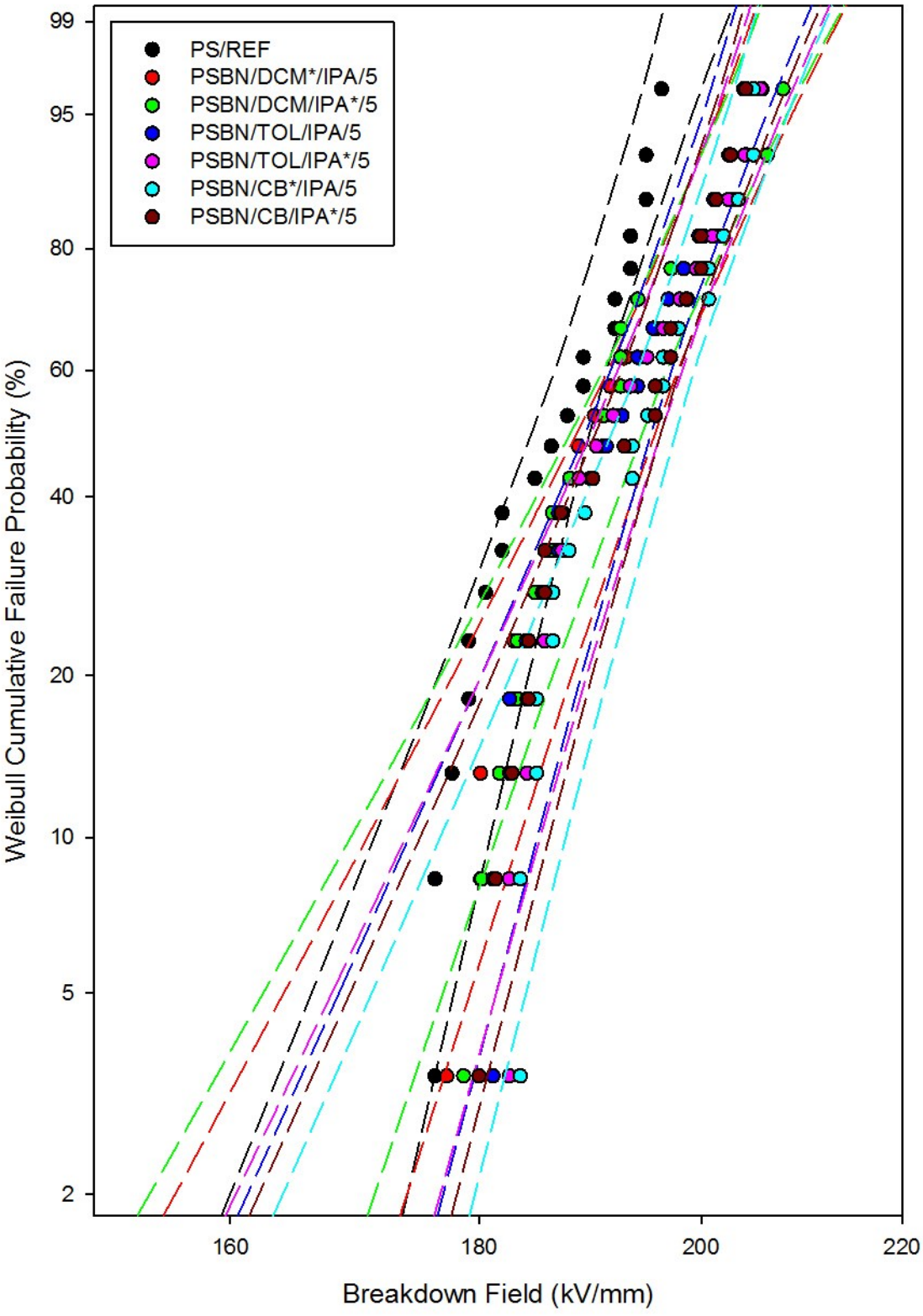

Figure 5.12: Weibull plots of the polystyrene/hBN nanocomposites

The breakdown behaviour of nanocomposites has been widely published with many contradictory results. Li et al. [156] reported an increase in breakdown strength in polystyrene nanocomposites based on alumina and titania fillers up to 5 wt %, where a maximum breakdown strength was observed with the inclusion of 1 wt % of particles. In contrast, Praeger et al. [157] reported a decrease in breakdown strength in polystyrene/silica nanocomposites at different filler loading levels up to 10 wt % of silica. The preparation route of the nanocomposites can also affect the dielectric properties. Singa et al. [18] reported similar results with epoxy nanocomposites based on titanium oxide, zinc oxide, and aluminum oxide with enhanced charge transport capabilities in comparison to the unfilled epoxy, due to the introduction of excess free charges by the inorganic particles.

The similarity in the breakdown strength behaviour observed in the six nanocomposites processed in the different solvents suggests that the breakdown strength is dependent on the dispersion of the nanoparticles. The role of particle distribution in the breakdown behaviour is still not very well understood as some contradictory results exist in the literature. For example, Li et al. [158] reported a direct relationship between the size of the agglomerates and the breakdown strength in polyethylene alumina nanocomposites. At an alumina content of more than 3 wt % with a uniform particle dispersion, the breakdown strength remained relatively unchanged from the unfilled polyethylene; however, the breakdown strength was significantly reduced at an alumina content more than 3 wt % where large agglomerates were present. Nguyen et al. [66] reported a similar trend in the breakdown strength of epoxy/silica nanocomposites, where the breakdown strength decreased although their system was very well dispersed, without the presence of large agglomerates. However, Yeung et al. [159] reported significant increases in the breakdown strength of epoxy/silica nanocomposites despite the presence of large agglomerates. Therefore, it is difficult to establish a direct relationship between the two parameters, the nanoparticle dispersion and the dielectric breakdown strength, which suggests that the particle dispersion may not be the primary factor affecting the breakdown strength of nanocomposites.

While the results in literature concerning the electrical properties of boron nitride nanocomposites are very limited, the available studies generally report an increase in breakdown strength in nanocomposites based on a boron nitride filler [60]–[62], [67], [69], [160], [161] which suggests that the enhanced breakdown property is a boron nitride specific effect. The breakdown strength of the nanocomposites slightly increased by ~5 kV/mm relative to the unfilled polystyrene, which makes the cause for this small improvement difficult to interpret. A direct explanation for the physical processes dominating the

breakdown behaviour of the nanocomposites is not straightforward as many processes might be causing the electrical degradation of the materials, which may be acting alone or in combination; however, a more detailed discussion of the breakdown behaviour of the polymer nanocomposites is presented in Chapter 6, where the effects of the hBN loading level and hBN dispersion/aggregation state are taken into account.

5.9 Conclusion

The SEM results of all the polystyrene nanocomposites revealed that solvent processing did not affect the dispersion state of the hBN particles in the polystyrene matrix, which is consistent with the XRD results that confirmed the lack of any intercalated or exfoliated structures. This suggested that the solvent/hBN and solvent/polymer interactions were weak. The TGA results confirmed that the correct amount of hBN was present in the system and showed that all nanocomposites exhibited a higher thermal degradation temperature than the unfilled polystyrene materials. The DSC results revealed that the glass transition temperature of all nanocomposites was higher than the unfilled polystyrene. The glass transition temperature of the materials processed in toluene and chlorobenzene appeared to be lower than the other materials, which could be due to the small amount of residual entrapped solvent. Dielectric spectroscopy measurements suggested that the incorporation of hBN particles did not significantly affect the dielectric losses of the polystyrene, although a slight increase in the real permittivity was observed. The breakdown strength of all nanocomposites was similar and slightly higher relative to the unfilled polystyrene, which again confirmed the negligible effect of solvent processing.

This chapter demonstrated that the sonication of the hBN particles in different solvents does not provide sufficient energy to separate the hBN layers. While more efforts in the exfoliation of hBN could be carried out, the aim of the chapter was to investigate the effect of solvent processing to determine which solvent is favourable in processing polystyrene nanocomposites. As the results in this chapter indicated that all nanocomposites exhibit a similar behaviour regardless of the solvent used in processing, it would be easy to conclude that the lack of change in behaviour is due to the lack of change in the dispersion state of the hBN particles. However, this conclusion would assume that the dispersion state is the key factor in determining the dielectric properties of nanocomposites. This chapter has shown that despite the similarity in the dispersion state of the hBN in the nanocomposites, the presence of large agglomerated structures did not negatively influence the breakdown behaviour of the nanocomposites which therefore suggests that proper dispersion of

nanoparticles may not be as important as hypothesized in improving the electrical properties of polymer nanocomposites.

Chapter 6: Polyethylene Hexagonal Boron Nitride Nanocomposites

6.1 Introduction

In the previous chapter, the effect of solvent processing on the dispersion state of hBN particles in polystyrene/hBN nanocomposites was studied. Despite the non-ideal dispersion of hBN and the presence of some hBN agglomerates, the presence of 5 wt % of hBN resulted in a slight increase in the breakdown strength relative to the unfilled polystyrene. That led to the hypothesis in this chapter, where the dispersion state of the hBN particles in the polymer is not considered a key factor that dominates the electrical performance of the hBN nanocomposites; any increase in breakdown strength can directly be related to a boron nitride specific property rather than its dispersion.

This chapter explores hBN nanocomposites based on a polyethylene matrix due to its suitability for high voltage applications [41]. Polyethylene is a thermoplastic polymer containing only hydrogen and carbon atoms, produced from the ethylene monomer, resulting in a chemical structure with repeating CH_2 units. Polyethylene consists of a chain of carbon atoms, covalently bonded with each other where each carbon is linked to a pair of hydrogen atoms [162]. The polyethylene chain, with a chemical formula $(-CH_2-CH_2-)_n$, is terminated with carbon atoms bonded to three hydrogen atoms. When polyethylene crystallises from the molten state, some chains organise themselves to form crystallites. Lamellar crystals, with a thickness in the orders of 10 nm and lateral dimensions of up to several micrometres, form during the crystallisation of polyethylene, and grow radially outwards from nucleation sites to form spherulites.

The regular crystalline structure of polyethylene is affected by the degree of chain branching, which consequently affects the crystallinity of the polymer. Polyethylene properties such as toughness, high modulus, and moisture resistance are a result of the crystalline regions. Higher degrees of crystallinity and increased density are a result of a larger number of polymer chains aligning with each other as there are less amorphous regions and more polymer chains per unit volume. Low density polyethylene (LDPE) has a high degree of branching, which hinders the crystallisation process, resulting in a less crystalline polymer

with lower density relative to high density polyethylene (HDPE). Due to the low degree of crystallinity, LDPE exhibits a low melting point and high flexibility. High density polyethylene (HDPE) consists mainly of unbranched chains which are packed closely to achieve a high degree of crystallinity. This results in a polymer with strong intermolecular forces and a high density. Because of its high degree of crystallinity, HDPE is known for having the lowest permeability and highest stiffness out of all the other types of polyethylene. Insulating materials used in electrical cables must be flexible at low temperatures and stable at high temperatures. A material with a high melting point, low dielectric losses, high breakdown strength, and good moisture resistance is ideal for high voltage cables. LDPE and HDPE have high enough melting points and moisture resistance to be used as suitable materials for electrical cables. However, at room temperature, HDPE is stiff due to its high young's modulus whereas LDPE is more flexible. On the other hand, LDPE suffers from poor mechanical performance at high temperatures. Therefore the addition of small amounts of HDPE into LDPE can enhance the mechanical performance, by increasing the young's modulus of LDPE, without the risk of making the resulting material brittle. Moreover, HDPE has a higher breakdown strength than LDPE so blending it into LDPE improves the overall breakdown strength of the resulting material [163]. This has been clearly demonstrated in the work of Hosier et al. [164] who investigated the effect of adding different HDPE fractions into LDPE on the dielectric performance of the materials relative to the pure LDPE. One of the main conclusions was the noticeable 15 % increase in breakdown strength in the polyethylene blend materials as compared to the pure LDPE. Where the breakdown strength of pure LDPE was measured to be 129 kV/mm, the breakdown strength for the polyethylene blend consisting of 80 wt % of LDPE and 20 wt % of HDPE was measured to be 148 kV/mm. Therefore, this is a suitable polymer matrix that can be used in this work.

Many of the results in the literature show that electrical properties of polymer nanocomposites deteriorate at high filler loading levels, as shown previously in Chapter 2 and later in Section 6.8 of this chapter. The aim of this chapter is to determine the effect of hBN loading level on the dielectric properties of polyethylene/hBN nanocomposites, especially on the electrical breakdown strength, and attempt to explain some of the possible mechanisms for their behaviour. A total of 6 different materials were prepared, which were tested for changes in structural, thermal, and electrical properties relative to an unfilled polyethylene blend material. Structural properties were investigated using scanning SEM, to study the dispersion state of the nanocomposites, and XRD, to examine the intercalation or

exfoliation state. Thermal properties were investigated using TGA, to confirm the filler content and DSC, to investigate changes in the melting and crystallisation temperatures as evidence of any interactions between the PE and the hBN. Electrical properties were investigated using dielectric spectroscopy and dielectric breakdown strength testing.

6.2 Preparation of the Polyethylene/hBN Nanocomposites

6.2.1 Materials

The polyethylene blend consists of LDPE grade LD100BW, obtained from ExxonMobil Chemicals, and HDPE grade Rigidex HD5813EA, obtained from BP Chemicals. The nanocomposites were prepared with the same hBN particles used previously to prepare the polystyrene nanocomposites.

6.2.2 Solvent Blending Procedure

To produce the polymer nanocomposites, the desired mass of LDPE, HDPE, and hBN was first weighed out, such that the final material is composed of a polymer blend with 80 wt % LDPE, 20 wt % HDPE and the desired wt % of hBN. The desired hBN mass was added in a small container, followed by the addition of ~15 mL xylene. In a separate round bottomed flask, the LDPE and HDPE pellets were added. The xylene/hBN solution was added to the flask with the addition of more xylene to give a 200 mL solution of 5% w/v (polymer/xylene) concentration. The mixture was heated to 140 °C, which is the boiling point of xylene, while simultaneously being stirred by a magnetic stirrer bar. After the xylene started boiling, the heat was lowered to allow it to boil gently. The mixture was left at low heat until all the polymer had dissolved. Then, 300 mL of the non-solvent methanol was poured into a beaker for the next step. The hot polymer/hBN/xylene mixture was poured into the methanol quickly with simultaneous, vigorous, stirring resulting in the precipitation of the polymer nanocomposite. The resulting nanocomposites were kept at ambient conditions in a ventilated fume cupboard for 7 days. After the material was taken out of the fume cupboard, it was placed in a vacuum oven with a rotary pump at 60 °C for 3 days, at which point the vast majority of the remaining xylene had evaporated. The material was then melt pressed at 180 °C in order to completely remove any xylene, other by-products or air. This was also done to convert the material into a more compact form, from which it is easier to produce films and samples. All samples were isothermally crystallised from the melt at 115 °C, in a temperature controlled oil bath, for 1 h and, then, directly quenched into water.

6.2.3 Material Formulations

The materials listed in Table 6.1 are denoted by "PEBN/hBN Content/Crystallisation method" where the "PEBN" refers to a polyethylene boron nitride nanocomposite, the "hBN Content" is the weight percent of the used hBN, and the "Crystallisation method" is either '115' or 'Q', where '115' refers to isothermal crystallisation at 115 °C and 'Q' refers to rapid crystallisation by quenching, as seen in Section 6.8.

Table 6.1: Polyethylene/hBN nanocomposite formulations

Material	Polyethylene content (wt %)	hBN content (wt %)	Crystallisation Method
PEBN/0/115	100	0	115
PEBN/2/115	98	2	115
PEBN/5/115	95	5	115
PEBN/10/115	90	10	115
PEBN/20/115	80	20	115
PEBN/30/115	70	30	115

6.3 Thermogravimetric Analysis

TGA was used to confirm the filler content of the nanocomposites. Figure 6.1 shows the TGA curve for all the materials. The results are summarised in Table 6.2, which confirm that all nanocomposites contain the expected amount of hBN, within slight variations, in the polyethylene matrix. Additionally, the curves clearly indicate that the nanocomposites start to degrade at a higher temperature than the unfilled polyethylene, regardless of the filler content. For comparative purposes, taking into account the temperature at which 10% (T_{10}) and 50% (T_{50}) of the material's initial mass has degraded is a good indication of the material's thermal stability. Table 6.2 lists the degradation temperatures of all the materials and their final residues.

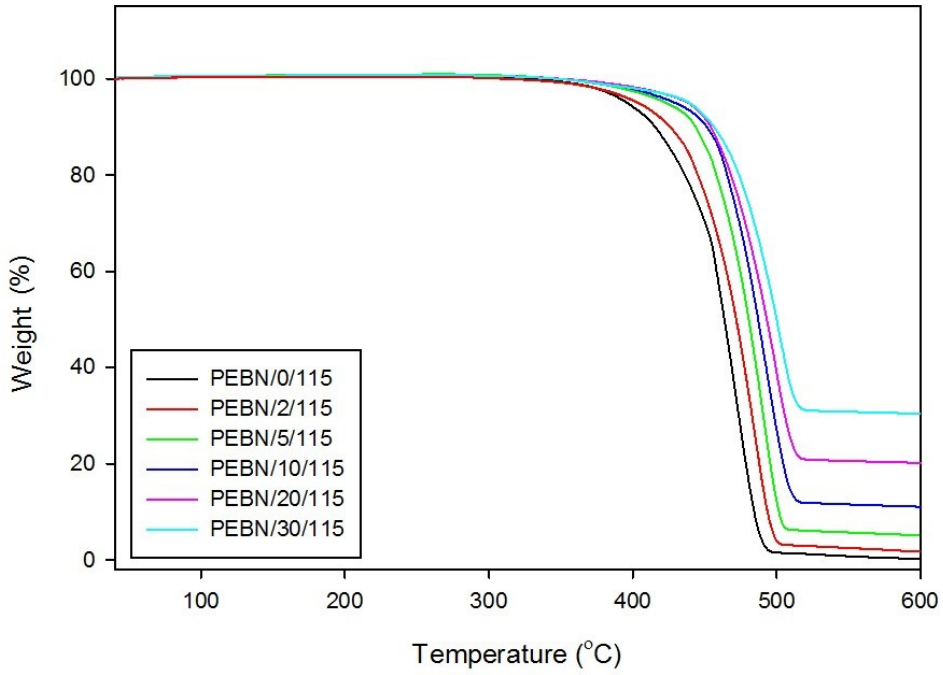

Figure 6.1: TGA curves for the different polyethylene/hBN nanocomposites

Table 6.2: Decomposition temperatures and residue for the polyethylene/hBN nanocomposites

Material	**Residue (wt %)**	**T_{10} (°C)**	**T_{50} (°C)**
PEBN/0/115	0.24	416	463
PEBN/2/115	1.88	425	471
PEBN/5/115	5.17	443	480
PEBN/10/115	11.03	451	487
PEBN/20/115	20.15	454	493
PEBN/30/115	29.99	456	500

Similar to the polystyrene nanocomposites investigated in chapter 5, all the polyethylene/hBN nanocomposites exhibit a higher $T_{10\%}$ and $T_{50\%}$ than the unfilled polyethylene, where the thermal stability improves with increasing hBN content. These results and trend appear to be consistent with other published work related to the thermal degradation of hBN nanocomposites [137], [165]. During the thermal degradation of the nanocomposites, the layers of the hBN act as barriers which limit the diffusion of gases into and out of the polymer nanocomposite. Dash et al. [166] experimentally found that there is a significant reduction in the oxygen permeability in soy/BN nanocomposites with increasing BN content, which confirms the oxygen barrier properties of the hBN layers. This barrier is formed by the hBN layers on the surface, which limits oxygen and heat flow and assists in the formation of char. As a result, layers consisting of boron nitride, which are impermeable to gases, and a thermally stable char are formed on the surface. Their combined effect, which prominently increases with increasing hBN content, further restricts both the diffusion of the volatile products evolved during the degradation of the polymer into the air and the oxygen into the nanocomposites, resulting in a reduced rate of the thermal degradation [165].

6.4 Scanning Electron Microscopy

Figure 6.2 shows representative SEM micrographs of the unfilled polyethylene prepared by isothermal crystallisation at 115 °C. The SEM micrographs clearly show space-filling banded spherulites, developed by the isothermally crystallised HDPE phase, separated from each other by regions of the rapidly quenched LDPE phase. These morphological features are typical of 115 °C isothermally crystallised polyethylene blend systems, which have been reported elsewhere in the literature [164], [167], [168].

The dispersion state of the 2 wt %, 5 wt %, 10 wt %, 20 wt %, and 30 wt % polyethylene/hBN nanocomposites is shown in the SEM micrographs in Figure 6.3, Figure 6.4, Figure 6.5, Figure 6.6, and Figure 6.7 respectively. A large degree of agglomeration is observed in all nanocomposites, more prominently at higher hBN content with 20 wt % and 30 wt % of hBN. The low magnification SEM micrographs in the figures clearly show that the hBN exists in a range of several different sizes, where both the degree of agglomeration and the size of agglomerates becomes larger with increasing amounts of hBN. Additionally, the variation in the hBN particle size becomes larger as the hBN content increases.

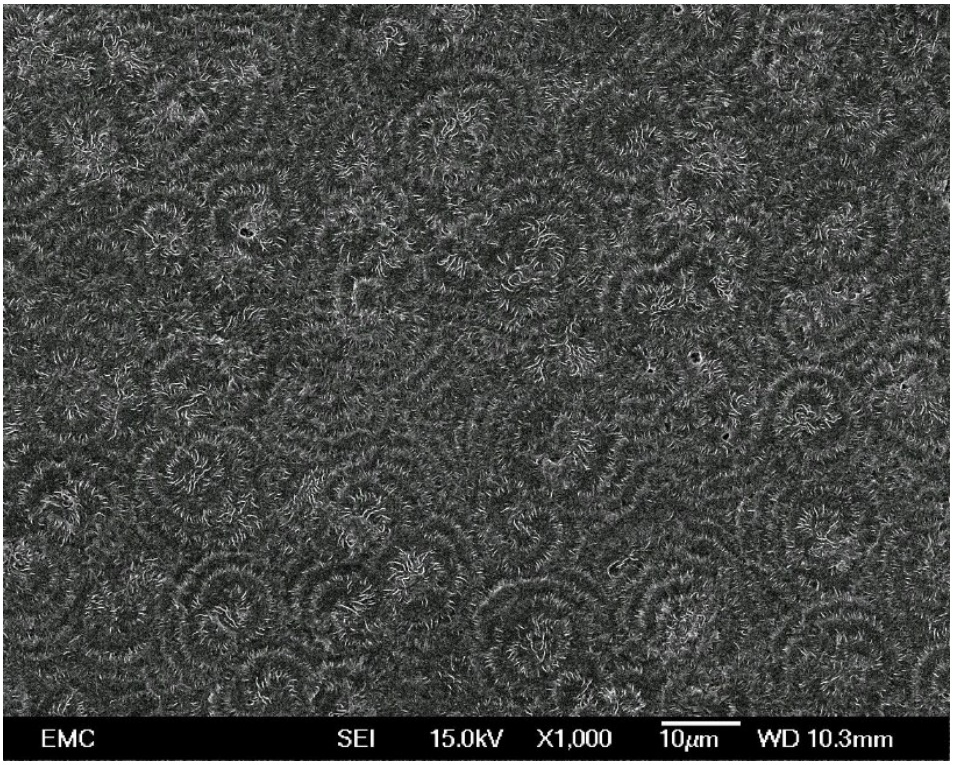

(a)

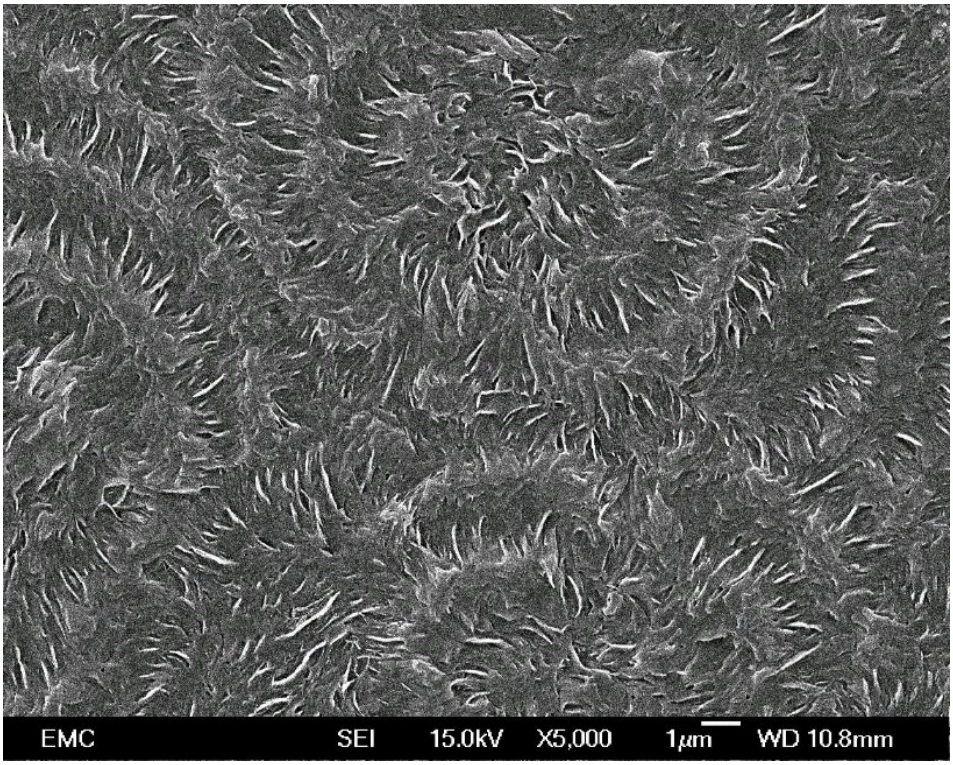

(b)

Figure 6.2: (a) Low magnification, (b) high magnification SEM micrographs of the unfilled polyethylene isothermally crystallised at 115 °C

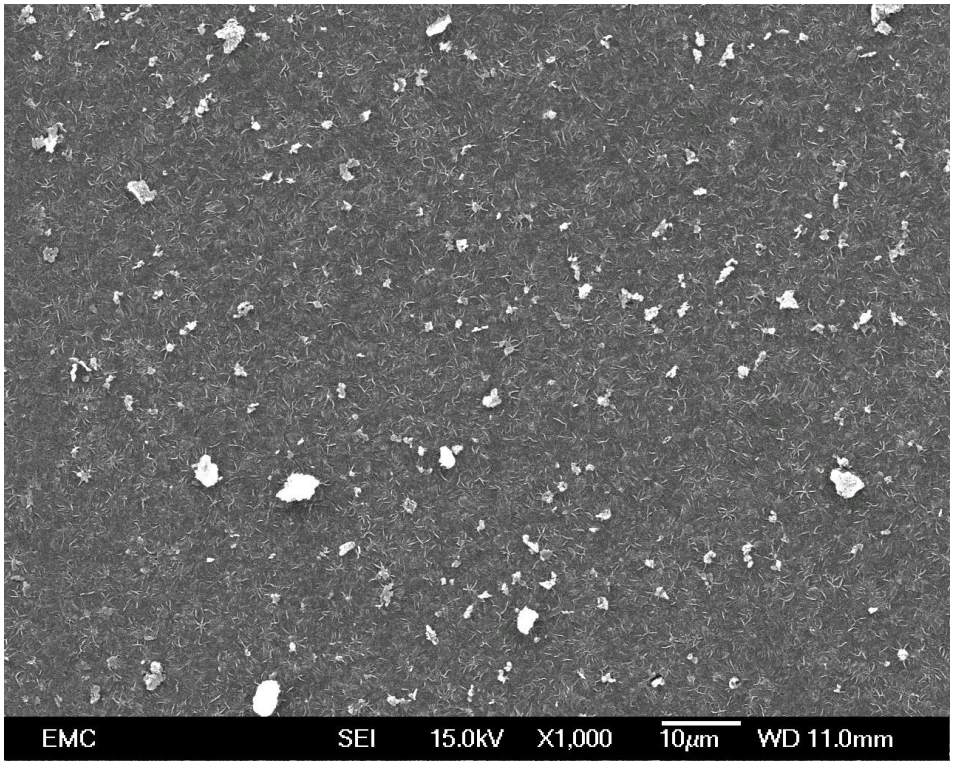

(a)

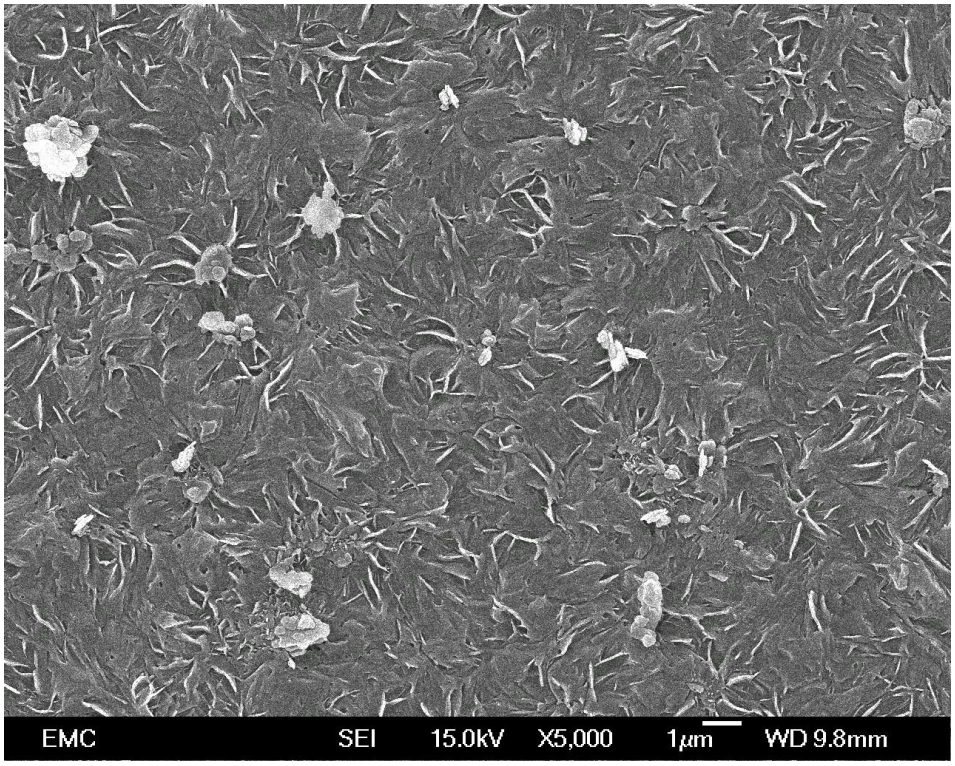

(b)

Figure 6.3: (a) Low magnification, (b) high magnification SEM micrographs of the 2 wt % polyethylene/hBN nanocomposites isothermally crystallised at 115 °C

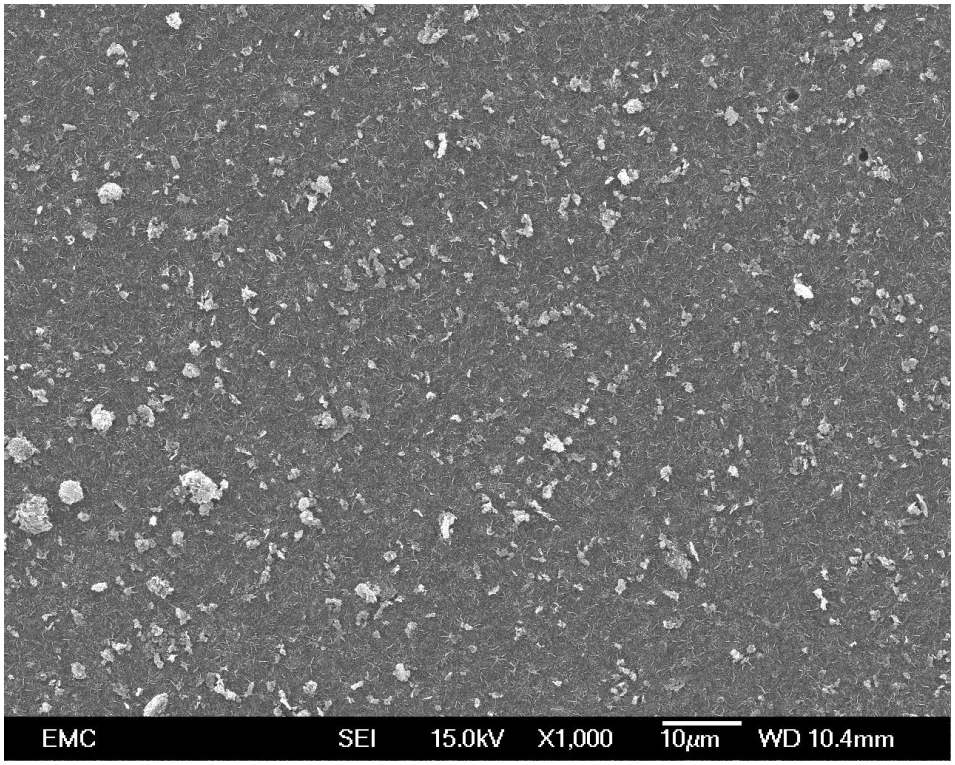

(a)

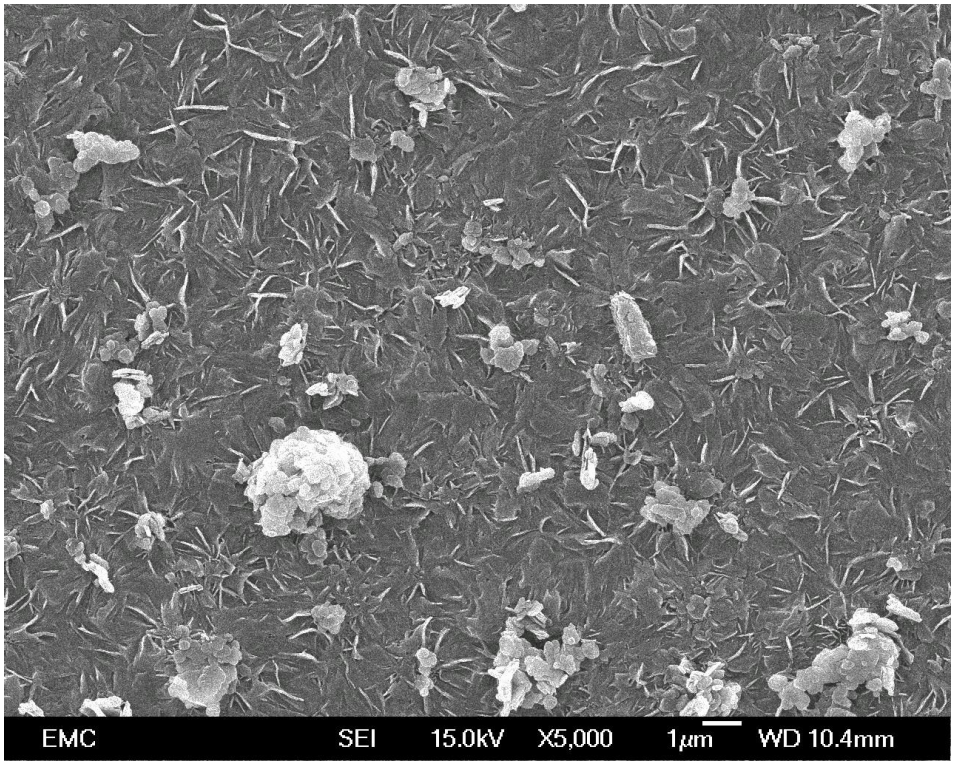

(b)

Figure 6.4: (a) Low magnification, (b) high magnification SEM micrographs of the 5 wt % polyethylene/hBN nanocomposites isothermally crystallised at 115 °C

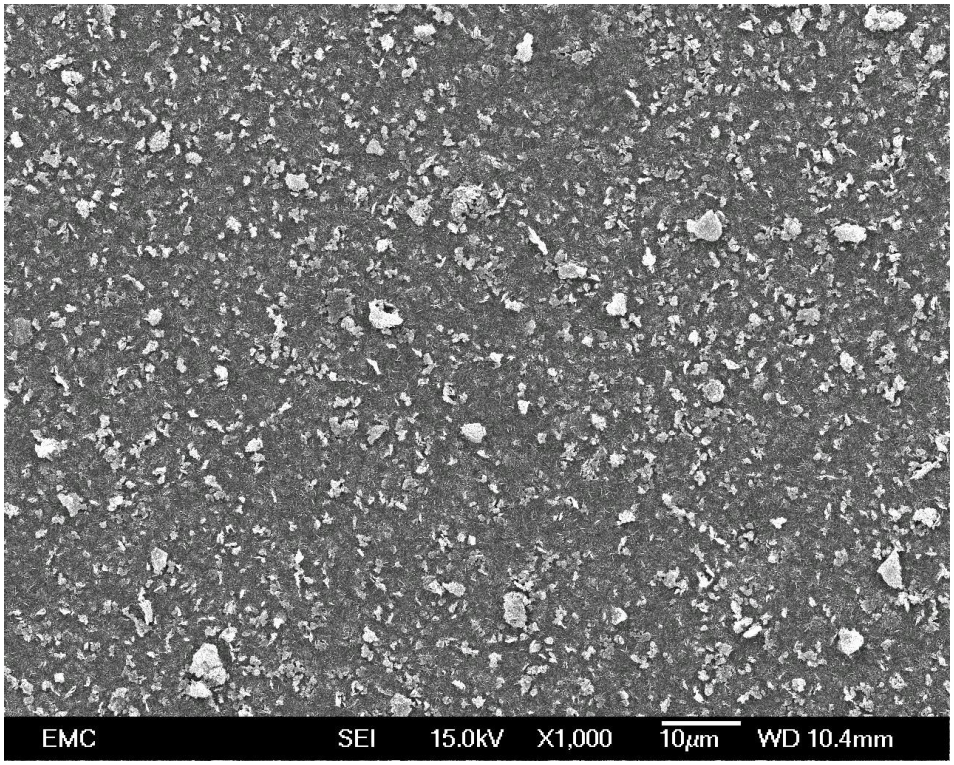

(a)

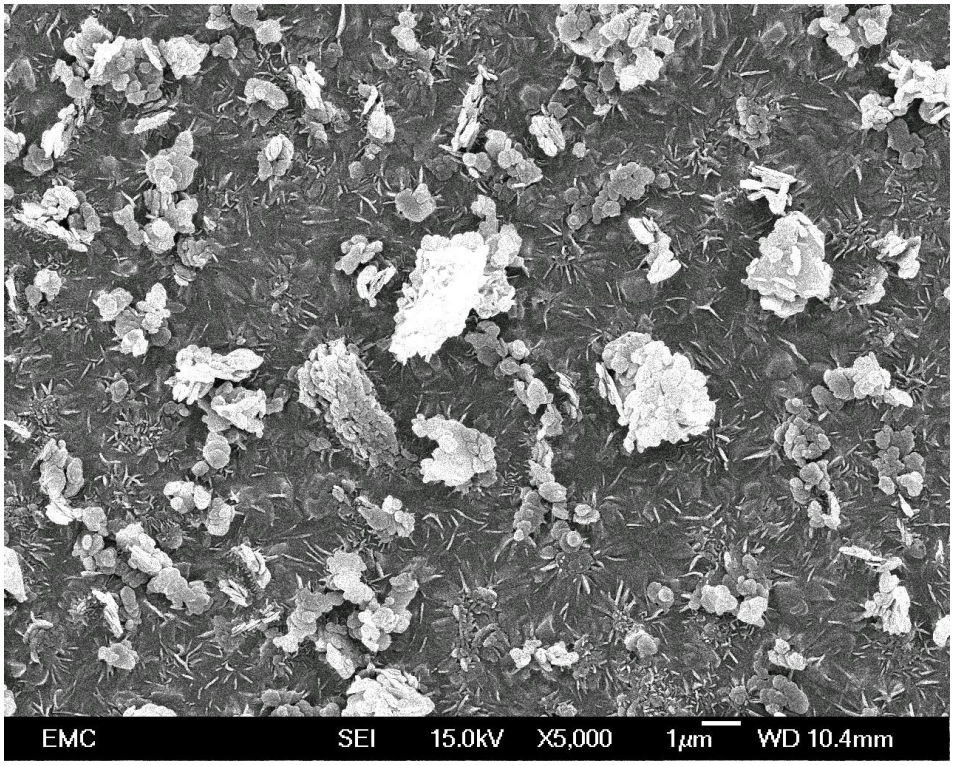

(b)

Figure 6.5: (a) Low magnification, (b) high magnification SEM micrographs of the 10 wt% polyethylene/hBN nanocomposites isothermally crystallised at 115 °C

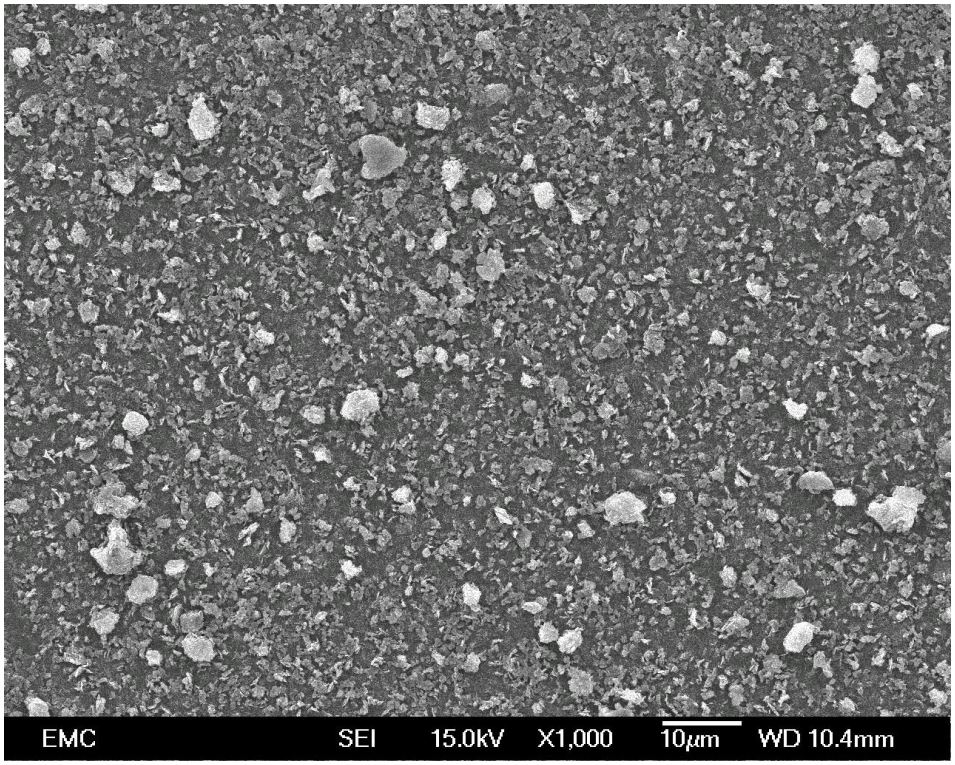

(a)

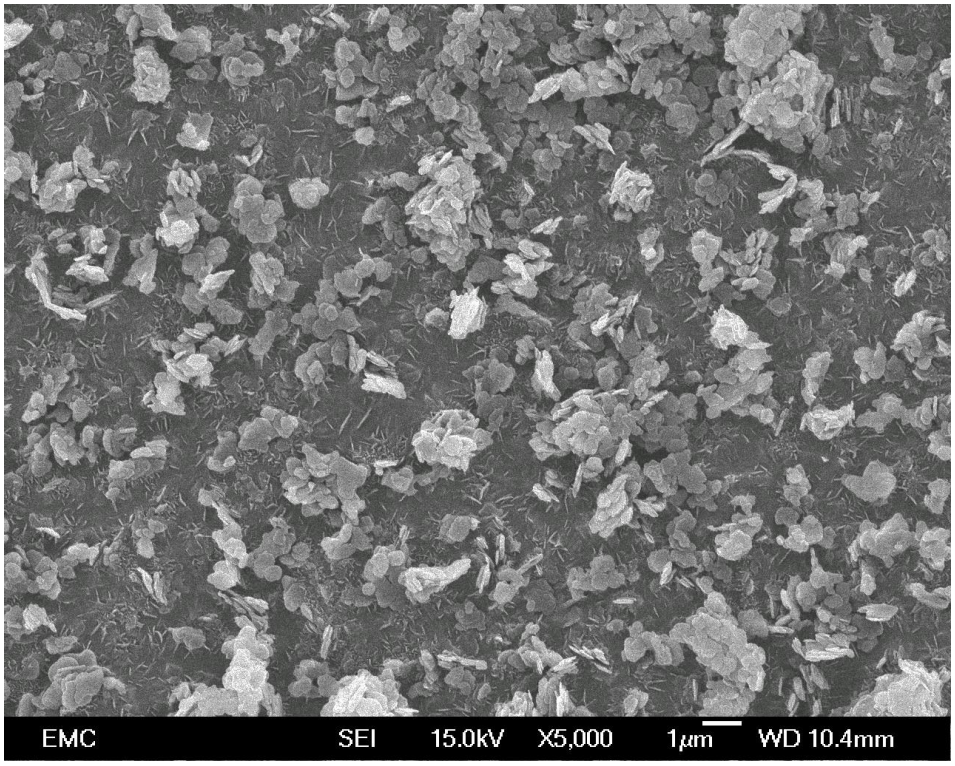

(b)

Figure 6.6: (a) Low magnification, (b) high magnification SEM micrographs of the 20 wt% polyethylene/hBN nanocomposites isothermally crystallised at 115 °C

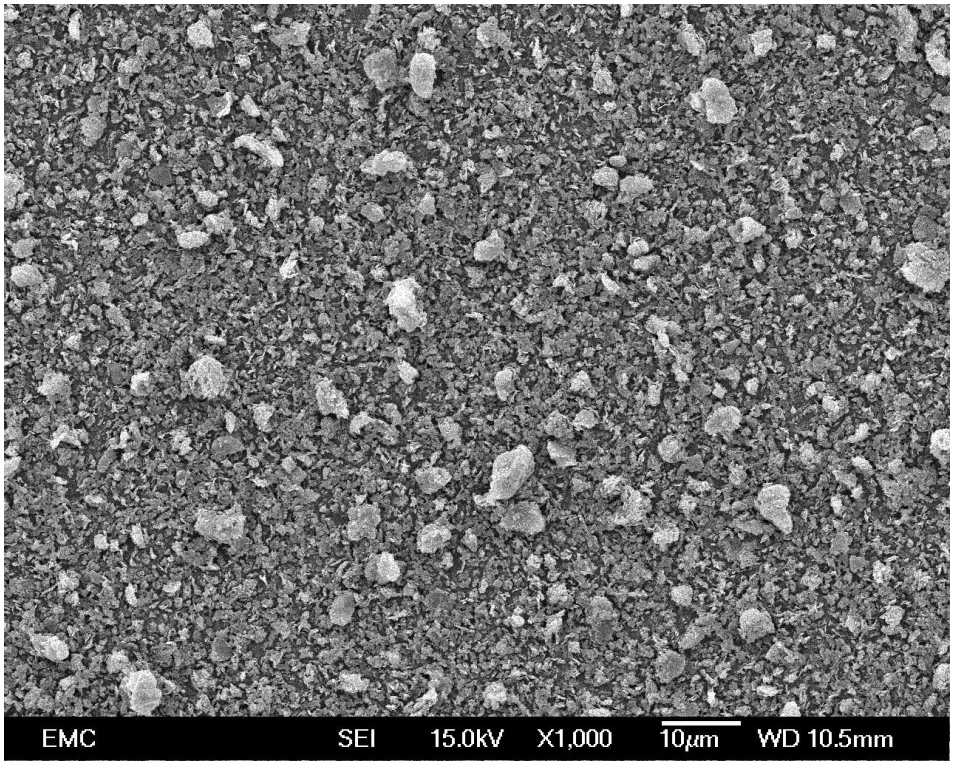

(a)

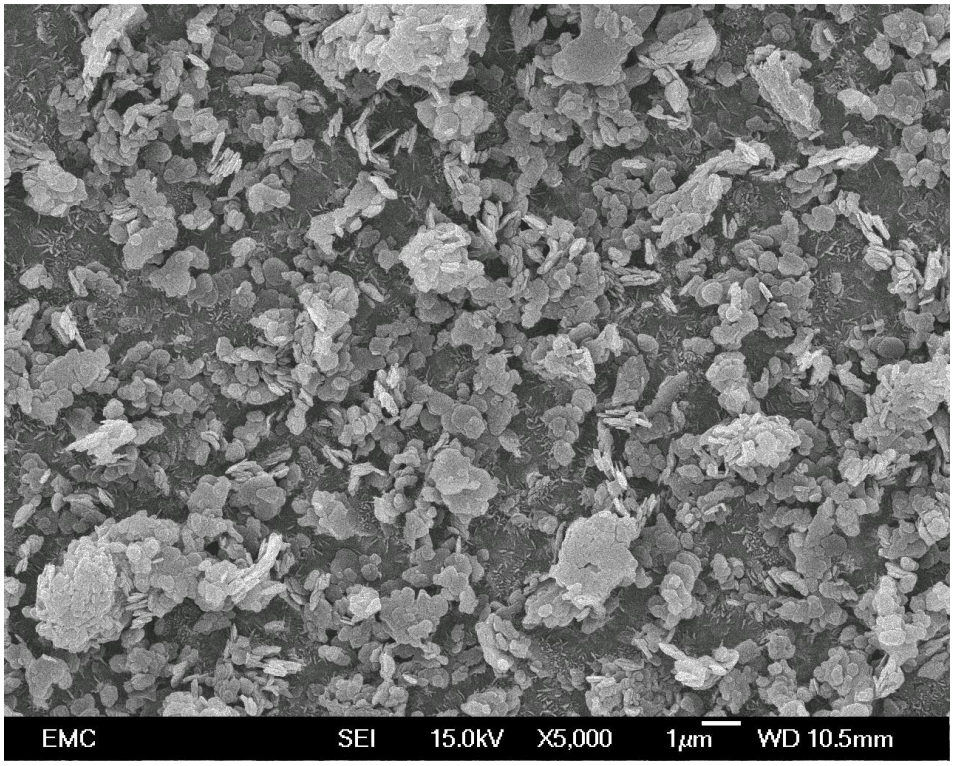

(b)

Figure 6.7: (a) Low magnification, (b) high magnification SEM micrographs of the 30 wt% polyethylene/hBN nanocomposites isothermally crystallised at 115 °C

The high magnification SEM micrographs of the nanocomposites revealed that the aggregates are made up of smaller particles, the hBN platelets, which are agglomerated at different orientations. The structure of the nanocomposites with low and high filler content are fundamentally different. In the low filler content nanocomposites, there are discrete hBN inclusions in a continuous matrix whereas there are regions of a continuous hBN percolating system in the high filler content nanocomposites. Despite the agglomeration, the hBN in all nanocomposites, which consists of some aggregated instead of exfoliated sheets, is uniformly distributed in all regions of the polymer matrix.

There are clear morphological features observed in the isothermally crystallised materials. Low magnification SEM micrographs of the isothermally crystallised nanocomposites showed that the banded spherulites, that were previously seen in the unfilled polyethylene, are no longer visible, even after the addition of small amounts, i.e. 2 wt %, of hBN. The whole texture of the polymer matrix is different to the unfilled polyethylene blend, where there is no evidence of banded spherulites. High magnification SEM micrographs show that there is a much more disordered polymer morphology, relative to the unfilled polyethylene, in the isothermally crystallised nanocomposite.

It is speculated that the change in the morphology upon the addition of hBN particles is due to a very strong nucleating effect brought about by the addition of hBN particles. The incorporation of hBN particles, which act as nucleating sites, cause more spherulites to develop at the same time where they are likely to impinge upon each other, which in turn limits their growth. This results in a disrupted banded spherulitic growth in the morphology, where the spherulites are not circular like the banded spherulites in the pure polyethylene matrix, and this effect becomes more pronounced with increasing hBN loading levels. This could be attributed to the stronger interaction between the boron nitride and the polymer matrix as the hBN content increases due to the increasing nucleating effect. Green et al. [169] found similar observations where they reported that the addition of montmorillonite (MMT) particles into polyethylene resulted in a system with a highly disordered morphology, due to the inhibition of crystal growth, similar to the hBN system studied here. Similar results have been reported by Chan et. al [170] in polypropylene/calcium carbonate nanocomposites, where the SEM images of the unfilled polypropylene showed spherulites 40 μm in size, whereas the nanocomposites with 9.2 vol % of filler showed no spherulites and a completely different morphology. As the extent of morphological disorder in the polyethylene matrix increases with increasing hBN content, the polymer becomes almost featureless at high hBN content and is unrecognisable from the isothermally crystallised unfilled polyethylene, as

seen from the high magnification SEM micrographs. This highly disordered morphology is a result of the ability of hBN to promote nucleation, which in turn limits the ordered growth of banded spherulites.

6.5 X-Ray Diffraction

The XRD pattern of the polyethylene/hBN nanocomposites is shown in Figure 6.8. Two distinct sharp peaks are immediately observed, at 2θ values ~21.4° and at ~23.7°, corresponding to the polyethylene (110) and (200) planes respectively, which agrees well with literature data [171]–[175].

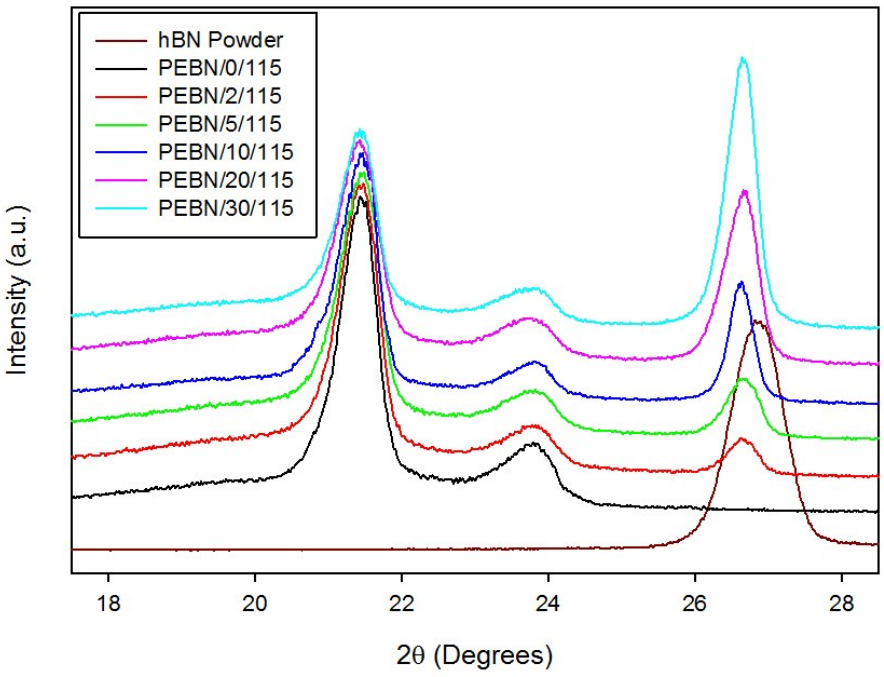

Figure 6.8: XRD patterns for the different polyethylene/hBN nanocomposites

The intensity of the crystalline peak at 2θ = 21.4° decreased with increasing hBN content, as the polymer fraction decreased. Similarly, Malucelli et al. [176] reported a similar observation in 5 wt % LDPE/alumina composites where the decrease in the intensity of the diffraction peak in the nanocomposites, in comparison to the unfilled LDPE, was related to a decrease in crystallinity. While the intensity of the polyethylene crystalline peak decreased with increasing hBN content, the intensity of the peak of the hBN phase of the nanocomposites increased due to the presence of more hBN particles and agglomerates. Similar results were observed in hBN nanocomposites where the intensity of the boron

nitride peak increased with increasing hBN content [177]. A distinct peak at a 2θ value of ~26.6° was present in all nanocomposites due to the presence of the hBN particles. The position of this peak is very close to the position of the peak in the pristine hBN powder which is at a 2θ value of ~26.8°. This suggests very little to no intercalation, similar to the investigated polystyrene/hBN nanocomposites in Chapter 5, as reflected in the interlayer spacing shown in Table 6.3.

Table 6.3: Interlayer spacing of the polyethylene/hBN nanocomposites

Material	**2θ**	**Interlayer spacing (nm)**
hBN	26.8191 °	0.33241
PEBN/2/115	26.5165 °	0.33641
PEBN/5/115	26.5963 °	0.33515
PEBN/10/115	26.5963 °	0.33565
PEBN/20/115	26.6570 °	0.33666
PEBN/30/115	26.6368 °	0.33742

Similar results were observed in polypyrrole/hBN nanocomposites where no difference in the interlayer spacing was reported at different hBN content [144], [178]. In addition, Saggar et al. [177] reported that the hBN peak does not shift to different angles after incorporating hBN into borosilicate glass, similar to the results in this study. This is consistent with SEM micrographs of the nanocomposites presented in Section 6.4, which clearly illustrated the presence of large hBN agglomerates where there is no evidence of intercalation and exfoliation of the hBN platelets. While there is no evidence of intercalation in the hBN nanocomposites, other nanocomposites based on layered particles such as MMT may exhibit different behaviours. For example, Malucelli et al. [179] prepared different modified epoxy/clay nanocomposites which resulted in large increases in the interlayer basal spacing as a result of an intercalated structure. Hwang et al. [180] studied the morphology of ethylene vinyl acetate (EVA)/MMA nanocomposites with MMT content between 1 wt % and 9 wt % using XRD, where an exfoliated layered structure was reported for nanocomposites with all filler loading levels. Similarly, Satapathy et al. [181] also reported the disappearance of the

MMT related peak in the XRD patterns of all epoxy/MMT nanocomposites containing 1 wt % to 10 wt % of MMT, suggesting a highly intercalated or exfoliated structure.

As described in the work of Malucelli et al. [182], the pristine structure of montmorillonite clay is highly polar as it contains metal cations in between the clay layers, which makes it hard to interact with non-polar polymers, and therefore it is necessary to replace these cations with organic groups such that the polymer becomes intercalated in between the clay layers. In contrast, hBN contains a small amount of surface functional groups and therefore prior to any surface treatments of hBN, the introduction of functional groups onto the surface of the hBN particles is required [95]. While surface treatment could enhance the interaction between the boron nitride and the polymer to produce an intercalated structure, the introduction of additional hydroxyl groups might be detrimental to the electrical properties of the nanocomposites and would counteract one of the principal motives of using such a highly hydrophobic particle in this research.

6.6 Differential Scanning Calorimetry

DSC was used as another tool to examine the interactions between the hBN and the polyethylene. Figure 6.9 shows the DSC melting traces for all the materials, where all systems exhibit two melting peaks: a lower temperature peak T_{m_1}, corresponding to the LDPE phase, and an upper temperature peak T_{m_2}, corresponding to the HDPE phase. Similar polyethylene blends have been studied extensively by Hosier et al. [164], [167] where the same observations have been reported. The shape of the melting endotherms in the nanocomposites is similar to the unfilled systems where the addition of any amount of hBN does not seem to affect the melting temperature, however, the shape of the HDPE melting endotherm becomes noticeably broader in the nanocomposites containing a high content of hBN, indicating the presence of high melting temperature polymer fractions.

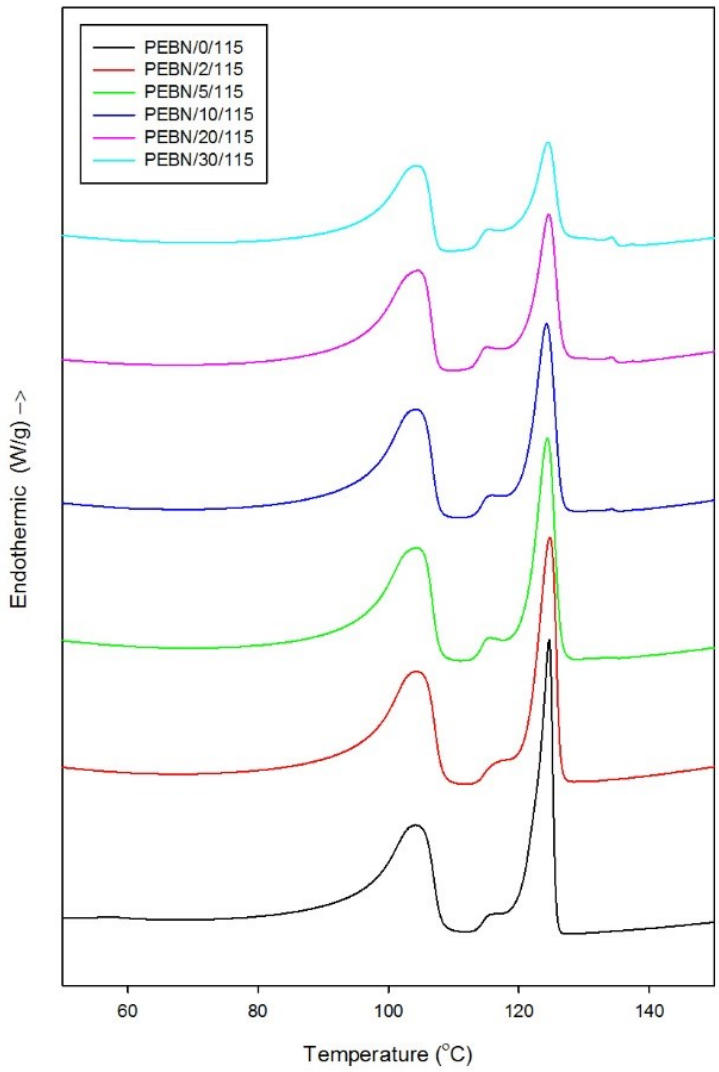

Figure 6.9: DSC melting traces for the polyethylene/hBN nanocomposites

Regarding the crystallisation traces in Figure 6.10, all the materials exhibit two crystallisation peaks: a lower temperature peak T_{c_1}, corresponding to the LDPE phase, and an upper temperature peak T_{c_2}, corresponding to the HDPE phase. The HDPE crystallisation peak is considerably affected even by the addition of small amounts of hBN while the LDPE crystallisation peak is unchanged by the addition of hBN; the crystallisation peak of the HDPE component shifts to higher temperatures with increasing filler content. This suggests that small amount of hBN has a strong nucleating effect on the HDPE component of the polymer matrix where the hBN acts as a nucleating agent providing nucleation sites for the spherulites to grow, which is consistent with the SEM results.

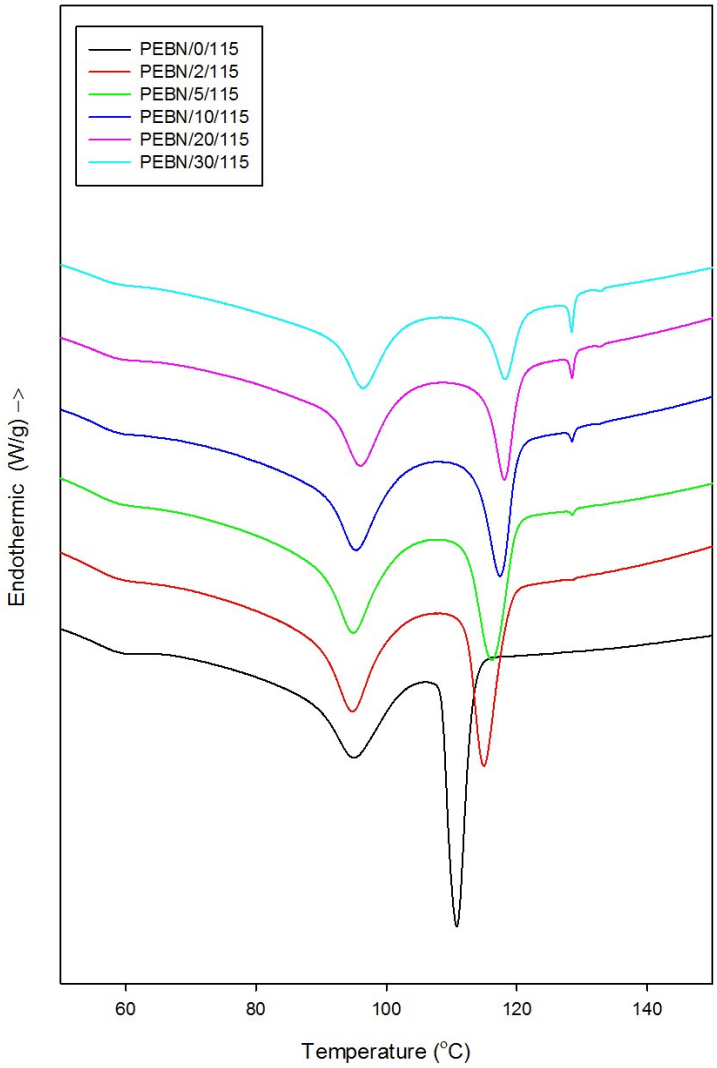

Figure 6.10: DSC crystallisation traces for the polyethylene/hBN nanocomposites

To validate the SEM findings, the crystallinity of the samples was calculated by the following equation:

$$\chi = \frac{\Delta H}{\omega_f \Delta H_0} \tag{6.1}$$

where ω_f is the weight fraction of the polymer, ΔH is the enthalpy of the sample, and ΔH_0 is the enthalpy of a 100% crystalline sample, which was reported to be 286.2 J/g for polyethylene [183].

The crystallinity values, along with the melting and crystallisation temperatures, are listed in Table 6.4. The crystallinity decreases with increasing hBN content, which is consistent with the SEM data, where the presence of the hBN appeared to largely hinder the crystal growth, which resulted in a highly disordered morphology.

Table 6.4: Melting temperature, crystallisation temperature, and crystallinity of the polyethylene/hBN nanocomposites

Material	T_{m_1}(°C)	T_{m_2}(°C)	T_{c_1}(°C)	T_{c_2}(°C)	χ (%)
PEBN/0/115	104.2	124.7	95.1	110.8	55.4
PEBN/2/115	104.2	124.7	94.7	115.0	49.1
PEBN/5/115	104.4	124.4	94.9	116.2	47.3
PEBN/10/115	104.2	124.2	95.3	117.4	44.1
PEBN/20/115	104.5	124.5	95.7	118.1	37.3
PEBN/30/115	104.3	124.5	96.1	118.7	28.6

An unexpected third crystallisation exotherm is observed at ~128 °C, which grows larger with increasing filler content, was also observed in Figure 6.10. While this effect is not generally observed in nanocomposite systems, the exact behaviour has been reported in the work of Zhang et al. [184], where they studied the crystallisation behaviour in PE/BN nanocomposites containing up to 50 wt % of hBN, so the results in this work are consistent with published data. The DSC melting traces in Figure 6.9 showed that the HDPE melting peak is broadened out as the hBN content increased, to produce a larger distribution of polyethylene crystal sizes that have melting temperatures up to 134 °C, which corresponds to the third crystallisation peak at 128 °C that was seen in the DSC crystallisation traces in Figure 6.10. The origin of this peak could also be due to the strong nucleating effect of the hBN particles. This strong nucleating effect of hBN has been reported by Puente et al. [185] where they reported that the addition of only 0.2 wt % into a poly (3-hydroxybutyrate)

polymer increased the crystallisation temperature from 91 °C to 121 °C, and this crystallisation temperature increased with increasing hBN content, thus exhibiting a very strong nucleating effect. Boron nitride particles have also been reported to behave in a similar manner in poly(3-hydroxybutyrate-co-3-hydroxyvalerate) and in poly(3-hydroxybutyrate-co-4-hydroxybutyrate) [186] polymers, in which they acted as highly effective nucleating agents. Therefore the polyethylene in this study appears to be rapidly forming crystals with different thicknesses, that take different times to crystallise, and thus a small amount is crystallising at these high temperatures. It could be that the highly crystalline nature of hBN provides a highly effective surface which largely increases the nucleation site density that enables the polymer to crystallise faster.

6.7 Dielectric Spectroscopy

The permittivity and dielectric losses are important parameters in the design of electrical insulation, and therefore it is necessary to study how they are affected upon the addition of hBN particles. Figure 6.11 shows the real relative permittivity of all the nanocomposites, where the unfilled polyethylene exhibited a real relative permittivity ~2.3 across the entire frequency range, which is consistent with published work on the dielectric response of polyethylene [77], [187]. The real relative permittivity behaviour of polyethylene is similar to the behaviour of polystyrene, where the permittivity is frequency independent. Polyethylene is non-polar and contains no permanent dipoles, therefore the only contributions to the permittivity are from an instantaneous, very high frequency electronic polarisation process [188]. The real relative permittivity of the nanocomposites increased with increasing hBN content, from ε_r' ~2.3 in the unfilled polyethylene to ε_r' ~2.8 in the nanocomposite containing 30 wt % of hBN, and a similar trend in epoxy/hBN composites has been reported previously [51]. In contrast, the real relative permittivity of dry polyethylene/silica nanocomposites has been shown to exhibit a different behaviour than the unfilled polyethylene where the permittivity increased with decreasing frequency [77], [187].

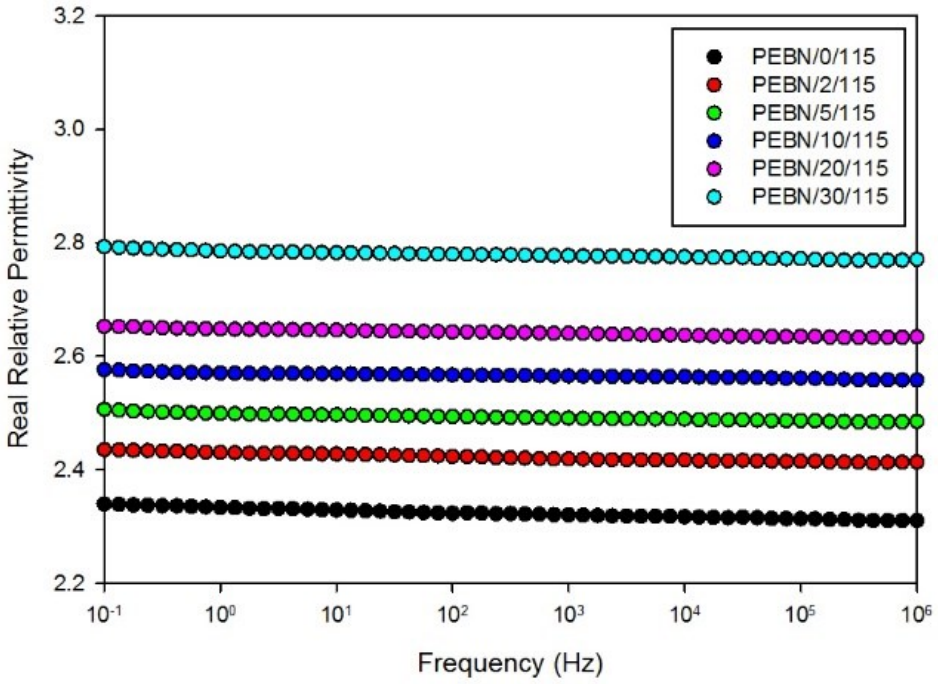

Figure 6.11: Real relative permittivity of the polyethylene/hBN nanocomposites

In order to confirm that this increase in permittivity is due to the presence of hBN itself, theoretical models were used to predict the permittivity of the hBN particles. Many theoretical models have been developed to determine the effective permittivity of a composite system. To examine the effect of adding hBN particles on the permittivity of the polyethylene/hBN nanocomposites, the Lichtenecker-Rother, Maxwell-Garnett, and Bruggeman effective medium equations [189], [190] have been used to determine the permittivity of the hBN.

The Lichtenecker-Rother equation is expressed as:

$$log\varepsilon_c{}' = \phi_p log\varepsilon_p{}' + (1-\phi_p) log\varepsilon_m{}' \tag{6.2}$$

The Maxwell-Garnett equation is expressed as:

$$\frac{\varepsilon_c{}' - \varepsilon_m{}'}{\varepsilon_c{}' + 2\varepsilon_m{}'} = \phi_p \frac{\varepsilon_p{}' - \varepsilon_m{}'}{\varepsilon_p{}' + 2\varepsilon_m{}'} \tag{6.3}$$

The Bruggeman equation is expressed as:

$$\frac{\varepsilon_c' - \varepsilon_m'}{\varepsilon_m' + 2\varepsilon_c'} = \frac{\phi_p}{1-\phi_p}\frac{\varepsilon_p' - \varepsilon_m'}{\varepsilon_p' + 2\varepsilon_c'} \tag{6.4}$$

where ϕ_p is the volume fraction of the particles, ε_p', ε_m', and ε_c' represent the real relative permittivity of the particle, the matrix, and the composite respectively.

At a fixed value of ε_m', the value of ε_c' varies with ϕ_p and thus the value of ε_p' can be calculated from the above equations. These models have been used to obtain the permittivity of the hBN particles by fitting the experimental data obtained from dielectric spectroscopy; the values of ε_m', ε_c' and ϕ_p are used from the dielectric spectroscopy data, which have been determined experimentally to produce a best-fit value of ε_p'. Plots of ε_c' as a function of ϕ_p are shown in Figure 6.12 with the best fit values of ε_p' containing 95% confidence bounds in all the three different equations. The best fit curves with 95% confidence bounds are shown in Figure 6.12 for the volume fractions of hBN that were used experimentally, and the extrapolated data are shown in Figure 6.13. The best fit values of ε_p' that conforms to the equations of the different models are listed in Table 6.5.

Table 6.5: Permittivity of hBN from the different models

Effective Medium Model	**Particle (hBN) Permittivity ε_p'**
Lichtenecker-Rother	5.81 ± 1.27
Maxwell-Garnett	5.49 ± 1.12
Bruggeman	8.51 ± 2.92

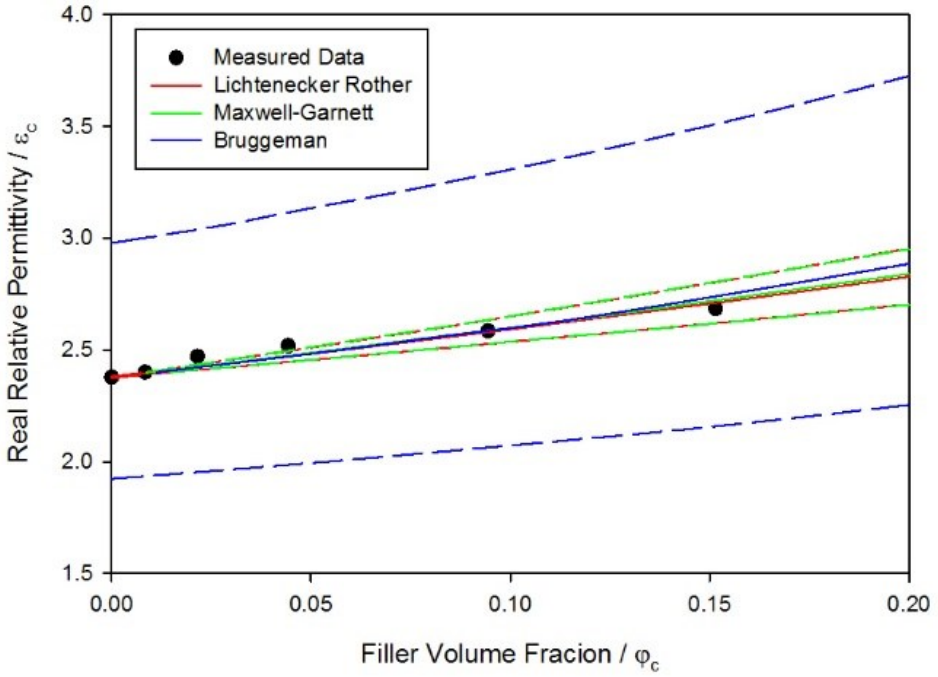

Figure 6.12: Real relative permittivity for the measured filler volume fractions

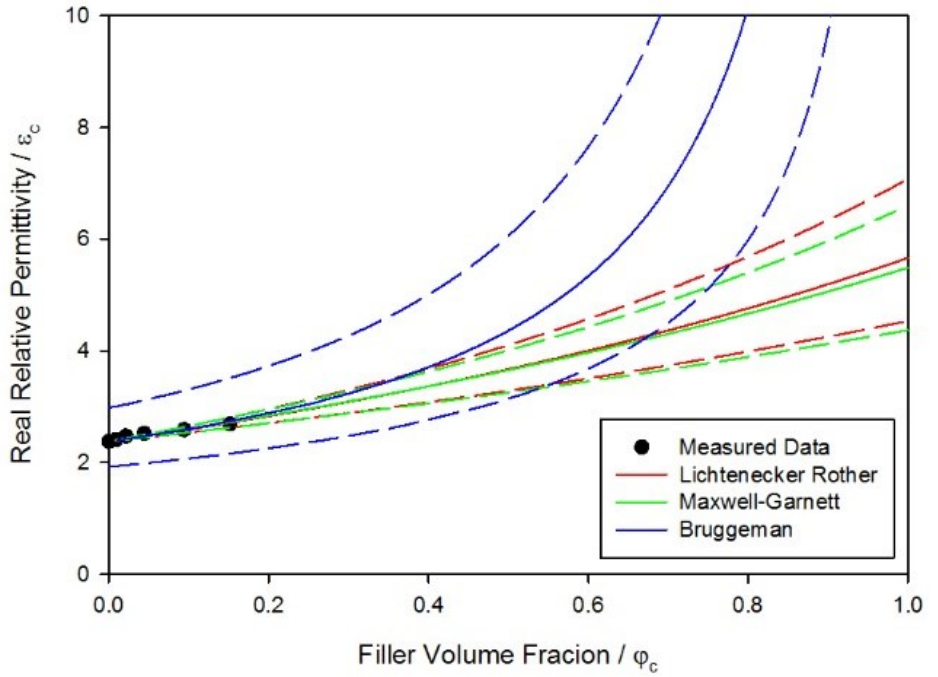

Figure 6.13: Extrapolated data for the rest of the filler volume fractions

The permittivity data is entirely consistent with a two phase model described by Lichtenecker-Rother and Maxwell-Garnett, although the Bruggeman model seems to yield high values of permittivity and appears to diverge to infinity with increasing filler volume, as observed from the extrapolated data; therefore it is not as reliable as the other two models which have also been reported by others for composite systems [191], [192]. The permittivity of hexagonal boron nitride has been reported in literature by a few researchers. For example, Kim et al. [193] reported a value of permittivity of hBN between 2 - 4, while Zhang et al. [194] reported a value of 4 - 5. Other researchers have reported permittivity values of ~4 of hBN particles [108], [195]. Thus the permittivity values of hBN obtained from these models agree with the literature data when the lower confidence bounds are considered, which explains the increase in real permittivity with increasing hBN loading level observed in the dielectric spectroscopy data.

To evaluate the dielectric losses of the materials, the imaginary relative permittivity of the materials was investigated and shown in Figure 6.14 as a function of frequency. The imaginary permittivity of the unfilled polyethylene is frequency independent and is characterised by very low losses (~$5x10^{-3}$), which appear as scattered data points at the noise limit of the equipment. In the hBN nanocomposites, the imaginary relative permittivity, and hence dielectric losses, slightly increased in the low frequency range although this increase cannot be validated as it is within the noise limit of the equipment. If there is indeed an increase in the imaginary permittivity at low frequencies, it may be attributed to a Maxwell/Wagner/Sillars interfacial polarisation process, where the low frequency contributions are a result of charge accumulation at the polyethylene/hBN interface or, alternatively, it may be due to electrode polarisation, where charge accumulation occurs at the electrode/sample interface [17].

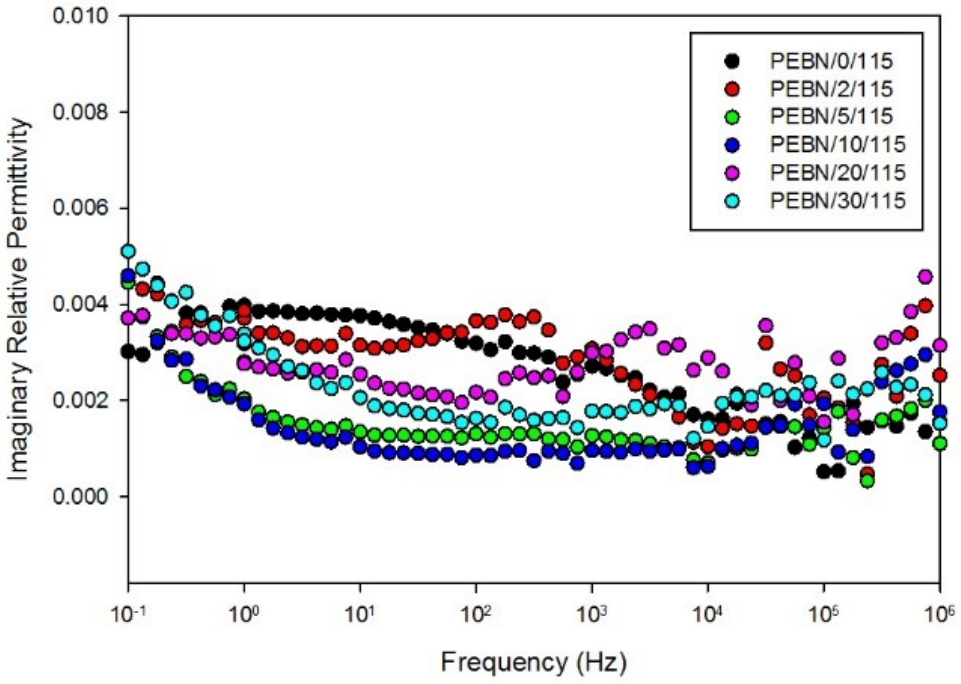

Figure 6.14: Imaginary relative permittivity of the polyethylene/hBN nanocomposites

The effect of interfacial polarisation is expected to become larger as a high amount of hBN is added, as more particles result in larger agglomerates and a higher possibility of charge build up. Although there is a slight increase in the imaginary permittivity at low frequencies, it is a very small increase, and within the noise limit of the equipment, and therefore the materials are characterised by very low losses that are comparable to the unfilled polyethylene. In contrast, polyethylene/silica nanocomposites [77], polyethylene/silicon nitride nanocomposites [187], and polyethylene/MMT nanocomposites [196] have been reported to exhibit much higher low frequency losses, even at a 10 wt % of filler. It is therefore surprising and extremely useful that the hBN nanocomposites, even at high hBN content up to 30 wt %, do not exhibit increased dielectric losses in comparison to the unfilled polyethylene. A thorough discussion of the dielectric response is provided in Chapter 7, where the effect of water is taken into account to further understand this behaviour.

6.8 Dielectric Breakdown Strength

The dielectric breakdown strength of all the materials was measured to examine the effect of the dispersion and aggregation state of the hBN. A representative Weibull plot for all the

polyethylene/hBN nanocomposites is shown in Figure 6.15, and the Weibull parameters are listed in Table 6.6.

Table 6.6: Weibull parameters of all the polyethylene/hBN nanocomposites

Material	**Scale parameter α (kV/mm)**	**Shape parameter β**
PEBN/0/115	162 ± 5	13 ± 4
PEBN/2/115	157 ± 4	19 ± 5
PEBN/5/115	163 ± 4	18 ± 5
PEBN/10/115	167 ± 6	11 ± 3
PEBN/20/115	179 ± 6	12 ± 4
PEBN/30/115	185 ± 4	21 ± 6

It can be seen that the 2 wt % nanocomposite exhibited a slightly lower breakdown strength than the unfilled polymer. However, it could be argued that they are equivalent due to the very similar breakdown values when the uncertainties from the confidence bounds are considered. Conversely, increasing the loading level above 2 wt % improved the breakdown strength compared to the unfilled polyethylene blend, where the breakdown strength monotonically increased with increasing hBN content from 5 wt % up to 30 wt %.

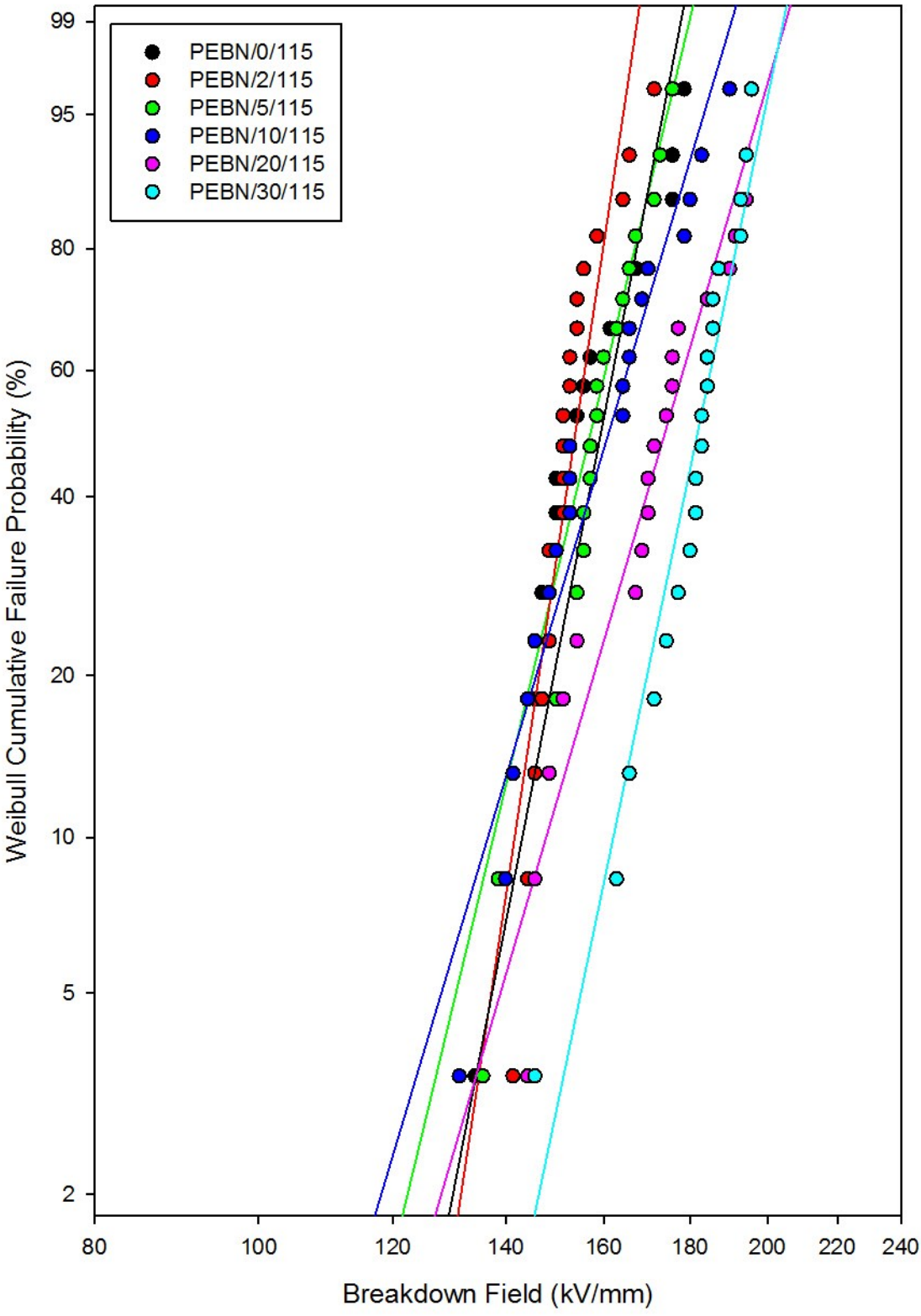

Figure 6.15: Weibull plots of the polyethylene/hBN nanocomposites

As mentioned in the previous chapter, the results in the literature regarding the breakdown strength of boron nitride composites are limited [60]–[62], [67], [69], [160], [161], and these results generally report that the incorporation of hBN particles results in an improved electrical performance. The effect of filler loading has been studied in a wide range of other systems by different researchers. For example, while Zazoum et al. [197] noticed an increase in breakdown strength in PE/clay nanocomposites at a 5 wt % of clay, Lioa et al. [198] only reported a maximum increase in breakdown strength at a 1 wt % MMT content in LDPE/MMT composites, and a reduction in breakdown strength at 3 wt % and 5 wt % of MMT content. Singha et al. [18] found that adding 0.1 wt % of titania and alumina fillers in epoxy significantly reduced the breakdown strength as compared to the pure epoxy. An interesting observation is that the breakdown strength in the titania nanocomposites decreased with titania content up to 0.5 wt %, then it started to increase with increasing filler content up to 10 wt %, although it was still lower than the breakdown strength of the pure epoxy. Gao et al. [199] tested the dielectric breakdown strength of epoxy/silica nanocomposites where they observed an increase in breakdown strength with increasing silica content up to 5 wt %, and then a significant decrease with further quantities of silica was observed. Singha et al. [18] reported that introducing any amount of filler caused a reduction in the breakdown strength in epoxy nanocomposites based on titania and alumina fillers. Calebrese et al. [200] found that the breakdown strength of polyamide-imide/alumina nanocomposites increased to a maximum by adding 7.5 wt % of alumina, and any further addition of alumina resulted in a decrease in breakdown strength, which was attributed to the poor particle dispersion. In contrast to the systems reported in the literature, the polyethylene/hBN nanocomposites in this research exhibited an enhanced breakdown strength despite the high loading level of hBN, which again suggests that this is specifically due to the boron nitride particles.

Where percolation effects are considered, a significant decrease in breakdown strength was almost always reported. For example, Grabowski et al. [58] has shown that adding up to 45 vol % of silica in PMMA significantly reduced the breakdown strength from ~800 V/μm to ~340 V/μm. An increase in breakdown strength was reported by Siddabattuni et al. [201] in 5 vol % epoxy/TiO_2 and epoxy/$BaTiO_3$ nanocomposites, containing surface modified titania and barium titanate nanoparticles, followed by a drastic reduction in breakdown strength at percolation when 15 vol % and 30 vol % of the particles were added. The breakdown strength of other $BaTiO_3$ based nanocomposites has been shown to drastically reduce at the percolation threshold [59]; a 20 vol % addition of $BaTiO_3$ in poly(vinylidene

fluoride-co-hexafluoro propylene) reduced the breakdown strength from ~380 V/μm to ~230 V/μm. The decrease in breakdown strength reported by many researchers was almost always attributed to the presence of large agglomerates at high filler loading levels that tend to form conductive pathways for the charge carriers; however, no clear correlation between the two properties has yet been established. The SEM images of the nanocomposites in this study clearly showed that there is a percolating network at high hBN content and almost all studies in the literature have reported that percolating systems always result in the deterioration of electrical properties. The formation of percolating networks at high filler contents creates electrically conductive pathways, allowing charge carriers to easily move through them, and therefore leading to a lower breakdown strength and high electrical conductivity. Therefore, the results presented here are peculiar as they clearly show that the percolation of hBN does not have a detrimental effect on the breakdown strength, where the charge transport is expected to occur in a system with continuous interfaces. As a result, the breakdown data are completely unexpected according to all the published literature as the opposite effect is always reported. The classical analysis is that once nanoparticles are added into a polymer, they tend to agglomerate and once they agglomerate the electrical properties of the nanocomposite deteriorates. However, this is clearly not the case as the breakdown strength improved although the system is agglomerated and percolating. Therefore, it is highly likely that the breakdown strength and charge transport have less to do with the distribution of the nanofiller and much more with how the nanofiller interacts with the charge carriers. The results presented above are therefore highly unexpected and clearly suggest that the dispersion of the boron nitride is not the main factor to consider when trying to improve the electrical properties in boron nitride based nanocomposites.

There can be many different possible mechanisms responsible for the electrical breakdown polymer nanocomposites. It has been suggested that the change in morphology of the polymer upon the addition of nanoparticles highly affects the interfacial regions in the material, which can increase the density of charge traps and effectively change the breakdown behaviour [202], [203]. The effect of clays on the morphology of polyethylene has been studied previously by Vaughan et al. [204], [205] who reported an increase in the breakdown strength in a 10 wt % polyethylene/MMT nanocomposites, where the MMT had no effect on the morphology of polyethylene. However, in another system containing a different grade of MMT, the nanocomposite was found to have a strong nucleating effect on the polyethylene, which inhibited crystal growth, resulting in a reduced spherulites size, but exhibited no change in breakdown strength although the MMT particles were well dispersed.

In another study, the presence of silica in polyethylene was shown to enhance nucleation, although it did not affect crystal growth, yet no changes in breakdown strength were reported [206]. While the breakdown strength may be affected by the changes in morphology, there does not appear to be a precise relationship between the two parameters. The SEM and DSC data clearly demonstrated the hBN particles considerably changed the morphology of the polyethylene matrix, which in turn could possibly be linked to this change in breakdown behaviour. In order to determine whether the breakdown strength observed here is due to the changes in polyethylene morphology or due to the presence of the hBN particles, another set of polyethylene/hBN nanocomposites were prepared, where the samples for breakdown testing were rapidly crystallised by direct quenching into ice water, rather than slow isothermal crystallisation, to minimise any morphological effects. The resulting SEM micrographs and DSC data of the unfilled quenched polyethylene and the quenched nanocomposites are shown in Appendix B, which showed very little structural detail and no change in crystallinity in all the samples, as the formation of spherulites has been suppressed by rapid crystallisation. It was seen that the trend in breakdown in the quenched samples is very similar to the isothermally crystallised samples, as shown in Figure 6.16.

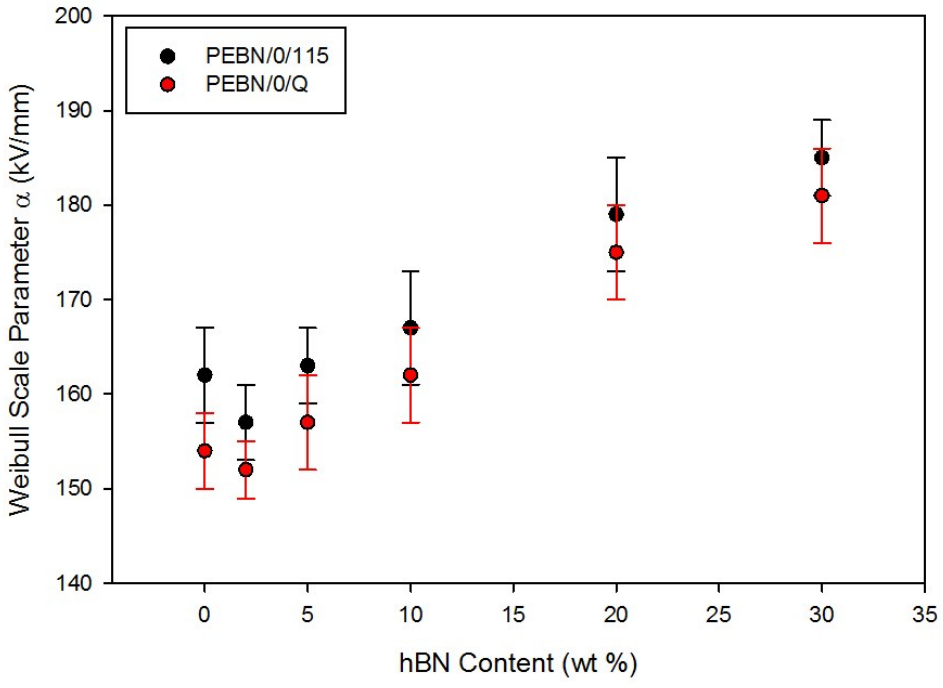

Figure 6.16: Relationship between hBN content and the breakdown strength in the isothermally crystallised and quenched polyethylene/hBN nanocomposites

There is a monotonic increase in the breakdown strength with increasing hBN content in the quenched samples, which follows the same trend observed in the isothermally crystallised samples. As both systems exhibit the same trend in breakdown strength, this suggests that the change in morphology of the isothermally crystallised systems does not play a major role in determining the breakdown strength behaviour, as the breakdown behaviour was unaffected in systems with the same crystallinity degree and in systems with a varying degree of crystallinity.

Since breakdown mechanisms as a result of morphological changes are unlikely in this case, it is necessary to determine other possible breakdown mechanisms. Nanoparticles, especially in the form of layered nanoplatelets, are thought to act as physical barriers which inhibit the propagation of electrical trees [207]–[209]. When the nanoplatelets are efficiently dispersed in the polymer matrix, the electrical tree will follow a tortuous path growing around the platelets which causes a longer time for the tree to reach the lower electrode, and thus a higher breakdown strength is observed. The effectiveness of the nanoparticles as electrical barriers could be determined by the breakdown strength of the nanoparticles relative to the surrounding polymer. If the breakdown strength of the particles is much lower than the polymer, the electrical tree may just penetrate the particles instead of propagating around it whereby the particles no longer act as barriers. The breakdown strength of hexagonal boron nitride particles has been reported to be in the range of 800 kV/mm to 1200 kV/mm [210], [211], which is much higher than the breakdown strength of polystyrene (~190 kV/mm) and polyethylene (~160 kV/mm), and therefore the tree will grow around the hBN electrical barriers, that is if the improved breakdown in the polystyrene/hBN and polyethylene/hBN nanocomposites is attributed to the inhibition of the tree propagation due to the barrier effect of the hBN platelets. However, electrical treeing is a long term process which is unlikely to occur in this type of short term breakdown strength test method employed in this study, and therefore this mechanism which is widely reported in the literature is excluded in this case.

While the idea of hBN particles, or any particle, acting as barriers to electrical trees does not hold true in short term breakdown strength tests, the idea of nanoparticles acting as traps for charge carriers, which effectively improve the breakdown behaviour, has been discussed thoroughly in the work of Li et al. [202], [212], [213] as a mechanism for enhanced breakdown strength. The term “trap” is typically associated with physical and chemical defects within the polymer, which can ultimately trap charge carriers and lower their energy state. Ishimoto et al. [214] found that the polyethylene nanocomposites containing micro and nano magnesium oxide exhibit a lower electrical conductivity than unfilled polyethylene,

which was explained by the presence of traps at the interface which capture the charge carriers. Similar results have been reported in the work of Roy et al. [215] where they investigated the electrical properties of silica/XLPE nanocomposites and experimentally confirmed that the nanocomposites introduced traps which act as scattering centres to reduce the mobility of charge carriers. Wang et al. [216] studied the relationship between the breakdown strength and charge trapping behaviour in polyethylene/alumina nanocomposites, where they experimentally determined the trap depth and trap density of the nanocomposites. The addition of 1 wt % and more alumina particles decreased the trap depth and trap density, which resulted in a decrease in breakdown strength. However, the addition of 0.5 wt % alumina nanofiller increased the trap depth and trap density, which effectively reduced the mobility of the charge carriers and increased the breakdown strength. The origin of these traps is usually associated with the chemical interactions between the surface functional groups of the nanoparticles and the polymer at the interface due to surface functionalisation of the nanoparticle [202].While the hBN particles could trap the charge carriers, the scarce amount of surface functional groups on hBN would therefore suggest that the increase in breakdown strength may not be solely due to the presence of charge traps. Therefore, it is proposed that the hBN platelets may not only trap charges, but they are most likely acting as electron scattering centres, which is a more probable than acting as barriers to electrical trees [215]. The platelet structure of hBN, as opposed to the spherical structure of many nanoparticles, could therefore act as effective scattering sites for charge carriers, causing a reduction in the mobility of the charge carriers, and therefore conduction current, which in turn increases the energy required for breakdown, and hence leading to an improved breakdown strength. Furthermore, the hBN platelets could suppress charge injection from the electrodes, which subsequently limits the mobility of the charge carriers in the polymer nanocomposite [212], and therefore effectively increasing the electric field required for the sample to breakdown.

6.9 Thermal Conductivity

As it was suggested that the most likely cause for the increased breakdown strength in the hBN nanocomposites is due to an electron scattering effect, other factors could also simultaneously lead to this enhanced performance. The thermal conductivity of an insulator is an important parameter to consider as it can have an effect on its breakdown strength. The thermal conductivity of LDPE and HDPE is ~0.33 W/m.K and ~0.45 W/m.K respectively [217] whereas the thermal conductivity of hBN is ~200 W/m.K [56]. As the thermal

conductivity of hBN is over 400 times larger than the thermal conductivity of polyethylene, the addition of hBN in the polymer matrix is expected to significantly increase the thermal conductivity of the resulting composite. Preliminary measurements of the thermal conductivity of the unfilled polyethylene sample and the 30 wt % polyethylene/hBN nanocomposite were undertaken. A relationship between the hBN filler content and the thermal conductivity would have been more useful, however, the measurements were limited to two samples as they were carried out externally by NETZSCH [218], [219]. The thermal conductivity measurements revealed that the thermal conductivity of the nanocomposite containing 30 wt % of hBN increased by 64 % relative to the unfilled polyethylene, which is consistent with published work on the thermal conductivity of hBN nanocomposites. For example, Zhou et al. [49], [220] found that the thermal conductivity of a 30 vol % HDPE/hBN composite is four times higher than that of pure HDPE, and reported an increase in the thermal conductivity with increasing hBN content. Similarly, Wang et al. [64] found that adding 40 wt % of hBN into epoxy increased the thermal conductivity by 5 times relative to the unfilled epoxy, and a general increase in thermal conductivity with increasing hBN content. The enhancement in thermal conductivity in polymer composites incorporating hBN as a filler has been widely reported in the literature in different host polymers [221], [222]. The relative increase in thermal conductivity values reported in most of the literature appears to be larger than the 64 % value reported in this study; however, some studies report comparable increases in the thermal conductivity. For example, the addition of 30 wt % of hBN into epoxy increased the thermal conductivity by ~57 % [223], which is similar to results in this study. The platelet-like structure of hBN yields anisotropic physical properties such as thermal conductivity and dielectric breakdown strength [224]. This leads to an orientational dependent thermal conductivity with components that are parallel and perpendicular to the basal plane, with values of ~200 W/m.K and ~2 W/m.K respectively [56] as shown in Figure 6.17. The SEM micrograph of the 30 wt % polyethylene/hBN nanocomposite in Figure 6.7 showed a random distribution of hBN particles at different orientations. As the thermal conductivity of the hBN particles perpendicular to the basal plane is ~100 times smaller than the thermal conductivity of the hBN particles parallel to the basal plane, this suggests that the measured thermal conductivity is an effect of the combined contributions from the particles parallel and perpendicular to the basal plane, which will not always necessarily lead to a large increase in the thermal conductivity. This could explain why the percentage increase in the thermal conductivity reported in this study is lower than the increases reported in the literature.

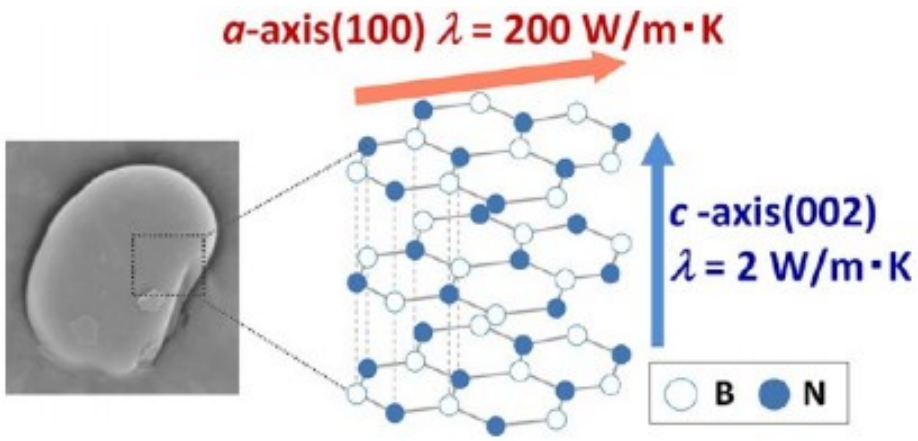

Figure 6.17: Anisotropic thermal conductivity of hBN [56]

While the idea of dispersion is a hot topic in the nanodielectric community, it is certainly not desired when attempting to enhance the thermal conductivity of a material [225]. A well dispersed system would result in a large interphase which significantly increases phonon scattering at the interfacial boundary regions, and thus increases the thermal resistance. In contrast, a percolating network of thermally conductive particles forms a thermal pathway which enables efficient phonon transport which in turn, largely increases the thermal conductivity of the material; this is exactly what is observed in the nanocomposite containing 30 wt % of hBN. As seen from the SEM micrographs in Figure 6.7, where a percolating pathway is observed, which increases the thermal conductivity by 64 % relative to the unfilled polyethylene.

While the studies reported earlier were consistent on reporting the significant increase in thermal conductivity in hBN composites, a limited number of studies have studied the relationship between the breakdown strength and thermal conductivity of these composites. Du et al. [69] reported that the breakdown strength in polypropylene/hBN nanocomposites increased from 289 kV/mm to 300 kV/mm, 320 kV/mm, and 336 kV/mm upon the addition of 3 wt %, 6 wt %, and 9 wt % of hBN respectively in polypropylene. This increase in breakdown strength was correlated with the increase in thermal conductivity with increasing hBN content. In the work described here, it is suggested the increase in breakdown strength in the polyethylene/hBN nanocomposites could possibly be partly attributed to the increase in thermal conductivity. The movement of charge carriers generates heat which increases the temperature of the dielectric. Thermal instability could occur if the temperature of the dielectric increases and the heat is not efficiently dissipated away. The increased thermal

conductivity of the 30 wt % nanocomposite could promote faster heat dissipation, and in turn prevent thermal runaway. The faster heat dissipation prevents any further thermal excitations of charge carriers, which consequently delays the breakdown process. Therefore, if no competing mechanisms are present, the thermal conductivity could play a major role in enhancing the breakdown strength of nanocomposites.

6.10 Conclusion

When considering the effect of hBN content on the dielectric properties of polyethylene/hBN nanocomposites, the hBN particles dominated the dielectric behaviour such that any property changes were a result of the presence of the hBN filler, which masked any dispersion-related and morphological effects under isothermal crystallisation. The hBN particles strongly interacted with the polyethylene matrix to produce a highly disordered morphology, which was consistent with the boron nitride acting as an effective nucleating agent, as evidenced from the DSC results. Although the hBN in the nanocomposites was uniformly distributed in the polyethylene matrix, there was a still a reasonable degree of agglomeration without any evidence of intercalation or exfoliation. Dielectric spectroscopy measurements have shown that the real permittivity increased with increasing hBN content, due to the higher permittivity of hBN particles relative to polyethylene. The measurements also showed that the presence of even high amounts of hBN did not lead to increased dielectric losses; this is a highly desirable property in electrical insulation systems. With regards to the breakdown behaviour, there was a monotonic increase in breakdown strength with increasing hBN content even when 30 wt % of hBN was included in the matrix, despite the existence of a percolating hBN network. Therefore, the breakdown strength in this study is not determined by the distribution of the particles but is primarily dominated by how the hBN particles interact with the charge carriers rather than how they interact with the polymer. The change in morphology can be concluded as not the primary reason for the changes in dielectric properties as both polyethylene morphologies exhibited a similar behaviour. It is proposed that it is highly likely that both the improved thermal conductivity in parallel with the ability of the hBN platelets to act as effective electron scattering centres serve to enhance the breakdown strength of the nanocomposites simultaneously. Regardless of the mechanisms involved, this chapter clearly demonstrated that the dispersion/aggregation state of the filler is not the key factor in improving the breakdown strength behaviour of polymer nanocomposites.

Chapter 7: Water Absorption in Polyethylene Hexagonal Boron Nitride Nanocomposites

7.1 Introduction

The previous chapter has shown that the breakdown strength behaviour in polyethylene/hBN nanocomposites was not directly related to the dispersion/aggregation state of the hBN particles. Therefore, the factors affecting the electrical performance of nanocomposites remain to be understood, as there still exists a considerable variability in the literature regarding the electrical performance of polymer nanocomposites. Possible reasons for the existing inconsistencies could be due to different material preparation techniques, nanoparticle agglomeration, unknown filler content, inconsistent sample storage conditions, and unknown water level content in the samples. Since many inconsistencies exist in the literature and not many have considered the effect of water, this could explain the source of some of the inconsistencies regarding the electrical performance of nanocomposites. Due to the existence of hydroxyl groups on the surface of most nanoparticles used in polymer nanocomposites, they are highly prone to absorbing moisture from their environment, which highly affects their electrical properties. Therefore, the water is preferentially absorbed at the hydrophilic surfaces of the nanoparticles rather than the relatively more hydrophobic polymer. :While the previous chapter has shown that a high hBN content resulted in an increase in breakdown strength, it is hypothesized that this could indirectly be detrimental to the electrical properties as the surfaces of the hBN could absorb water, especially when a high content is used, whilst operating in challenging and humid environments, which would highly affect its breakdown behaviour. The work in this chapter is therefore set out to investigate the role of the surface chemistry through the influence of absorbed water on the electrical properties of a hydrophobic nanocomposite system under different humid conditions. Electrical tests including dielectric spectroscopy, dielectric breakdown strength, and electrical conductivity were performed on samples that were stored under different conditions to understand how water affects the electrical properties of polyethylene/hBN nanocomposites

7.2 Sample Conditioning

One of the major challenges in the design of electrical insulation is the ability of the insulator to maintain its electrical performance after exposure to water. In this study, polyethylene/hBN test samples were placed in conditions with different relative humidity (RH) levels. The samples were conditioned as follows:

- "Ambient": Samples were exposed to laboratory ambient conditions (20 ± 2 °C and 50 ± 20% RH) for periods up to 14 days.
- "Dry": Samples were in placed in a vacuum oven, which contains dry desiccant pellets, at room temperature for periods up to 14 days.
- "Wet": Samples were completely immersed in water at room temperature for periods up to 14 days.
- "Wet to Dry": These are the wet samples which were subsequently placed in a vacuum oven at room temperature for periods up to 14 days.

The mass of these samples was recorded at regular intervals until the mass no longer changed and reached saturation – it is in equilibrium with the environment. Table 7.1 shows the mass change after saturation in the samples under all conditions. The unfilled polyethylene sample exhibited the same behaviour under all conditions, where an insignificant change in mass wasi observed, suggesting that it does not absorb water under these conditions.

Table 7.1: Mass changes after conditioning of the polyethylene/hBN nanocomposites

Material	**Conditioning Regime**			
	Ambient	**Dry**	**Wet**	**Wet to Dry**
PEBN/0	<0.02 %	<0.02 %	<0.02 %	<0.02 %
PEBN/2	<0.02 %	<0.02 %	+ 0.0239 %	- 0.0221 %
PEBN/5	<0.02 %	<0.02 %	+ 0.0372 %	- 0.0366 %
PEBN/10	<0.02 %	<0.02 %	+ 0.0493 %	- 0.0459 %
PEBN/20	<0.02 %	<0.02 %	+ 0.0667 %	- 0.0684 %
PEBN/30	<0.02 %	<0.02 %	+ 0.0805 %	- 0.0792 %

The nanocomposites did not gain or lose mass in “Ambient” and “Dry” conditions as the mass change in these conditions was less than 0.01%, so any mass changes under these conditions were seen as mass fluctuations due to uncertainties in the measurements. As the nanocomposites did not absorb any water/moisture from the environment in “Ambient” conditions and do not have any absorbed water to lose in “Dry” conditions, this suggests that they are completely dry in these two conditions. In “Wet” conditions, the nanocomposites gained some mass due to the presence of water, and as the hBN content increased, the amount of absorbed water clearly increased. The mass of the samples stopped changing after ~2 days of being immersed in water. Although the nanocomposites absorbed some water, it is a very insignificant amount of water. For example, the 30 wt % nanocomposite absorbed only ~0.08% of water, which an insignificant amount when compared to a 10 wt % polyethylene/silica nanocomposite which can potentially absorb more than 1 % of water in some cases [77], [187]. The mass of the “Wet to Dry” samples clearly indicated that the nanocomposites can lose all the absorbed water when the “Wet” samples were dried under vacuum conditions, as the masses returned to their starting value. The “Wet” samples have been dried in order to determine whether water absorption is a reversible effect. The mass change with respect to time could not be plotted as the mass changes before saturation were too small to be detected, and the mass measurements contained many uncertainties as the amount of absorbed water was too low.

7.3 Dielectric Spectroscopy

While the presence of water is expected to negatively influence the electrical performance of insulators, it can nevertheless be thought of as an effective dielectric probe of the interfacial regions. As such, the polyethylene/hBN interface and the surface chemistry of the hBN particles can directly be examined using dielectric spectroscopy. Figure 7.1 and Figure 7.2 show the real and imaginary relative permittivity respectively of all the materials under “Dry” conditions. The figures show that the real relative permittivity of all materials is frequency independent and increases with increasing hBN content due to the higher permittivity of hBN particles, as discussed in the previous chapter. The imaginary relative permittivity of all materials is characterised by very low losses, as the measurements are within the noise limit of the equipment. These measurements are consistent with the dielectric spectroscopy measurements obtained in the previous chapter, which confirms the reproducibility of the results.

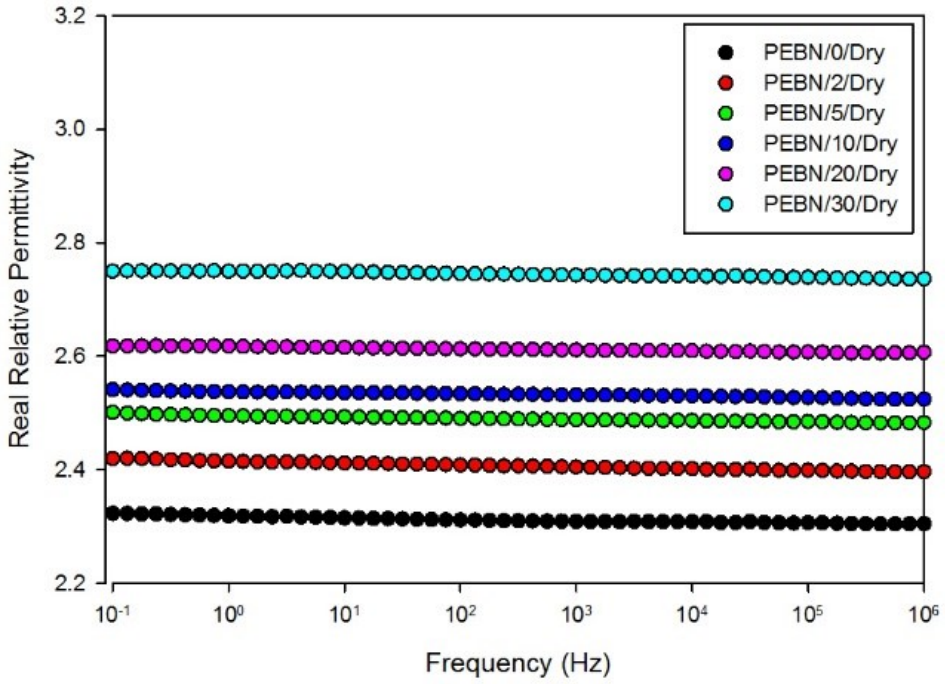

Figure 7.1: Real relative permittivity of the "Dry" polyethylene/hBN nanocomposites

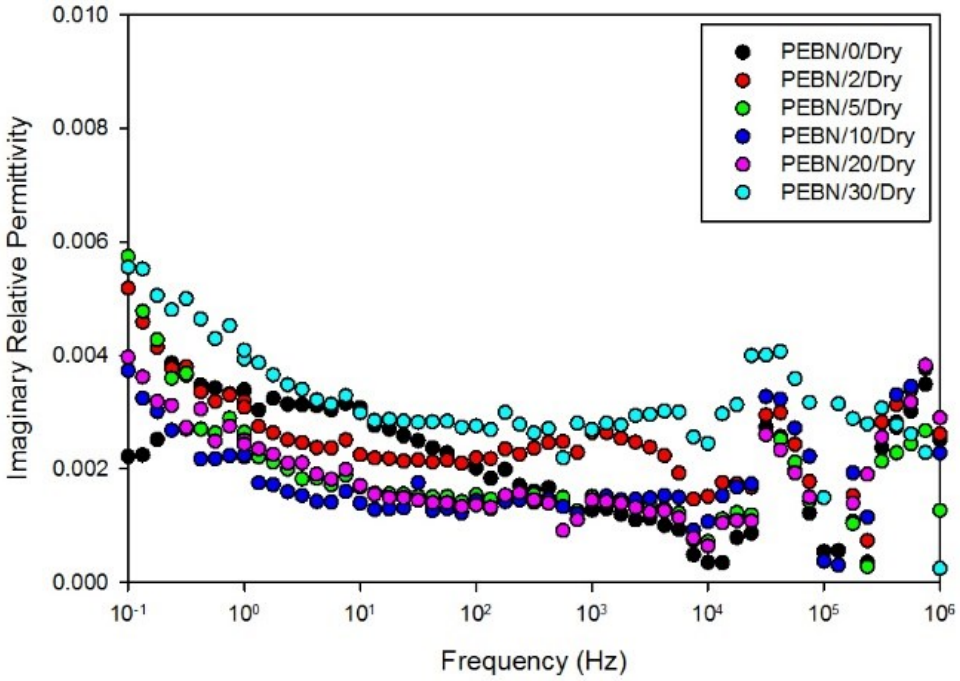

Figure 7.2: Imaginary relative permittivity of the "Dry" polyethylene/hBN nanocomposites

Figure 7.3 and Figure 7.4 show the real and imaginary relative permittivity respectively of all the materials under "Ambient" conditions. The figure shows that the behaviour of both the real and imaginary relative permittivity of the "Ambient" samples is identical to the behaviour of the "Dry" sample with no frequency dependent behaviour or relaxation peaks, which suggests they are both completely dry. This is consistent with the mass measurements which shows no mass changes even after being exposed to ambient conditions with ~50 % RH. This is in contrast to polyethylene nanocomposites containing silica and silicon nitride particles, which tend to absorb water under ambient conditions [21]. Unlike the hBN nanocomposites in this study, dielectric spectroscopy of the silica and silicon nitride based nanocomposites under "Ambient" conditions revealed relaxation features attributed to bound water molecules at the nanoparticle interfaces. The importance of this finding should be emphasized, as water absorption in nanocomposites under ambient conditions could be a source of the variability in the literature. The literature data could therefore reflect incorrect information as the properties of nanocomposites are inadvertently reported as effects of water rather than the inclusion of nanoparticles.

As the nanocomposites do not absorb any water under "Ambient" conditions, it was necessary to expose them to a 100 % RH environment to understand the influence of water. Figure 7.5 and Figure 7.6 show the real and imaginary relative permittivity respectively of all the materials under "Wet" conditions, after complete water saturation. The real relative permittivity of the unfilled polyethylene in "Wet" conditions is similar to measurements under "Dry" and "Ambient" conditions, with no noticeable changes. This is consistent with the lack of variation of mass of the unfilled polyethylene under all types of conditioning. In contrast, the nanocomposites exhibit a marked change in the real relative permittivity behaviour under "Wet" conditioning, which is consistent with the increase of mass when exposed to water. Although the amount of absorbed water is very small (< 0.1 % in all nanocomposites), it is easily detected through measurements of permittivity, as water is a highly polar molecule with a very large permittivity in comparison to the dry nanocomposites. Unlike the behaviour of the "Dry" and "Ambient" samples, the real relative permittivity of all the "Wet" nanocomposite samples is frequency dependent, which increases with decreasing frequency. This suggests that the water exists in different modes or states in these systems, which is able to polarise at different frequencies. As the hBN content increases, the variation in the value of permittivity across the measured frequency range increases due to the larger amount of present water in the system.

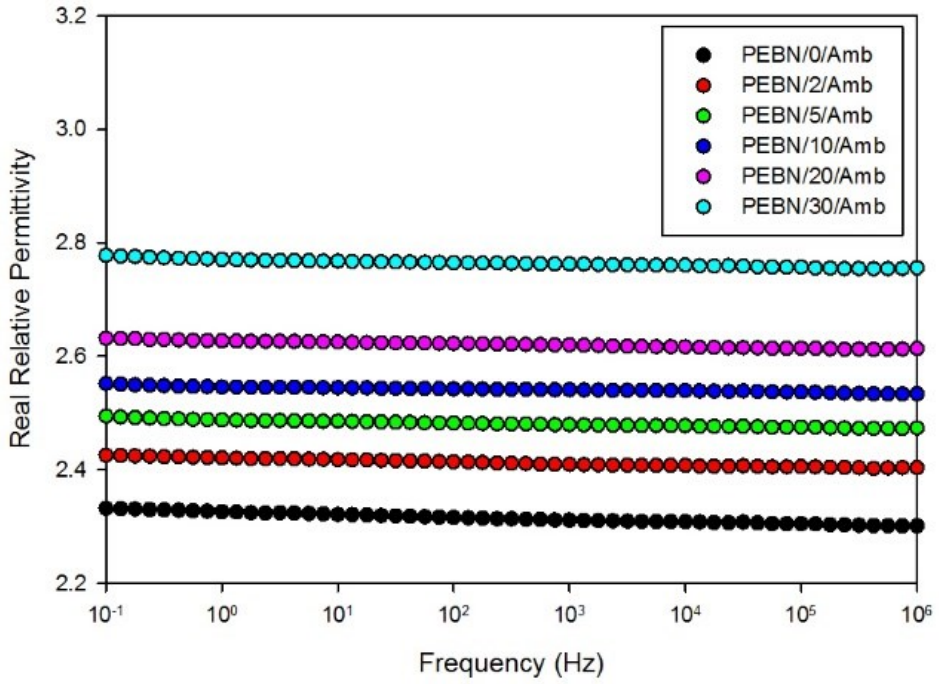

Figure 7.3: Real relative permittivity of the "Ambient" polyethylene/hBN nanocomposites

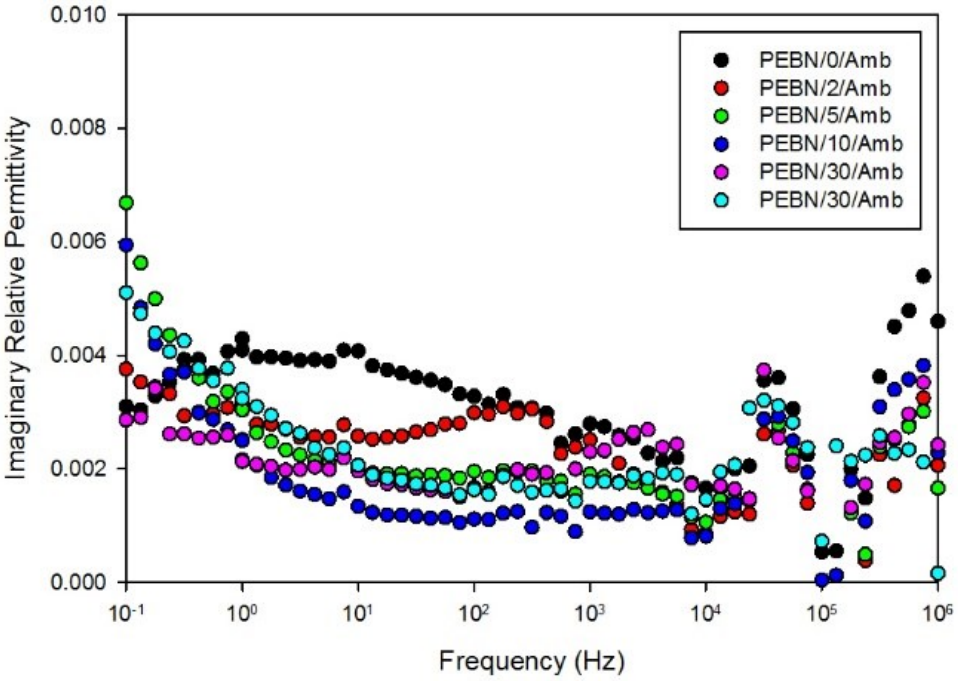

Figure 7.4: Imaginary relative permittivity of the "Ambient" polyethylene/hBN nanocomposites

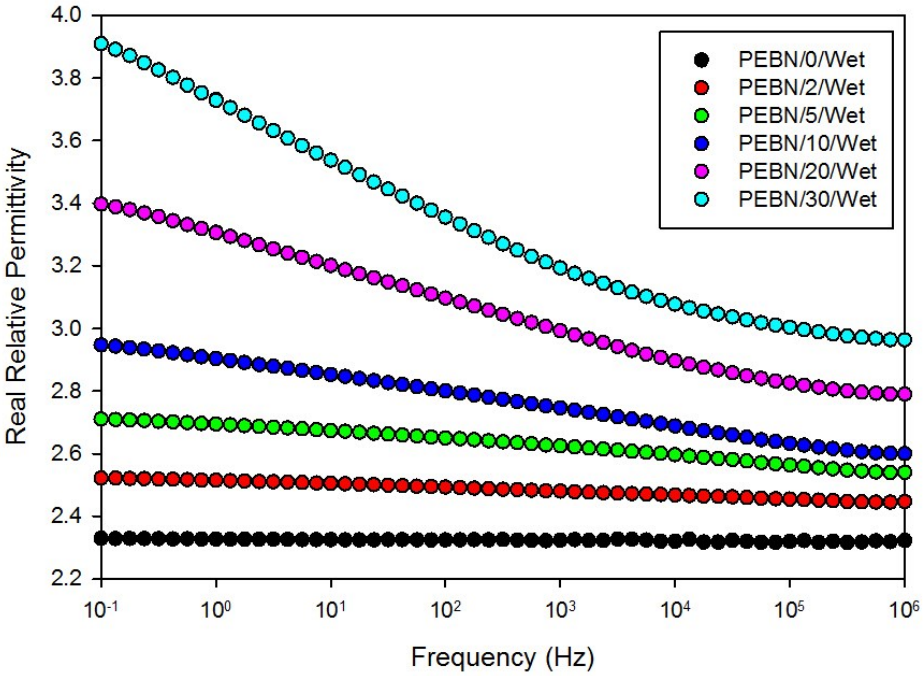

Figure 7.5: Real relative permittivity of the "Wet" polyethylene/hBN nanocomposites

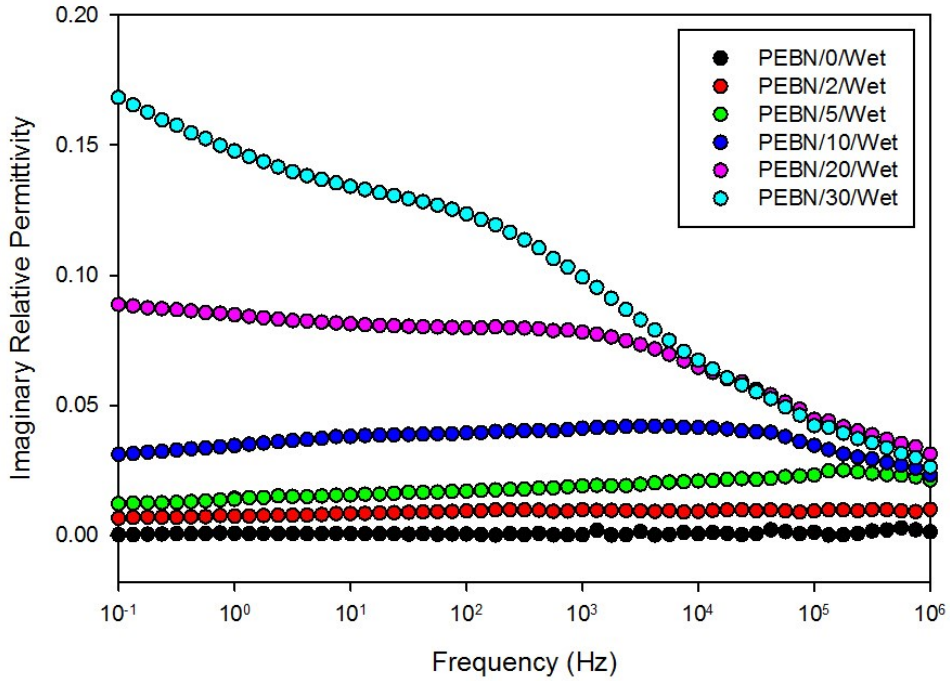

Figure 7.6: Imaginary relative permittivity of the "Wet" polyethylene/hBN nanocomposites

The imaginary relative permittivity of the "Wet" nanocomposites with 10 wt % of hBN or lower behave in a similar manner, where the dielectric losses increase with increasing hBN content and appears to exhibit a broad loss peak centred at ~$5x10^4$ Hz, which is a relaxation feature attributed to the polarisable content in the materials due to the present water. The broad loss peak confirmed that the water exists in a variety of states as suggested earlier from the real relative permittivity data. The dielectric response behaviour changes as the amount of hBN increases to more than 10 wt %, where a subtle relaxation peak appears at 10^3 Hz and 10^2 Hz in the 20 wt % and 30 wt % nanocomposites respectively, with a slight upturn at low frequencies, which is more evident in the 30 wt % nanocomposite. While these features are attributed to the amount of water in the system, the variation of the dielectric response under different water immersion times would reveal more information about the state of the water in the system and the origins of these features.

Figure 7.7 shows the time-dependent real relative permittivity behaviour of all the samples under different water immersion times. It is noteworthy that that Y-axis scale of the different graphs in the figure is different for a clearer illustration of the changes in the real relative permittivity in the individual nanocomposite samples. The figure shows that the real relative permittivity behaviour of all nanocomposites is similar and the value of the real relative permittivity gradually increases as the water immersion time, or amount of absorbed water, increases due to the larger amount of polarisable material present in the system. As more water is absorbed, the quantity of water molecules increases thereby increasing the amount of polar dipoles that can readily respond to the applied electric field, which in turn is manifested as a higher real relative permittivity. This is consistent with published work on the dielectric response of polyethylene nanocomposites with silica and silicon nitride particles under wet conditions [21], [77], although the change in permittivity due to water is much lower in this study. For example, the real relative permittivity of a polyethylene nanocomposite containing 5 wt % of silica increased by ~70% after immersion in water [21], whereas the real relative permittivity of polyethylene nanocomposites with 5 wt % of hBN in this study only increased by 7% after water immersion.

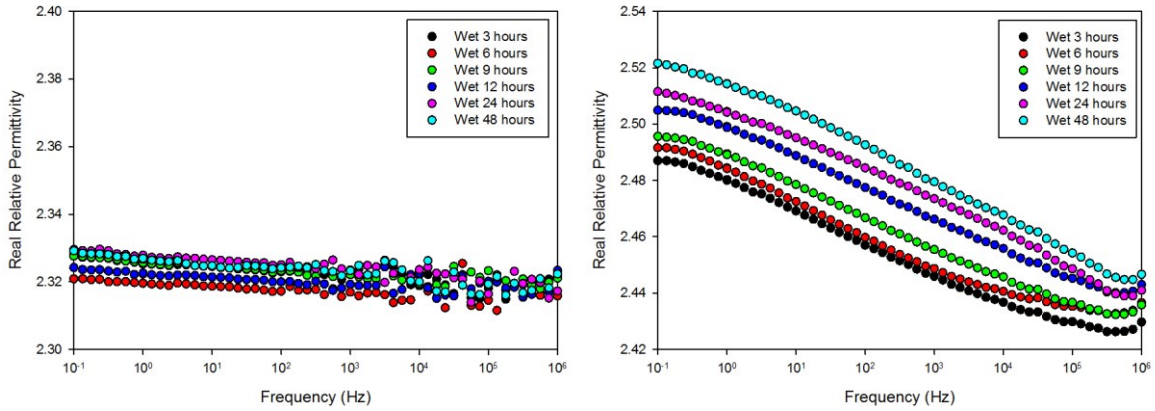

(a) (b)

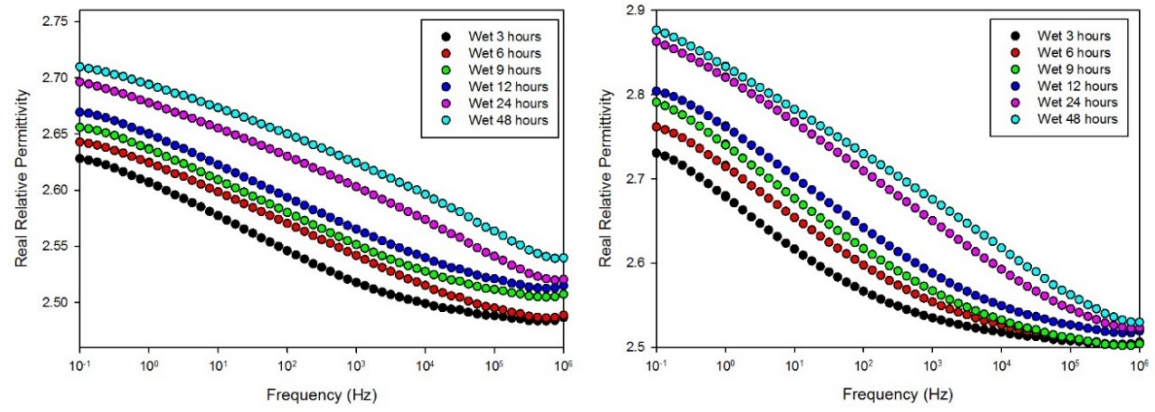

(c) (d)

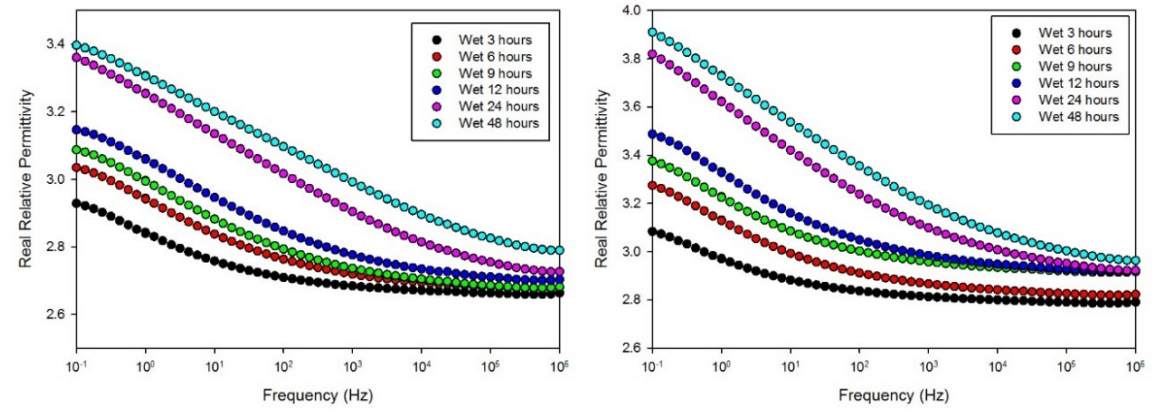

(e) (f)

Figure 7.7: Real relative permittivity of the "Wet" polyethylene/hBN nanocomposites containing (a) 0 wt %, (b) 2 wt %, (c) 5 wt %, (d) 10 wt %, (e) 20 wt %, and (f) 30 wt % of hBN

Figure 7.8 shows the time-dependent imaginary relative permittivity behaviour of all the samples under different water immersion times. It is noteworthy that that Y-axis scale of the different graphs in the figure is different for a clearer illustration of the changes in the imaginary relative permittivity. Considering the nanocomposites containing 10 wt % of hBN and lower, there appears to be a broad loss peak which slightly shifts to higher frequencies as the time, which the samples are exposed to water, increases and the magnitude of this loss peak increases with increasing hBN content. This is clearer in the 5 wt % and 10 wt % nanocomposite than in the 2 wt % due to the larger quantity of absorbed water. Similarly, studied on the water absorption in poly(ethylene-co-butyl acrylate)/alumina nanocomposites [226], polyethylene/silica nanocomposites [77], and polyethylene/silicon nitride nanocomposites [21] have shown that the dielectric losses increase with increasing filler content, where the loss peaks shift to higher frequencies with increasing water content, and therefore this effect is comparable to the results in the available published work on the water absorption behaviour of nanocomposites. The broad loss peaks in the imaginary relative permittivity are in line with the increase in real relative permittivity across the entire measured frequency range; this confirms the existence of many different states of water in the system. This has been highlighted in the work of Zou et al. [72]–[74] where they developed a water shell model to describe the dielectric properties of epoxy/silica nanocomposites under wet conditions. The existence of different states of water suggests that water layers with different thicknesses exist around the hBN particles, which correspond to relaxations at different frequencies, due to the different mobility of the different water layers. This is consistent with the SEM images shown in the previous chapter which show uniform yet agglomerated structures in the nanocomposites where the hBN particles exist in different sizes in the polyethylene matrix, resulting in different interfacial regions with different states of water.

The imaginary relative permittivity behaviour of the 20 wt % and 30 wt % nanocomposites appears to be different from the nanocomposites containing 10 wt % of hBN content and lower, which suggests different mechanisms are in effect in the nanocomposites containing high loading levels of hBN particles. First, Figure 7.8 (e) and Figure 7.8 (f) show the existence of distinct mid-frequency relaxation features, leading to a low frequency upturn, after 24 hours of water immersion. These relaxations, which are absent in the dry nanocomposites, appear as a result of interfacial polarisation of the water molecules at the polyethylene/hBN interface, and shift to higher frequencies with increasing water content.

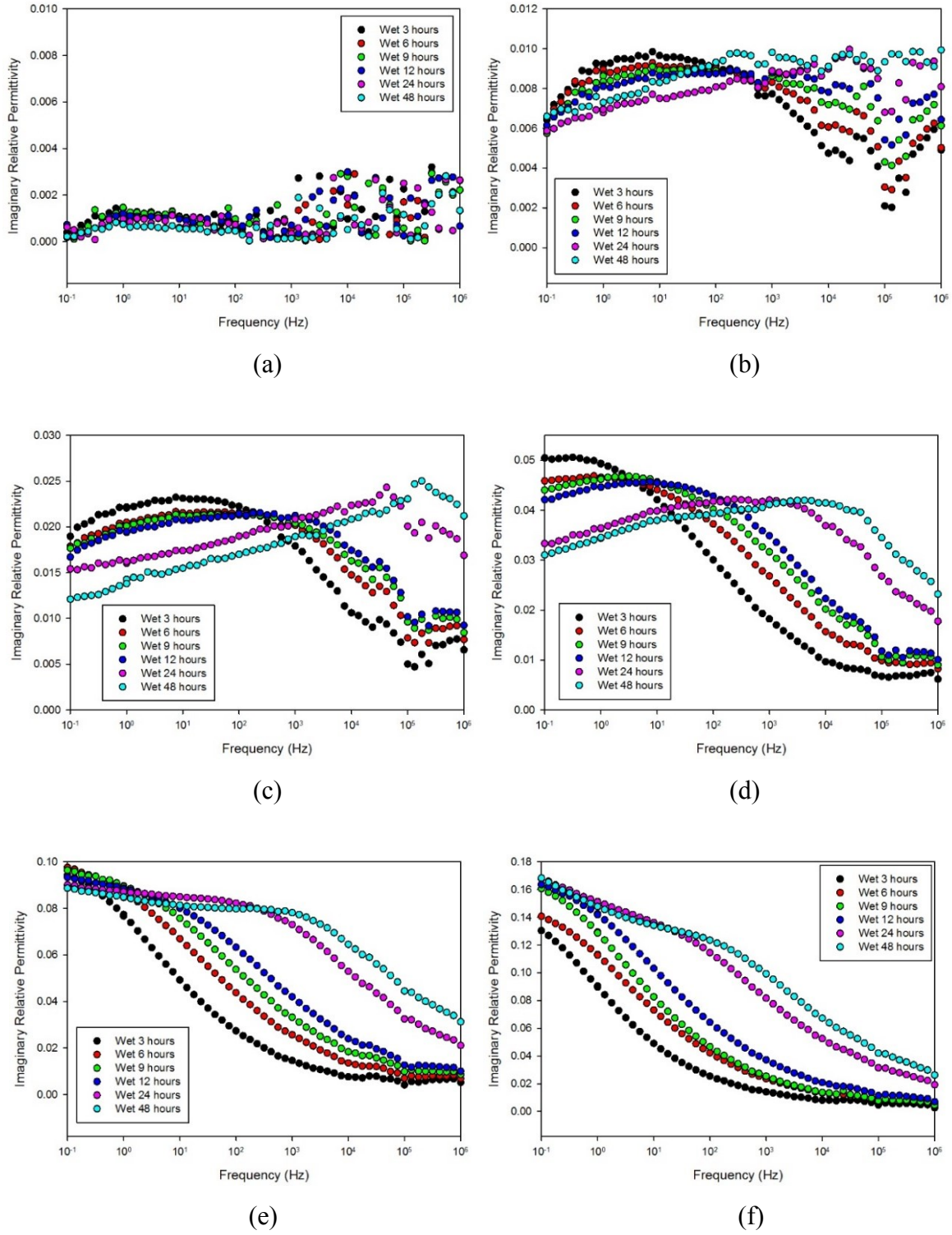

Figure 7.8: Imaginary relative permittivity of the "Wet" polyethylene/hBN nanocomposites containing (a) 0 wt %, (b) 2 wt %, (c) 5 wt %, (d) 10 wt %, (e) 20 wt %, and (f) 30 wt % of hBN

These distinct peaks only appear after 24 hours of water immersion, as they could have been located at frequencies lower than the measured frequency range when the samples were immersed in water for less than 24 hours. It is interesting to note that the relaxation peak of the 30 wt % nanocomposite, which contains more water, is at a lower frequency than the broad loss peak of the 20 wt % nanocomposite, which seems to be contradictory as a larger amount of water generally implies a larger amount of mobile species, which in turn leads to higher frequency relaxations. However, this could be ascribed to the different nature of the bound water molecules and their interaction with the different amounts of available hBN particles, implying that the water molecules are more tightly bound in the 30 wt % nanocomposite thus restricting the mobility of the water. Nevertheless, the dielectric losses are larger in the 30 wt % sample than the 20 wt % sample, especially at lower frequencies, although much smaller than the losses observed in polyethylene nanocomposites containing 10 wt % or less of silica or silicon nitride particles [77], [227].

Second, the imaginary relative permittivity of the highly loaded nanocomposites increases at low frequencies, and its magnitude increases with increasing water absorption, whereas the imaginary relative permittivity of the nanocomposites with low loading levels decreases at low frequencies to exhibit the broad relaxation peaks. The upturn in the imaginary relative permittivity at low frequencies, which is more evident in the 30 wt % nanocomposite, could imply the presence of a percolating water network which facilitates electrical conduction. The increase in the imaginary permittivity with decreasing frequency has been described in the work of Dissado et al. [228] as a consequence of quasi-DC conduction due to the formation of electrically conductive paths. This is usually observed when the slopes of the real and imaginary permittivity are parallel, with a slope of -1 in the log-log plot of the imaginary permittivity with frequency, which has been observed in nanocomposites containing a percolating water network [21], [74], [75]. A log-log plot of the real and imaginary permittivity of the 20 wt % and the 30 wt % is shown in Figure 7.9, which shows a relatively flat behaviour, with slopes of -0.0253 and -0.0531 respectively, which are much lower than -1, and therefore strongly suggests that a percolating water network does not exist in these systems. In contrast to the hBN systems here, the presence of a percolating water network has been reported by Hui et al. [75] where they observed mid-frequency loss peaks in a 5 wt % XLPE/silica nanocomposite, due to the bound water, which is different to the behaviour of the 12.5 wt % nanocomposite in which the imaginary permittivity increases with decreasing frequency with a high slope, low frequency upturn due to water percolation at high filler content. Similar features have also been reported in a 9 wt % epoxy/silica

nanocomposite containing a water percolating network at high RH levels [74]. Therefore it is highly unexpected that a 30 wt %, water saturated nanocomposite does not exhibit a similar behaviour despite the existence of a percolating structure of hBN particles, as further shown in the high magnification SEM micrographs in Figure 7.10 and Figure 7.11.

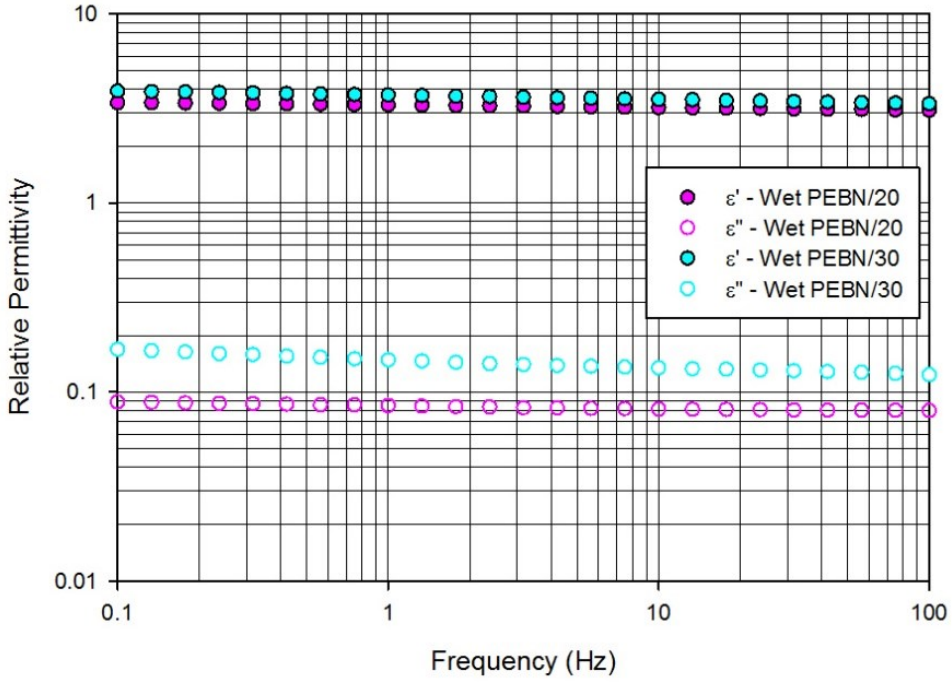

Figure 7.9: Log-log plot of the relative permittivity of the "Wet" 20 wt % and 30 wt % polyethylene/hBN nanocomposites

As the slight upturn at lower frequencies may not be associated with water percolation, it may, rather, be indicative of a broad relaxation peak centred at much lower frequencies than in the measured frequency range. Since the measurements are performed in systems that are effectively not in equilibrium, it is important to perform very quick measurements. The nanocomposites that have been immersed in water have been found to easily lose water to their surroundings under ambient conditions and therefore dielectric spectroscopy measurements at frequencies lower than 0.01 Hz would provide misleading data as the measurements would require in excess of 3 hours. The wet 30 wt % nanocomposite can lose up to ~10 % of the absorbed water when exposed to ambient conditions for 3 hours and therefore measurements at lower frequencies would not accurately represent the dielectric behaviour of the as-produced material.

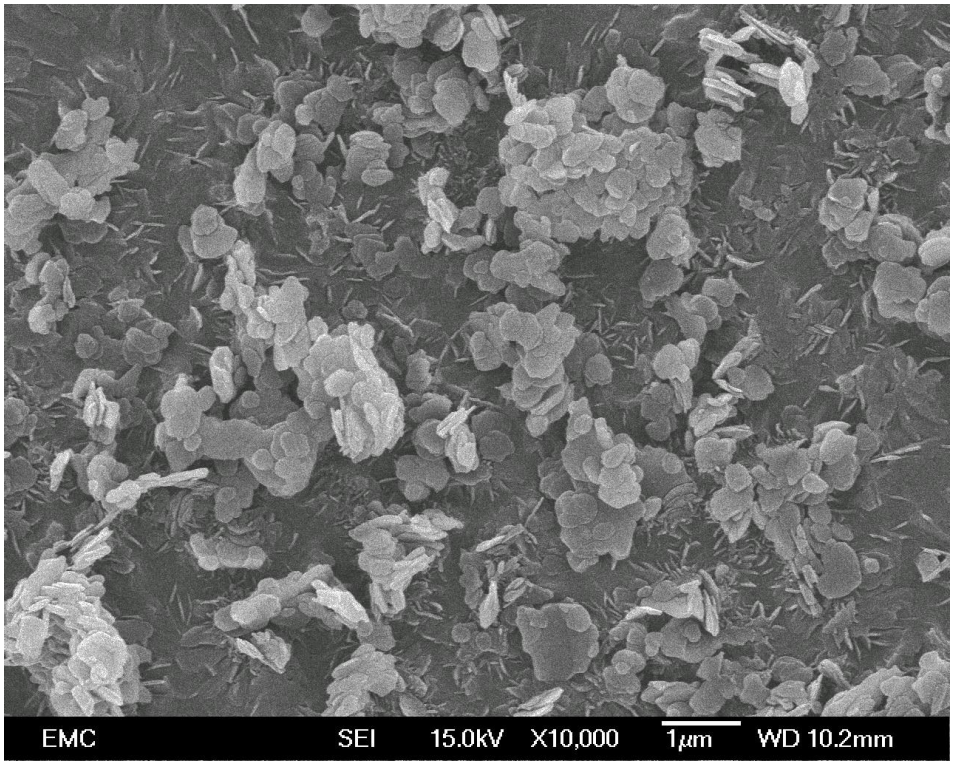

Figure 7.10: High magnification SEM micrograph of the 20 wt % polyethylene/hBN nanocomposite

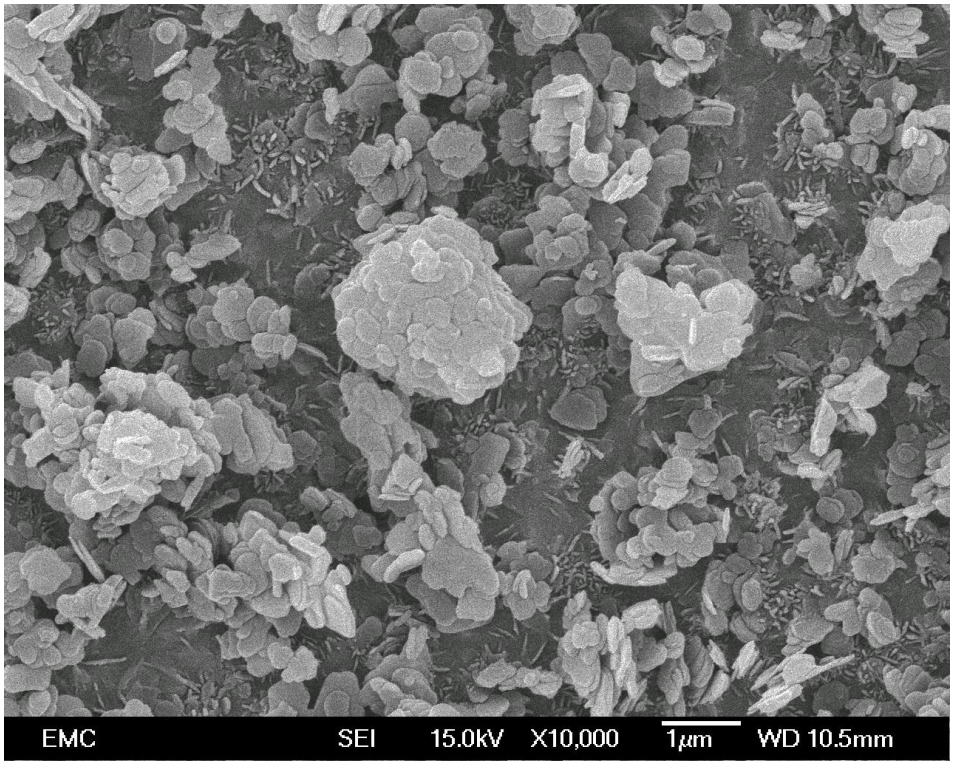

Figure 7.11: High magnification SEM micrograph of the 30 wt % polyethylene/hBN nanocomposite

The same "upturn" at lower frequencies was shown in the 10 wt % nanocomposite that was immersed in water for 3 hours, which later appeared as a broad peak at higher frequencies after further immersion in water. The same mechanism could be in effect in the highly loaded nanocomposites where this broad peak could be located at much lower frequencies. A peak at lower frequencies could be due to slow relaxations because of the stronger bonding of water to the hydroxyl groups as larger amounts of hydroxyl groups are available for bonding with increasing hBN content. Zhang et al. [229] showed that the inclusion of alumina nanoparticles in both epoxy and polyethylene produced a low frequency loss peak attributed to the tightly bound water molecules. They suggested that the absorbed water accumulates at different sites in the nanocomposites than the pure epoxy due to the large interfacial surfaces when the nanoparticles are introduced. Similarly, Praeger et al. [230] reported a very similar behaviour in wet polyethylene nanocomposites containing 10 wt % of calcined silica where a small relaxation peak appears at ~10^4 Hz, and the imaginary permittivity increases with decreasing frequency, leading to a broader low frequency relaxation peak centred around ~1 Hz. The "Wet" hBN nanocomposites in this study could have a similar behaviour, with the mechanisms discussed previously, where the low frequency peak observed at 1 Hz in the wet 10 wt % polyethylene/calcined silica nanocomposite in the work of Praeger et al. [230] is located at much lower frequencies in the 20 wt % and 30 wt % nanocomposites, below 0.1 Hz. Alternatively, the water molecules could be physically restrained within the large hBN aggregates which consequently hinders the motion of these water molecules. The physical confinement of water molecules results in slower dipolar reorientation, which could be manifested as a very low frequency relaxation peak.

It is important to understand the reason why a water percolating network does not form in a system containing a percolating hBN network, as a percolating water network at much lower filler loading levels has been previously reported in the literature. [21], [74], [75]. The systems reported previously have incorporated spherical particles rather than layered particles, which suggests that the nature of the water shells in layered and spherical particles are fundamentally different. Fabiani et al. [231] studied the effect of water absorption on nanocomposites containing layered fillers with different aspect ratios. They used a polyethylene-covinylacetate polymer with a high aspect ratio fluorohectorite filler (aspect ratio > 100) and a low aspect ratio boehmite filler (aspect ratio ~1). The real permittivity behaviour of the wet fluorohectorite sample is similar to the wet hBN samples in our case, however, the permittivity for a wet 5 wt % fluorohectorite sample increased by 87% whereas the permittivity for the wet 5 wt % hBN sample in our study increased merely by 7 %. The

authors demonstrate that water shells can interconnect more easily in particles with a higher aspect ratio which can create a percolation path between water shells, depending on the filler and water content. This contradicts the findings in this study which revealed that a percolating water network is not readily formed in hBN layered nanocomposites. While percolation is achieved at lower filler loading levels in nanocomposites containing layered fillers rather than spherical fillers, the formation of a percolating water network could be determined by a combination of both the aspect ratio and the surface chemistry of the filler rather just one factor. Indeed, the study of Fabiani et al. [231] has considered the presence of hydroxyl groups around all the surfaces of the fluorohectorite filler which is likely to easily result in a percolating water network. Therefore, the dielectric spectroscopy highly suggest that the hydroxyl groups on the hBN are most likely present only on the edge surfaces, rather than the entire surface, of the hBN particles. Up to date, dielectric spectroscopy which examines the surface chemistry of hBN particles has not been reported in the literature, and therefore the results in this work show indirect yet strong evidence that the hBN particles are characterised by hydrophobic basal surfaces, free of hydroxyl groups, with slightly hydrophilic edge surfaces as a result of a small amount of hydroxyl groups on the edges, possibly due to manufacturing defects. This is highly consistent with the TGA and FTIR results of the hBN particles in Chapter 4, which indicated a very small mass loss and the existence of a small amount of hydroxyl groups respectively. This implies that water clusters may preferentially form around the edges of the hBN platelets rather than form complete water shells around the entire hBN particles, thereby inhibiting the formation of a percolating water network. While the overlapping of water clusters between some neighbouring hBN particles or hBN aggregates should not be excluded, the existence of a percolating water network forming complete conducting paths between the two electrodes is, however, highly unlikely.

Not many studies have been done on the effect of water absorption in boron nitride based composites due to their hydrophobic nature. Unlike the systems shown in this study which are only based on boron nitride, most studies in the literature exploring the effects of water absorption have been performed on nanocomposites with silica or other oxide based fillers. Some researchers have attempted to turn hydrophilic particles into a hydrophobic state by either changing the surface chemistry of the nanoparticles through surface functionalisation or through calcination, where the hydroxyl groups are completely eliminated, therefore fundamentally changing the water absorption kinetics, and the dielectric response, due to the changed interfacial region [74], [232]–[234]. For example, the work of Lau et al. [77] has

shown that the permittivity and dielectric losses in polyethylene silica nanocomposites were reduced by changing the interfacial structure when the hydroxyl groups on the surface of the silica particles were substituted with the non-polar propyl (C_3H_7) groups that do not easily absorb water. In the same system, Praeger et al. [230] eliminated the hydroxyl groups on the surface of silica through calcination, which resulted in a system with a drastically lower water absorption capability and a changed dielectric response. In the case of hBN, calcination or surface functionalisation is not required due to the hydrophobic surface state of the hBN particles which, in its as-received state, is not prone to absorbing water. This highlights the importance of the surface chemistry of the nanoparticles, which changes their surrounding interfacial region and thus affecting the amount of water that can be absorbed by the material.

While the hBN nanocomposites have been shown to have a highly hydrophobic surface, they nevertheless absorb some water and therefore it is important to know if this is a reversible effect; hence, the "Wet" samples have been subjected to vacuum drying. The effects of water on the real and imaginary relative permittivity, which have been previously observed, are completely eliminated when the "Wet" samples have been completely dried, as shown in Figure 7.12 and Figure 7.13. After drying, the dielectric response of all nanocomposites becomes identical to the "Dry" and "Ambient" samples. The values of the real and imaginary relative permittivity have been reduced to the same values as in the "Dry" and "Ambient" samples, where they have become constant and frequency independent once again, which is consistent with the mass measurements as the samples have lost all the mass they previously gained due to the amount of water they absorbed. The results from mass measurements and complex permittivity suggest that the water absorbed in the nanocomposites is free water that is not tightly bound at the polymer/nanoparticle interface, thus it was easily removed by vacuum drying. Since boron nitride absorbs a small amount of water, any amount of absorbed water is likely to be loosely bound. When water is tightly bound to the surface of the hBN particles, its effects will appear in the dielectric loss measurements at lower frequencies whereas the effects of loosely bound water are apparent at higher frequencies due to the higher mobility of the loosely bound water molecules. It has been shown that polyethylene/silica nanocomposites contain both tightly and loosely bound water which are manifested in the imaginary relative permittivity as two distinct relaxation peaks at low and high frequencies respectively [77], [227]. If any tightly bound water molecules exist in the systems here, their relaxation peak would be at a very low frequency lower than the minimum measured frequency of 0.1 Hz.

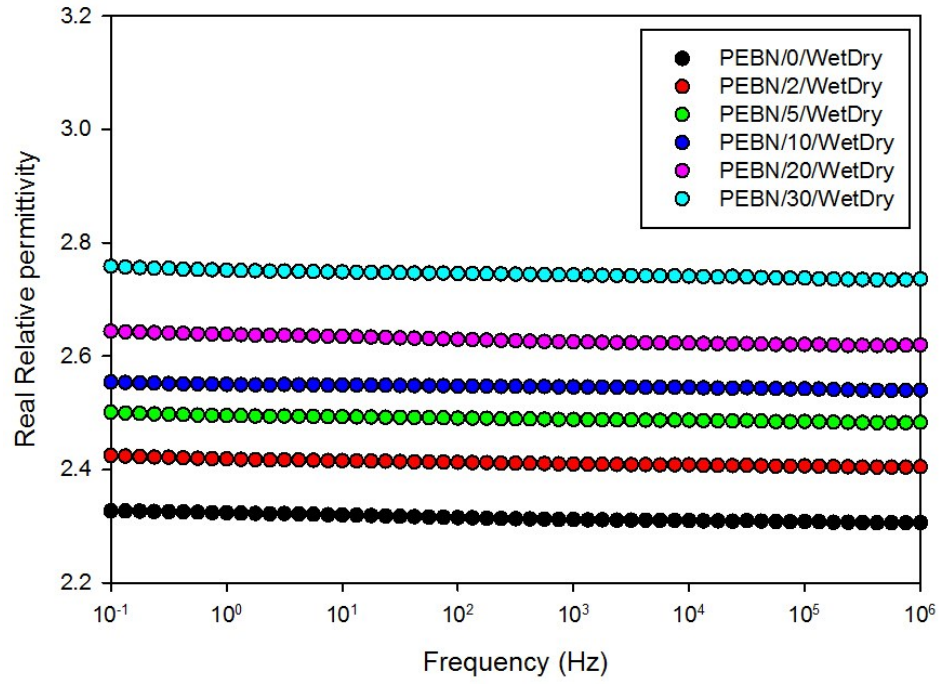

Figure 7.12: Real relative permittivity of the "Wet to Dry" polyethylene/hBN nanocomposites

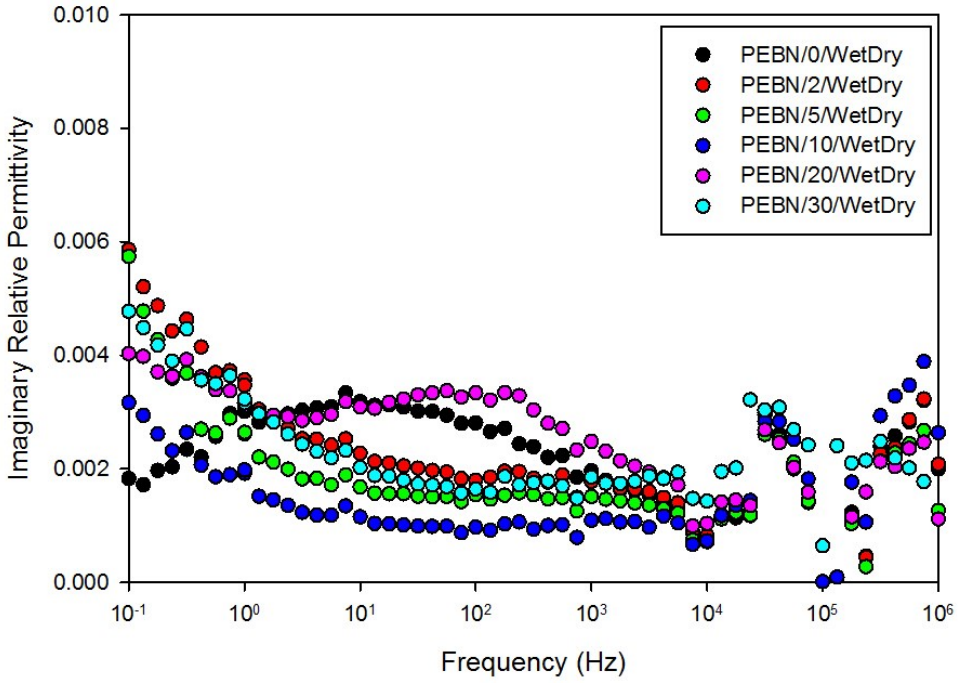

Figure 7.13: Imaginary relative permittivity of the "Wet to Dry" polyethylene/hBN nanocomposites

Although the behaviour of the highly loaded nanocomposites was considered to be an effect of tightly bound water, the low frequency upturn and mid-frequency relaxation peaks observed in the "Wet" samples were completely eliminated after drying, and therefore it can be assumed that any water related relaxation features observed in the dielectric response is attributed to loosely bound water molecules held together with the hydroxyl groups by weak hydrogen bonding.

7.4 Dielectric Breakdown Strength

As the breakdown strength test is a destructive test, only water saturated samples were tested and the effect of water immersion time was not considered. Figure 7.14 and Figure 7.15 show representative Weibull plots for the "Dry" and "Ambient" samples. As expected, the unfilled sample shows similar breakdown strength in both conditions, which is consistent with previously discussed data as it does not absorb water. The scale parameter of the unfilled sample is ~168 kV/mm under all conditions. When the "Dry" and "Ambient" nanocomposite samples are considered, there is a clear pattern, whereby the breakdown strength increases with increasing hBN content, and the highest breakdown field (~189 kV/mm) is observed in the PEBN/30 sample with a 13% increase relative to the unfilled sample. It can be seen from Table 7.2 that while some of the scale parameter values in the nanocomposites with low filler content might not be statistically different relative to the unfilled sample, the breakdown values at high filler content do not fall within the statistical uncertainties in the unfilled sample. Therefore the breakdown data become more meaningful in the nanocomposites with higher hBN content. Although it is not a substantial increase in breakdown strength, this suggests that this monotonic increase in the dielectric breakdown strength behaviour with increasing filler content is a real effect. It should be noted that the scale parameter of the 2 wt % nanocomposite is higher than the scale parameter of the unfilled sample. While the breakdown measurements in the previous chapter revealed the opposite effect, the values are still within experimental uncertainties and therefore the results are still considered reproducible. Additionally, there was less variation in the produced sample thicknesses used to produce these results, as compared to the samples in Chapter 6, which resulted in a higher β value.

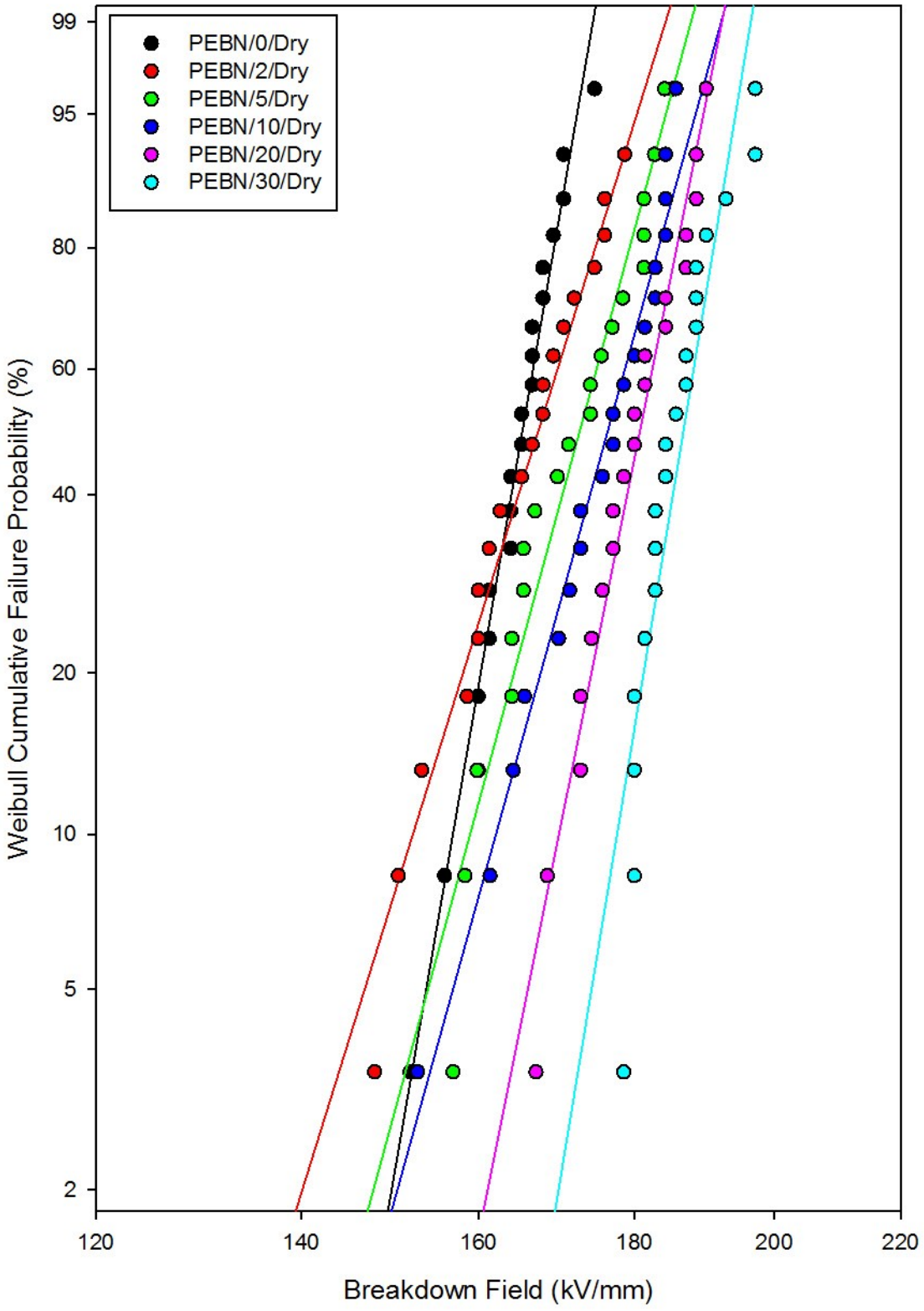

Figure 7.14: Weibull plots of the "Dry" polyethylene/hBN nanocomposites

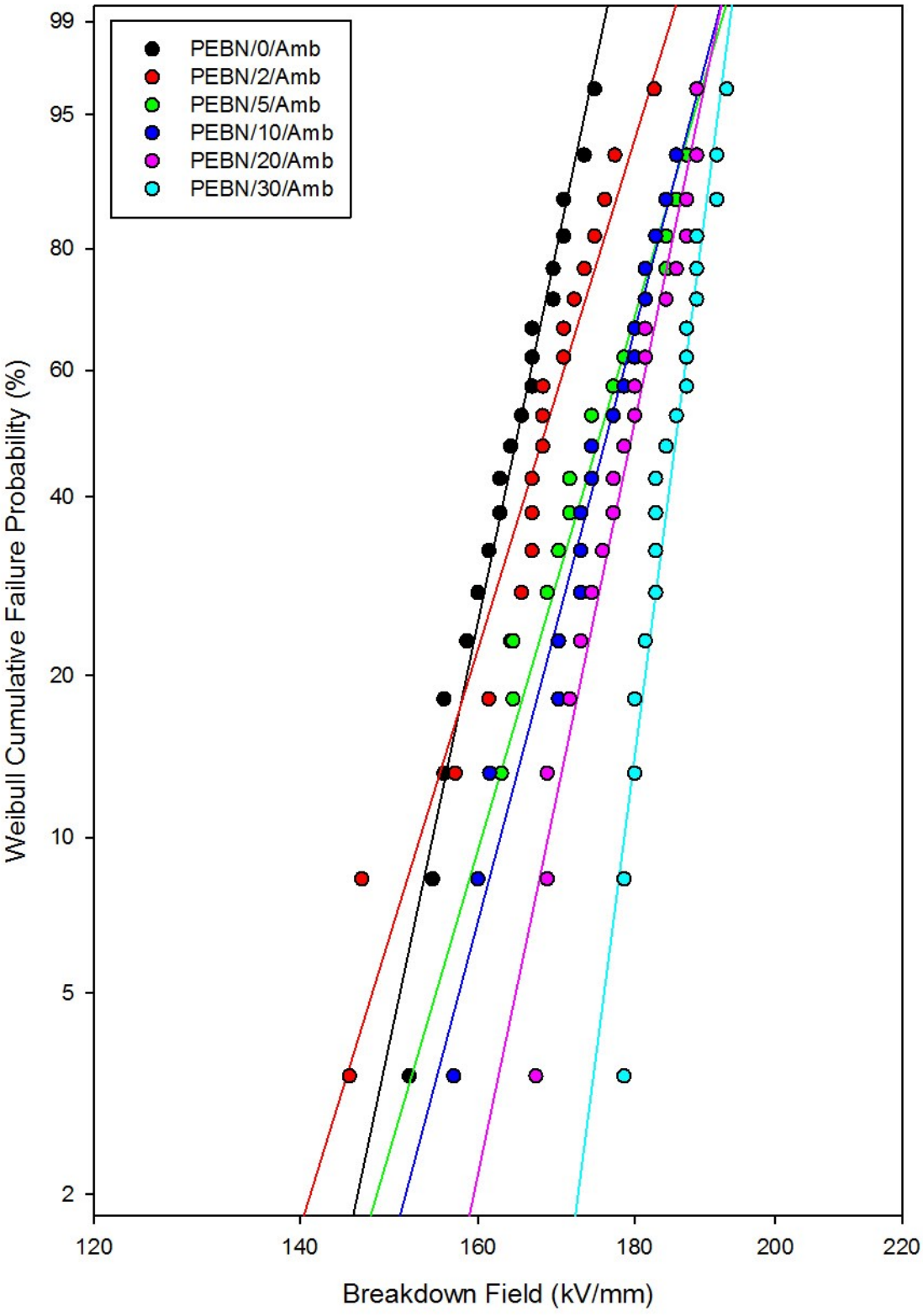

Figure 7.15: Weibull plots of the "Ambient" polyethylene/hBN nanocomposites

When considering the “Wet” samples, the breakdown strength of the nanocomposite samples was reduced relative to their corresponding “Dry” samples, and not relative to the unfilled sample, as observed in Figure 7.16. Any amount of water inclusions will deteriorate the electrical performance as the presence of water will aid charge transport. The shape parameter in the “Wet” samples has also decreased, indicating an increased scatter in the measured data. While the breakdown strength of the unfilled sample is ~167 kV/mm, the breakdown strength, of the “Dry” and “Wet” 30 wt % sample is 189 kV/mm and 176 kV/mm respectively, with a 7 % reduction after water immersion. While the breakdown strength of the “Wet” samples is lower than the “Dry” samples, however, it is still higher than the breakdown strength of the unfilled sample at higher filler content.

The breakdown strength of the “Wet to Dry” samples are similar to the “Dry” and “Ambient” samples, as shown in Figure 7.17, since all the water was successfully removed as seen from the mass change and dielectric spectroscopy data. The Weibull parameters for the samples under all conditioning regimes are listed in Table 7.2 .

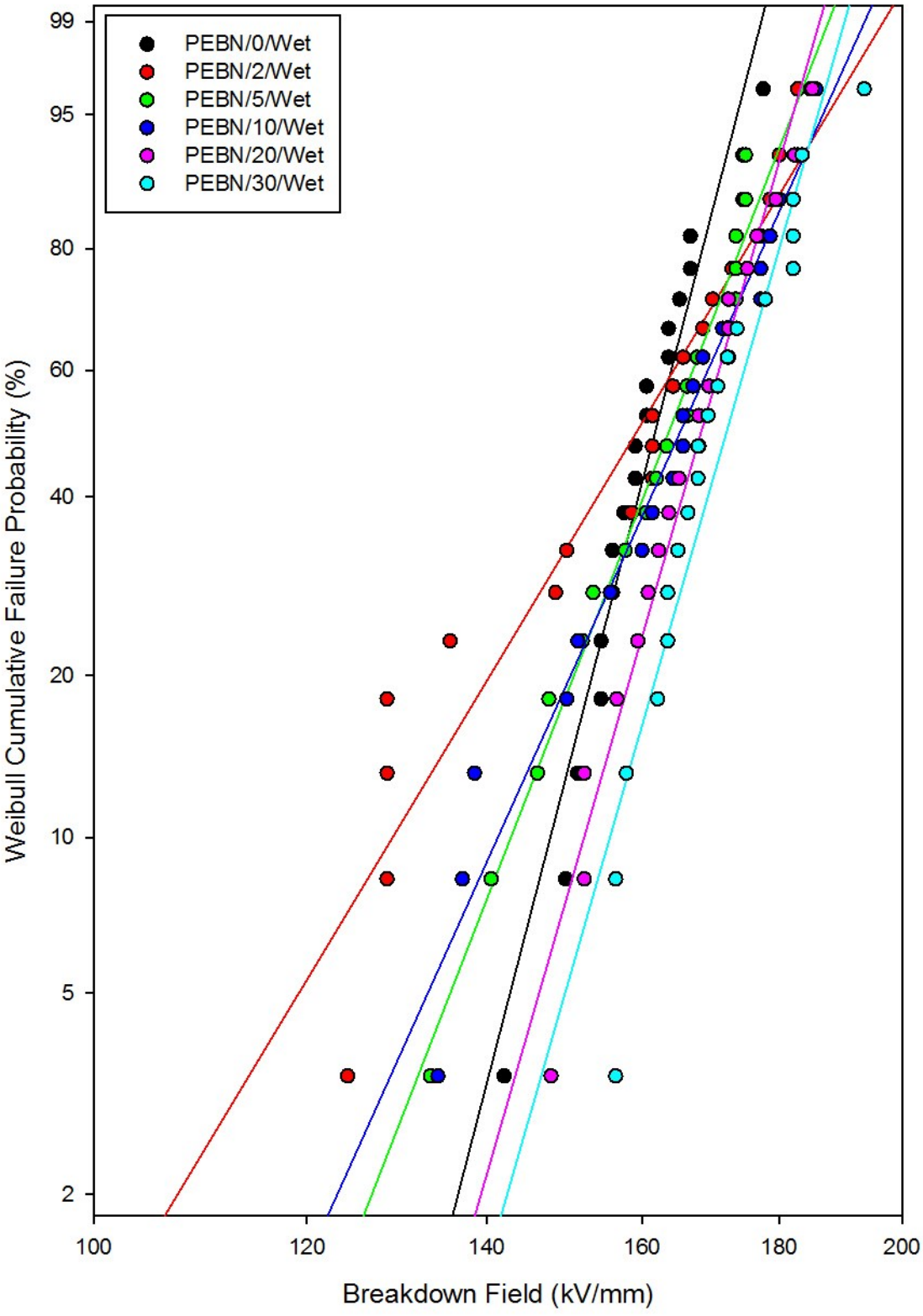

Figure 7.16: Weibull plots of the "Wet" polyethylene/hBN nanocomposites

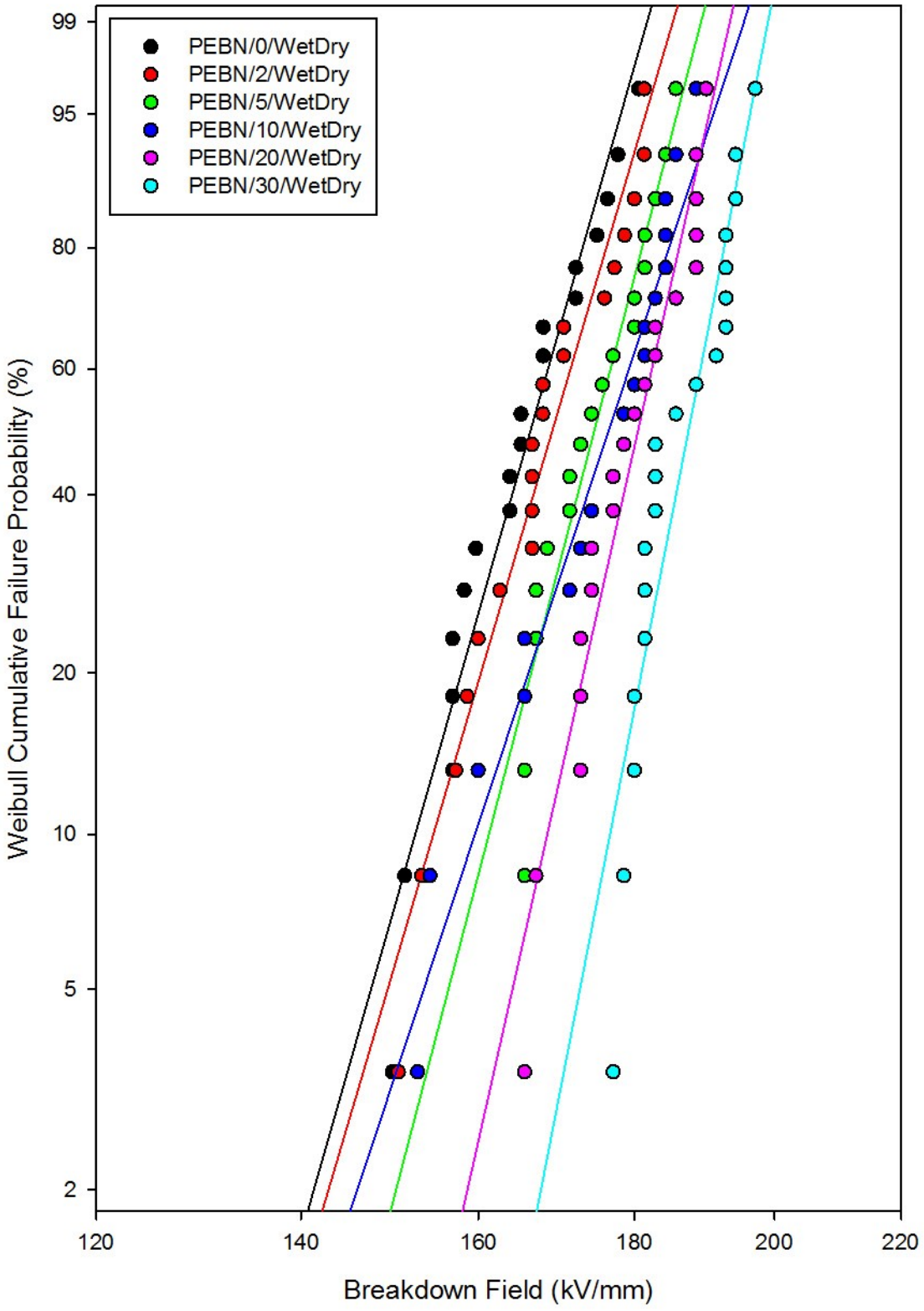

Figure 7.17: Weibull plot of the "Wet to Dry" polyethylene/hBN nanocomposites

Table 7.2: Weibull parameters of the polyethylene/hBN nanocomposites under all conditioning regimes

		PEBN/0	PEBN/2	PEBN/5	PEBN/10	PEBN/20	PEBN/30
Dry	**α (kV/mm)**	167 ± 2	171 ± 3	176 ± 3	179 ± 3	183 ± 2	189 ± 2
	β	38 ± 10	19 ± 5	24 ± 7	27 ± 8	32 ± 9	33 ± 8
Ambient	**α (kV/mm)**	167 ± 3	172 ± 3	175 ± 3	180 ± 2	182 ± 2	187 ± 2
	β	30 ± 8	23 ± 7	22 ± 6	26 ± 7	31 ± 9	46 ± 13
Wet	**α (kV/mm)**	165 ± 4	165 ± 6	168 ± 5	170 ± 5	172 ± 4	176 ± 4
	β	20 ± 5	11 ± 3	15 ± 4	14 ± 4	19 ± 5	17 ± 4
Wet to Dry	**α (kV/mm)**	169 ± 3	172 ± 4	175 ± 3	180 ± 4	183 ± 3	190 ± 2
	β	21 ± 6	22 ± 6	26 ± 8	24 ± 8	29 ± 8	33 ± 9

Some researchers who studied the effect of water absorption in nanocomposites have always reported a decrease in breakdown strength in the wet samples relative to the dry samples. For example, Fabiani et al. [231] used a polyethylene-co-vinylacetate polymer nanocomposite based on a 5 wt % fluorohectorite and boehmite filler. In both cases, the wet samples had a lower breakdown strength than the dry samples although the effect was much greater in the fluorohectorite nanocomposite due to its high aspect ratio, which is likely to form a percolating water network. Hosier et al. [227] reported the addition of 10 wt % of silica in polyethylene caused a slight reduction in the breakdown strength relative to the unfilled polyethylene under dry conditions. In wet conditions, they found that there is a significant reduction in breakdown strength, with a 65% and 75% reduction relative to the dry nanocomposite and unfilled polymer respectively. Hui et al. [75] studied the effect of water absorption on the breakdown strength in XLPE/silica nanocomposites. At 5 wt % and 12.5 wt % of silica, the breakdown strength reduced by 20 % and 60 % relative to the corresponding dry samples. These reductions are much more significant than the reductions in breakdown strengths reported in this study, although much higher concentrations of hBN are used here. As discussed earlier, the lack of available hydroxyl groups prevents the materials from absorbing much water, which does not significantly aid charge transport and lower the breakdown behaviour. There might be two competing mechanisms affecting the breakdown behaviour simultaneously here: the charge trapping/scattering effect which serves to enhance the breakdown field and the presence of electrically conductive inclusions, i.e. water molecules, which serve to aid charge transport. This is consistent with the idea that a percolating water network is not formed in these systems as the "Wet" hBN nanocomposites still maintain a breakdown strength relatively higher than the unfilled polyethylene. Any electrical conduction contribution from the observed low frequency upturn in the imaginary relative permittivity in the 20 wt % and 30 wt % nanocomposites is not significant and does not dominate the charge transport dynamics of the system. Indeed, the value of the imaginary relative permittivity at 0.1 Hz in the 30 wt % nanocomposite is less than 0.2, which is significantly much lower than the value of $\sim 10^4$ in a wet 10 wt % polyethylene silicon nitride nanocomposite [21] whose behaviour is dominated by charge transport through a percolating water network. Nonetheless, these nanocomposites continue to give excellent breakdown performance, at higher hBN concentrations in particular, even when exposed to the most humid conditions.

While many studies in the literature report the enhancement of electrical properties as the dispersion of the nanoparticles is improved, this study continues to show that this is not

always the case, even in a highly loaded and agglomerated system containing water. Experimental results, together with numerical simulations, in the work of Hosier et al. [21] have shown that a water percolating network can easily form in a well-dispersed 10 wt % silicon nitride polyethylene nanocomposite, while a highly agglomerated 10 wt % silica polyethylene nanocomposite cannot form a water percolating network. A well-dispersed system allows the overlapping of water shells all around the uniform structure which can easily form a percolating network, whereas the water shells only overlap locally in a highly agglomerated structure which does not achieve percolation. A percolating water network, which can easily form in a well-dispersed system where nanoparticles become very close to each other, provides a conductive path for charge carriers, which in turn aids charge transport and leads to a more rapid electrical breakdown of the material. While these results do not directly claim that agglomerated systems are more superior to well-dispersed systems, they do, however, suggest that well-dispersed systems can sometimes be undesirable. The relatively high breakdown strength of the wet nanocomposites in this study, which contain highly aggregated structures, agrees with the dielectric spectroscopy results and confirms that a percolating water network does not exist.

The presence of water without a percolating water network can also be very detrimental to the breakdown strength of the material. For example, Praeger et al. [230], [235] prepared two polyethylene/silica nanocomposites: a hydrophilic nanocomposite containing as-received silica (with many surface hydroxyl groups) and a hydrophobic nanocomposite with calcinated silica (where the surface hydroxyl groups have been removed by processing at high temperatures). Their study revealed that the dispersion in both nanocomposites was very similar and both contained large agglomerates of silica; however, there was a large difference in the breakdown behaviour of both systems. The major findings in the study was that the breakdown strength of the nanocomposite processed with the as-received silica decreased to approximately half of its value under ambient conditions, relative to its breakdown strength under dry conditions, while the nanocomposite processed with the calcinated silica retained its high breakdown strength under ambient conditions. While both nanocomposites exhibited a lower breakdown strength under wet conditions relative to their breakdown strength under dry conditions, the breakdown strength of the wet nanocomposite containing calcinated silica was approximately twice as large as the breakdown strength of the nanocomposite containing the as-received silica due to its reduced capability to absorb water. The findings of their study are consistent with the results of this work where the breakdown strength of nanocomposites is believed to be largely dominated by the presence

of water rather the structural or nanoparticle agglomeration effects. While many studies in the literature claim that functionalising the surface of nanoparticles leads to better dispersion and therefore improved breakdown strength, the improved breakdown strength in the nanocomposites with functionalised nanoparticle surfaces could potentially just be an effect of the presence of fewer available hydroxyl groups to bind with water molecules rather than an effect of better nanoparticle dispersion. The generally believed and accepted concept by the nanodielectrics community which states that better nanoparticle dispersion leads to improved electrical properties is therefore not always entirely true, and in fact could easily deteriorate the electric properties of the material under specific environmental conditions.

7.5 Electrical Conductivity

The effect of water absorption on the electrical conductivity of all the samples was measured, to aid the breakdown strength data. Figure 7.18 and Figure 7.19 show the electrical conductivity values measured as a function of time for the "Dry" and "Ambient" samples respectively, which are very similar. The conductivity of the unfilled sample falls rapidly at the start of the application of the field, due to polarisation effects, and gradually reduces with time until it reaches a steady state condition. On the other hand, the nanocomposites have a constant, lower, and time independent behaviour in comparison to the unfilled material; however, this does not represent the true conductivity behaviour of the nanocomposites due to the highly scattered data. At a filler content of 10 wt % and higher, the values of conductivity appear to overlap as the pico-ammeter is limited to current values corresponding to those conductivity values. It should be noted that many efforts have been made to produce samples with different geometries to yield a higher conduction current in order obtain a more accurate conductivity reading, however the current remained too low therefore suggesting that the conductivity of the nanocomposite samples is in fact likely to be much lower than that of the unfilled polyethylene sample. The low conductivity values of the nanocomposites in comparison to the unfilled polyethylene is in agreement with the breakdown results, where the nanocomposites exhibited an increased breakdown strength.

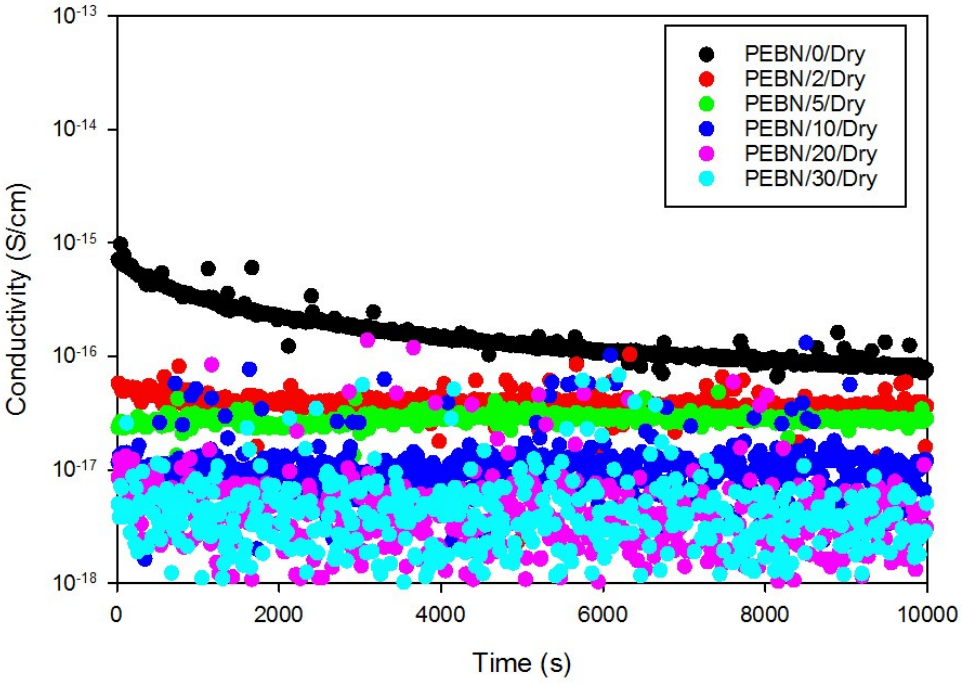

Figure 7.18: Conductivity of the "Dry" polyethylene/hBN nanocomposites

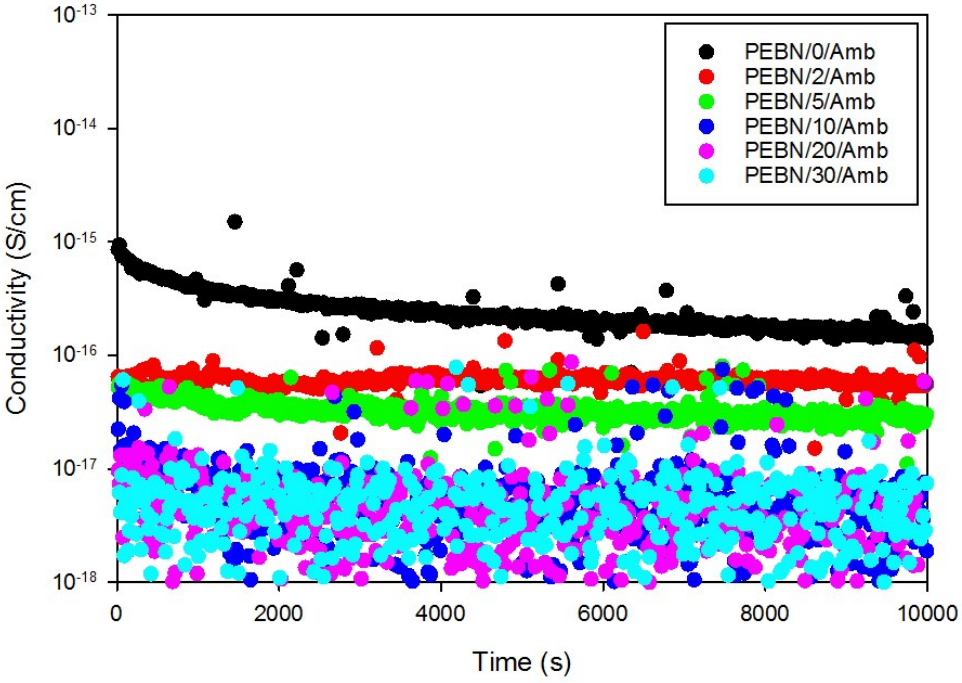

Figure 7.19: Conductivity of the "Ambient" polyethylene/hBN nanocomposites

Similar results have been reported in LDPE nanocomposites based on 3 wt % of magnesia and alumina fillers [236], and 3 wt % of a ZnO filler [237] where the nanocomposites exhibited a lower conductivity than the pure LDPE. In terms of hBN nanocomposites, Tsekmes et al. [238] reported a decrease in conductivity in a 5 wt % epoxy/hBN nanocomposite. However, the results in the literature usually report an increase in conductivity upon the addition of nanoparticles. For example, Ciuprina et al. [239] found that the conductivity values in LDPE nanocomposites based on silica, titania, and alumina fillers were all higher than the unfilled LDPE. Similarly, Sengwa et al. [240] found that the addition of 5 wt% of clay in a PEO-PMMA blend resulted in an increase in the conductivity when compared to the unfilled polymer. Where percolation effects are considered, Mendoza et al. [241] found that the conductivity of chitosan/clay nanocomposites increased significantly with increasing clay content in nanocomposite containing up to 40 wt % of clay, due to the conductive pathways caused by the percolating network, causing charge carriers to flow along the interfaces, thereby increasing the conductivity. This effect is not observed in the polyethylene/hBN nanocomposites investigated in this study, which is consistent with the idea that a conductive, percolating path does not exist. Therefore the conductivity data is consistent with the breakdown data where the conductivity decreases with increasing filler content, so the charge transport in this system is limited even at the percolation limit.

Figure 7.20 shows the electrical conductivity values measured as a function of time for the "Wet" samples. While the conductivity of the unfilled polyethylene is unaffected by conditioning, the conductivity of the "Wet" nanocomposites samples is initially slightly higher than the unfilled polyethylene; however, the conductivity values of the "Wet" nanocomposites eventually become lower with time. This initial rapid decrease in conductivity followed by a constant reduction with time is possibly attributed to the reducing water content in the nanocomposites with time, as the experiment was conducted under ambient conditions, and exposure of the nanocomposite in ambient conditions was also found to dry the nanocomposites where the mass of the samples dropped due to water loss.

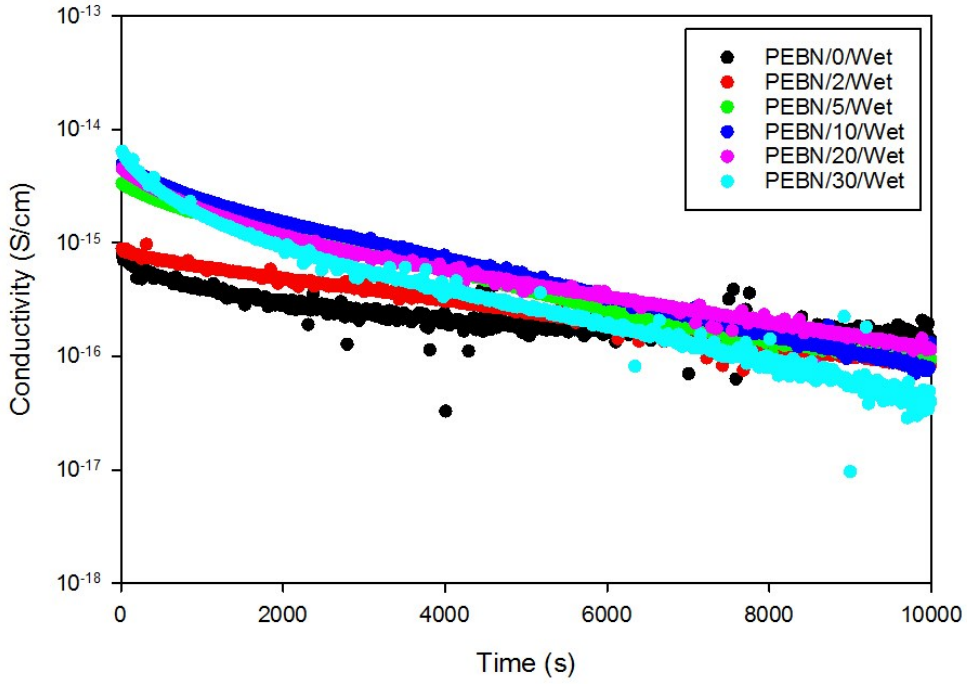

Figure 7.20: Conductivity of the "Wet" polyethylene/hBN nanocomposites

In contrast, Hosier et al. [227] reported a noticeable increase in conductivity in polyethylene nanocomposites based on silica and silicon nitride fillers under wet conditions, most possibly due to the more hydrophilic surfaces of the nanoparticles in their study. Therefore the conductivity results of the polyethylene/hBN nanocomposites here are consistent with the idea that water molecules are loosely bound to the surface of hBN, and also demonstrate why long dielectric spectroscopy measurements to a frequency of 0.01 Hz would provide unreliable results due to the observed rapid mass loss under ambient conditions.

The conductivity of the “Wet to Dry” samples is again identical to the “Dry” and “Ambient” samples, as shown in Figure 7.21, as there is no residual water after vacuum drying. The electrical conductivity behaviour can be attributed to the surface chemistry of the nanoparticles, which can aid or prevent charge transport. While many researchers have studied the conductivity behaviour of different nanocomposites, the general conclusion is that the inclusion of nanoparticles increases the conductivity of the material relative to the unfilled polymer. This is very different from the findings in this study where the exact opposite behaviour is reported, due to the lack of interconnected, conductive pathways, which is attributed to the surface chemistry of the hBN. All of these results are consistent

with the previous dielectric spectroscopy and electrical breakdown results suggesting that these nanocomposites have an enhanced electrical performance.

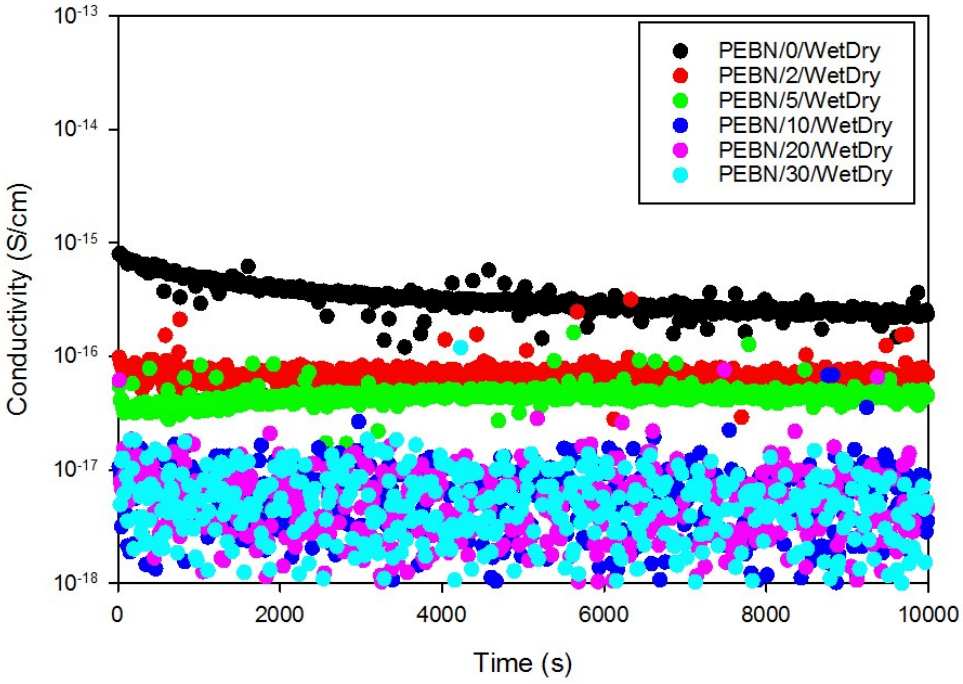

Figure 7.21: Conductivity of the "Wet to Dry" polyethylene/hBN nanocomposites

7.6 Conclusion

The dielectric response of the unfilled polyethylene was unaffected by any type of conditioning due to the hydrophobic nature of the polyethylene polymer. The dielectric response of the “Dry” and “Ambient” nanocomposites is very similar as the nanocomposites did not absorb any water under ambient conditions. Under dry and ambient conditions, the real relative permittivity of the nanocomposites was frequency independent and increased with increasing hBN content. The imaginary relative permittivity was frequency independent and within the noise limit of the equipment, which suggested that the nanocomposites exhibited very low losses under these conditions. The dielectric response of the “Wet” nanocomposites was significantly different than the “Dry” and “Ambient” nanocomposites despite absorbing a small amount of water. The measurements showed that the nanocomposites exhibited a broad relaxation peak due to the presence of water, which shifted to higher frequencies with increasing water content. The nanocomposites were able to lose all the amount of absorbed water after drying, which revealed that the interactions

between the hBN and water are very weak, due to the very small amount of available hydroxyl groups.

The breakdown strength and electrical conductivity measurements showed similar trends. The breakdown strength and conductivity of the "Dry" and "Ambient" samples were similar and exhibited an improved performance relative to the unfilled polyethylene. The breakdown strength increased with increasing hBN content and the conductivity decreased with increasing hBN content. The breakdown strength of the "Wet" samples decreased upon water immersion relative to the "Dry" nanocomposites although it was still higher than the unfilled polyethylene. The conductivity of the "Wet" samples increased with increasing hBN content due to the inclusion of water which highly affected the conductivity of the bulk material. The breakdown strength and conductivity behaviour of the "Wet" samples after drying ("Wet to Dry") became similar to the "Dry" and "Ambient" samples as the "Wet to Dry" samples lost all of the absorbed water.

These results suggest that the presence of water plays a major role in the electrical properties of nanocomposites. The main difference seen in this study and the published results in the literature is attributed to the different surface states of the used fillers: the hydrophilic and spherical surface of silica, which is commonly used, is surrounded by hydroxyl groups and therefore readily absorbs water to form conducting water shells whereas the hydrophobic surface of hBN does not favour water absorption due to the presence of a small amount of hydroxyl groups on the edge surfaces which cannot form water shells around the entire hBN particles; this property could be vital in the design of nanocomposites for high voltage electrical insulation. The surface chemistry of the nanoparticles, rather than the dispersion of nanoparticles within the polymer, affects how they interact with the charge carriers and may be the dominating factor in determining the electrical performance of nanodielectrics.

Chapter 8: Conclusions

8.1 Summary and Conclusions

A wide range of nanocomposites have been prepared in this work to understand the variability of the reported electrical properties of polymer nanocomposites in the literature. In order to underpin some of the fundamental mechanisms that determine the electrical properties of polymer nanocomposites, the research work presented here was set out to:

i) Investigate the chemical interactions between the hexagonal boron nitride filler and different solvents, and thus different dispersion states.
ii) Investigate the effect of nanoparticle agglomeration on the electrical properties of polymer nanocomposites.
iii) Investigate the role of surface chemistry of the nanoparticles, or the interface, in determining the electrical properties of polymer nanocomposites.

Initially, hBN nanocomposites were prepared using a polystyrene polymer matrix due to its amorphous nature, which enabled the hBN dispersion to be readily imaged without any morphological effects from the interactions between the polymer and the filler. Using a solution blending method, a total of six nanocomposites were prepared using three different solvents with a 5 wt % of hBN. The hBN particles were either sonicated in the solvent or the non-solvent prior to incorporation into the polystyrene. SEM examination revealed that the dispersion of the hBN in all six nanocomposites was relatively unchanged regardless of the used solvent. Therefore the hypothesis that different chemical interactions arise between the hBN and different solvents was not true in this case, as no noticeable degree of intercalation or exfoliation of the hBN particles was observed qualitatively in the SEM or quantitatively in the XRD analysis. While it was expected that this approach would lead to nanocomposites with different dispersion states, this was clearly not achieved. Although all nanocomposites exhibited a similar dispersion state, the hBN particles appeared to be uniformly distributed in the polymer.

Due to the polar nature of the B-N bond, a relatively strong bonding between the hBN layers exists which makes it difficult to separate the layers. Thus the energy from sonication in a solvent may not be sufficient in separating the hBN layers. Sonicating in a solvent after

modifying the surface of hBN with hydroxyl groups could aid in the separation of the hBN layers as this would result in stronger interactions with the solvent; however, the introduction of hydroxyl groups could be detrimental to the electrical properties of the nanocomposites. All the nanocomposites exhibited similar electrical properties as a result of similar dispersion states of the hBN particles, and therefore it is difficult to conclude whether this effect was due to the nanocomposites exhibiting similar hBN dispersion states or similar amounts of hBN particles. However, as the nanocomposites exhibited a slight increase in breakdown strength, despite having aggregated structures, it is therefore suggested that the dispersion state may not be a dominant factor affecting the breakdown strength of nanocomposites.

Following the investigation of the polystyrene/hBN nanocomposites, a range of polyethylene/hBN nanocomposites were prepared to investigate the effect of the dispersion/aggregation state of the hBN on the breakdown strength. Polyethylene samples were obtained by slow cooling through isothermal crystallisation where a total of 5 nanocomposites of different hBN content were prepared in addition to the unfilled polyethylene. The samples contained 2 wt %, 5 wt %, 10 wt %, 20 wt %, and 30 wt % of hBN. SEM analysis revealed that the distribution of hBN particles in the nanocomposites containing 10 wt % and less of hBN was fundamentally different than the nanocomposites containing 20 wt % or more of hBN. There were discrete hBN inclusions in the polymer matrix in the nanocomposites containing low loading levels of hBN while there were continuous hBN inclusions forming a percolating hBN structure in the nanocomposites containing high loading levels of hBN. In addition, the presence of hBN resulted in a severely disordered morphology, especially at high hBN loading levels, due to the ability of hBN to serve as an effective nucleating agent which inhibited crystal growth. While it could be argued that the changes in dielectric properties are brought about by the changes in polymer morphology, the effect of morphology on the dielectric properties was very subtle in comparison to the effects brought about by the addition of hBN such that presence of hBN masked any effects from the morphological changes in the isothermally crystallised polyethylene. To confirm this behaviour, quenched samples were prepared where the development of spherulites was suppressed by rapid crystallisation, and these materials exhibited a very similar breakdown strength behaviour which increased with increasing hBN content. Furthermore, the amorphous polystyrene/hBN nanocomposites exhibited an increase in breakdown strength, thereby suggesting that the presence of the filler, rather than the polymer morphology, determines the dielectric properties of the nanocomposites. Contrary to the general belief that nanocomposites with filler loading greater than 10 wt %

would highly deteriorate the electrical properties, the work in this study has shown not only did a 10 wt % polyethylene/hBN nanocomposite improved the dielectric breakdown strength, but also a percolating structure containing 30 wt % even further enhanced the dielectric breakdown strength. As the decreased breakdown strength of many nanocomposite systems reported in the literature was attributed to the presence of large agglomerates, the work here has shown otherwise and therefore the presence of agglomerates, while could affect the breakdown strength, may not always be the dominant factor to consider when trying to improve the electrical properties of polymer nanocomposites.

It has been speculated that the presence of water shells around nanoparticles governs the electrical properties of the nanocomposites here, and the nature of the systems in this work suggests that investigating the water absorption capabilities would be helpful. While the unfilled polymer did not seem to have absorbed any amount of water, all nanocomposites have absorbed some amount of water, as seen from increases in mass measurements, which was proportional to the amount of filler they contained. The samples only absorbed water when they were directly immersed in water, as exposure to ambient conditions showed no effect on their dielectric properties as compared to the dry conditions. The effects of water were very clear when the permittivity and dielectric losses were studied using dielectric spectroscopy, which revealed that the hydroxyl groups are most likely located on the edge surfaces of the hBN particles rather than the basal surfaces, which prevented the formation of a percolating water network. While samples under dry and ambient conditions showed slight increases in permittivity with a frequency independent behaviour and no apparent dielectric losses, the real permittivity of the "Wet" samples increased with reducing frequency and the dielectric losses were increased with increasing filler content. The dielectric breakdown strength of the "Dry" samples increased with increasing filler content while the breakdown strength of the "Wet" samples was lower than their corresponding "Dry" samples due to the water content. The conductivity of the "Dry" nanocomposites was always lower than the unfilled polyethylene. The conductivity of the "Wet" nanocomposite samples was higher than the unfilled polyethylene sample and appeared to have a slight dependence on time, although it was likely due to the samples losing water under ambient conditions. Under drying conditions, all the water was completely lost from the system and the performance of the resulting nanocomposites, referred to as "Wet to Dry" in the study, became identical to the "Dry" and "Ambient" samples. As the water was clearly free and not tightly bound to the interface in these nanocomposites, it was easily introduced and lost under the appropriate environmental conditions.

While the materials under “Dry” and “Ambient” conditions exhibited a superior performance with higher hBN content in comparison to the unfilled polyethylene, it is important to note that they were still slightly affected by the presence of water. However, this study clearly demonstrated that the effect of water in these nanocomposites was not very drastic as they absorbed an insignificant amount of water even at very high filler concentrations when compared to other studies, which incorporated more hydrophilic fillers. Although the nanocomposites absorbed some amount of water, this water could be easily removed from the nanocomposites through exposure to vacuum or ambient conditions for a very short time. This is due to the hydrophobic nature of the hexagonal boron nitride, in its as-received state without surface modification, which contains small amount of hydroxyl groups that are not as readily available to interact with water molecules as other types of fillers. This property of hBN prevents the nanocomposite from absorbing significant amounts of water and thus allowing the nanocomposites to continue to have a superior performance under all conditions.

The investigation on the role of water on the electrical properties revealed a major conclusion: the electrical properties of polymer nanocomposites are determined by the interaction between the surface of the nanofiller and the charge carriers rather than by the distribution or dispersion state of the nanofiller. Therefore much of the reported work in the literature regarding the improved dispersion due to surface functionalisation leading to improved breakdown strength could in fact be false. The most probable cause for the improved breakdown strength due to surface functionalisation is likely not to be due to better dispersion but rather could be due to the elimination or substitution of available surface hydroxyl groups which would reduce the amount of absorbed water under ambient and wet conditions. Choosing a hydrophobic nanofiller is ideal if a polymer nanocomposite is prepared with the goal of enhancing electrical properties. This would also eliminate the need of unnecessary nanofiller surface modification, which would be required if a hydrophilic filler is used. From an electrical engineering perspective, the interaction between nanodielectrics and the water in the environment must be controlled if they are to be used in any industrial application. This work served to give insight about both the inconsistencies regarding electrical properties of nanodielectrics and some of the major misconceptions about the factors that determine their electrical properties.

8.2 Future Work

It has been shown that graphite is easier to exfoliate than hBN despite having the same interlayer spacing, and nanocomposites incorporating exfoliated graphite were reported to reach the percolation threshold below 1 wt % of graphene content [242]. Although the research based on the hBN nanocomposites in this work revealed that the dispersion of nanoparticles is not the key to improving the electrical properties, exfoliation of hBN particles to achieve the same electrical performance as the 30 wt %, or percolation, with a lower hBN content would be worth studying. From an industrial and practical point of view, this would achieve a more efficient use of the hBN particles while lowering the cost of manufacturing of the nanocomposite if produced on a large-scale, as the cost of hBN is more expensive than the cost of polyethylene.

While the materials were immersed in water for a relatively short time for a few days, it would be worthwhile to conduct this experiment for a much longer duration to resemble practical situations. As high voltage subsea cables lay on the seabed for many years, the initiation of water trees becomes an issue which would lead to the premature failure of the cable insulation. It would be highly useful to investigate the role of nanoparticles on the formation of water trees in polyethylene.

A preliminary investigation of the thermal conductivity of the hBN nanocomposites was presented in this work. The thermal conductivity of dielectrics is important in high voltage cable as a higher thermal conductivity would allow a higher current carrying capacity. While the work here has shown that the addition of hBN enhanced the thermal conductivity, additional work is mandatory to understand how the thermal conductivity can be improved further for high voltage cable systems.

Appendices

Appendix A Theoretical Considerations for the Interactions Between the Hexagonal Boron Nitride and Solvents

Since a solvent blending method was used to prepare the nanocomposites, the choice of solvent is an important factor to consider. The solvent must first be compatible with the polymer and be able to efficiently disperse the hBN particles. Energy is required to overcome the van der Waals bonds between the stacked layers of hexagonal boron nitride to separate the individual sheets [243]. This process is known as exfoliation and two common methods found in the literature include mechanical and liquid exfoliation. Figure A.1 illustrates the exfoliation process of a layered material with the assistance of sonication to obtain nanosheets. Good solvents are those that have a similar surface energy to the layered material to chemically stabilise the exfoliated sheets and reduce their tendency to stack on top of each other again.

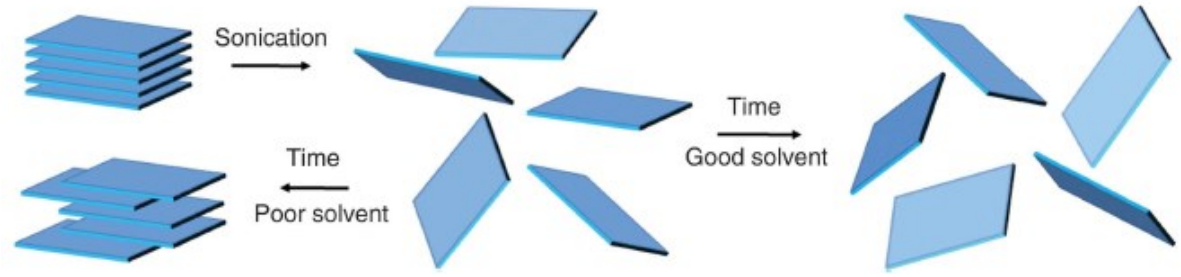

Figure A.1: Liquid exfoliation process by sonication in a solvent

The main reason for exfoliation is to significantly increase the surface area of the material thus enhancing consequent chemical and physical interactions. Although mechanical exfoliation can produce perfect crystalline structure sheets, the yield from this method is extremely low. Recent work on ball-milling techniques using gentle shear forces has yielded hBN sheets with lateral dimensions in the range of hundreds of nanometres and a thickness of a few nanometres, but some impurities have been introduced. Liquid exfoliation methods involve the use of sonication of the particles in a solvent to disperse the layers of boron nitride [244]. This is a more efficient method to produce large quantities of individual boron nitride layers than mechanical exfoliation. The dispersion of hexagonal boron nitride has

been studied in a variety of solvents. Tiano et al. [245] found that the following solvents were effective in dispersing BNNTs: N,N'-dimethylacetamide, N,N'-dimethylformamide, acetone, methanol, isopropyl alcohol, tetrahydrofuran, and N-methyl-2-pyrrolidone while the following solvents were found to be poor in dispersing the BNNTs: hexane, ethanol, pyridine, toluene, dimethylsulfoxide, acetic acid, dichloromethane, and chloroform. Cao et al. [127] used a 3:2 ammonia water solution: isopropyl alcohol mixture to exfoliate hexagonal boron nitride where they obtained a stable, well dispersed solution without precipitation for over a month. The effectiveness of IPA as a solvent for boron nitride exfoliation has been reported by other researchers [127], [246]. Han et al. [247] sonicated hBN for 1 h in a 1,2-dichloroethane solution of poly(m-henyl-enevinylene-co-2,5-dictoxy-p-phenylenevininylene) to break up the crystals of hBN. Few-layer hBN sheets were produced with lateral dimensions in the micron range. The solvent 1,2-dichloroethane was used because of its low boiling point which allows the easy removal of solvent.

Mixing the boron nitride with any solvent will lead to a change in entropy and enthalpy in the system, which can be related by:

$$\Delta G_{mix} = \Delta H_{mix} - T\Delta S_{mix} \tag{A.1}$$

where G is the Gibbs free energy of the system, H is the enthalpy of the system, S is the entropy of the system, and T is the temperature [245].

The mixing processes will be energetically favourable if the following condition is met:

$$\Delta G_{mix} < 0 \tag{A.2}$$

For large or long rigid like particles such as nanotubes or nanosheets, the entropy of mixing is very small and thus the enthalpy of mixing must be very small or as negative as possible to satisfy the above condition, which minimises the Gibbs free energy.

An approximation for ΔH_{mix} can be expressed using the Hildebrand-Scatchard equation:

$$\frac{\Delta H_{mix}}{V_{mix}} = \phi(1-\phi)(\delta_N - \delta_S)^2 \tag{A.3}$$

where $\Delta H_{mix}/V_{mix}$ is the enthalpy of mixing per unit volume, ϕ is the volume fraction of the particle , δ_N is the Hildebrand solubility parameter of the particle, δ_S is the Hildebrand solubility parameter of the solvent [248].

As this equation is approximate, it is useful to point out that there are clear shortcomings of this theory such that only positive enthalpies of mixing are allowed, which would result in a positive Gibbs free energy therefore a spontaneous reaction would not occur. Nevertheless, this theory is useful as it suggests that if $\delta_S \approx \delta_N$, the enthalpy of mixing will be minimised and a suitable solvent can be chosen to minimise the Gibbs free energy.

The Hildebrand solubility parameter can be expressed as:

$$\delta = \sqrt{E_{Sur}} \tag{A.4}$$

where E_{sur} is the surface energy of either the particle or the solvent. For hexagonal boron nitride, the surface energy is defined as the energy required to overcome the Van der Waals forces between two layers and separate them. For liquids, it is more appropriate to define surface energy in terms of the surface tension:

$$\gamma = E_{Sur}^{Sol} - TS_{Sur}^{Sol} \tag{A.5}$$

where γ is the surface tension of the solvent, E_{Sur}^{Sol} is the surface energy of the solvent, S_{Sur}^{Sol} is the surface entropy of the solvent, and *T* is the temperature in Kelvin [249].

The surface entropy of a liquid is a quantity that defines the relationship between the surface tension of a liquid and temperature, and can be expressed as:

$$S_{Sur}^{Sol} = -\left(\frac{\partial \gamma}{\partial T}\right) \tag{A.6}$$

So rewriting the equation in terms of the surface energy of the liquid:

$$E_{Sur}^{Sol} = \gamma - T\left(\frac{\partial \gamma}{\partial T}\right) \tag{A.7}$$

The energy for exfoliation of the hexagonal boron nitride platelets is minimised when the surface energy of the solvent matches the surface energy of the particles. Extensive

experimental work has been done on the surface energy of carbon nanotubes and graphene but there are very few studies of the surface energy of hexagonal boron nitride. Rathod et al. [250] measured the surface energy of a range of boron nitride powders and Seth et al. [251] characterised the same powders in an earlier study. This is the most frequently cited reference from other researchers when referring to the surface energy of boron nitride. They found that the boron nitride powders have a surface energy in the range of 44 – 66 mJ/m^2. The surface tension and surface entropy for different available solvents have been experimentally determined and reported in the literature [252]. With these values, the above equation can be used to calculate the surface energy of the different solvents at room temperature, which is listed in Table A.1 with the other surface properties of the liquid.

Table A.1: Surface Energy of the Different Solvents

Solvent	$\boldsymbol{\gamma}$ **(mJ/m^2)**	$\frac{\partial \gamma}{\partial T}$ **(mJ/m^2 K)**	E_{Sur}^{Sol}**(mJ/m^2)**
Xylene	30.10	-0.1101	62.36
Dichloromethane	26.50	-0.1284	64.12
Toluene	28.40	-0.1189	63.24
Chlorobenzene	33.60	-0.1191	68.50
Isopropyl Alcohol	23.00	-0.0789	46.12
Methanol	22.70	-0.0773	45.35

With the exception of chlorobenzene, the surface energy values for all the solvents lie within the reported measured range of the surface energy of the boron nitride. The surface energy values of xylene, dichloromethane, toluene, and chlorobenzene are very similar, which lie within the upper range of the reported values of the surface energy of boron nitride, while the surface energy values of IPA and methanol are almost identical, which lie within the lower range of the reported values of the surface energy of boron nitride. Therefore these solvents are ideal for this research as they are expected to result in different interactions with the hBN, which would result in different dispersion states.

It should be noted that hBN solutions in all the solvents listed in Table A.1 have been previously examined by SEM, however, the micrographs showed a considerable amount of agglomeration, which was possibly attributed to the re-aggregation of the hBN after the evaporation of the solvent on the SEM stubs. Additionally, the size of the hBN in the solvents was examined by dynamic light scattering (DLS), however this resulted in a high degree of uncertainty and unrepeatability. Therefore both sets of results were considered to be unsuitable for analysis.

Appendix B Morphology and Breakdown Strength of the Quenched Polyethylene Hexagonal Boron Nitride Nanocomposites

B.1 Introduction

In section 6.8, the breakdown strength of the isothermally crystallised samples was compared to the quenched sample, and it was concluded that both sets of samples followed the same breakdown behaviour trend. The data in this appendix shows that the morphology of the quenched samples is largely unaffected by the presence of the hBN particles, which aids the results in Section 6.8 that show that the increase in breakdown strength was not caused by the morphological changes in the polyethylene.

B.2 Differential Scanning Calorimetry

Figure B.1 shows the DSC data for all the quenched polyethylene/hBN nanocomposites. The quenched samples exhibit a very broad endotherm at lower temperatures, corresponding to a distribution of polyethylene crystals consisting mainly of LDPE and some HDPE crystals which did not crystallise at higher temperatures due to the rapid crystallisation. The DSC data show that the crystallinity of the quenched nanocomposites, as seen in Figure B.1, is lower than the isothermally crystallised nanocomposites, as seen in Section 6.6. Furthermore, the crystallinity values of the all the quenched nanocomposites are very similar to the crystallinity of the unfilled polyethylene, which suggests that the hBN does not suppress crystal growth as in the isothermally crystallised samples, and that the crystallinity in the quenched samples is largely determined by the crystallisation method rather than the presence of the hBN particles.

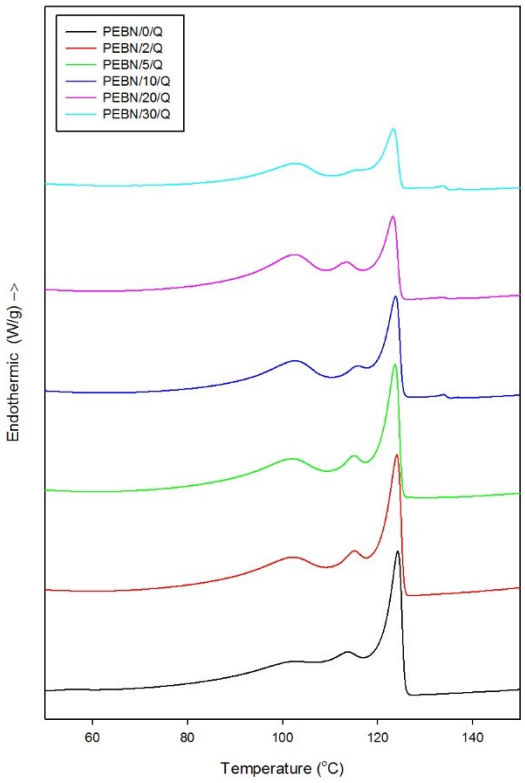

Material	T_{m_1}(°C)	T_{m_2}(°C)	χ (%)
PEBN/0/Q	103.0	122.9	32.1
PEBN/2/Q	102.2	123.2	32.2
PEBN/5/Q	102.0	123.1	30.7
PEBN/10/Q	102.7	123.3	29.4
PEBN/20/Q	102.5	123.5	30.2
PEBN/30/Q	102.8	123.4	29.8

Figure B.1: DSC melting traces with the corresponding melting temperature and crystallinity

B.3 Scanning Electron Microscopy

Figure B.2 shows the SEM micrographs of all the quenched polyethylene/hBN nanocomposites. While the presence of some spherulitic features may undoubtedly exist, there is a lack of structural or morphogical detail in the SEM micrographs in comparison to the isothermally crystallised samples shown in Section 6.4; crystallisation by quenching suppresses crystal growth, as seen in the DSC crystallinity values, which results in similar crystallinity values in all of the samples, regardless of the hBN content. Therefore the SEM and DSC results highly suggest that the hBN does not alter the morphology of the polyethylene.

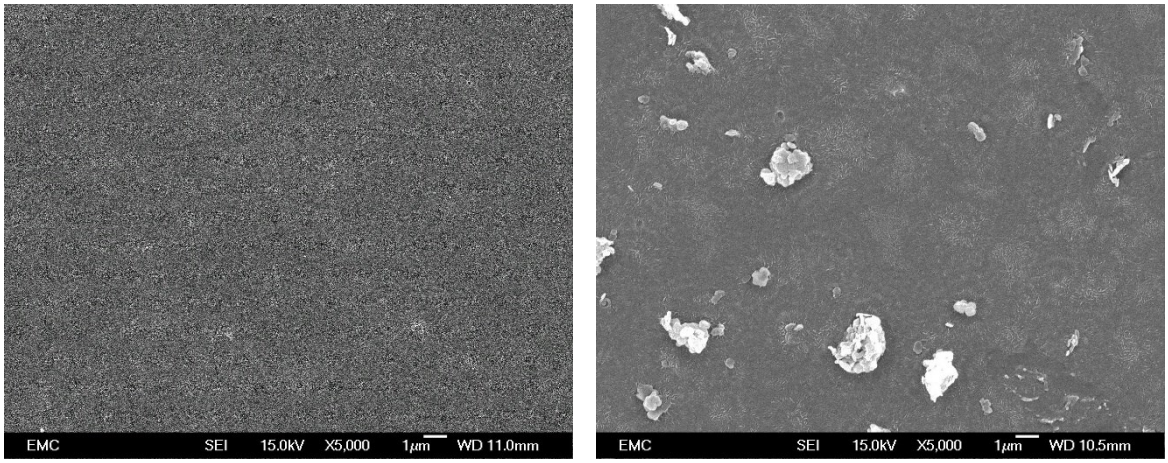

(a) (b)

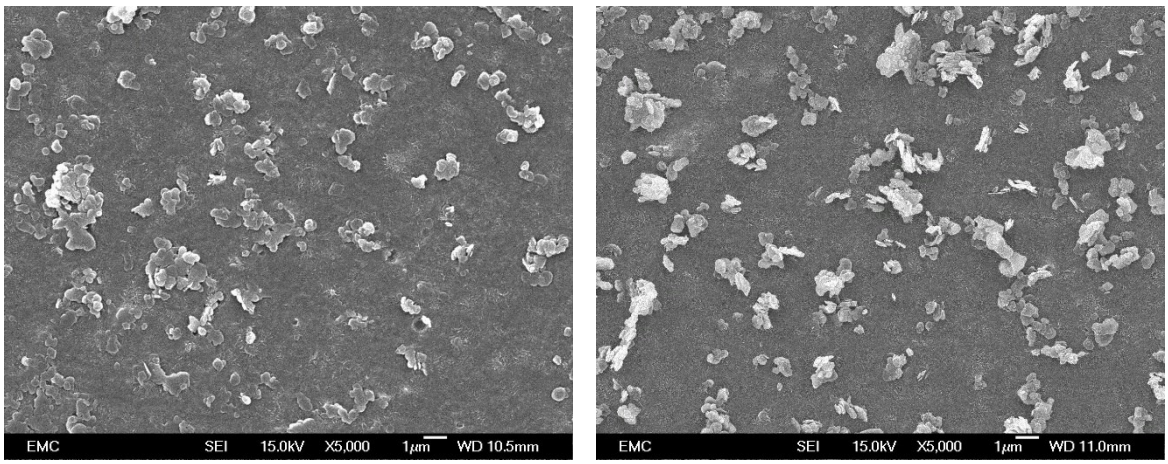

(c) (d)

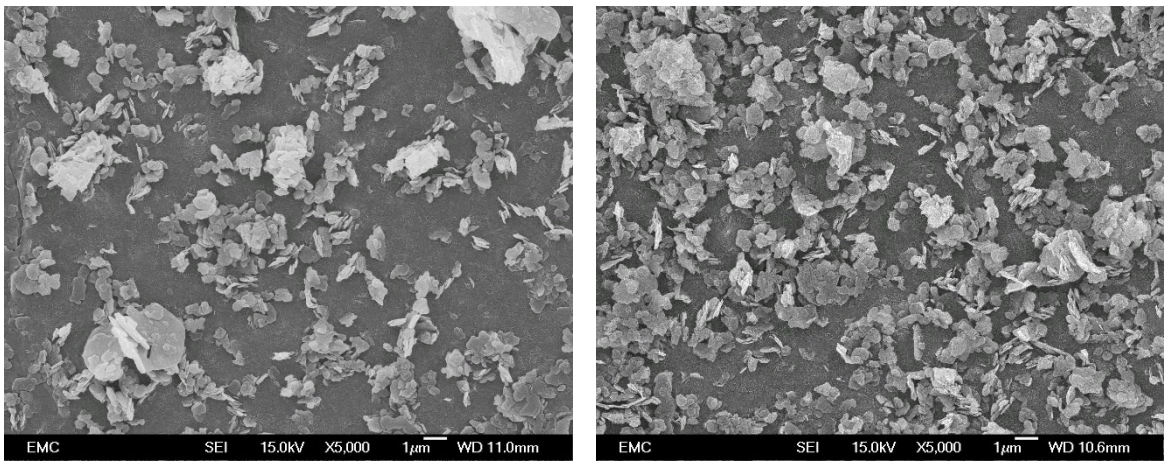

(e) (f)

Figure B.2: SEM micrographs of the quenched polyethylene/hBN nanocomposites containing (a) 0 wt%, (b) 2 wt %, (c) 5 wt %, (d) 10 wt %, (e) 20 wt%, and (f) 30 wt % hBN content

B.4 Dielectric Breakdown Strength

Figure B.3 shows the Weibull plots of the quenched polyethylene/hBN nanocomposites with the corresponding Weibull parameters. The figure shows a monotonic increase in breakdown strength with increasing hBN content; this is similar to the trend seen in the isothermally crystallised samples. The quenched polyethylene/hBN nanocomposites, which resulted in no change in crystallinity, and the isothermally crystallised samples, which resulted in a significant change in crystallinity and morphology, both exhibit the same pattern in breakdown behaviour therefore suggesting that the morphological changes are not the cause for the enhanced breakdown strength.

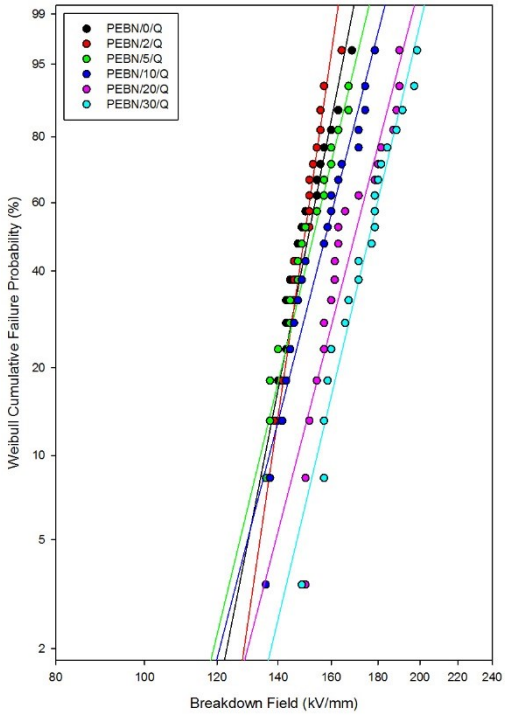

Material	Scale parameter α (kV/mm)	Shape parameter β
PEBN/0/Q	154 ± 4	16 ± 5
PEBN/2/Q	152 ± 3	22 ± 6
PEBN/5/Q	157 ± 5	13 ± 4
PEBN/10/Q	162 ±56	13 ± 4
PEBN/20/Q	175 ± 5	13 ± 4
PEBN/30/Q	181 ± 5	14 ± 4

Figure B.3: Weibull plots of the quenched polyethylene/hBN nanocomposites

References

[1] D. Gielen, F. Boshell, and D. Saygin, "Climate and energy challenges for materials science," *Nature Materials*, vol. 15, no. 2, pp. 117–120, 2016.

[2] P. Lakshmanan, J. Liang, and N. Jenkins, "Assessment of collection systems for HVDC connected offshore wind farms," *Electric Power Systems Research*, vol. 129, pp. 75–82, 2015.

[3] J. K. Nelson, "Overview of nanodielectrics : insulating materials of the future," in *Electrical Insulation Conference and Electrical Manufacturing Expo*, 2007, pp. 229–235.

[4] T. J. Lewis, "Nanometric dielectrics," *IEEE Transactions on Dielectrics and Electrical Insulation*, vol. 1, no. 5, pp. 812–825, 1994.

[5] A. Okada and A. Usuki, "Twenty years of polymer-clay nanocomposites," *Macromolecular Materials and Engineering*, vol. 291, no. 12, pp. 1449–1476, Dec. 2006.

[6] G. Motors, "Auto applications drive commercialization of nanocomposites," *Plastics, Additives, & Compounding*, 2002.

[7] F. Gao, "Clay / polymer composites : the story," *Materials Today*, no. November, pp. 50–55, 2004.

[8] P. O. Henk, T. W. Kortsen, and T. Kvarts, "Increasing the electrical discharge endurance of acid anhydride cured DGEBA epoxy resin by dispersion of nanoparticle silica," *High Performance Polymers*, vol. 11, pp. 281–296, 1999.

[9] J. K. Nelson, J. Fothergill, L. A. Dissado, and W. Peasgood, "Towards an understanding of nanometric dielectrics," *Conference on Electrical Insulation and Dielectric Phenomena*, pp. 295–298, 2002.

[10] Y. Wang, C. Wang, W. Chen, and K. Xiao, "Effect of stretching on electrical properties of LDPE/MgO nanocomposites," *IEEE Transactions on Dielectrics and Electrical Insulation*, vol. 23, no. 3, pp. 1713–1722, 2016.

[11] Y. Chen and J. Wu, “Investigation on relationship between breakdown strength enhancement of composites and dielectric characteristics of nanoparticle,” *IEEE Transactions on Dielectrics and Electrical Insulation*, vol. 23, no. 2, pp. 927–934, 2016.

[12] S. A. Mansour, R. A. Elsad, and M. A. Izzularab, “Dielectric properties enhancement of PVC nanodielectrics based on synthesized ZnO nanoparticles,” *Journal of Polymer Research*, vol. 23, no. 5, p. 85, 2016.

[13] Z. Li, K. Okamoto, Y. Ohki, and T. Tanaka, “Role of nano-filler on partial discharge resistance and dielectric breakdown strength of micro-Al203 / epoxy composites,” *Proceedings of the 9th International Conference on Properties and Applications of Dielectric Materials*, pp. 753–756, 2009.

[14] S. Siddabattuni, T. P. Schuman, and F. Dogan, “Improved polymer nanocomposite dielectric breakdown performance through barium titanate to epoxy interface control,” *Materials Science and Engineering: B*, vol. 176, no. 18, pp. 1422–1429, Nov. 2011.

[15] X. Huang, Z. Ma, Y. Wang, P. Jiang, Y. Yin, and Z. Li, “Polyethylene / Aluminum Nanocomposites : Improvement of Dielectric Strength by Nanoparticle Surface Modification,” *Journal of Applied Polymer Science*, vol. 113, pp. 3577–3584, 2009.

[16] K. Y. Lau, A. S. Vaughan, G. Chen, and I. L. Hosier, “Polyethylene nanodielectrics: The effect of nanosilica and its surface treatment on electrical breakdown strength,” *Conference on Electrical Insulation and Dielectric Phenomena*, pp. 21–24, Oct. 2012.

[17] J. K. Nelson and J. C. Fothergill, “Internal charge behaviour of nanocomposites,” *Nanotechnology*, vol. 15, no. 5, pp. 586–595, May 2004.

[18] S. Singha and M. Thomas, “Dielectric properties of epoxy nanocomposites,” *IEEE Transactions on Dielectrics and Electrical Insulation*, vol. 15, no. 1, pp. 12–23, 2008.

[19] T. Andritsch, R. Kochetov, P. H. F. Morshuis, and J. J. Smit, “Dielectric properties and space charge behavior of MgO-epoxy nanocomposites,” *International Conference on Solid Dielectrics*, pp. 5–8, 2010.

[20] K. Y. Lau, A. S. Vaughan, G. Chen, and I. L. Hosier, “Dielectric response of polyethylene nanocomposites: The effect of surface treatment and water absorption,”

Conference on Electrical Insulation and Dielectric Phenomena, pp. 275–278, Oct. 2012.

[21] I. L. Hosier, M. Praeger, A. S. Vaughan, and S. G. Swingler, "The effects of water on the dielectric properties of silicon based nanocomposites," *IEEE Transactions on Nanotechnology*, vol. PP, no. 99, pp. 1–10, 2016.

[22] T. Okazaki, S. Okuzumi, S. Imazawa, Y. Murakami, M. Nagao, Y. Sekiguchi, C. C. Reddy, and Y. Murata, "Electric characteristics of MgO/LDPE nanocomposite up to breakdown under DC ramp voltage," *Conference on Electrical Insulation and Dielectric Phenomena*, pp. 654–657, 2009.

[23] A. Ersoy and H. R. Hiziroglu, "Electrical breakdown of polyurethane-based nanocomposites," *Proceedings of the 2010 IEEE International Conference on Solid Dielectrics, ICSD 2010*, pp. 10–12, 2010.

[24] P. Preetha and M. J. Thomas, "AC breakdown characteristics of epoxy nanocomposites," *IEEE Transactions on Dielectrics and Electrical Insulation*, vol. 18, no. 5, pp. 1526–1534, 2011.

[25] S. Li, G. Yin, and J. Li, "Breakdown performance of low density polyethylene nanocomposites," *IEEE 10th International Conference on the Properties and Applications of Dielectric*, pp. 10–13, 2012.

[26] R. Kochetov, T. Andritsch, P. H. F. Morshuis, and J. J. Smit, "Evaluation of the influence of various nanofillers on the AC breakdown strength of epoxy-based nanocomposites," in *International Conference on Electrical Insulating Materials*, 2011, pp. 383–386.

[27] W. Wang, S. Li, F. Tang, and J. Li, "Characteristics on breakdown performance of polyethylene/silica dioxide nanocomposites," *Conference on Electrical Insulation and Dielectric Phenomena*, pp. 521–524, 2012.

[28] P. Preetha and M. J. Thomas, "AC breakdown characteristics of epoxy alumina nanocomposites," *Conference on Electrical Insulation and Dielectric Phenomena*, pp. 26–29, 2010.

[29] K. Y. Lau, A. S. Vaughan, G. Chen, I. L. Hosier, and A. F. Holt, "On Interfaces and the DC Breakdown Performance of Polyethylene / Silica Nanocomposites," *Conference on Electrical Insulation and Dielectric Phenomena*, pp. 679–682, 2014.

[30] S. Singha and M. Thomas, “Reduction of Permittivity in Epoxy Nanocomposites,” in *Conference on Electrical Insulation and Dielectric Phenomena*, 2008, pp. 726–729.

[31] T. Andritsch, R. Kochetov, P. H. F. Morshuis, and J. J. Smit, “The complex permittivity of epoxy based nanocomposites with alumina and magnesium oxide fillers at very low temperatures,” *Conference on Electrical Insulation and Dielectric Phenomena*, pp. 306–309, 2011.

[32] T. J. Lewis, “Interfaces: nanometric dielectrics,” *Journal of Physics D: Applied Physics*, vol. 38, no. 2, pp. 202–212, Jan. 2005.

[33] T. J. Lewis, “Interfaces and nanodielectrics are synonymous,” *International Conference on Solid Dielectrics*, 2004.

[34] T. J. Lewis, “Interfaces are the dominant feature of dielectrics at the nanometric level,” *IEEE Transactions on Dielectrics and Electrical Insulation*, vol. 11, no. 5, pp. 739–753, Oct. 2004.

[35] T. Tanaka, M. Kozako, N. Fuse, and Y. Ohki, “Proposal of a multi-core model for polymer nanocomposite dielectrics,” *IEEE Transactions on Dielectrics and Electrical Insulation*, vol. 12, no. 4, pp. 669–681, Aug. 2005.

[36] T. Tanaka, “Dielectric nanocomposites with insulating properties,” *IEEE Transactions on Dielectrics and Electrical Insulation*, vol. 12, no. 5, pp. 914–928, Oct. 2005.

[37] S. Raetzke and J. Kindersberger, “Role of interphase on the resistance to high-voltage arcing, on tracking and erosion of silicone/SiO2 nanocomposites,” *IEEE Transactions on Dielectrics and Electrical Insulation*, vol. 17, no. 2, pp. 607–614, Apr. 2010.

[38] T. Andritsch, R. Kochetov, P. H. F. Morshuis, and J. J. Smit, “Proposal of the polymer chain alignment model,” *Conference on Electrical Insulation and Dielectric Phenomena*, pp. 624–627, Oct. 2011.

[39] K. N. Mathes, “A brief history of development in electrical insulation,” in *Proceedings of the 20th Electrical Electronics Insulation Conference*, 1991, pp. 147–150.

[40] G. Teyssedre and C. Laurent, “Advances in high-field insulating polymeric materials over the past 50 years,” *IEEE Electrical Insulation Magazine*, vol. 29, no. 5, pp. 26–35, 2013.

[41] W. J. Plate, T. H. Ling, and J. F. Nuccio, “Reassessment of Polyethylene Power Cable,” *IEEE Transactions on Power Apparatus and Systems*, vol. 82, no. 69, pp. 990–1002, 1963.

[42] L. Hartshorn, N. J. L. Megson, and E. Hushton, “Plastics and electrical insulation,” *Journal of the Institution of Electrical Engineers*, vol. 83, no. 502, pp. 474–487, 1938.

[43] R. M. Eichhorn, “Treeing in Solid Extruded Electrical Insulation,” *IEEE Transactions on Electrical Insulation*, vol. 12, no. 1, pp. 2–18, 1977.

[44] R. B. Blodgett and R. G. Fisher, “Insulations and Jackets ror Cross-Linked Polyethylene Cables,” *IEEE Transactions on Power Apparatus and Systems*, vol. 82, no. 69, pp. 971–980, 1963.

[45] M. Ishida, T. Okamoto, and K. Izumi, “Morphological improvement of the insulation for EHV XLPE cables by an additive,” in *Conference Record of the 1990 IEEE International Symposium on Electrical Insulation*, 1990, pp. 309–312.

[46] T. L. Hanley, R. P. Burford, R. J. Fleming, and K. W. Barber, “A general review of polymeric insulation for use in HVDC cables,” *IEEE Electrical Insulation Magazine*, vol. 19, no. 1, pp. 13–24, 2003.

[47] M. S. Khalil, “International research and development trends and problems of HVDC cables with polymeric insulation,” *IEEE Electrical Insulation Magazine*, vol. 13, no. 6, pp. 35–47, 1997.

[48] X. Huang, P. Jiang, and T. Tanaka, “A review of Dielectric Polymer Composites with High Thermal Conductivity,” *IEEE Electrical Insulation Magazine*, vol. 27, no. 4, pp. 8–16, 2011.

[49] W. Zhou, S. Qi, Q. An, H. Zhao, and N. Liu, “Thermal conductivity of boron nitride reinforced polyethylene composites,” *Materials Research Bulletin*, vol. 42, no. 10, pp. 1863–1873, 2007.

[50] C. Vanga-Bougana, S. Savoie, M. Frechette, and E. David, “Synthesis and Characterization of Ultra High Molecular Weight Polyethylene Filled with Boron

Nitride Micro and Nano-Particles," in *Electrical Insulation Conference*, 2015, pp. 234–237.

[51] W. Zhou, J. Zuo, X. Zhang, and a. Zhou, "Thermal, electrical, and mechanical properties of hexagonal boron nitride-reinforced epoxy composites," *Journal of Composite Materials*, no. August, Aug. 2013.

[52] B. X. Du and M. Xiao, "Effects of Thermally Conducting Particles on Resistance to Tracking Failure of Polyimide/BN Composites," *IEEE Transactions on Dielectrics and Electrical Insulation*, vol. 21, no. 4, pp. 1565–1572, 2014.

[53] T. Heid, M. Frechette, and E. David, "Epoxy/BN micro- and submicro-composites: Dielectric and thermal properties of enhanced materials for high voltage insulation systems," *IEEE Transactions on Dielectrics and Electrical Insulation*, vol. 22, no. 2, pp. 1176–1185, 2015.

[54] M. Reading, A. S. Vaughan, and P. L. Lewin, "An investigation into improving the breakdown strength and thermal conduction of an epoxy system using boron nitride," in *Conference on Electrical Insulation and Dielectric Phenomena*, 2011, pp. 636–639.

[55] F. Saysouk, S. Diaham, M. Locatelli, B. Belkerk, and Y. Scudeller, "Enhancement of Thermal Conduction of Polyimide / Boron Nitride Nanocomposites," in *Conference on Electrical Insulation and Dielectric Phenomena*, 2013, pp. 543–546.

[56] M. Tanimoto, T. Yamagata, K. Miyata, and S. Ando, "Anisotropic Thermal Diffusivity of Hexagonal Boron Nitride-Filled Polyimide Films: Effects of Filler Particle Size, Aggregation, Orientation, and Polymer Chain Rigidity," *ACS Applied Materials and Interfaces*, vol. 5, no. 10, pp. 4374–4382, 2013.

[57] S. N. Monteiro, A. L. D. Skury, M. G. De Azevedo, and G. S. Bobrovnitchii, "Cubic boron nitride competing with diamond as a superhard engineering material - An overview," *Journal of Materials Research and Technology*, vol. 2, no. 1, pp. 68–74, 2013.

[58] C. A. Grabowski, S. P. Fillery, N. M. Westing, C. Chi, J. S. Meth, M. F. Durstock, and R. A. Vaia, "Dielectric breakdown in silica-amorphous polymer nanocomposite films: The role of the polymer matrix," *ACS Applied Materials and Interfaces*, vol. 5, no. 12, pp. 5486–5492, 2013.

[59] P. Kim, N. M. Doss, J. P. Tillotson, P. J. Hotchkiss, M. Pan, S. R. Marder, J. Li, J. P. Calame, and J. W. Perry, "High Energy Density Nanocomposites Based on Surface-Modified BaTiO3 and a Ferroelectric Polymer," *ACS Nano*, vol. 3, no. 9, pp. 2581–2592, 2009.

[60] T. Andritsch, R. Kochetov, Y. T. Gebrekiros, P. H. F. Morshuis, and J. J. Smit, "Short term DC breakdown strength in epoxy based BN nano- and microcomposites," *IEEE International Conference on Solid Dielectrics*, pp. 1–4, 2010.

[61] I. A. Tsekmes, R. Kochetov, P. H. F. Morshuis, and J. J. Smit, "AC Breakdown Strength of Epoxy-Boron Nitride Nanocomposites : Trend & Reproducibility," in *Electrical Insulation Conference*, 2015, pp. 446–449.

[62] I. A. Tsekmes, R. Kochetov, P. H. F. Morshuis, and J. J. Smit, "DC Breakdown Strength of Epoxy-Boron Nitride Nanocomposites : Trend and Reproducibility," in *Conference on Electrical Insulation and Dielectric Phenomena*, 2015, pp. 479–482.

[63] Z. Wang, T. Iizuka, M. Kozako, Y. Ohki, and T. Tanaka, "Development of epoxy/BN composites with high thermal conductivity and sufficient dielectric breakdown strength part I-Sample preparations and thermal conductivity," *IEEE Transactions on Dielectrics and Electrical Insulation*, vol. 18, no. 6, 2011.

[64] Z. Wang, T. Iizuka, M. Kozako, Y. Ohki, and T. Tanaka, "Development of epoxy/BN composites with high thermal conductivity and sufficient dielectric breakdown strength part II-breakdown strength," *IEEE Transactions on Dielectrics and Electrical Insulation*, vol. 18, no. 6, pp. 1963–1972, 2011.

[65] S. L. Chung and J. S. Lin, "Thermal Conductivity of Epoxy Resin Composites Filled with Combustion Synthesized h-BN Particles," *Molecules*, vol. 21, no. 5, pp. 1–11, 2016.

[66] V. Nguyen, a. Vaughan, P. Lewin, and a. Krivda, "The effect of resin stoichiometry and nanoparticle addition on epoxy/silica nanodielectrics," *IEEE Transactions on Dielectrics and Electrical Insulation*, vol. 22, no. 2, pp. 895–905, 2015.

[67] L. Xing, Q. Li, G. Zhang, X. Zhang, F. Liu, L. Liu, Y. Huang, and Q. Wang, "Self-Healable Polymer Nanocomposites Capable of Simultaneously Recovering Multiple Functionalities," *Advanced Functional Materials*, vol. 26, no. 20, pp. 3524–3531, 2016.

[68] J. C. Fothergill, “Filamentary Electromechanical Breakdown,” *IEEE transactions on electrical insulation*, vol. 26, no. 6, pp. 1124–1129, 1991.

[69] B. X. Du and B. Cui, “Effects of thermal conductivity on dielectric breakdown of micro, nano sized BN filled polypropylene composites,” *IEEE Transactions on Dielectrics and Electrical Insulation*, vol. 23, no. 4, pp. 2116–2125, 2016.

[70] G. Zhu, S. Dong, J. Hu, Y. Kan, P. He, L. Gao, X. Zhang, and H. Zhou, “In situ growth behavior of boron nitride nanotubes on the surface of silicon carbide fibers as hierarchical reinforcements,” *RSC Advances*, vol. 6, no. 17, pp. 14112–14119, 2016.

[71] N. P. Bansal, J. B. Hurst, and S. R. Choi, “Boron Nitride Nanotubes-Reinforced Glass Composites,” *Journal of the American Ceramic Society*, vol. 89, no. 1, pp. 388–390, 2006.

[72] C. Zou, M. Fu, J. C. Fothergill, and S. W. Rowe, “Influence of absorbed water on the dielectric properties and glass-transition temperature of silica-filled epoxy nanocomposites,” *Conference on Electrical Insulation and Dielectric Phenomena*, pp. 321–324, 2006.

[73] C. Zou, J. C. Fothergill, and S. W. Rowe, “A ‘Water Shell’ Model for the Dielectric Properties of Hydrated Silica-filled Epoxy Nano-composites,” *International Conference on Solid Dielectrics*, pp. 389–392, 2007.

[74] C. Zou, J. C. Fothergill, and S. W. Rowe, “The effect of water absorption on the dielectric properties of epoxy nanocomposites,” *IEEE Transactions on Dielectrics and Electrical Insulation*, vol. 15, no. 1, pp. 106–117, 2008.

[75] L. Hui, L. S. Schadler, and J. K. Nelson, “The Influence of Moisture on the Electrical Properties of Crosslinked Polyethylene / Silica Nanocomposites,” *IEEE Transactions on Dielectrics and Electrical Insulation*, vol. 20, no. 2, pp. 641–653, 2013.

[76] J. van Wijk, N. van Deventer, E. Harmzen, J. Meuldijk, and B. Klumperman, “Formation of hybrid poly(styrene-co-maleic anhydride)–silica microcapsules,” *Journal of Materials Chemistry B*, vol. 2, no. 30, pp. 4826–4835, 2014.

[77] K. Y. Lau, a S. Vaughan, G. Chen, I. L. Hosier, and a F. Holt, “On the dielectric response of silica-based polyethylene nanocomposites,” *Journal of Physics D: Applied Physics*, vol. 46, no. 9, p. 095303, 2013.

[78] P. Marx, A. J. Wanner, Z. Zhang, H. Jin, I.-A. Tsekmes, J. J. Smit, W. Kern, and F. Wiesbrock, “Effect of interfacial polarization and water absorption on the dielectric properties of epoxy-nanocomposites,” *Polymers*, vol. 9, no. 6, pp. 1–16, 2017.

[79] K. Sato, H. Horibe, T. Shirai, Y. Hotta, H. Nakano, H. Nagai, K. Mitsuishi, and K. Watari, “Thermally conductive composite films of hexagonal boron nitride and polyimide with affinity-enhanced interfaces,” *Journal of Materials Chemistry*, vol. 20, no. 14, pp. 2749–2752, 2010.

[80] U. W. Gedde, *Polymer physics*. Chapman & Hall, 1995.

[81] Y. Lin, T. Williams, and J. Connell, “Soluble, exfoliated hexagonal boron nitride nanosheets,” *The Journal of Physical Chemistry Letters*, vol. 1, no. 1, pp. 277–283, Jan. 2010.

[82] W. E. Hall, “Method of forming polyethylene powders,” US 2945020 A, 1960.

[83] J. Scheirs, *Compositional and Failure Analysis of Polymers: A Practical Approach*. Wiley, 2000.

[84] P. Goodhew, J. Humphreys, and R. Beanland, *Electron microscopy and analysis*, Third Edit. Taylor and Francis, 2001.

[85] R. H. Olley, D. C. Bassett, and D. J. Blundell, “Permanganic etching of PEEK,” *Polymer*, vol. 27, no. 3, pp. 344–348, 1986.

[86] Y. Waseda, E. Matsubara, and K. Shinodo, *X-Ray Diffraction Crystallography: Introduction, Examples and Solved Problems*. Springer, 2011.

[87] B. Stuart, *Infrared Spectroscopy: Fundamentals and Applications*. John Wiley & Sons Inc., 2004.

[88] V. Mittal, *Characterization Techniques for Polymer Nanocomposites*. Wiley-VCH, 2012.

[89] D. A. Skoog, F. J. Holler, and T. Nieman, *Principles of Instrumental Analysis*, 5th Editio. Brooks Cole, 1998.

[90] T. Blythe and D. Bloor, *Electrical properties of polymers*, 2nd ed. Cambridge University Press, 2005.

[91] L. A. Dissado and J. C. Fothergill, *Electrical degradation and breakdown in polymers*. London: Peter Peregrinus, 1992.

[92] W. Weibulll, "A statistical distribution function of wide applicability," *Journal of Applied Mechanics*, 1951.

[93] J. C. Fothergill, "Estimating the cumulative probability of failure data points to be Plotted on weibull and other probability paper," *IEEE Transactions on Electrical Insulation*, vol. 25, no. 3, pp. 489–492, 1990.

[94] M. Xu, T. Liang, M. Shi, and H. Chen, "Graphene-like two-dimensional materials.," *Chemical reviews*, vol. 113, no. 5, pp. 3766–98, May 2013.

[95] Q. Weng, X. Wang, X. Wang, Y. Bando, and D. Golberg, "Functionalized hexagonal boron nitride nanomaterials: emerging properties and applications," *Chemical Society Reviews*, vol. 45, pp. 3989–4012, 2016.

[96] N. Ooi, a. Rairkar, L. Lindsley, and J. B. Adams, "Electronic structure and bonding in hexagonal boron nitride," *Journal of Physics: Condensed Matter*, vol. 18, no. 1, p. 97, 2006.

[97] G. Cassabois, P. Valvin, and B. Gil, "Hexagonal boron nitride is an indirect bandgap semiconductor," *Nature photonics*, vol. 10, no. 4, pp. 262–267, 2016.

[98] M. Neshastehriz, I. Smid, and a. E. Segall, "In-Situ Agglomeration and De-agglomeration by Milling of Nano-Engineered Lubricant Particulate Composites for Cold Spray Deposition," *Journal of Thermal Spray Technology*, vol. 23, no. 7, pp. 1191–1198, 2014.

[99] G.-C. Wang and T.-M. Lu, *RHEED Transmission Mode and Pole Figures: Thin Film and Nanostructure Texture Analysis*. New York, USA: Springer, 2014.

[100] J. Wulff, *Structure and Properties of Materials*. New York, USA: Wiley, 1964.

[101] Y. Xue, Q. Liu, G. He, K. Xu, L. Jiang, X. Hu, and J. Hu, "Excellent electrical conductivity of the exfoliated and fluorinated hexagonal boron nitride nanosheets.," *Nanoscale research letters*, vol. 8, no. 1, p. 49, Jan. 2013.

[102] Y. Xue, X. Jin, Y. Fan, R. Tian, X. Xu, J. Li, J. Lin, J. Zhang, L. Hu, and C. Tang, "Large-Scale Synthesis of Hexagonal Boron Nitride Nanosheets and Their

Improvement in Thermal Properties of Epoxy Composites," *Polymers Composites*, vol. 35, no. 9, pp. 1707–1715, 2014.

[103] M. Du, Y. Wu, and X. Hao, "A facile chemical exfoliation method to obtain large size boron nitride nanosheets," *CrystEngComm*, vol. 15, no. 9, p. 1782, 2013.

[104] H. Ulus, T. Üstün, V. Eskizeybek, Ö. S. Şahin, A. Avci, and M. Ekrem, "Boron nitride-MWCNT/epoxy hybrid nanocomposites: Preparation and mechanical properties," *Applied Surface Science*, vol. 318, pp. 37–42, 2014.

[105] B. Yu, W. Xing, W. Guo, S. Qiu, W. Xin, S. Lo, and Y. Hu, "Thermal exfoliation of hexagonal boron nitride for effective enhancements on thermal stability, flame retardancy and smoke suppression of epoxy resin nanocomposites via sol-gel process," *Journal of Materials Chemistry A*, vol. 4, pp. 7330–7340, 2016.

[106] O. Hod, "Graphite and hexagonal boron-nitride have the same interlayer distance. Why?," *Journal of Chemical Theory and Computation*, vol. 8, no. 4, pp. 1360–1369, 2012.

[107] W. Paszkowicz, J. B. Pelka, M. Knapp, T. Szyszko, and S. Podsiadlo, "Lattice parameters and anisotropic thermal expansion of hexagonal boron nitride in the 10-297.5 K temperature range," *Applied Physics A: Materials Science & Processing*, vol. 75, no. 3, pp. 431–435, 2002.

[108] J. Hou, G. Li, N. Yang, L. Qin, M. E. Grami, Q. Zhang, N. Wang, and X. Qu, "Preparation and Characterization of Surface Modified Boron Nitride Epoxy Composites with Enhanced Thermal Conductivity," *RSC Advances*, vol. 4, pp. 44282–44290, 2014.

[109] L. K. Pillari, V. Umasankar, P. Elamathi, and G. Chandrasekar, "Synthesis and characterization of nano hexagonal boron nitride powder and evaluating the influence on aluminium alloy matrix," *Materials Today: Proceedings*, vol. 3, no. 6, pp. 2018–2026, 2016.

[110] M. T. Huang and H. Ishida, "Surface study of hexagonal boron nitride powder by diffuse reflectance Fourier transform infrared spectroscopy," *Surface and Interface Analysis*, vol. 37, no. 7, pp. 621–627, 2005.

[111] P. A. Encarnacion, "Electron Field Emission From Boron Nitride Thin Films," PhD Thesis, The University of Michigan, 2008.

[112] N. Kostoglou, K. Polychronopoulou, and C. Rebholz, "Thermal and chemical stability of hexagonal boron nitride (h-BN) nanoplatelets," *Vacuum*, vol. 112, pp. 42–45, 2015.

[113] L. Wang, R. Hang, Y. Xu, C. Guo, and Y. Qian, "From ultrathin nanosheets, triangular plates to nanocrystals with exposed (102) facets, a morphology and phase transformation of sp2 hybrid BN nanomaterials," *RCS Advances*, vol. 4, no. 27, pp. 14233–14240, 2014.

[114] W. Li, Y. Xu, Y. Zhou, W. Ma, S. Wang, and Y. Dai, "Silica nanoparticles functionalized via click chemistry and ATRP for enrichment of Pb(II) ion," *Nanoscale Research Letters*, vol. 7, no. 1, p. 1, 2012.

[115] D. Bracho, V. N. Dougnac, H. Palza, and R. Quijada, "Functionalization of silica nanoparticles for polypropylene nanocomposite applications," *Journal of Nanomaterials*, vol. 2012, 2012.

[116] H. Jin, P. H. F. Morshuis, J. J. Smit, and T. Andritsch, "The effect of surface treatment of silica nanoparticles on the breakdown strength of mineral oil," *IEEE International Conference on Dielectric Liquids*, pp. 1–4, 2014.

[117] Z. Guo, T. Pereira, O. Choi, Y. Wang, and H. T. Hahn, "Surface functionalized alumina nanoparticle filled polymeric nanocomposites with enhanced mechanical properties," *Journal of Materials Chemistry*, vol. 16, no. 27, p. 2800, 2006.

[118] Y. Tai, J. Miao, J. Qian, R. Xia, and Y. Zhang, "An effective way to stabilize silicon nitride nanoparticles dispersed in rubber matrix by a one-step process," *Materials Chemistry and Physics*, vol. 112, no. 2, pp. 659–667, 2008.

[119] W. Peng, X. Huang, J. Yu, P. Jiang, and W. Liu, "Electrical and thermophysical properties of epoxy/aluminum nitride nanocomposites: Effects of nanoparticle surface modification," *Composites Part A: Applied Science and Manufacturing*, vol. 41, no. 9, pp. 1201–1209, 2010.

[120] J. Gray, *Polystyrene: Properties, Performance, and Applications*. Nova Science Publishers, 2011.

[121] R. Ding, Y. Hu, Z. Gui, R. Zong, Z. Chen, and W. Fan, "Preparation and characterization of polystyrene/graphite oxide nanocomposite by emulsion polymerization," *Polymer Degradation and Stability*, vol. 81, no. 3, pp. 473–476, 2003.

[122] W. H. Zhang, X. D. Fan, W. Tian, and W. W. Fan, "Polystyrene/nano-SiO 2 composite microspheres fabricated by pickering emulsion polymerization: Preparation, mechanisms and thermal properties," *Express Polymer Letters*, vol. 6, no. 7, pp. 532–542, 2012.

[123] S. V. Krishna and G. Pugazhenthi, "Properties and Thermal Degradation Kinetics of Polystyrene/Organoclay Nanocomposites Synthesized by Solvent Blending Method: Effect of Processing Conditions and Organoclay Loading," *Journal of Applied Polymer Science*, vol. 120, no. 3, pp. 1322–1336, 2011.

[124] C. R. Martins, G. Ruggeri, and M. a. De Paoli, "Synthesis in Pilot Plant Scale and Physical Properties of Sulfonated Polystyrene," *Journal of the Brazilian Chemical Society*, vol. 14, no. 5, pp. 797–802, 2003.

[125] Y. Han, Y. Wu, M. Shen, X. Huang, J. Zhu, and X. Zhang, "Preparation and properties of polystyrene nanocomposites with graphite oxide and graphene as flame retardants," *Journal of Materials Science*, vol. 48, no. 12, pp. 4214–4222, 2013.

[126] K. Suresh, R. V. Kumar, and G. Pugazhenthi, "Processing and characterization of polystyrene nanocomposites based on CoAl layered double hydroxide," *Journal of Science: Advanced Materials and Devices*, vol. 1, no. 3, pp. 351–361, 2016.

[127] L. Cao, S. Emami, and K. Lafdi, "Large-scale exfoliation of hexagonal boron nitride nanosheets in liquid phase," *Materials Express*, vol. 4, no. 2, pp. 165–171, 2014.

[128] B. Q. Dai and G. L. Zhang, "A DFT study of hBN compared with graphite in forming alkali metal intercalation compounds," *Materials Chemistry and Physics*, vol. 78, no. 2, pp. 304–307, 2003.

[129] Z. Lin, A. Mcnamara, Y. Liu, K. S. Moon, and C. P. Wong, "Exfoliated hexagonal boron nitride-based polymer nanocomposite with enhanced thermal conductivity for electronic encapsulation," *Composites Science and Technology*, vol. 90, pp. 123–128, 2014.

[130] R. C. Zhang, D. Sun, A. Lu, S. Askari, M. Macias-Montero, P. Joseph, D. Dixon, K. Ostrikov, P. Maguire, and D. Mariotti, "Microplasma Processed Ultrathin Boron Nitride Nanosheets for Polymer Nanocomposites with Enhanced Thermal Transport Performance," *ACS Applied Materials and Interfaces*, vol. 8, no. 21, pp. 13567–13572, 2016.

[131] W. Lei, V. N. Mochalin, D. Liu, S. Qin, Y. Gogotsi, and Y. Chen, "Boron nitride colloidal solutions, ultralight aerogels and freestanding membranes through one-step exfoliation and functionalization," *Nature Communications*, vol. 6, p. 8849, 2015.

[132] J. Rieger, "The glass transition temperature of polystyrene," *Journal of Thermal Analysis*, vol. 46, pp. 965–972, 1996.

[133] L.-P. Blanchard, J. Hesse, and S. L. Malhotra, "Effect of Molecular Weight on Glass Transition by Differential Scanning Calorimetry," *Canadian Journal of Chemistry*, vol. 52, no. 18, pp. 3170–3175, 1974.

[134] B. Wunderlich, D. M. Bodily, and M. H. Kaplan, "Theory and measurements of the glass-transformation interval of polystyrene," *Journal of Applied Physics*, vol. 35, no. 1, pp. 95–102, 1964.

[135] A. Yoshioka and K. Tashiro, "Solvent effect on the glass transition temperature of syndiotactic polystyrene viewed from time-resolved measurements of infrared spectra at the various temperatures and its simulation by molecular dynamics calculation," *Macromolecules*, vol. 37, no. 2, pp. 467–472, 2004.

[136] W. Zhou, J. Zuo, X. Zhang, and a. Zhou, "Thermal, electrical, and mechanical properties of hexagonal boron nitride-reinforced epoxy composites," *Journal of Composite Materials*, vol. 48, no. 20, pp. 2517–2526, 2014.

[137] T.-L. Li and S. L.-C. Hsu, "Preparation and properties of thermally conductive photosensitive polyimide/boron nitride nanocomposites," *Journal of Applied Polymer Science*, vol. 121, no. 2, pp. 916–922, 2011.

[138] X. Cao, L. James Lee, T. Widya, and C. Macosko, "Polyurethane/clay nanocomposites foams: Processing, structure and properties," *Polymer*, vol. 46, no. 3, pp. 775–783, 2005.

[139] L. Torre, G. Lelli, and J. M. Kenny, "Synthesis and characterization of sPS/montmorillonite nanocomposites," *Journal of Applied Polymer Science*, vol. 100, no. 6, pp. 4957–4963, 2006.

[140] M. Praeger, A. S. Vaughan, and S. G. Swingler, "A dielectric spectroscopy study of the polystyrene / nanosilica model system," in *International Conference on Solid Dielectrics*, 2013, pp. 859–862.

[141] A. F. Holt, “Towards Intelligent Insulation,” PhD Thesis, University of Southampton, 2013.

[142] A. Von Hippel and L. G. Wesson, “Polystyrene plastics as high frequency dielectrics,” *Industrial & Engineering Chemistry*, vol. 38, no. 11, pp. 1121–1129, 1946.

[143] H. Couderc, M. Fréchette, and E. David, “Thermal and Dielectric Properties Evaluation of Low Density Polyethylene – Boron Nitride – Carbon Black Nanocomposites,” in *Conference on Electrical Insulation and Dielectric Phenomena*, 2015, pp. 535–538.

[144] S. Madakbaş, F. Şen, M. V. Kahraman, and F. Dumludağ, “Preparation, characterization, thermal, and dielectric properties of polypyrrole/h-BN nanocomposites,” *Advances in Polymer Technology*, vol. 33, no. 4, pp. 1–8, 2014.

[145] I. A. Tsekmes, R. Kochetov, P. H. F. Morshuis, and J. J. Smit, “Evaluating the Effect of Particle Distribution and Dispersion on the Dielectric Response of Boron Nitride - Epoxy Nanocomposites,” in *Electrical Insulation Conference*, 2014, pp. 329–332.

[146] I. A. Tsekmes, R. Kochetov, P. H. F. Morshuis, and J. J. Smit, “The role of particle distribution in the dielectric response of epoxy – boron nitride nanocomposites,” *Journal of Materials Science*, vol. 50, no. 3, pp. 1175–1186, 2015.

[147] H. W. Wang, K. C. Chang, H. C. Chu, S. J. Liou, and J. M. Yeh, “Significant Decreased Dielectric Constant and Loss of Polystyrene-Clay Nanocomposite Materials by Using Long-Chain Intercalation Agent,” *Journal of Applied Polymer Science*, vol. 92, no. 4, pp. 2402–2410, 2004.

[148] A. Krivda, T. Tanaka, M. Frechette, J. Castellon, D. Fabiani, G. C. Montanari, R. Gorur, P. Morshuis, S. Gubanski, J. Kindersberger, A. Vaughan, S. Pelissou, Y. Tanaka, L. E. Schmidt, G. Iyer, T. Andritsch, J. Seiler, and M. Anglhuber, “Characterization of epoxy microcomposite and nanocomposite materials for power engineering applications,” *IEEE Electrical Insulation Magazine*, vol. 28, no. 2, pp. 38–51, 2012.

[149] R. Kochetov, T. Andritsch, P. H. F. Morshuis, and J. J. Smit, “Anomalous behaviour of the dielectric spectroscopy response of nanocomposites,” *IEEE Transactions on Dielectrics and Electrical Insulation*, vol. 19, no. 1, pp. 107–117, 2012.

[150] R. Kochetov, T. Andritsch, U. Lafont, P. H. F. Morshuis, and J. J. Smit, "Effects of inorganic nanofillers and combinations of them on the complex permittivity of epoxy-based composites," in *IEEE International Symposium on Electrical Insulation*, 2010, pp. 1–5.

[151] T. Andritsch, R. Kochetov, P. H. F. Morshuis, and J. J. Smit, "Short term DC breakdown and complex permittivity of Al2O3- and MgO-epoxy nanocomposites," in *Conference on Electrical Insulation and Dielectric Phenomena*, 2010, pp. 1–4.

[152] I. A. Tsekmes, P. H. F. Morshuis, J. J. Smit, and R. Kochetov, "Enhancing the Thermal and Electrical with the Addition of Nanofillers," *IEEE Electrical Insulation Magazine*, vol. 31, no. 3, pp. 32–42, 2015.

[153] X. Y. Huang, P. K. Jiang, and C. U. Kim, "Electrical properties of polyethylene/aluminum nanocomposites," *Journal of Applied Physics*, vol. 102, no. 12, 2007.

[154] X. Huang, P. Jiang, C. Kim, Q. Ke, and G. Wang, "Preparation, microstructure and properties of polyethylene aluminum nanocomposite dielectrics," *Composites Science and Technology*, vol. 68, no. 9, pp. 2134–2140, Jul. 2008.

[155] M. H. Sabuni and J. K. Nelson, "The Effects of Plasticizer on the Electric Strength of Polystyrene," *Journal of Materials Science*, vol. 14, no. 12, pp. 2791–2796, 1979.

[156] S. Li, W. Wang, F. Ni, and G. Yin, "Surface flashover in vacuum and bulk breakdown in polystyrene nanocomposites," in *International Conference on Electrical Insulating Materials*, 2011, pp. 486–490.

[157] M. Praeger, A. S. Vaughan, and S. G. Swingler, "The breakdown strength and localised structure of polystyrene as a function of nanosilica fill-fraction," in *International Conference on Solid Dielectrics*, 2013, pp. 863–866.

[158] W. Li, H. Hillborg, and U. W. Gedde, "Influence of process conditions and particle dispersion on the ac breakdown strength of polyethylene-aluminium oxide nanocomposites," *IEEE Transactions on Dielectrics and Electrical Insulation*, vol. 22, no. 6, pp. 3536–3542, 2015.

[159] C. Yeung and A. S. Vaughan, "On the effect of nanoparticle surface chemistry on the electrical characteristics of epoxy-based nanocomposites," *Polymers*, vol. 8, no. 4, p. 16, 2016.

[160] R. Ayoob, T. Andritsch, and A. S. Vaughan, “The effect of material processing on the dielectric properties of polystyrene boron nitride nanocomposites,” in *IEEE Electrical Insulation Conference*, 2015, pp. 333–336.

[161] R. Ayoob, T. Andritsch, A. S. Vaughan, and Y. Meng, “The Effect of Exfoliation on the Breakdown Strength of Polystyrene Boron Nitride Composites,” *Conference on Electrical Insulation and Dielectric Phenomena*, pp. 675–678, 2014.

[162] A. J. Peacock, *Handbook of polyethylene: structures, properties, and applications*. Marcel Dekker, Inc., 2000.

[163] I. L. Hosier, “Morphology and electrical properties of polyethylene blends,” PhD Thesis, University of Reading, 1996.

[164] I. L. Hosier, A. S. Vaughan, and S. G. Swingler, “Structure – property relationships in polyethylene blends : the effect of morphology on electrical breakdown strength,” *Journal of Materials Science*, vol. 2, pp. 4523–4531, 1997.

[165] M. Öner, a. a. Çöl, C. Pochat-Bohatier, and M. Bechelany, “Effect of incorporation of boron nitride nanoparticles on the oxygen barrier and thermal properties of poly(3-hydroxybutyrate-co-hydroxyvalerate),” *RSC Advances*, vol. 6, no. 93, pp. 90973–90981, 2016.

[166] S. Dash and S. K. Swain, “Effect of nanoboron nitride on the physical and chemical properties of soy protein,” *Composites Science and Technology*, vol. 84, pp. 39–43, 2013.

[167] I. L. Hosier, a. S. Vaughan, and S. G. Swingler, “On the effects of morphology and molecular composition on the electrical strength of polyethylene blends,” *Journal of Polymer Science Part B: Polymer Physics*, vol. 38, no. 17, pp. 2309–2322, 2000.

[168] I. L. Hosier, A. S. Vaughan, and S. G. Swingler, “On the effects of morphology and molecular momposition on the electrical strength of polyethylene blends,” *Journal of Polymer Science: Part B: Polymer Physics*, vol. 38, pp. 2309–2322, 2000.

[169] C. D. Green and A. S. Vaughan, “Morphology and crystallisation kinetics of polyethylene/montmorillonite nanocomposites,” *Conference on Electrical Insulation and Dielectric Phenomena*, pp. 635–638, 2007.

[170] C.-M. Chan, J. Wu, J.-X. Li, and Y.-K. Cheung, “Polypropylene/calcium carbonate nanocomposites,” *Polymer*, vol. 43, no. 10, pp. 2981–2992, 2002.

[171] A. A. Alsaygh, J. Al-Hamidi, D. Alsewailem, I. M. Al-Najjar, and V. L. Kuznetsov, “Characterization of polyethylene synthesized by zirconium single site catalysts,” *Appl Petrochem Research*, vol. 4, no. 1, pp. 79–84, 2014.

[172] M. Laridjani and P. Leboucher, “The structural dilemma of bulk polyethylene: An intermediary structure,” *PLoS ONE*, vol. 4, pp. 1–17, 2009.

[173] N. S. Murthy, H. Minor, C. Bednarczyk, and S. Krimm, “Structure of the Amorphous Phase in Oriented Polymers,” *Macromolecules*, vol. 26, pp. 1712–1721, 1993.

[174] B. Inci and K. B. Wagener, “Decreasing the alkyl branch frequency in precision polyethylene: Pushing the limits toward longer run lengths,” *Journal of the American Chemical Society*, vol. 133, no. 31, pp. 11872–11875, 2011.

[175] C. W. Bunn, “The crystal structre of long-chain normal paraffin hydrocarbons. The ‘Shape’ of the CH2 group,” *Transactions of the Faraday Society*, vol. 35, pp. 482–491, 1939.

[176] G. Malucelli, P. Palmero, S. Ronchetti, A. Delmastro, and L. Montanaro, “Effect of various alumina nano-fillers on the thermal and mechanical behaviour of low-density polyethylene-Al2O3 composites,” *Polymer International*, vol. 59, no. 8, pp. 1084–1089, 2010.

[177] R. Saggar, H. Porwal, P. Tatarko, I. Dlouhý, and M. J. Reece, “Boron nitride nanosheets reinforced glass matrix composites,” *Advances in Applied Ceramics*, vol. 114, no. S1, pp. S26–S33, 2015.

[178] A. Sultan, S. Ahmad, T. Anwer, and F. Mohammad, “Binary doped polypyrrole and polypyrrole/boron nitride nanocomposite: preparation, characterization and application in detection of liquefied petroleum gas leaks,” *RSC Advances*, vol. 5, pp. 105980–105991, 2015.

[179] G. Malucelli, R. Bongiovanni, M. Sangermano, S. Ronchetti, and A. Priola, “Preparation and characterization of UV-cured epoxy nanocomposites based on o-montmorillonite modified with maleinized liquid polybutadienes,” *Polymer*, vol. 48, no. 24, pp. 7000–7007, 2007.

[180] S. S. Hwang, S. P. Liu, P. P. Hsu, J. M. Yeh, J. P. Yang, and C. L. Chen, "Morphology, mechanical, and rheological behavior of microcellular injection molded EVA-clay nanocomposites," *International Communications in Heat and Mass Transfer*, vol. 39, no. 3, pp. 383–389, 2012.

[181] S. Satapathy, G. C. Mohanty, and P. L. Nayak, "Synthesis and characterization of layered silicate / epoxy nanocomposite," *Advances in Applied Science Research*, vol. 3, no. 6, pp. 3981–3986, 2012.

[182] G. Malucelli, S. Ronchetti, N. Lak, A. Priola, N. T. Dintcheva, and F. P. La Mantia, "Intercalation effects in LDPE/o-montmorillonites nanocomposites," *European Polymer Journal*, vol. 43, no. 2, pp. 328–335, 2007.

[183] B. Wunderlich and C. M. Cormier, "Heat of fusion of polyethylene," *Journal of Polymer Science*, vol. 5, no. A-2, pp. 987–988, 1967.

[184] X. Zhang, H. Wu, S. Guo, and Y.-Z. Wang, "Understanding in Crystallization of Polyethylene: The Role of boron nitride (BN) particles," *RSC Advances*, vol. 5, pp. 99812–99819, 2015.

[185] J. A. S. Puente, A. Esposito, F. Chivrac, and E. Dargent, "Effect of boron nitride as a nucleating agent on the crystallization of bacterial poly(3-hydroxybutyrate)," *Journal of Applied Polymer Science*, vol. 128, no. 5, pp. 2586–2594, 2013.

[186] L. Wang, X. Wang, W. Zhu, Z. Chen, J. Pan, and K. Xu, "Effect of Nucleation Agents on the Crystallization ofPoly(3-hydroxybutyrate-co-4-hydroxybutyrate) (P3/4HB)," *Journal of Applied Polymer Science*, vol. 116, no. 2, pp. 1116–1123, 2010.

[187] I. L. Hosier, M. Praeger, a S. Vaughan, and S. G. Swingler, "Electrical properties of polymer nano-composites based on oxide and nitride fillers," *Electrical Insulation Conference*, no. June, pp. 438–441, 2015.

[188] D. Nwabunma and T. Kyu, *Polyolefin Composites*. Wiley, 2008.

[189] V. Myroshnychenko and C. Brosseau, "Finite-element modeling method for the prediction of the complex effective permittivity of two-phase random statistically Isotropic heterostructures," *Journal of Applied Physics*, vol. 97, no. 4, pp. 044101–1 – 044101–14, 2005.

[190] M. Kühn and H. Kliem, "A numerical method for the calculation of dielectric nanocomposites," *IEEE Transactions on Dielectrics and Electrical Insulation*, vol. 17, no. 5, pp. 1499–1508, 2010.

[191] O. Boorman, I. L. Hosier, M. Praeger, R. Torah, A. S. Vaughan, T. Andritsch, S. G. Swingler, and J. Topham, "Barium Titanate and the Dielectric Response of Polystyrene-based Composites," in *Conference on Electrical Insulation and Dielectric Phenomena*, 2014, pp. 707–710.

[192] J. Topham, O. Boorman, I. L. Hosier, M. Praeger, R. Torah, A. S. Vaughan, T. Andritsch, and S. G. Swingler, "Dielectric Studies of Polystyrene-based , High-permittivity Composite Systems," in *Conference on Electrical Insulation and Dielectric Phenomena*, 2014, pp. 711–714.

[193] K. K. K. K. K. Kim, A. Hsu, X. Jia, S. M. S. M. M. Kim, Y. Shi, M. Dresselhaus, T. Palacios, and J. Kong, "Synthesis and Characterization of Hexagonal Boron Nitride Film as a Dielectric Layer for Graphene Devices," *ACS Nano*, vol. 6, no. 10, pp. 8583–8590, 2012.

[194] T. Zhang, M.-Q. Wu, S.-R. Zhang, J. Xiong, J.-M. Wang, D.-H. Zhang, F.-M. He, and Z.-P. Li, "Permittivity and its temperature dependence in hexagonal structure BN dominated by the local electric field," *Chinese Physics B*, vol. 21, no. 7, p. 077701, 2012.

[195] T.-L. Li and S. L.-C. Hsu, "Enhanced thermal conductivity of polyimide films via a hybrid of micro-and nano-sized boron nitride," *The Journal of Physical Chemistry B*, vol. 114, no. 20, pp. 6825–6829, 2010.

[196] C. D. Green, "Polyethylene-montmorillonite nanocomposites," PhD Thesis, University of Southampton, 2008.

[197] B. Zazoum, E. David, and a. D. Ngô, "Correlation between Structure and Dielectric Breakdown in LDPE/HDPE/Clay Nanocomposites," *ISRN Nanomaterials*, vol. 2014, pp. 1–9, 2014.

[198] R. Liao, G. Bai, L. Yang, H. Cheng, Y. Yuan, and J. Guan, "Improved electric strength and space charge characterization in LDPE composites with montmorillonite fillers," *Journal of Nanomaterials*, vol. 2013, 2013.

[199] M. Gao, P. Zhang, and F. Wang, “Effect of percolation and interfacial characteristics on breakdown behavior of nano-silica/epoxy composites,” *8th International Forum on Strategic Technology*, vol. 1, pp. 120–123, 2013.

[200] C. Calebrese, L. Hui, L. S. Schadler, and J. K. Nelson, “A review on the importance of nanocomposite processing to enhance electrical insulation,” *IEEE Transactions on Dielectrics and Electrical Insulation*, vol. 18, no. 4, pp. 938–945, 2011.

[201] S. Siddabattuni, T. P. Schuman, and F. Dogan, “Dielectric Properties of Polymer − Particle Nanocomposites In fl uenced by Electronic Nature of Filler Surfaces,” *ACS Applied Materials & Interfaces*, vol. 5, no. 6, pp. 1917–1927, 2013.

[202] W. Wang, D. Min, and S. Li, “Understanding the conduction and breakdown properties of polyethylene nanodielectrics: Effect of deep traps,” *IEEE Transactions on Dielectrics and Electrical Insulation*, vol. 23, no. 1, pp. 564–572, 2016.

[203] R. C. Smith, C. Liang, M. Landry, J. K. Nelson, and L. S. Schadler, “The mechanisms leading to the useful electrical properties of polymer nanodielectrics,” *IEEE Transactions on Dielectrics and Electrical Insulation*, vol. 15, no. 1, pp. 187–196, 2008.

[204] A. S. Vaughan, S. G. Swingler, and Y. Zhang, “Polyethylene Nanodielectrics: The Influence of Nanoclays on Structure Formation and Dielectric Breakdown,” *IEEJ Transactions on Fundamentals and Materials*, vol. 126, no. 1057–1063, 2006.

[205] C. D. Green, A. S. Vaughan, G. R. Mitchell, and T. Liu, “Structure Property Relationships in Polyethylene / Montmorillonite Nanodielectrics,” *IEEE Transactions on Dielectrics and Electrical Insulation*, vol. 15, no. 1, pp. 134–143, 2008.

[206] K. Y. Lau, “Structure and electrical properties of silica-based polyethylene nanocomposites,” PhD Thesis, University of Southampton, 2013.

[207] M. G. Danikas and T. Tanaka, “Nanocomposites - A review of electrical treeing and breakdown,” *IEEE Electrical Insulation Magazine*, vol. 25, no. 4, pp. 19–25, 2009.

[208] R. Vogelsang, T. Farr, and K. Fröhlich, “The effect of barriers on electrical tree propagation in composite insulation materials,” *IEEE Transactions on Dielectrics and Electrical Insulation*, vol. 13, no. 2, pp. 373–382, 2006.

[209] S. Alapati and M. J. Thomas, “Electrical Treeing in Polymer Nanocomposites,” *International Journal of Emerging Electric Power Systems*, pp. 351–355, 2009.

[210] Y. Hattori, T. Taniguchi, K. Watanabe, and K. Nagashio, “Layer-by-layer dielectric breakdown of hexagonal boron nitride,” *ACS Nano*, vol. 9, no. 1, pp. 916–921, 2015.

[211] G. H. Lee, Y. J. Yu, C. Lee, C. Dean, K. L. Shepard, P. Kim, and J. Hone, “Electron tunneling through atomically flat and ultrathin hexagonal boron nitride,” *Applied Physics Letters*, vol. 99, no. 24, pp. 1–4, 2011.

[212] S. Li, D. Min, W. Wang, and G. Chen, “Linking traps to dielectric breakdown through charge dynamics for polymer nanocomposites,” *IEEE Transactions on Dielectrics and Electrical Insulation*, vol. 23, no. 5, pp. 2777–2785, 2016.

[213] S. Li, G. Yin, G. Chen, J. Li, S. Bai, L. Zhong, Y. Zhang, and Q. Lei, “Short-term breakdown and long-term failure in nanodielectrics: A review,” *IEEE Transactions on Dielectrics and Electrical Insulation*, vol. 17, no. 5, pp. 1523–1535, 2010.

[214] K. Ishimotol, T. Tanaka, Y. Ohki, Y. Sekiguchi, Y. Murata, and M. Gosyowaki, “Comparison of Dielectric Properties of Low-density Polyethylene / MgO Composites with Different Size Fillers,” in *Conference on Electrical Insulation and Dielectric Phenomena*, 2008, pp. 208–211.

[215] M. Roy, J. K. Nelson, R. K. MacCrone, and L. S. Schadler, “Candidate mechanisms controlling the electrical characteristics of silica/XLPE nanodielectrics,” *Journal of Materials Science*, vol. 42, no. 11, pp. 3789–3799, 2007.

[216] W. Wang and S. Li, “Correlation between Trap Parameters and Breakdown Strength of Polyethylene / Alumina Nanocomposites,” in *International Symposium on Electrical Insulating Materials*, 2014, pp. 73–76.

[217] X. Huang, P. Jiang, and T. Tanaka, “A review of dielectric polymer composites with high thermal conductivity,” *IEEE Electrical Insulation Magazine*, vol. 27, no. 4, pp. 8–16, 2011.

[218] NETZSCH, “Electronic Communication,” 2015.

[219] A. S. Vaughan, “Personal Communication,” 2015.

[220] W. Zhou, S. Qi, H. Li, and S. Shao, “Study on insulating thermal conductive BN/HDPE composites,” *Thermochimica Acta*, vol. 452, no. 1, pp. 36–42, 2007.

[221] Z. Lin, Y. Yao, A. McNamara, K. S. Moon, and C. P. Wong, "Single/few-layer boron nitride-based nanocomposites for high thermal conductivity underfills," *Proceedings - Electronic Components and Technology Conference*, pp. 1437–1441, 2012.

[222] C. Zhi, Y. Bando, T. Terao, C. Tang, H. Kuwahara, and D. Golberg, "Towards thermoconductive, electrically insulating polymeric composites with boron nitride nanotubes as fillers," *Advanced Functional Materials*, vol. 19, no. 12, pp. 1857–1862, 2009.

[223] B. X. Du and M. Xiao, "Thermal accumulation and tracking failure process of BN-filler epoxy-matrix composite," *IEEE Transactions on Dielectrics and Electrical Insulation*, vol. 20, no. 6, pp. 2270–2276, 2013.

[224] Y. Hattori, T. Taniguchi, K. Watanabe, and K. Nagashio, "Anisotropic Dielectric Breakdown Strength of Single Crystal Hexagonal Boron Nitride," *ACS Applied Materials & Interfaces*, vol. 8, no. 41, pp. 27877–27884, 2016.

[225] W. Tian and R. Yang, "Phonon transport and thermal conductivity percolation in random nanoparticle composites," *Computer Modeling in Engineering and Sciences*, vol. 24, no. 2–3, pp. 123–141, 2008.

[226] N. Jäverberg, H. Edin, P. Nordell, S. Nawaz, H. Hillborg, B. Azhdar, and U. W. Gedde, "Dielectric properties of alumina-filled poly (ethylene-co-butyl acrylate) nanocomposites Part II- wet studies," *IEEE Transactions on Dielectrics and Electrical Insulation*, vol. 19, no. 2, pp. 391–399, 2012.

[227] I. L. Hosier, M. Praeger, a F. Holt, a S. Vaughan, and S. G. Swingler, "Effect of water absorption on dielectric properties of nano-silica / polyethylene composites," *Conference on Electrical Insulation and Dielectric Phenoma*, pp. 651–654, 2014.

[228] L. A. Dissado and R. M. Hill, "Anomalous low-frequency dispersion. Near direct current conductivity in disordered low-dimensional materials," *Journal of the Chemical Society, Faraday Transactions 2: Molecular and Chemical Physics*, vol. 80, no. 3, pp. 291–319, 1984.

[229] C. Zhang and G. C. Stevens, "The dielectric response of polar and non-polar nanodielectrics," *IEEE Transactions on Dielectrics and Electrical Insulation*, vol. 15, no. 2, pp. 606–617, 2008.

[230] M. Praeger, I. L. Hosier, a S. Vaughan, and S. G. Swingler, "The effects of surface hydroxyl groups in polyethylene-silica nanocomposites," in *IEEE Electrical Insulation Conference*, 2015, pp. 201–204.

[231] D. Fabiani, G. Montanari, and L. Testa, "Effect of aspect ratio and water contamination on the electric properties of nanostructured insulating materials," *IEEE Transactions on Dielectrics and Electrical Insulation*, vol. 17, no. 1, pp. 221–230, 2010.

[232] D. Ma, T. a Hugener, R. W. Siegel, A. Christerson, E. Mårtensson, C. Önneby, and L. S. Schadler, "Influence of nanoparticle surface modification on the electrical behaviour of polyethylene nanocomposites," *Nanotechnology*, vol. 16, no. 6, pp. 724–731, 2005.

[233] C. W. Reed, "Functionalization of nanocomposite dielectrics," *International Symposium on Electrical Insulation*, pp. 0–3, 2010.

[234] M. Roy, J. K. Nelson, R. K. Maccrone, L. S. Schadler, C. W. Reed, and R. Keefe, "Polymer nanocomposite dielectrics-the role of the interface," *IEEE Transactions on Dielectrics and Electrical Insulation*, vol. 12, no. 4, pp. 629–643, 2005.

[235] M. Praeger, I. L. Hosier, A. S. Vaughan, and S. G. Swingler, "Calcined Silica for Enhanced Polyethylene Nano Composites," *Applied Physics Letters*, vol. Submitted, 2015.

[236] A. T. Hoang, L. Pallon, D. Liu, Y. V. Serdyuk, S. M. Gubanski, and U. W. Gedde, "Charge Transport in LDPE Nanocomposites Part I—Experimental Approach," *Polymers*, vol. 8, no. 3, p. 19, 2016.

[237] F. Tian, Q. Lei, X. Wang, and Y. Wang, "Investigation of electrical properties of LDPE/ZnO nanocomposite dielectrics," *IEEE Transactions on Dielectrics and Electrical Insulation*, vol. 19, no. 3, pp. 763–769, 2012.

[238] I. A. Tsekmes, R. Kochetov, P. H. F. Morshuis, and J. J. Smit, "Impact of Particle Distribution on the Electrical Conductivity of Epoxy Nanocomposites," in *Electrical Insulation Conference*, 2015, pp. 337–340.

[239] F. Ciuprina and I. Plesa, "DC and AC Conductivity of LDPE Nanocomposites," in *International Symposium on Advanced Topics in Electrical Engineering*, 2011.

[240] R. J. Sengwa and S. Choudhary, “Dielectric Dispersion and Relaxation in Polymer Blend Based Nanodielectric Film,” *Macromolecular Symposia*, vol. 362, no. 1, pp. 132–138, 2016.

[241] M. Oviedo Mendoza, O. A. de Fuentes, E. Prokhorov, G. Luna Barcenas, and E. P. Ortega, “Correlation between Electrical Properties and Potentiometric Response of CS-Clay Nanocomposite Membranes,” *Advances in Materials Science and Engineering*, vol. 2015, pp. 1–6, 2015.

[242] E. Tkalya, M. Ghislandi, A. Alekseev, C. Koning, and J. Loos, “Latex-based concept for the preparation of graphene-based polymer nanocomposites,” *Journal of Materials Chemistry*, vol. 20, no. 15, pp. 3035–3039, 2010.

[243] D. Golberg, Y. Bando, Y. Huang, T. Terao, M. Mitome, and C. Tang, “Boron nitride nanotubes and nanosheets,” *ACS Nano*, vol. 4, no. 6, pp. 2979–2993, 2010.

[244] V. Nicolosi, M. Chhowalla, M. G. Kanatzidis, M. S. Strano, and J. N. Coleman, “Liquid exfoliation of layered materials,” *Science*, vol. 340, no. 6139, pp. 1226419–1226419, Jun. 2013.

[245] A. Tiano, L. Gibbons, M. Tsui, S. Applin, R. Silva, C. Park, and C. Fay, “Thermodynamic Approach to Boron Nitride Nanotube Solubility and Dispersion,” *Nanoscale*, pp. 4348–4359, 2016.

[246] K. L. Marsh, M. Souliman, and R. B. Kaner, “Co-solvent exfoliation and suspension of hexagonal boron nitride.,” *Chemical communications (Cambridge, England)*, vol. 51, no. 1, pp. 187–90, 2015.

[247] W. Han, L. Wu, Y. Zhu, K. Watanabe, and T. Taniguchi, “Structure of chemically derived mono- and few-atomic-layer boron nitride sheets,” *Applied Physics Letters*, vol. 93, no. 22, p. 223103, 2008.

[248] A. F. M. Barton, “Solubility parameters,” *Chemical Reviews*, vol. 75, pp. 731–753, 1975.

[249] J. Lyklema, “The surface tension of pure liquids,” *Colloids and Surfaces A: Physicochemical and Engineering Aspects*, vol. 156, no. 1–3, pp. 413–421, 1999.

[250] N. Rathod and S. G. Hatzikiriakos, “The effect of surface energy of boron nitride on polymer processability,” *Polymer Engineering and Science*, vol. 44, no. 8, pp. 1543–1550, 2004.

[251] M. Seth, S. G. Hatzikiriakos, and T. M. Clere, “Gross melt fracture elimination: The role of surface energy of boron nitride powders,” *Polymer Engineering and Science*, vol. 42, no. 4, pp. 743–752, 2002.

[252] I. M. Smallwood, *Handbook of organic solvent properties*. John Wiley & Sons Inc., 1996.